The assessment of the uncertainty of the hydrodynamical SYMPHONIE2015 model and its implications for Lagrangian dispersal studies

Elise Vissenaekens

Sorbonne University

ED129: Environmental sciences

Laboratory of Ecogeochemistry of Benthic environments UMR 8222 (LECOB)

The assessment of the uncertainty of the hydrodynamical SYMPHONIE2015 model and its implications for Lagrangian dispersal studies.

By Elise Vissenaekens

PhD in oceanography

Supervised by Katell Guizien

Presented and defended on 27/01/2022

In front of a jury consisting of:

- Durrieu de Madron, Xavier, Research scientist, Examinator
- Estournel, Claude, Research director, Reporter
- Guizien, Katell, Research director, Thesis supervisor
- Magaldi, Marcello, Senior researcher, Reporter
- Ourmières, Yann, Lecturer, Examinator
- Stemmann, Lars, professor, President

Acknowledgments

First and foremost, I would like to thank my PhD supervisor Katell Guizien. Without your continuous effort and optimism, this would not have been possible. Moreover, I would like to thank Nathalie, who helped me survive the French bureaucracy. Furthermore, I would like to thank my family, for their continuous support throughout my university adventures. Especially my father, who let his only daughter travel more than a thousand miles away from him and who came to visit every holiday, just so I could see my dog (and see my father too, presumably). I would like to thank my dog Nala, for surviving cancer when I was away and simply for being the best girl ever. A special thanks to my friends Wouter and Marie, whose skype sessions got me through a worldwide pandemic and a PhD. I would also like to thank my crazy colleagues, Corentin and Mathilde, for shooting Nerf darts at me whenever I was too stressed. The memes you sent me will forever stay in my heart. Since this PhD involved a lot of coding, I would like to thank the contributors of Stack Overflow, without who many students would have never graduated.

Table of contents

English abstract

To give sound management advice, the connectivity in coastal areas must be thoroughly understood. The red thread throughout this PhD is analysing the uncertainty of the SYMPHONIE2015 model and its effect on larval dispersal simulations.

In the first chapter, the robustness of the model to assumption violation was tested. This was done by calculating six relative and absolute statistical indicators during and outside of wind, wave and stratification events. The results showed that the model's performance is not affected by these events.

In the second chapter, the instant error was calculated. Then, the cumulative error distributions were compared to each other in space and time. In time, the intraseasonal differences in error distributions were smaller than the interseasonal ones. In space, eight groups of error distributions could be formed. No link was found between the model's performance and the modelling characteristics. Similar to chapter one, no link was found between the model's performance and stratification and wave interaction. However, a strong correlation between the current speed and the error distributions was found.

In chapter three, the instant error was added as noise to the Lagrangian dispersal simulations and compared to the original run to assess the effect of the models' error on connectivity. The median difference in transfer rate between the runs with and without noise is zero for most zones. However, when there is a difference in transfer rate, the runs with noise often underestimate the connectivity. Moreover, the relative difference in transfer rate can vary from -100% to 100%.

Knowing the uncertainties in dispersal simulations can aid in using them for management advice.

French abstract

Pour donner de bons conseils de gestion, la connectivité dans les zones côtières doit être parfaitement comprise. Le fil rouge de cette thèse est l'analyse de l'incertitude du modèle SYMPHONIE2015 et son effet sur les simulations de dispersion larvaire.

Dans le premier chapitre, la robustesse du modèle à la violation des hypothèses a été testée. Cela a été fait en calculant six indicateurs statistiques relatifs et absolus pendant et en dehors des événements de vent, de vagues et de stratification. Les résultats ont montré que les performances du modèle ne sont pas affectées par ces événements.

Dans le deuxième chapitre, l'erreur instantanée a été calculée. Ensuite, les distributions d'erreurs cumulées ont été comparées les unes aux autres dans l'espace et dans le temps. Avec le temps, les différences intrasaisonnières dans les distributions d'erreurs étaient plus petites que les différences intersaisonnières. Dans l'espace, huit groupes de distributions d'erreurs pourraient être formés. Aucun lien n'a été trouvé entre les performances du modèle et les caractéristiques de modélisation. Comme au chapitre un, aucun lien n'a été trouvé entre les performances du modèle et la stratification et l'interaction des vagues. Cependant, une forte corrélation entre la vitesse du courant et les distributions d'erreurs a été trouvée.

Dans le chapitre trois, l'erreur instantanée a été ajoutée en tant que bruit aux simulations de dispersion lagrangienne et comparée à l'exécution initiale pour évaluer l'effet de l'erreur des modèles sur la connectivité. La différence médiane de taux de transfert entre les analyses avec et sans bruit est nulle pour la plupart des zones. Cependant, lorsqu'il y a une différence de taux de

transfert, les runs avec du bruit sous-estiment souvent la connectivité. De plus, la différence relative de taux de transfert peut varier de -100 % à 100 %.

Connaître les incertitudes dans les simulations de dispersion peut aider à les utiliser pour des conseils de gestion.

General introduction

The ocean has a large impact on the atmosphere, land and biosphere. It covers 71% of the earth's surface (Hoegh-Guldberg et al., 2014) and provides many ecosystem services such as food, transport and tourism (Barbier, 2017). Literature states that these services increase with increasing biodiversity (Loreau et al., 2001; Tilman, 2001; Sala & Knowlton, 2006; Worm et al., 2006; Butler et al., 2007; Hector & Bagchi, 2007; Palumbi et al., 2009). Despite its importance, it is continuously threatened by anthropogenic influences like overfishing (Christensen et al., 2007), pollution (Sindermann, 1995), acidification (Hoegh-Guldberg et al., 2014) and global warming (Hoegh-Guldberg et al., 2014). Moreover, the amount of people living by the coast is continuously increasing (Small & Nicholls, 2003; Neumann et al., 2015). This increased stress on the ocean can create conflicts between the different ecosystem services, reducing their efficiency (Douvere, 2008; Collie et al., 2013).

Anthropogenic influences on the ocean can cause habitat fragmentation. Habitat fragmentation is defined by Wilcove et al. (1986) as the transformation of a large habitat into smaller, isolated patches. Habitat fragmentation can cause a reduction in biodiversity and population abundance (Saunders et al., 1991; Fahrig, 2003; Boström et al., 2006; Cushman, 2006; Ha & Williams, 2018; Yeager et al., 2020).

The increased anthropogenic influence on the ocean is why marine spatial planning (MSP) is increasingly applied (Foley et al., 2010; Lubchenco & Sutley, 2010). Frazão Santos et al. (2018) defined MSP as a way to organize the use of ocean space and interactions between human uses and the marine environment. Unfortunately, many MSPs are mainly based on economic growth,

a.k.a. blue growth, rather than marine conservation (Qiu & Jones, 2013; Frazão Santos et al., 2018).

Luckily, there has been increased interest in protecting the world's oceans (Sala et al., 2018) with more and bigger marine protected areas (MPAs) being implemented in MSPs as a result (Lubchenco & Grorud-Colvert, 2015; Sala et al., 2018). During the United Nations' Convention on Biological Diversity (CBD) in 2010 it was decided that by 2020, 10% of the ocean should be protected (Sala et al., 2018). However, Sala et al. (2018) found that only 3.6% of the ocean is actually in an MPA since many of the reported MPAs are either not yet installed or not sufficiently protected from extractive activities. Moreover, scientists state that at least 30% should be protected to properly protect the ocean's biodiversity (O'Leary et al., 2016; Sala et al., 2018). Overall, no-take reserves have a positive effect on biomass and species richness (Lester et al., 2009). However, Lester et al. (2009) found that for algae and invertebrates, this is not always the case. This makes sense, since most of the MPAs were implemented to sustain fisheries (Guizien et al., 2012). This is why giving sound scientific advice on where to install MPA's is crucial for the protection of species of all taxa.

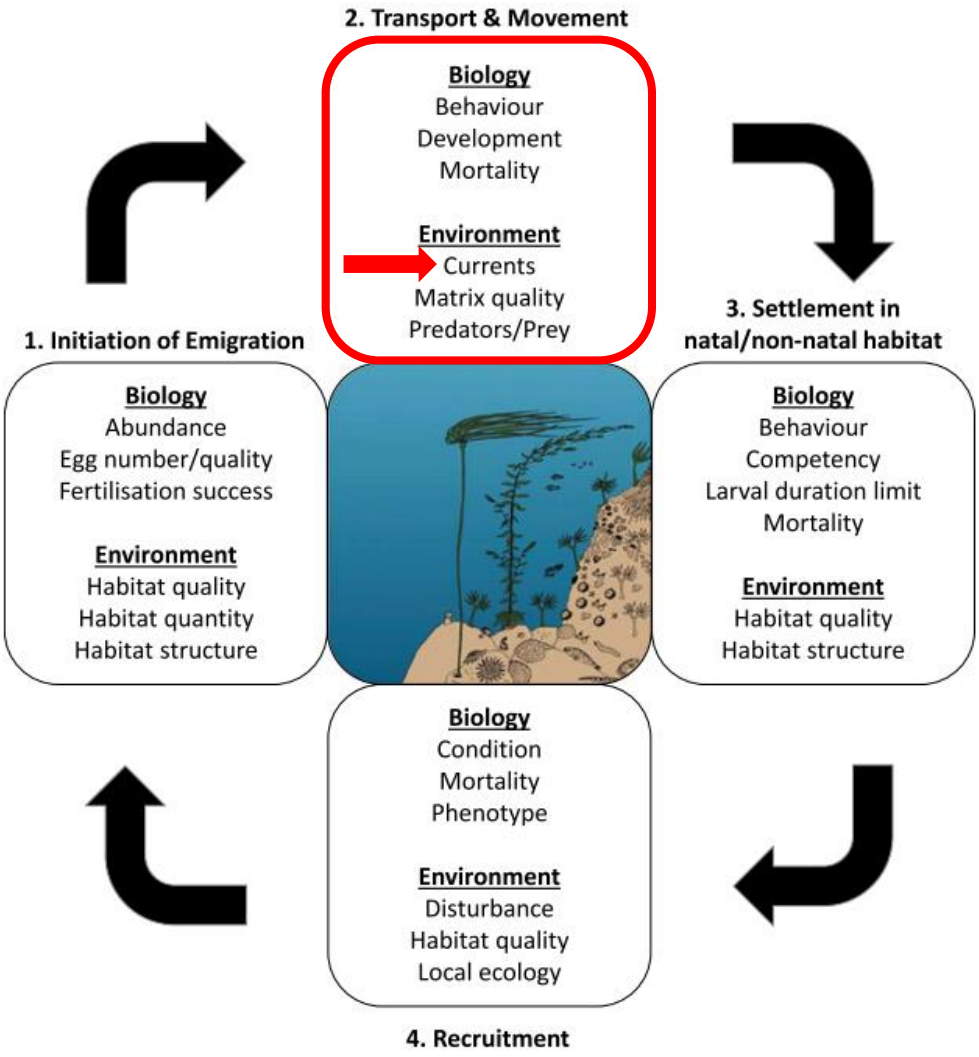

Figure I.1: The four stages needed for successful larval dispersal of benthic marine organisms to create population connectivity (Modified from Treml et al., 2015; Swearer et al., 2019).

To fully understand how to protect sessile invertebrates, one must look at their lifecycle, since most of them have a pelagic larval stage (Thorson, 1946; Young, 1990) with variable durations (Scheltema, 1986; Victor, 1986; Guizien et al., 2020). The four stages of their lifecycle are: Initiation of emigration, transport & movement, settlement and recruitment (figure I.1; Pineda et al., 2007). The persistence of a species is also highly dependent on interactions within the population.

A population is a group of individuals who are able to interact/reproduce with each other, although several different definitions are used (Waples & Gaggiotti, 2006). Through dispersal, species can move between habitats and create metapopulations (Levins, 1969; Hanski, 1991). Many different concepts and models for metapopulations have been developed throughout the years (Figure I.2). Of course, different species living in the same habitat can also interact with each other through predation, competition, parasitism, mutualism or commensalism (Lang & Benbow, 2013). This is called a community and dispersal between different communities forms metacommunities (Wilson, 1992).

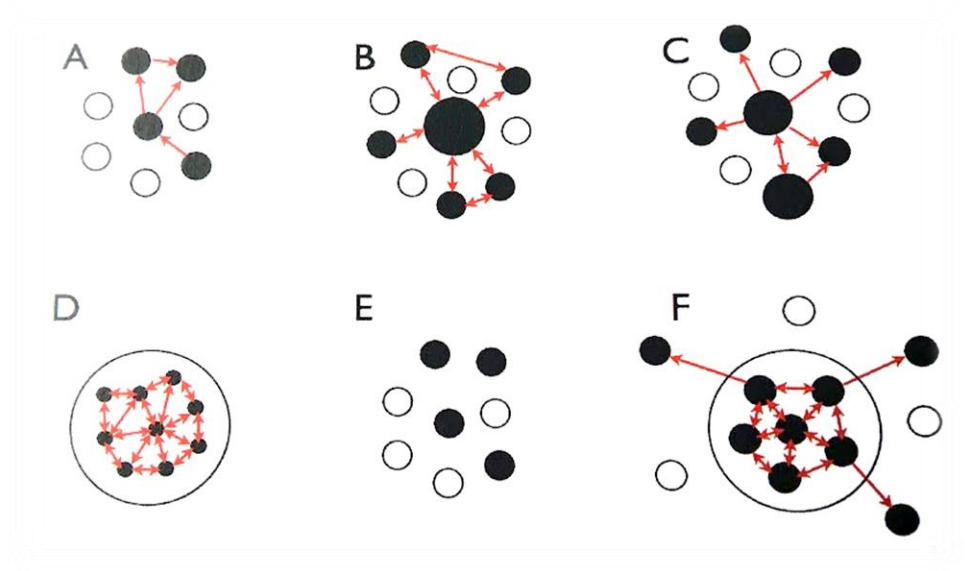

Figure I.2: Different models of metapopulations: A) Levins' model (1969), B) mainland-island model, C) source-sink model, D) fragmented population model, E) unstable fragmented population model, F) intermediate model. Red arrows depict dispersal. Taken from Moritz (2010), adapted from Harrison (1991).

Unfortunately, MPAs are often installed in places with a high biodiversity (Briton et al., 2018), without taking metapopulation or metacommunity functioning into consideration (Halpern & Warner, 2003). More often than not, the size of the reserve is a lot smaller than the spatial extent of the population (Allison et al., 1998; Palumbi, 2004; Gaines et al., 2010). One solution would be to enlarge the MPAs, but given the previously mentioned increase in people living at the coast,

this is an improbable scenario. Another option is to create a network of connected MPAs, as several studies have shown the benefits of this (Crowder et al., 2000; Neubert, 2003; Costello & Polasky, 2008). Unfortunately, single, isolated reserves are still the norm (Lester et al., 2009). In order for these isolated reserves to be beneficial to the protected species, there must be a self-persistent population with population growth (Hastings & Botsford, 2006). That way, there can be benefits through larval export, with the marine reserve becoming a source population (Crowder et al., 2000). Source populations have higher birth rates than death rates and higher emigration rates than immigration rates, contrary to sink populations (Pulliam, 1988; Crowder et al., 2000). However, these reserves must be sufficiently large in order to be self-sufficient (Botsford et al., 2001), which often is not the case (Gaines et al., 2010). Small, non-self-sufficient patches must be connected to other populations in order for the species to persist. This is why a network of reserves can help stabilise the system (Gaines et al., 2010). Moreover, networks can help the recolonisation of destroyed patches after a natural or manmade disaster (Allison et al., 2003; Hastings et al., 2006). Therefore, larval dispersal plays a decisive role in the persistence of a species.

This PhD seeks to understand the second stage of larval dispersal: Transport & movement, which is a processes heavily influenced by ocean currents. Ocean currents are regulated by a variety of factors. Not only bathymetry and salinity have an effect, but also atmospheric influences such as wind and temperature. When looking at the Mediterranean Sea's climate in particular, it has quite a specific climate due to its latitudinal position. The winters are wet and mild, due to the position of the westerly wind belt at this time. During summer, the weather is hot and dry for several months, as it is under the influence of subtropical high pressure systems (Harding et al., 2009).

The Mediterranean is a semi-enclosed sea which is connected to the Red Sea through the Suez canal, the Black Sea via the Sea of Marmara and the Atlantic ocean through the Strait of Gibraltar. The classical circulation features are depicted in figure I.3 (MERMEX group, 2011). The general circulation features of the Mediterranean have also been described by many other papers (e.g. Malanotte-Rizzoli & Bergamasco, 1991; Robinson & Golnaraghi, 1993; Millot, 1994; Roussenov et al., 1995; Pinardi & Masetti, 2000; Molcard et al., 2002). In shallow waters (0-200 m) there is an inflow of Atlantic water through the Strait of Gibraltar. In the eastern Mediterranean, it becomes the Levantine intermediate water (200-600 m). Through the Strait of Sicily, this warmer and saltier water can travel west again. Once there, the water can densify and turn into deep water through the constant force of cold and dry winds (MEDOC GROUP, 1969; Lascaratos, 1993; Theocharis et al., 1993; Marshall & Schott, 1999; Pinardi & Masetti, 2000; Mikolajczak, 2019). In the north-western Mediterranean, the Northern Current can be found (Millot, 1999; MERMEX group, 2011; Barrier et al., 2016; Mikolajczak, 2019). It runs past the continental shelf of the Gulf of Lion, which is the part of the Mediterranean Sea this PhD focusses on.

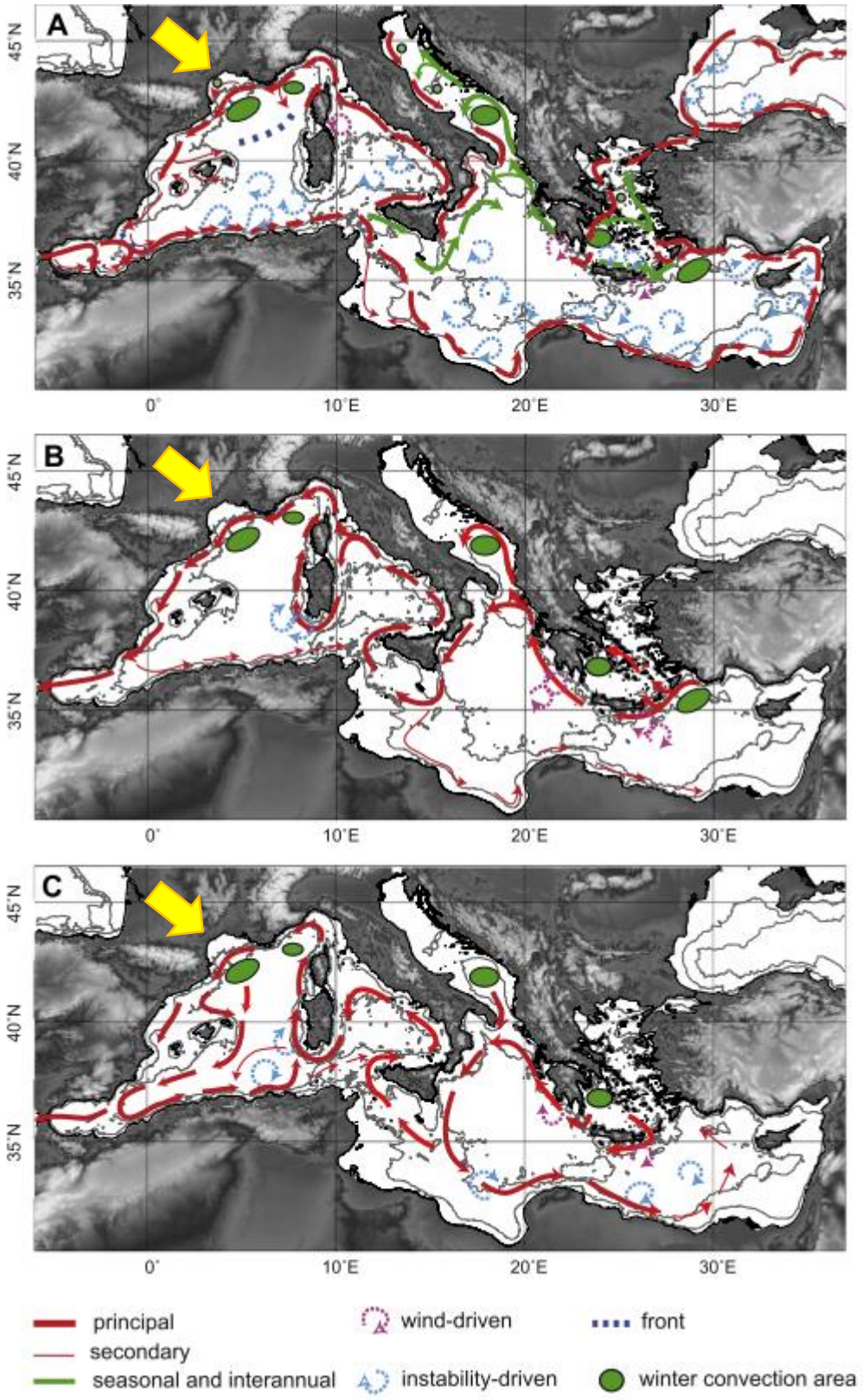

Figure I.3. (A) Circulation of surface water masses (taken from Mermex group, 2011; redrawn from Millot and Taupier-Letage (2005a). (B) Circulation of intermediate water masses, and (C) represents circulation of deep water masses. The thin lines represent the 1000-m and 2000-m isobaths). Yellow arrow shows Gulf of Lion.

The Gulf of Lion is often under the influence of continental winds blowing from the north and northwest (Mistral and Tramontane resp.). These winds are cold and dry, which causes the water to become colder and thus denser. This makes them sink to the bottom in a process called dense shelf water cascading. The canyons play a big role in guiding this dense water to deeper parts of the ocean (Herrmann et al., 2008; Puig et al., 2008; Ulses et al., 2008; Puig et al., 2013; Mikolajczak, 2019). Overall, the waves in the Gulf of Lion are quite small. However, extreme waves can occur (Guizien, 2009). Both the wind and the waves can dissipate the summer stratification in the Gulf of Lion, which is usually present during spring and autumn (Millot, 1990). Stratification can also be caused by rivers. The biggest river that flows into the Gulf of Lion is the Rhône River, which causes a large plume of fresh water and sediment (Estournel et al., 2001). The Gulf of Lion's coastal sediment consists of sand, silts, mud and some patches of rocky hard substrate (Aloïsi, 1973; Bourrin, 2007). Recently, several artificial reefs have been installed (Blouet et al., 2021), enlarging the amount of hard substrate. These patches of hard substrate could be used as stepping stones by sessile species with pelagic larval dispersal.

When anticipating the dispersal of living beings, it is important to take into account that the obtained results are only temporarily relevant. Namely, the population dynamics, spread and habitat are constantly changing due to natural or anthropogenic causes. For example, global warming is causing a geographical shift in suitable habitat for many species (Chen et al., 2011). To survive this, they can either move to more suitable habitat or evolve, both of these processes require dispersal (Berg et al., 2010; Bellard et al., 2012).

Although dispersal has been studied in situ through for example genetic techniques (Hedgecock et al., 2007) and tagging (e.g. Bailey, 1997), it is often modelled using biophysical models that

consist two factors: Biological and physical factors. The biological factors include mortality, growth, behaviour, pelagic larval duration (PLD), spawning period and spawn area. This PhD focusses mainly on the physical influences on modelled larval dispersal, namely ocean current flow.

The type of circulation model used varies according to the different scales and processes they aim to simulate, ranging from global ocean models to regional models. Current flow models, just like all models, are approximations of reality, meaning they are not perfect and have uncertainties. Since models are often used to aid in decision making (e.g. Beger et al., 2010; Kough et al., 2013; Andrello et al., 2015; Gallego et al., 2017; Bode et al., 2019), they need to be reliable. This is why it is important to validate the model's uncertainties. Many different techniques have been used to assess the hydrodynamic models' uncertainties: The simulations were compared to in situ measured hydrological parameters like salinity and temperature (e.g. Gustafsson et al., 1998; Reffray et al., 2004; André et al., 2005; Kara et al., 2006; Chelton et al., 2007; Pairaud et al., 2011; Renault et al., 2012; Marzocchi et al., 2015; Seyfried et al., 2017; Akhtar et al., 2018) or the simulations were compared to in situ measured hydrodynamical parameters like flow speed and direction (chapters 1 and 2, e.g. Petrenko et al., 2005; Halliwell et al., 2011; Ross et al., 2016). Other techniques are inter-model comparisons (between model comparisons; e.g. Delhez et al., 2004) or intra-model comparisons (within model comparisons; e.g. Ezer & Mellor, 2000; Seyfried et al., 2017; Ridenour et al., 2019).

In this PhD, the uncertainty of a hydrodynamical SYMPHONIE2015 simulation is quantified. It was developed in the Toulouse Aerology Laboratory (Laboratoire d'Aérologie Toulouse) (Marsaleix et al., 2008, 2009, 2012) and solves Navier Stokes equations to calculate the speed and direction of

the current at every grid point. In this PhD, the same grid is used as in Briton et al. (2018). The model uses the hydrostatic assumption and the Boussinesq approximation. The hydrostatic assumption states that the vertical movement of the water is smaller than the horizontal movement. The Boussinesq approximation assumes density variations can be neglected, except in the terms associated with buoyancy forcing. Of course, assumptions are not always met.

This is why the first chapter evaluates the model during and outside of assumption violation. This is done by comparing in situ hydrodynamical observations to modelled currents during and outside three types of events: Waves, wind and stratification. During waves, the hydrostatic assumption is violated. During strong wind events, the turbulent closure scheme might by inadequate. The turbulence closure scheme distributes the total flow energy between the turbulent energy resulting from all velocity fluctuations at the subgrid scale and the mean flow (Boussinesq, 1903; Prandtl, 1925). During stratification events, the Boussinesq approximation is not valid. By comparing the performance of the model during these events to the performance of the model outside of these events (reference period), the model's robustness to assumption violation is tested.

In the second chapter, the uncertainty of the Eulerian model is calculated at every instant, whereas in the first chapter, it was averaged over the duration of the event. However, the uncertainty of the model will affect the drift of the larvae at every step, which is why the instant error needs to be assessed as well. In the second chapter, spatiotemporal variations in the model's uncertainty were researched and linked to modelling and environmental characteristics. The SYMPHONIE2015 model also has a Lagrangian routine to study larval dispersal. In a Lagrangian model, the trajectory of each individual particle is calculated (Saidi et al., 2014).

Another aim of this PhD is to assess the validity of simulated dispersal and connectivity, which is what the third chapter does.

In the third chapter, the overall uncertainty found in the second chapter was added as a noise to the drift trajectories of a Lagrangian drift simulation. The particles were released from artificial reefs in the Gulf of Lion and their connectivity to other reefs (both artificial and natural) was calculated. This way, the effect of the model's uncertainty on the dispersal and connectivity of drifting larvae was assessed.

References

Akhtar, N., Brauch, J., & Ahrens, B. (2018). Climate modeling over the Mediterranean Sea: impact of resolution and ocean coupling. Climate Dynamics, 51(3), 933–948. https://doi.org/10.1007/s00382-017-3570-8

Allison, G. W., Gaines, S. D., Lubchenco, J., & Possingham, H. P. (2003). Ensuring persistence of marine reserves: Catastrophes require adopting an insurance factor. Ecological Applications, 13(1), 8–24.

Allison, G. W., Lubchenco, J., & Carr, M. H. (1998). Marine reserves are necessary but not sufficient for marine conservation. Ecological Applications, 8(1 SUPPL.), 79–92. https://doi.org/10.2307/2641365

Aloïsi, J.C., Got, H. and Monaco, A. (1973). Carte géologique du précontinent languedocien au 1/250000ième., International Institute for Aerial Survey and Earth Sciences (I.T.C.) (Eds.), Netherlands.

André, G., Garreau, P., Garnier, V., & Fraunié, P. (2005). Modelled variability of the sea surface circulation in the North-western Mediterranean Sea and in the Gulf of Lions. Ocean Dynamics, 55(3–4), 294–308. https://doi.org/10.1007/s10236-005-0013-6

Andrello, M., Jacobi, M. N., Manel, S., Thuiller, W., & Mouillot, D. (2015). Extending networks of protected areas to optimize connectivity and population growth rate. Ecography, 38(3), 273–282. https://doi.org/10.1111/ecog.00975

Bailey, K. M. (1997). Structural dynamics and ecology of flatfish populations. Journal of Sea Research, 37(3–4), 269–280. https://doi.org/10.1016/S1385-1101(97)00018-X

Barbier, E.B. (2017). Marine ecosystem services. Current Biology, 27(11), R507–R510. https://doi.org/10.1016/j.cub.2017.03.020

Barrier, N., Petrenko, A. A., & Ourmières, Y. (2016). Strong intrusions of the Northern Mediterranean Current on the eastern Gulf of Lion: insights from in-situ observations and high resolution numerical modelling. Ocean Dynamics, 66(3), 313–327. https://doi.org/10.1007/s10236-016-0921-7

Beger, M., Linke, S., Watts, M., Game, E., Treml, E., Ball, I., & Possingham, H. P. (2010). Incorporating asymmetric connectivity into spatial decision making for conservation. Conservation Letters, 3(5), 359–368. https://doi.org/10.1111/j.1755-263X.2010.00123.x

Bellard, C., Bertelsmeier, C., Leadley, P., Thuiller, W., & Courchamp, F. (2012). Impacts of climate change on the future of biodiversity. Ecology Letters, 15(4), 365–377. https://doi.org/10.1111/j.1461-0248.2011.01736.x.Impacts

Berg, M. P., Toby Kiers, E., Driessen, G., van der Heijden, M., Kooi, B. W., Kuenen, F., Liefting, M., Verhoef, H. A., & Ellers, J. (2010). Adapt or disperse: Understanding species persistence in a changing world. Global Change Biology, 16(2), 587–598. https://doi.org/10.1111/j.1365-2486.2009.02014.x

Blouet, S., Quittet, L., Agin, G., Thorin, S., Dalias, N., Marobin, D., Lenfant, P., Guizien, K., (2021). Database of the location and typology of artificial reefs in the Gulf of Lion (NW Mediterranean Sea).

Bode, M., Leis, J. M., Mason, L. B., Williamson, D. H., Harrison, H. B., Choukroun, S., & Jones, G. P. (2019). Successful validation of a larval dispersal model using genetic parentage data. PLoS Biology, 17(7), 1–13. https://doi.org/10.1371/journal.pbio.3000380

Boström, C., Jackson, E. L., & Simenstad, C. A. (2006). Seagrass landscapes and their effects on associated fauna: A review. Estuarine, Coastal and Shelf Science, 68(3–4), 383–403. https://doi.org/10.1016/j.ecss.2006.01.026

Botsford, L. W., Hastings, A., & Gaines, S. D. (2001). Dependence of sustainability on the configuration of marine reserves and larval dispersal distance. Ecology Letters, 4(2), 144-150.

Bourrin, F. (2007). Variability and fate of sedimentary inputs from coastal rivers : example of the Têt river - Roussillon coastal area system in the gulf of Lions. [Doctoral dissertation, Perpignan university]

Boussinesq, J. (1903). Théorie analytique de la chaleur mise en harmonie avec la thermodynamique et avec la théorie mécanique de la lumière: Refroidissement et échauffement par rayonnement, conductibilité des tiges, lames et masses cristallines, courants de convection, théorie. In Cours de physique mathématique de la Faculté des sciences (2nd ed.). Gauthiers-Vars.

Briton, F., Cortese, D., Duhaut, T., & Guizien, K. (2018). High-resolution modelling of ocean circulation can reveal retention spots important for biodiversity conservation. Aquatic Conservation: Marine and Freshwater Ecosystems, 28(4), 882–893. https://doi.org/10.1002/aqc.2901

Butler, S. J., Vickery, J. A., & Norris, K. (2007). Farmland biodiversity and the footprint of agriculture. Science, 315(5810), 381-384.

Chelton, D. B., Schlax, M. G., & Samelson, R. M. (2007). Summertime coupling between sea surface temperature and wind stress in the California current system. Journal of Physical Oceanography, 37(3), 495–517. https://doi.org/10.1175/JPO3025.1

Chen, I. C., Hill, J. K., Ohlemüller, R., Roy, D. B., & Thomas, C. D. (2011). Rapid range shifts of species associated with high levels of climate warming. Science, 333(6045), 1024–1026. https://doi.org/10.1126/science.1206432

Christensen, V., Aiken, K. A., & Villanueva, M. C. (2007). Threats to the ocean: On the role of ecosystem approaches to fisheries. Social Science Information, 46(1), 67–86. https://doi.org/10.1177/0539018407073656

Collie, J. S., Vic Adamowicz, W. L., Beck, M. W., Craig, B., Essington, T. E., Fluharty, D., Rice, J., & Sanchirico, J. N. (2013). Marine spatial planning in practice. Estuarine, Coastal and Shelf Science, 117, 1–11. https://doi.org/10.1016/j.ecss.2012.11.010

Costello, C., & Polasky, S. (2008). Optimal harvesting of stochastic spatial resources. Journal of Environmental Economics and Management, 56(1), 1–18. https://doi.org/10.1016/j.jeem.2008.03.001

Crowder, L. B., Lyman, S. J., Figueira, W. F., & Priddy, J. (2000). Source-sink population dynamics and the problem of siting marine reserves. Bulletin of Marine Science, 66(3), 799–820.

Cushman, S. A. (2006). Effects of habitat loss and fragmentation on amphibians: A review and prospectus. Biological Conservation, 128(2), 231–240. https://doi.org/10.1016/j.biocon.2005.09.031

Delhez, É. J. M., Damm, P., De Goede, E., De Kok, J. M., Dumas, F., Gerritsen, H., Jones, J. E., Ozer, J., Pohlmann, T., Rasch, P. S., Skogen, M., & Proctor, R. (2004). Variability of shelf-seas

hydrodynamic models: Lessons from the NOMADS2 Project. Journal of Marine Systems, 45(1–2), 39–53. https://doi.org/10.1016/j.jmarsys.2003.09.003

Douvere, F. (2008). The importance of marine spatial planning in advancing ecosystem-based sea use management. Marine Policy, 32(5), 762–771. https://doi.org/10.1016/j.marpol.2008.03.021

Estournel, C., Broche, P., Marsaleix, P., Devenon, J. L., Auclair, F., & Vehil, R. (2001). The Rhone River plume in unsteady conditions: Numerical and experimental results. Estuarine, Coastal and Shelf Science, 53(1), 25–38. https://doi.org/10.1006/ecss.2000.0685

Ezer, T., & Mellor, G. L. (2000). Sensitivity studies with the North Atlantic sigma coordinate Princeton Ocean Model. Dynamics of Atmospheres and Oceans, 32(3–4), 185–208. https://doi.org/10.1016/S0377-0265(00)00047-6

Fahrig, L. (2003). Effects of Habitat Fragmentation on Biodiversity. Annual Review of Ecology, Evolution, and Systematics, 34, 487–515. https://doi.org/10.1146/annurev.ecolsys.34.011802.132419

Foley, M. M., Halpern, B. S., Micheli, F., Armsby, M. H., Caldwell, M. R., Crain, C. M., Prahler, E., Rohr, N., Sivas, D., Beck, M. W., Carr, M. H., Crowder, L. B., Emmett Duffy, J., Hacker, S. D., McLeod, K. L., Palumbi, S. R., Peterson, C. H., Regan, H. M., Ruckelshaus, M. H., Sandifer, P. A., Steneck, R. S. (2010). Guiding ecological principles for marine spatial planning. Marine Policy, 34(5), 955–966. https://doi.org/10.1016/j.marpol.2010.02.001

Frazão Santos, C., Ehler, C. N., Agardy, T., Andrade, F., Orbach, M. K., & Crowder, L. B. (2018). Marine spatial planning. World Seas: An Environmental Evaluation Volume III: Ecological

Issues and Environmental Impacts, September, 571–592. https://doi.org/10.1016/B978-0-12-805052-1.00033-4

Gaines, S. D., White, C., Carr, M. H., & Palumbi, S. R. (2010). Designing marine reserve networks for both conservation and fisheries management. Proceedings of the National Academy of Sciences of the United States of America, 107(43), 18286–18293. https://doi.org/10.1073/pnas.0906473107

Gallego, A., Gibb, F. M., Tullet, D., & Wright, P. J. (2017). Bio-physical connectivity patterns of benthic marine species used in the designation of Scottish nature conservation marine protected areas. ICES Journal of Marine Science, 74(6), 1797–1811. https://doi.org/10.1093/icesjms/fsw174

Guizien, K. (2009). Spatial variability of wave conditions in the Gulf of Lions (NW Mediterranean Sea). Life and Environment, 59(3/4), 261–270. https://www.researchgate.net/publication/250306276

Guizien, K., Belharet, M., Marsaleix, P., & Guarini, J. M. (2012). Using larval dispersal simulations for marine protected area design: Application to the Gulf of Lions (northwest Mediterranean). Limnology and Oceanography, 57(4), 1099–1112. https://doi.org/10.4319/lo.2012.57.4.1099

Guizien, K., Viladrich, N., Martínez-Quintana, & Bramanti, L. (2020). Survive or swim: different relationships between migration potential and larval size in three sympatric Mediterranean octocorals. Scientific Reports, 10(1), 1–12. https://doi.org/10.1038/s41598-020-75099-1

Gustafsson, N., Nyberg, L., & Omstedt, A. (1998). Coupling of a high-resolution atmospheric model and an ocean model for the Baltic Sea. Monthly Weather Review, 126(11), 2822–2846. https://doi.org/10.1175/1520-0493(1998)126<2822:COAHRA>2.0.CO;2

Ha, G., & Williams, S. L. (2018). Eelgrass community dominated by native omnivores in Bodega Bay, California, USA. Bulletin of Marine Science, 94(4), 1333–1353. https://doi.org/10.5343/bms.2017.1091

Halliwell, J. R., Shay, L. K., Brewster, J. K., & Teague, W. J. (2011). Evaluation and sensitivity analysis of an ocean model response to Hurricane Ivan. Monthly Weather Review, 139(3), 921–945. https://doi.org/10.1175/2010MWR3104.1

Halpern, B. S., & Warner, R. R. (2003). Matching marine reserve design to reserve objectives. Proceedings of the Royal Society B: Biological Sciences, 270(1527), 1871–1878. https://doi.org/10.1098/rspb.2003.2405

Hanski, I. (1991). Single-species metapopulation dynamics: concepts, models and observations. Biological Journal of the Linnean Society, 42(1–2), 17–38. https://doi.org/10.1111/j.1095-8312.1991.tb00549.x

Harding, A., Palutikof, J., & Holt, T. (2009). The climate system. The physical geography of the Mediterranean, 69-88.

Harrison, S. (1991). Local extinction in a metapopulation context: an empirical evaluation. Biological Journal of the Linnean Society, 42(1–2), 73–88. https://doi.org/10.1111/j.1095-8312.1991.tb00552.x

Hastings, A., & Botsford, L. W. (2006). Persistence of spatial populations depends on returning home. Proceedings of the National Academy of Sciences of the United States of America, 103(15), 6067–6072. https://doi.org/10.1073/pnas.0506651103

Hector, A., & Bagchi, R. (2007). Biodiversity and ecosystem multifunctionality. Nature, 448(7150), 188-190.

Hedgecock, D., Barber, P. H., & Edmands, S. (2007). Genetic approaches to measuring connectivity. Oceanography, 20(SPL.ISS. 3), 70–79. https://doi.org/10.5670/oceanog.2007.30

Herrmann, M., Estournel, C., Déqué, M., Marsaleix, P., Sevault, F., & Somot, S. (2008). Dense water formation in the Gulf of Lions shelf: Impact of atmospheric interannual variability and climate change. Continental Shelf Research, 28(15), 2092–2112. https://doi.org/10.1016/j.csr.2008.03.003

Hoegh-Guldberg, O., Cai, R., Poloczanska, E.S., Brewer, P.G., Sundby, S., Hilmi, K., Fabry, V.J. & Jung, S. (2014). The Ocean. In: Climate Change 2014: Impacts, Adaptation, and Vulnerability. Part B: Regional Aspects. Contribution of Working Group II to the Fifth Assessment Report of the Intergovernmental Panel on Climate Change [Barros, V.R.,. Field, C.B, Dokken, D.J., Mastrandrea, M.D., Mach, K.J., Bilir, T.E., Chatterjee, M., Ebi, K.L., Estrada, Y.O., Genova, R.C., Girma, B., Kissel, E.S., Levy, A.N., MacCracken, S., Mastrandrea, P.R., and White, L.L. (eds.)]. Cambridge University Press pp. 1655-1731.

Kara, A. B., Barron, C. N., Martin, P. J., Smedstad, L. F., & Rhodes, R. C. (2006). Validation of interannual simulations from the 1/8° global Navy Coastal Ocean Model (NCOM). Ocean Modelling, 11(3–4), 376–398. https://doi.org/10.1016/j.ocemod.2005.01.003

Kough, A. S., Paris, C. B., & Butler IV, M. J. (2013). Larval Connectivity and the International Management of Fisheries. PLoS ONE, 8(6). https://doi.org/10.1371/journal.pone.0064970

Lang, J. M. & Benbow, M. E. (2013). Species Interactions and Competition. Nature Education Knowledge 4(4):8

Lascaratos, A. (1993). Estimation of deep and intermediate water mass formation rates in the Mediterranean Sea. Deep-Sea Research Part II, 40(6), 1327–1332. https://doi.org/10.1016/0967-0645(93)90072-U

Lester, S. E., Halpern, B. S., Grorud-Colvert, K., Lubchenco, J., Ruttenberg, B. I., Gaines, S. D., Airamé, S., & Warner, R. R. (2009). Biological effects within no-take marine reserves: A global synthesis. Marine Ecology Progress Series, 384, 33–46. https://doi.org/10.3354/meps08029

Levins, R. (1969). Some Demographic and Genetic Consequences of Environmental Heterogeneity for Biological Control. American Entomologist, 15(3), 237–240.

Loreau, M., Naeem, S., Inchausti, P., Bengtsson, J., Grime, J.P., Hector, A., Hooper, D.U., Huston, M.A., Raffaelli, D., Schmid, B., Tilman, D. & Wardle, D.A. (2001). Biodiversity and ecosystem functioning: current knowledge and future challenges. Science, 294(5543), 804-808. https://doi.org/10.1126/science.1064088

Lubchenco, J., & Grorud-Colvert, K. (2015). Making waves: The science and politics of ocean protection. Science, 350(6259), 382–383. https://doi.org/10.1126/science.aad5443

Lubchenco, J. & Sutley, N. (2010). Proposed U.S. policy for ocean, coast, and Great Lakes stewardship. Policy forum. Science 328, 1485-1486. http://dx.doi.org/10.1126/

Malanotte-Rizzoli, P., & Bergamasco, A. (1991). The wind and thermally driven circulation of the eastern Mediterranean Sea. Part II: The baroclinic case. Dynamics of Atmospheres and Oceans, 15(3-5), 355-419.

Marsaleix, P., Auclair, F., Duhaut, T., Estournel, C., Nguyen, C., & Ulses, C. (2012). Alternatives to the Robert-Asselin filter. Ocean Modelling, 41, 53–66. https://doi.org/10.1016/j.ocemod.2011.11.002

Marsaleix, P., Auclair, F., & Estournel, C. (2009). Low-order pressure gradient schemes in sigma coordinate models: The seamount test revisited. Ocean Modelling, 30(2–3), 169–177. https://doi.org/10.1016/j.ocemod.2009.06.011

Marsaleix, P., Auclair, F., Floor, J. W., Herrmann, M. J., Estournel, C., Pairaud, I., & Ulses, C. (2008). Energy conservation issues in sigma-coordinate free-surface ocean models. Ocean Modelling, 20(1), 61–89. https://doi.org/10.1016/j.ocemod.2007.07.005

Marshall, J., & Schott, F. (1999). Open-Ocean Convection: Observations, Theory, and Models. Reviews of Geophysics, 37(98), 1–64.

Marzocchi, A., Hirschi, J. J. M., Holliday, N. P., Cunningham, S. A., Blaker, A. T., & Coward, A. C. (2015). The North Atlantic subpolar circulation in an eddy-resolving global ocean model. Journal of Marine Systems, 142, 126–143. https://doi.org/10.1016/j.jmarsys.2014.10.007

MEDOC GROUP (1969). Observation of Formation of Deep Water in the Mediterranean Sea, 1969. Nature, 227(5262), 1037–1040. https://doi.org/10.1038/2271037a0

MERMEX group (2011) Marine ecosystems' responses to climatic and anthropogenic forcings in the Mediterranean. Progress in Oceanography, 91, 97-166

Mikolajczak, G. (2019). Dynamique de l'eau et des apports particulaires originaires du Rhône sur la marge continentale du Golfe du Lion. [Doctoral dissertation, Toulouse university]

Millot, C. (1990). The Gulf of Lions' hydrodynamics. Continental Shelf Research, 10(9–11), 885–894. https://doi.org/10.1016/0278-4343(90)90065-T

Millot, C. (1994). Models and data: a synergetic approach in the western Mediterranean Sea. In: Malanotte-Rizzoli, P., Robinson, A.R. (Eds.), Ocean Processes in Climate Dynamics: Global and Mediterranean Examples. Kluwer Academic Publishers, Dordrecht, The Netherlands, 1994, pp. 407–425

Millot, C. (1999). Circulation in the Western Mediterranean Sea. Journal of Marine Systems, 20(1–4), 423–442. https://doi.org/10.1016/S0924-7963(98)00078-5

Millot, C. & Taupier-Letage, I. (2005). Additional evidence of LIW entrainment across the Algerian Basin by mesoscale eddies and not by a permanent westward- flowing vein. Progress in Oceanography 66 (2-4), 231–250.

Molcard, A., Pinardi, N., Iskandarani, M., & Haidvogel, D. B. (2002). Wind driven general circulation of the Mediterranean Sea simulated with a spectral element ocean model. Dynamics of Atmospheres and Oceans, 35(2), 97–130. https://doi.org/10.1016/S0377-0265(01)00080-X

Moritz, C. (2010). Dynamics of marine metacommunities: theory and application to Annelid polychaetes in the Mediterranean Sea. [Doctoral dissertation, Toulouse university]

Neubert, M. G. (2003). Marine reserves and optimal harvesting. Ecology Letters, 6(9), 843-849.

Neumann, B., Vafeidis, A. T., Zimmermann, J., & Nicholls, R. J. (2015). Future coastal population growth and exposure to sea-level rise and coastal flooding - A global assessment. PLoS ONE, 10(3). https://doi.org/10.1371/journal.pone.0118571

O'Leary, B. C., Winther-Janson, M., Bainbridge, J. M., Aitken, J., Hawkins, J. P., & Roberts, C. M. (2016). Effective Coverage Targets for Ocean Protection. Conservation Letters, 9(6), 398–404. https://doi.org/10.1111/conl.12247

Pairaud, I., Gatti, J., Bensoussan, N., Verney, R., & Garreau, P. (2011). Hydrology and circulation in a coastal area off Marseille: Validation of a nested 3D model with observations. Journal of Marine Systems, 88(1), 20–33. https://doi.org/10.1016/j.jmarsys.2011.02.010

Palumbi, S. R. (2004). Marine reserves and Ocean neighborhoods: The spatial scale of marine populations and their management. Annual Review of Environment and Resources, 29, 31–68. https://doi.org/10.1146/annurev.energy.29.062403.102254

Palumbi, S. R., Sandifer, P. A., Allan, J. D., Beck, M. W., Fautin, D. G., Fogarty, M. J., Halpera, B. S., Incze, L. S., Leong, J. A., Norse, E., Stachowicz, J. J., & Wall, D. H. (2009). Managing for ocean biodiversity to sustain marine ecosystem services. Frontiers in Ecology and the Environment, 7(4), 204–211. https://doi.org/10.1890/070135

Petrenko, A., Leredde, Y., & Marsaleix, P. (2005). Circulation in a stratified and wind-forced Gulf of Lions, NW Mediterranean Sea: In situ and modeling data. Continental Shelf Research, 25(1), 7–27. https://doi.org/10.1016/j.csr.2004.09.004

Pinardi, N., & Masetti, E. (2000). Variability of the large scale general circulation of the Mediterranean Sea from observations and modelling: A review. Palaeogeography,

Palaeoclimatology, Palaeoecology, 158(3–4), 153–173. https://doi.org/10.1016/S0031-0182(00)00048-1

Pineda, J., Hare, J. A., & Sponaugle, S. (2007). Larval transport and dispersal in the coastal ocean and consequences for population connectivity. Oceanography, 20(SPL.ISS. 3), 22–39. https://doi.org/10.5670/oceanog.2007.27

Prandtl, L. (1925). 7. Bericht über Untersuchungen zur ausgebildeten Turbulenz. ZAMM-Journal of Applied Mathematics and Mechanics/Zeitschrift für Angewandte Mathematik und Mechanik, 5(2), 136-139.

Puig, P., Madron, X. D. de, Salat, J., Schroeder, K., Martín, J., Karageorgis, A. P., Palanques, A., Roullier, F., Lopez-Jurado, J. L., Emelianov, M., Moutin, T., & Houpert, L. (2013). Thick bottom nepheloid layers in the western Mediterranean generated by deep dense shelf water cascading. Progress in Oceanography, 111, 1–23. https://doi.org/10.1016/j.pocean.2012.10.003

Puig, P., Palanques, A., Orange, D. L., Lastras, G., & Canals, M. (2008). Dense shelf water cascades and sedimentary furrow formation in the Cap de Creus Canyon, northwestern Mediterranean Sea. Continental Shelf Research, 28(15), 2017–2030. https://doi.org/10.1016/j.csr.2008.05.002

Pulliam, H. R. (1988). Sources , Sinks , and Population Regulation. The American Naturalist, 132(5), 652–661.

Qiu, W., & Jones, P. J. S. (2013). The emerging policy landscape for marine spatial planning in Europe. Marine Policy, 39(1), 182–190. https://doi.org/10.1016/j.marpol.2012.10.010

Reffray, G., Fraunié, P., & Marsaleix, P. (2004). Secondary flows induced by wind forcing in the Rhône region of freshwater influence. Ocean Dynamics, 54(2), 179–196. https://doi.org/10.1007/s10236-003-0079-y

Renault, L., Chiggiato, J., Warner, J. C., Gomez, M., Vizoso, G., & Tintoré, J. (2012). Coupled atmosphere-ocean-wave simulations of a storm event over the Gulf of Lion and Balearic Sea. Journal of Geophysical Research: Oceans, 117(C9), n/a-n/a. https://doi.org/10.1029/2012JC007924

Ridenour, N. A., Hu, X., Jafarikhasragh, S., Landy, J. C., Lukovich, J. V., Stadnyk, T. A., Sydor, K., Myers, P. G., & Barber, D. G. (2019). Sensitivity of freshwater dynamics to ocean model resolution and river discharge forcing in the Hudson Bay Complex. Journal of Marine Systems, 196(May), 48–64. https://doi.org/10.1016/j.jmarsys.2019.04.002

Robinson, A.R., Golnaraghi, M. (1993). Circulation and dynamics of the eastern Mediterranean Sea; quasi-synoptic data-driven simulations. Part II. Deep Sea Research. Topical Studies of Oceanography 40 (6), 1207–1246.

Ross, N. O., Fraysse, M., Pinazo, C., Pairaud, I. (2016). Impact of an intrusion by the Northern Current on the biogeochemistry in the eastern Gulf of Lion, NW Mediterranean . Estuarine Coastal And Shelf Science , 170, 1-9. https://doi.org/10.1016/j.ecss.2015.12.022

Roussenov, V., Stanev, E., Artale, V., Pinardi, N. (1995). A seasonal model of the Mediterranean Sea general circulation. Journal of Geophysical Research 100, 13515–13538.

Saidi, M. S., Rismanian, M., Monjezi, M., Zendehbad, M., & Fatehiboroujeni, S. (2014). Comparison between Lagrangian and Eulerian approaches in predicting motion of micron-sized

particles in laminar flows. Atmospheric Environment, 89, 199–206. https://doi.org/10.1016/j.atmosenv.2014.01.069

Sala, E., & Knowlton, N. (2006). Global marine biodiversity trends. Annual Review of Environment and Resources, 31, 93–122. https://doi.org/10.1146/annurev.energy.31.020105.100235

Sala, E., Lubchenco, J., Grorud-Colvert, K., Novelli, C., Roberts, C., & Sumaila, U. R. (2018). Assessing real progress towards effective ocean protection. Marine Policy, 91(February 2018), 11–13. https://doi.org/10.1016/j.marpol.2018.02.004

Saunders, D., Hobbs, R., & Margules, C. (1991). Biological Consequences of Ecosystem Fragmentation: A Review. Conservation Biology, 5(1), 18–32. https://doi.org/10.1111/j.1523-1739.1991.tb00384.x

Scheltema, R. S. (1986). On dispersal and planktonic larvae of benthic invertebrates: an eclectic overview and summary of problems. Bulletin of marine science, 39(2), 290-322.

Seyfried, L., Marsaleix, P., Richard, E., & Estournel, C. (2017). Modelling deep-water formation in the north-west Mediterranean Sea with a new air-sea coupled model: Sensitivity to turbulent flux parameterizations. Ocean Science, 13(6), 1093–1112. https://doi.org/10.5194/os-13-1093-2017

Sindermann, C. J. (1995). Ocean pollution: effects on living resources and humans. CRC press.

Small, C., & Nicholls, R. J. (2003). A global analysis of human settlement in coastal zones. Journal of Coastal Research, 19(3), 584–599.

Swearer, S. E., Treml, E. A., & Shima, J. S. S. (2019). A Review of Biophysical Models of Marine Larval Dispersal. In Oceanography and Marine Biology (Vol. 57, pp. 325–356). CRC Press.

Theocharis, A., Georgopoulos, D., Lascaratos, A., & Nittis, K. (1993). Water masses and circulation in the central region of the Eastern Mediterranean. Deep-Sea Research II, 40(6), 1121–1142.

Thorson, G. (1946). Reproduction and larval development of Danish marine bottom invertebrates, with special reference to the planktonic larvae in the Sound (Oresund). Meddelelser fra Kommissionen For Danmarks Fiskeriog Havundersøkelser. Serie: Plankton IV: 1–523

Tilman, D. (2001). Functional Diversity. In Encyclopedia of Biodiversity volume 3, 109–120).

Treml, E. A., Ford, J. R., Black, K. P., & Swearer, S. E. (2015). Identifying the key biophysical drivers, connectivity outcomes, and metapopulation consequences of larval dispersal in the sea. Movement Ecology, 3(1), 1–16. https://doi.org/10.1186/s40462-015-0045-6

Ulses, C., Estournel, C., Bonnin, J., Durrieu de Madron, X., & Marsaleix, P. (2008). Impact of storms and dense water cascading on shelf-slope exchanges in the Gulf of Lion (NW Mediterranean). Journal of Geophysical Research, 113(C2), C02010. https://doi.org/10.1029/2006JC003795

Victor, B. C. (1986). Duration of the planktonic larval stage of one hundred species of Pacific and Atlantic wrasses (family Labridae). Marine Biology, 90(3), 317–326. https://doi.org/10.1007/BF00428555

Waples, R. S., & Gaggiotti, O. (2006). What is a population? An empirical evaluation of some genetic methods for identifying the number of gene pools and their degree of connectivity. Molecular Ecology, 15(6), 1419–1439. https://doi.org/10.1111/j.1365-294X.2006.02890.x

Wilcove, D. S., McLellan, C. H., & Dobson, A. P. (1986). Habitat fragmentation in the temperate zone. In Conservation Biology (The Science of Scarcity and Diversity), 237–256.

Wilson, D. S. (1992). Complex Interactions in Metacommunities , with Implications for Biodiversity and Higher Levels of Selection. Ecology, 73(6), 1984–2000.

Worm, B., Barbier, E.B., Beaumont, N., Duffy, E.J., Folke, C., Halpern, B.S., Jackson, J.B.C., Lotze, H.K., Micheli, F., Palumbi, S.R., Sala, E., Selko, K.A., Stachowicz, J.J., & Watson, R. (2006). Impacts of biodiversity loss on ocean ecosystem services. Science, 314(5800), 787–790. https://doi.org/10.1126/science.1137946

Yeager, L. A., Estrada, J., Holt, K., Keyser, S. R., & Oke, T. A. (2020). Are Habitat Fragmentation Effects Stronger in Marine Systems? A Review and Meta-analysis. Current Landscape Ecology Reports, 5(3), 58–67. https://doi.org/10.1007/s40823-020-00053-w

Young, C.M. (1990). Larval ecology of marine invertebrates: a sesquicentennial history. Ophelia 32(1–2), 1–48.

Chapter 1: Accuracy of high resolution coastal flow speed simulations during and outside wind, wave and stratification events (Gulf of Lion, NW Mediterranean).

Elise Vissenaekens[a,*], Katell Guizien[a], Xavier Durrieu de Madron[b], Ivane Pairaud[c], Yann Leredde[d], Pere Puig[e], François Bourrin[b]

[a]CNRS-Sorbonne Université, Laboratoire d'Ecogéochimie des Environnements Benthiques, LECOB, Observatoire Océanologique de Banyuls Sur Mer, 66650 Banyuls sur Mer, France

[b]CNRS-Université Perpignan Via Domitia,, Centre de Recherche et de Formation sur les Environnements Méditerranéens, CEFREM, 52 avenue Paul Alduy, 66860 Perpignan, France

[c]Institut Français de Recherche pour l'Exploitation de la Mer, IFREMER, Laboratoire Environnement Ressources Provence Azur Corse, BP 330, 83507, La Seyne sur Mer, France

[d]CNRS–Université Montpellier-2, Géosciences Montpellier, place Eugène-Bataillon, 34095 Montpellier cedex 5, France

[e] ICM-CSIC, Passeig Marítim de la Barceloneta 37–49, 08003 Barcelona, Spain

*Corresponding author: elise.vissenaekens@telenet.be

1.1 Abstract

Accurately predicting the flow speed is crucial for applications of coastal ocean circulation simulations such as sediment, larval or contaminant dispersal. This study aims to assess the accuracy of simulated flow speed in a coastal circulation model in comparison with field observations. Deviation between simulated and observed flow speed was assessed in four shallow, coastal locations and four deep, offshore locations in the Gulf of Lion (NW Mediterranean Sea) using six indicators (bias, relative bias, root mean square error, Hanna & Heinold index, correlation and scatter index). Model performance was compared between reference periods and during three categories of events (wind, waves and stratification) when model assumptions were expected to be violated. The model displayed a higher performance at shallow stations, probably due to grid refinement at these stations. Neither wind, wave nor stratification events seem to affect the model's performance. However, the scarcity of wave and stratification events advocates for extending the study. Moreover, there was a low correlation between modelled and observed flow speed, likely caused by short term time/space mismatches. Nonetheless, the simulation's uncertainties were similar or lower than those found in comparable studies that estimated uncertainty based on flow speed and not on hydrological variables.

Keywords:

Hydrodynamics, modelling, current observations, uncertainty quantification, Mediterranean, Gulf of Lion

Funding:

Elise Vissenaekens was funded by the French Ministère de la Recherche through a doctoral grant from Doctoral school Sciences de l'Environnement Ile de France of Sorbonne Université.

1.2 Introduction

Ocean currents are the key drivers of dissolved and particulate compound transport. At the global scale, the thermohaline circulation regulates the earth's climate (McCarthy et al., 2015; Clark et al., 2019). Wind-driven, upwelling currents arrange nutrient transport and mixing and regulate primary production at the regional scale (Falkowski et al., 1998). From regional to coastal scales, ocean currents play an imperative role in sediment transport and pollution diffusion (James, 2002; Dufois et al., 2008; Warner et al., 2008; Mansui et al., 2020). At all spatial scales, vessel navigation and marine population connectivity (from large mammal migration to benthic species' larval dispersal) are affected by ocean currents (Cowen et al., 2000; Briton et al., 2018; Putman, 2018; Mannarini & Carelli, 2019). These applications are currently simulated with Lagrangian dispersal models which, in contrast to Eulerian models, disregard mixing processes and only account for transport processes.

Unfortunately, ocean velocity observations, which are necessary to describe these transport processes, are often limited in either time or space. Satellite-mounted or land-based radars and Lagrangian drifters can measure the currents over a wide area, but only near the ocean's surface (Dohan et al., 2010; Mader et al., 2016). Some in situ current meters do provide flow measurement time series along vertical profiles (e.g. Acoustic Doppler Current Profiler, ADCP), but single point measurements are still common (Schroeder et al., 2013; Durrieu de Madron et al., 2019). ADCPs, which were previously only deployed at fixed moorings (Guizien et al., 1999) are now being mounted on the hulls of ships (Sextant, 1996) or on autonomous underwater vehicles (Dohan et al., 2010; Bourrin et al. 2015; Gentil et al. 2020). Ultimately, ocean current measuring devices are either deployed on the horizontal or on the vertical plane, which strongly

limits their applicability to study transport processes. For this reason, transport processes are mainly studied using current simulations.

Ocean circulation models vary according to the different scales and processes they aim to simulate. Tide models are bidimensional models, predicting sea surface elevation and depth-integrated horizontal flow transport, whose main application is navigation (Le Provost & Lyard, 2000). Global ocean circulation models (OGCMs) are three-dimensional models resolving the ocean dynamics at coarse spatial scales everywhere on earth (1/12°). They either rely on atmospheric coupling for climate predictions (Siedler et al., 2001; Chassignet et al., 2007; Somot et al., 2008) or on one-way atmospheric forcing for modelling ocean energy, fishery management and ship routing (Drevillon et al., 2018). Coastal circulation models are three-dimensional models forced by atmospheric models, most of the time without air-sea interaction, simulating the ocean flow dynamics and hydrology on a limited area. These models aim to simulate meso-scale to sub-meso-scale ocean processes, like eddies (Hu et al., 2009; Hu et al., 2011), dense water cascading (Ulses et al., 2008) and river plumes (Marsaleix et al., 1998). They use a horizontal spatial resolution which can be more precise than 100 m and a vertical resolution which can be more precise than 1 m (Estournel et al., 2003; Briton et al., 2018). Such models are considered capable of describing the processes controlling the transport of dissolved and/or particulate matter in a variety of applications (oil spills, land-sea transfer, ecosystem modelling, population connectivity). Regional circulation models have also been coupled to wave models for sediment transport and beach erosion prediction (Ulses et al., 2008; Dufois et al., 2008; Warner et al., 2008). Examples of these models are the Model for Applications at Regional Scale (MARS 3D; Lazure & Dumas, 2008; Dumas & Langlois, 2009), the COupled Hydrodynamical Ecological model for

REgioNal Shelf seas (COHERENS; Dulière et al., 2019), the Regional Ocean Modelling System (ROMS; Moore et al., 2011) and SYMPHONIE (Marsaleix et al., 2008, 2009a).

However, circulation simulations are subject to various sources of uncertainties, either linked to the model's implementation or to the model's intrinsic assumptions. The model's implementation includes the spatial and temporal resolution of the baroclinic modes and the precision of the forcing data (atmospheric forcing, river runoff, bathymetry and open boundary forcing). The sensitivity to the grid's spatial resolution (Kirtman et al., 2012; Kvile et al., 2018; Cai et al., 2020) and to atmospheric and open boundary forcing (Kourafalou et al., 2009) has been thoroughly illustrated.

In addition to uncertainties coming from model implementations, uncertainties can come from the model's intrinsic assumptions, such as hydrostaticity, the Boussinesq approximation, the turbulent closure scheme and air-sea interaction. The hydrostatic assumption that the vertical variation of the pressure is dominated by gravity acceleration (resulting in negligible vertical velocities compared to horizontal ones) is not met during wave events (Marshall et al., 1997; Zhang et al., 2014). The Boussinesq approximation (density variations can be neglected except in the terms associated with buoyancy forcing) may not be met in the upper stratified ocean, since water density can vary up to 5%, particularly in coastal areas under riverine influence. Therefore, the Boussinesq approximation can cause inaccuracies in the Eulerian simulated velocity of the same magnitude as the water density variation (McDougall et al., 2002). Turbulence closure is also a vital part of any flow dynamics model as it distributes the total flow energy between the turbulent energy resulting from all velocity fluctuations at the subgrid scale and the mean flow (Boussinesq, 1903; Prandtl, 1925). This splitting of the flow energy is essential to describe

transport and mixing processes in the numerical simulations. Turbulence closure is expected to play a more prominent role when energetic transfer happens at scales smaller than the spatio-temporal grid, such as during wind-wave (Fisher et al., 2018) or river flooding events (Reffray et al., 2004). This poses the question if modelled current velocities are valid during certain periods in the course of the simulation when the classical assumptions of ocean models are not met.

In the present study, we assessed the uncertainties of regional circulation speed simulations performed in the NW Mediterranean Sea with the hydrostatic Boussinesq model SYMPHONIE2015, implemented at one of the finest spatiotemporal resolution to date for bathymetry, atmospheric data and river data. The simulations, which were performed from 2010 to June 2013, are compared to hydrodynamic observations available in the area during this period. To estimate the effect of model assumption violation, one must first thoroughly understand the uncertainty of the model when the assumptions are valid, to have a base of comparison. To do so, the uncertainties in flow speed in different locations and periods were assessed when the model's assumptions were valid (reference period in absence of wind, waves and stratification) and when assumptions were violated (strong wind events, wave events and stratification events). Model performance was assessed by comparing six indicators calculated during each event type and observation station to their statistical distribution outside of these events.

1.3 Materials and methods

1.3.1 Study area

The Gulf of Lion is located in the north-western part of the Mediterranean Sea and has a wide continental shelf with a mean depth of 70 m (Aloisi et al., 1973). It is delineated by a steep shelf break, incised by a dense network of submarine canyons. Its coastal circulation mainly results from the interaction between the thermohaline Northern Current, which flows along the shelf break from the northeast to the southwest and the frequent continental winds blowing from the north and northwest (Mistral and Tramontane resp.), which induce winter convection (Millot, 1990). The south-easterly and southerly winds, which blow less frequently, occur mainly from autumn to spring and can cause large swells (Guizien, 2009).

The Gulf of Lion's coastal circulation is also influenced by the outflow of one of the largest Mediterranean rivers, the Rhône River, and a series of smaller rivers with typical Mediterranean flash-flooding regimes (Guizien et al., 2007; Ludwig et al., 2009). The size of the freshwater plume from the Rhône River depends on the atmospheric conditions, the strength of the river flow and the sea water circulation (Millot, 1990; Many et al., 2016; Many et al., 2018). The surface layers in the Gulf of Lion can stratify thermally between spring and autumn and are recurrently destabilised nearshore by coastal upwelling (Millot, 1990; Petrenko et al., 2005).

1.3.2 Water current observations

Horizontal velocity measurements were gathered from eight locations in the Gulf of Lion between 2010 and June 2013 (figure 1). Observations included the shallow coastal ADCP moorings BeSete, Mesurho, POEM, and SOLA and the deep moorings Planier, Cap de Creus (Creus), Lacaze-Duthiers

(LD) and Lion with one or more single point, acoustic Doppler current meters (SP-ADCMs). The time periods for which flow speed data was acquired are in table 1. Additional information on the observations, such as equipment specifications, can be found in the appendix table A.1.

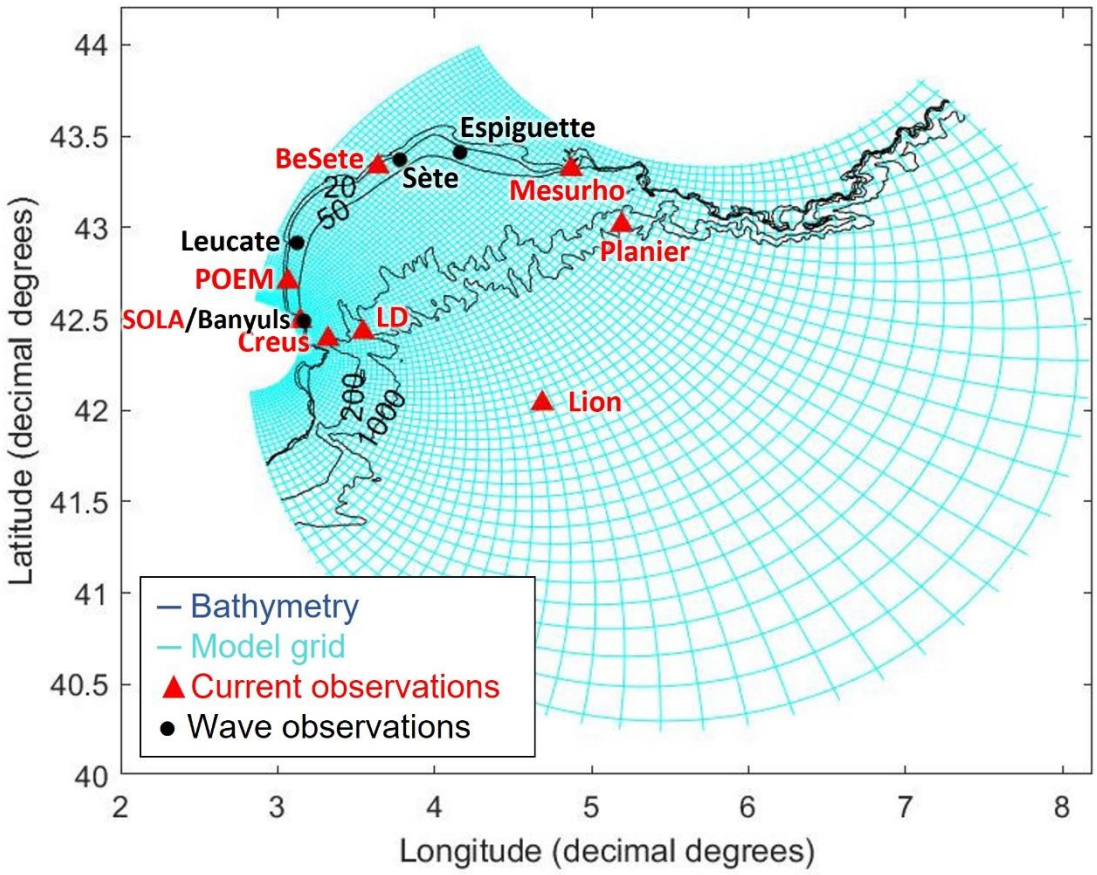

Figure 1: The Gulf of Lion. Main bathymetrical contours (20, 50, 200, 1000 m) of the Gulf of Lion including the dipolar model grid (680 × 710; with one blue line every 10 cells; North pole (44.2°N, 5.3°E); South pole (42.37°N, 2.82°E); grid point (170; 710) corresponding to (47°N, S°E); and the reference latitude for Mercator projection was 52° N). Further information on the grid can be found in Briton et al., (2018). The locations of the fixed moorings with current meters are in red: BeSete, Creus, LD (Lacaze-Duthiers), Lion, Mesurho (Measuring buoy at the mouth of the Rhône River), Planier, POEM (Observational Platform of the Mediterranean Environment/Plateforme d'Observation de l'Environnement Méditerranéen), SOLA (SOMLIT Observatory of the Arago Laboratory/SOMLIT Observatoire de Laboratoire Arago) and with the wave meters in black: Banyuls, Espiguette, Leucate, Sète.

Table 1: Timetable of acquired flow speed data per observation station. X indicates there was data available during this month.

Year	2010												2011												2012												2013					
Month	1	2	3	4	5	6	7	8	9	10	11	12	1	2	3	4	5	6	7	8	9	10	11	12	1	2	3	4	5	6	7	8	9	10	11	12	1	2	3	4	5	6
Creus	X	X	X	X	X	X					X	X	X	X	X	X	X	X					X	X	X	X	X	X	X													
LD	X	X	X	X	X	X	X	X	X	X	X	X	X	X	X	X	X	X	X	X	X	X	X	X	X	X	X	X	X	X	X	X	X	X								
Lion	X	X	X	X	X	X	X	X	X	X	X	X	X	X	X	X	X	X	X	X	X	X	X	X	X	X	X	X	X	X	X	X	X	X	X	X	X	X	X	X	X	X
Planier	X	X	X	X	X	X	X	X	X	X	X	X	X	X	X	X	X	X	X	X	X	X	X	X	X	X	X	X	X	X	X	X	X	X	X							
Mesurho											X	X	X	X	X							X	X	X	X	X	X	X		X	X			X	X	X	X	X				
POEM														X	X	X																										
SOLA	X	X	X																																							
BeSete			X	X	X	X	X	X	X	X	X	X	X																	X	X	X	X	X	X	X	X	X	X		

The observations were filtered to remove erroneous data. For the deep stations, if the velocity measurements presented abnormal values (defined as spikes of intensity with respect to the daily average greater than three times the standard deviation), they were replaced by the average of the previous and the following valid value. For the shallow stations, the upper three meters of the water column were not taken into account, to avoid measuring air speed amid sea surface fluctuations. Moreover, all observations were filtered over time to detect unrealistically fast changes in water speed. The maximum change in water speed tolerated was 30 cm/s over one hour. Another filter was applied on the vertical level and the maximum change in water speed tolerated was 10 cm/s over one meter.

1.3.3 Ocean circulation simulations

The Boussinesq hydrostatic ocean model SYMPHONIE (Marsaleix et al., 2008, 2009a, 2009b, 2012; SIROCCO, n.d.) was set up to perform regional ocean circulation simulations at a very high resolution in the Gulf of Lion (Briton et al., 2018). A bipolar, curvilinear, 680x710 horizontal grid was used to mesh the Gulf of Lion yielding a minimum resolution of 80 m at the coast and a maximum resolution of 2.7 km in the open ocean (figure 1, Bentsen et al., 1999). Generalized σ-coordinates were used for vertical meshing, with 29 vertical levels (Briton et al., 2018).

Simulations were carried out over the period 2010- June 2013 and were forced by sea-surface and open-sea boundary conditions from the regionally downscaled climate simulations NM12-FREE (6–7 km horizontal resolution; Hamon et al., 2016) and the discharge of twelve rivers (Agly, Argens, Aude, Baillaury, Ebro, Grand Rhône, Hérault, Orb, Petit Rhône, Tech, Têt, Var; Banque Hydro, n.d.). The model's internal and external timesteps were 25.48s and 1.59s, respectively. Since this model setup is largely similar to the one performed by Briton et al. (2018), more information on the model setup can be found in their paper.

The simulated velocities were extracted four times per hour on minute 0, 20, 30 and 40 to correspond with the times the observations were measured. On the horizontal, the simulated flow speeds were extracted at the grid point closest to the observations' location (less than 132 m apart). On the vertical, since the simulation's vertical levels did not match the observations' depths, the simulated speeds were interpolated at the same depth as the observations. If the actual water depth was larger than the water depth in the simulation (bathymetric discrepancy), the simulated speeds were interpolated at the depth with the same distance from the bottom as the observation.

In order to test the effect of model hypotheses violation on model performance, uncertainties were assessed separately in the presence of strong wind (turbulence closure or atmospheric forcing reliability), waves (hydrostatic hypothesis violation), in stratified conditions (Boussinesq approximation violation) and then compared to uncertainties during the reference period (low wind conditions, without waves and unstratified; figure 2).

1.3.4 Wind event selection

Wind stress data was extracted from the atmospheric simulations used to force the ocean circulation simulations at the closest atmospheric model grid point from the Planier and POEM stations (6-8 km horizontal resolution, figure 1). Wind events were defined as having a wind stress bigger than 0.4041 Pa (corresponding to ~50 km/hr with a drag coefficient of 0.00171 and an air density of 1.225 kg/m³ according to Smith, 1988, appendix equation B.1) during more than 12 hr at both stations.

Numerous wind events (37) were detected with wind stresses between 0.6903 Pa and 2.4939 Pa. The event duration frequency enabled grouping these events according to their duration into four different classes (12-24 hr, 24-36 hr, 36-48 hr, 48-60 hr, appendix figure A.1; figure 2).

1.3.5 Wave event selection

Wave events were selected from the observations during the years 2010 - June 2013 at four stations of the In Situ National Data Archiving Center of Waves (Centre d'Archivage National des Données de Houle In Situ, CANDHIS). The four stations (Banyuls, Espiguette, Leucate, Sète, figure 1) enabled the detection of different wave events propagating in different directions in relation to the Gulf of Lion's coastline (Guizien, 2009). Wave events were defined as having a peak period (Tp) larger than 8 s, a significant period (Tz) larger than 5 s and a zeroth order moment wave height (Hm0) larger than 3 m for more than 12 hours. These criteria resulted in the selection of five wave events with different durations (figure 2):

- 12 hr (max.: Tp = 12.5 s, Tz = 8.0 s, Hm0 = 4.2 m),
- 15 hr (max.: Tp = 11.8 s, Tz = 8.0 s, Hm0 = 5.5 m),

- 21 hr (max.: Tp = 10.5 s, Tz = 8.3 s, Hm0 = 4.1 m),
- 40 hr (max.: Tp = 10.5 s, Tz = 7.8 s, Hm0 = 5.6 m) and
- 86 hr (max.: Tp = 10.5 s, Tz = 7.7 s, Hm0 = 4.4 m).

1.3.6 Stratification events

Stratification events were defined as the period during which the maximum value of the Brunt-Väisälä frequency (N^2, appendix equation B.2) over the entire water column was larger than 0.005 s^{-2} for at least 12 hours (Gill, 1982). The Brunt-Väisälä frequency was computed using simulated salinity and temperature profiles at each station (Fofonoff & Millard, 1983) and was calculated between all available depth levels. The maximum over all these depth levels needed to be bigger than 0.005 s^{-2} for over 12 hours. This allowed us to assess the stratification events at each station separately, contrary to the wave and wind events, which were assumed to be active over the entire Gulf of Lion.

No stratification events were detected at the stations SOLA, LD, Lion and Planier, while at Mesurho, which was closest to the Rhône River, the water column was almost always stratified. Since at the aforementioned stations, there was either an absence of stratification events or of reference conditions, there could be no comparison between the two. Therefore, none of these stations were used for testing the effect of the Boussinesq hypothesis violation on the model's performance. The only stations that were considered were BeSete and POEM (shallow stations) with four stratification events at BeSete (figure 2):

- 81 hr (max. N^2=0.0084 s^{-2}),
- 143 hr (max. N^2=0.0124 s^{-2}),
- 194 hr (max. N^2= 0.0202 s^{-2}) and

- 249 hr (max. N^2=0.0150 s^{-2})

and three stratification events at POEM (figure 2):

- 74 hr (max. N^2=0.0953 s^{-2}),
- 79 hr (max. N^2=0.0310 s^{-2}) and
- 103 hr (max. N^2=0.0211 s^{-2})

1.3.7 Reference Period

The reference period was defined as an unstratified period (N^2 < 0.005 s^{-2}), without waves (Tp < 8 s, Tz < 5 s and Hm0 < 3 m) and with low wind conditions. Low wind conditions corresponded to a wind stress of less than 0.2586 Pa (wind velocity less than ~40 km/h; Smith, 1988) in the atmospheric simulations. The Mesurho station is the only station which is almost constantly stratified and therefore, it is still stratified during the reference period. There are no wind or wave events during the reference period at this station.

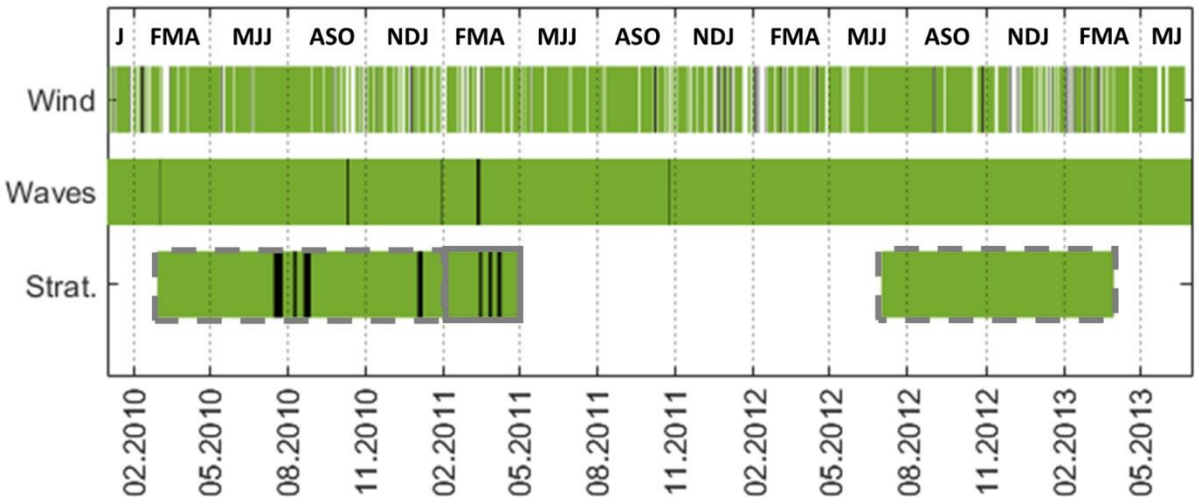

Figure 2: Timetable with selected events (Black). Green is the reference period. For the wind events, the white zones are zones with intermediate wind. For the stratification event, striped line (- -) is the reference period for Besete and the full line (-) is the reference period for POEM. In the white zone, no observational data was available for these two stations. The wind and wave events are applied over all stations. The dashed vertical lines (:) indicate the seasons and the letter triplets are the first letters of the months in that season.

1.3.8 Statistical indicators

The deviation between observed and simulated current speed was described by six time- and depth-averaged statistical indicators (mathematical definitions are given in appendix B, equations B.3-B.8). These indicators are integrated over the entire water column and the entire event duration. Only the current speed is taken into account. The bias is the difference between the simulated and observed mean (appendix equation B.3). It indicates systematic under- (negative value) or overestimation (positive value) of the simulated flow speed. The relative bias is the absolute bias normalized by the square root of the mean of the product of observed and simulated flow speed (appendix equation B.4). The root mean square error (RMSE) is the square root of the quadratic mean of differences between simulated and observed velocities (appendix equation B.5). It adds to the bias as a measure of random deviation and indicates the accuracy of simulations. The Hanna & Heinold index (HH; Hanna and Heinold, 1985) normalized the RMSE by the mean of the product of the observed and simulated flow speed (appendix equation B.6). It indicates the relative uncertainty from the mean flow and avoids biasing when the model underestimates the currents (negative bias, Mentaschi et al., 2013). The scatter index (SI) is the quadratic mean of the difference between simulated and observed flow speed fluctuations around the mean, normalized by the mean of the product of observed and simulated flow speed (appendix equation B.7). It indicates if the simulated flow speed fluctuates more or less around the mean than the observed flow speed. The correlation index is the product of simulated and observed fluctuations around the mean flow speed, normalized by the product of the standard deviation of the simulated and observed flow speed (appendix equation B.7). It varies between -1 and +1. Values close to 1 indicate co-variation (-1 indicates opposed variation) in the dynamics

of simulated and observed flow speed, while values close to 0 indicate the dynamics of simulated and observed flow are different.

1.3.9 Assessment of model performance during specific events

Each of the aforementioned indicators are expected to vary with the duration, the moment and the location on which they were calculated, either randomly or systematically. Systematic variation indicates a worse model performance. To test the model's performance under specific conditions (such as strong wind, waves or density stratification), the value of each of these indicators was computed during and in absence of such conditions over a same duration. To compare the events to the reference period, reference cumulative frequency distributions (CFDs) were established for each indicator and each station for the same duration as the event to test. To do so, a set of 200 time periods with an equal event duration as the event to test was randomly selected from the reference period and used to build this reference CFD for the indicator. These 200 time periods each had unique starting moments, but in the case of stations with a short observation period, partial overlap is possible. A bootstrap procedure was applied to produce 250 repeats of the reference CFD. Those repeats were used to estimate the most probable reference frequency distribution and a confidence interval around it. The most probable reference CFD for the indicator was thus defined by the 50% quartile (median) of the 250 repeats. For the wave and stratification events, the reference CFDs were calculated using the same duration as the event to

test. For the wind events, the reference CFD was calculated over a duration equal to the duration of the middle of the class this event belonged to (e.g. A wind event of 14 hr would belong to the class of 12-24hr and be compared to the CFD calculated over 18 hr, as this is the middle of the class). Please see appendix figure A.2 for more information.

Reference CFDs were used to determine the corresponding cumulative frequencies of each indicator/station/event by assessing the event's indicator value compared to the reference CFD (Figure 3, additional schematic in appendix figure A.2). Those corresponding cumulative frequencies were used to assess the model's performance, by comparing its value to a threshold value. For RMSE, HH and SI and relative bias, if the corresponding cumulative frequency of the indicator value during the event was larger than 75%, it was considered to have a higher uncertainty during the event. For the correlation, the uncertainty of the model is the lowest when the correlation is closer to 1. Therefore, there was a bad model performance when the corresponding cumulative frequency was less than 25%. For the bias, the uncertainty is the lowest when bias is close to zero. Therefore, bad model performance was determined by a corresponding cumulative frequency below 12.5% or above 87.5%.

The proportion of events during which the model performed worse than during the reference period was calculated per station, per indicator and per event type. Those proportions were averaged across all indicators and stations to assess whether there was a difference in model performance per station, indicator or event type.

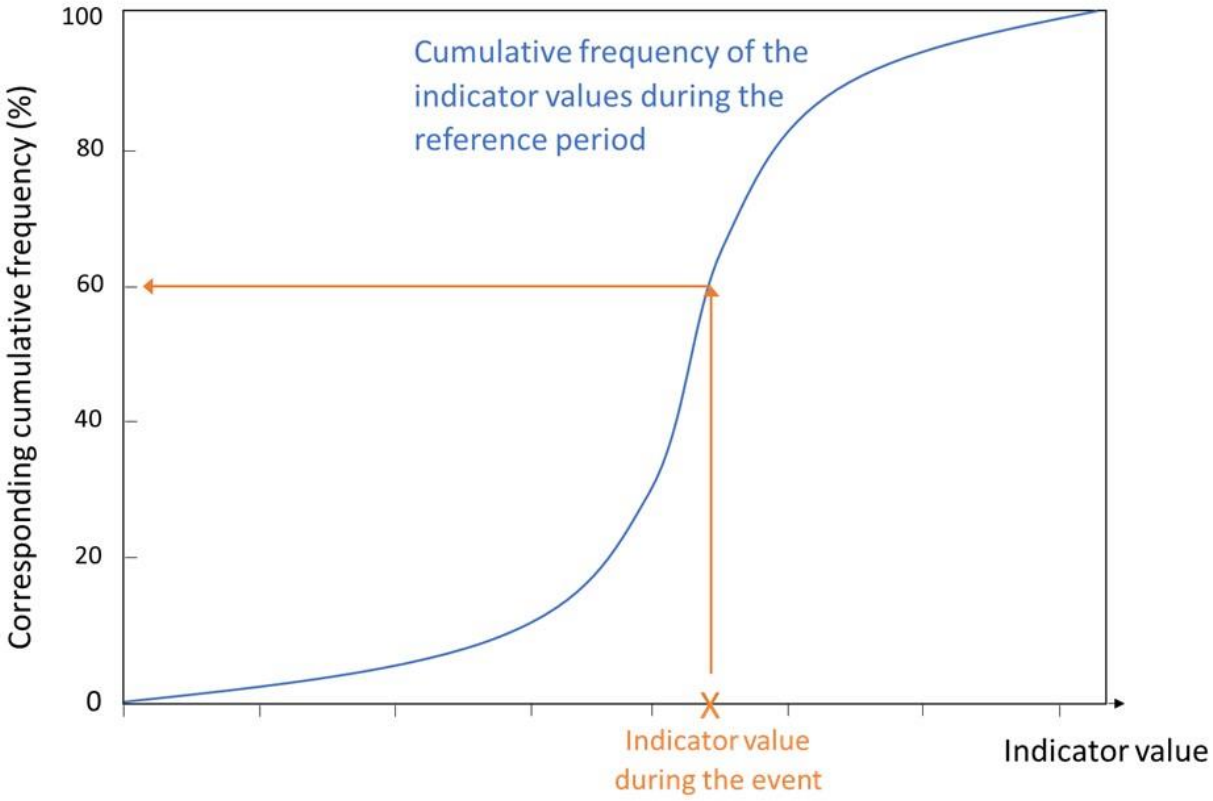

Figure 3: Corresponding cumulative frequency example. The corresponding cumulative frequency of the indicator value during the event can be read on the y-axis of when placing the indicator value calculated during the event (orange X) on the cumulative frequency of the indicator values during the reference period (blue line).

1.4 Results

The reference period CFD of each accuracy indicator in absence of wind, waves and stratification was computed for durations ranging from 12 hr to 249 hr at each station (Figure 4 for a duration of 42 hr). Overall, the simulated flow speed was underestimated at deep stations during the reference period, with bias median values calculated over 42 hr ranging from -3 cm/s at the Lion station to -1.2 cm/s in Creus and LD (figure 4A). At the shallow stations, the flow speed could be either underestimated (BeSete and SOLA, bias median values of -1.2 cm/s and -0.6 cm/s resp.) or overestimated (Mesurho and POEM, bias median values of 3.6 cm/s and 0.6 cm/s; figure 4A). In both groups of stations, bias values spread was large, with the first and third quartile being -5.4

and 0 cm/s at deep stations and -4.2 and 6.6 cm/s at shallow stations. After normalizing by the current magnitude in each station, the relative bias was smaller at the shallow stations (with median values ranging from 30% at BeSete and SOLA to 40% at POEM) than at the deep stations (with median values ranging from 35% at Creus to 85% at Lion, figure 4B). The relative scatter index (SI) was variable amongst the stations, with a similar variability among deep and shallow stations (median values ranging from 65% at Lion to 93% at Mesurho; figure 4C). As a result, the HH indicator was larger at deep stations (median values ranging from 95% at LD and Creus to 110% at Lion) than at shallow stations (median values ranging from 75% at SOLA and BeSete to 83% at Mesurho, figure 4E). Noteworthy, the median HH values were larger than 70% at all stations. In absolute values, the median RMSE was similar at deep and shallow stations, ranging from 2.5 cm/s at Planier and BeSete to 5.6 cm/s at Creus and 5.3 cm/s at Mesurho (Figure 4D). However, the RMSE's third quartile was less homogenous across deep stations, which had values ranging from 3.2 cm/s to 12.6 cm/s, than across shallow stations, with values ranging from 3.2 cm/s to 6.7 cm/s. Although the correlation was low at all stations, it was higher at the shallow stations than at the deep stations (figure 4F). Median (third quartile) values ranged from 0.03 (0.14, resp.) at BeSete to 0.13 (0.23, resp.) at POEM while median values in deep stations had a median of -0.01 for LD and Lion and were always less than 0.01.

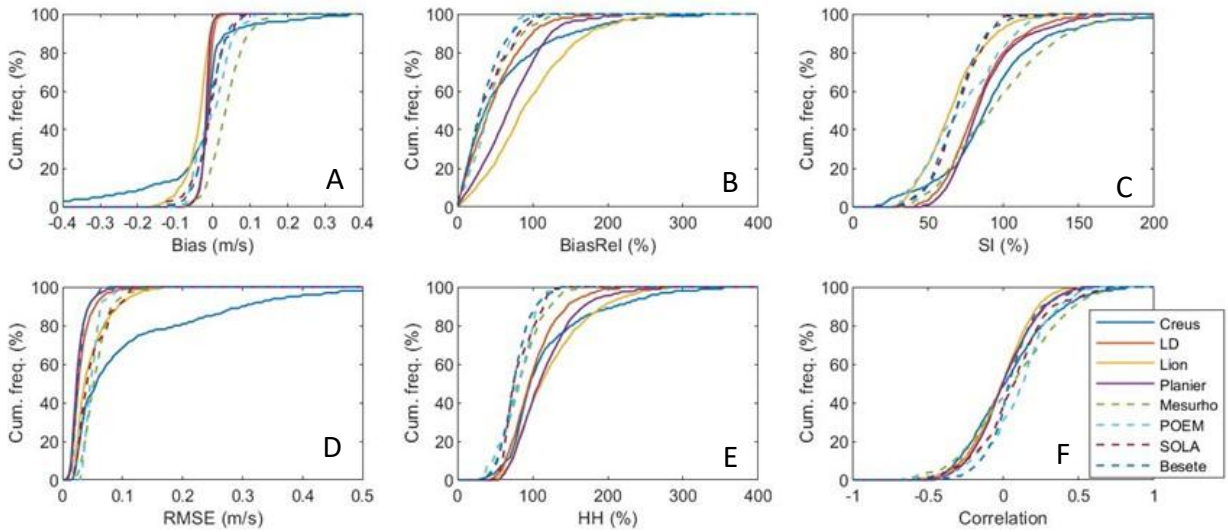

Figure 4: 42 hr reference period CFD. The indicators' cumulative frequencies integrated over 42 hr at all stations during the reference period. Shallow stations are depicted with a dashed line, deep stations with a solid line. A) Bias, B) Relative bias, C) SI, D) RMSE, E) HH, F) Correlation.

Although the CFDs of the accuracy indicators clustered according to the duration of the event, the deviation between the CFDs calculated over 12-24 hours and those calculated over more than 72 remained limited (Appendix figure A.3). The median correlation at BeSete varied between 0.02 and 0.06 and the maximum between 0.33 and 0.63 for integration duration increasing from 12-24 hr to 72< hr (Figure 5). While the correlation and bias (relative and absolute) improved with increasing integration duration, the SI worsened. With increasing integration duration, the deviation between the first and third quartile of the RMSE and HH indicators decreased and the median value increased (Figure 5 for the correlation at BeSete, appendix figure A.3 for the other indicators).

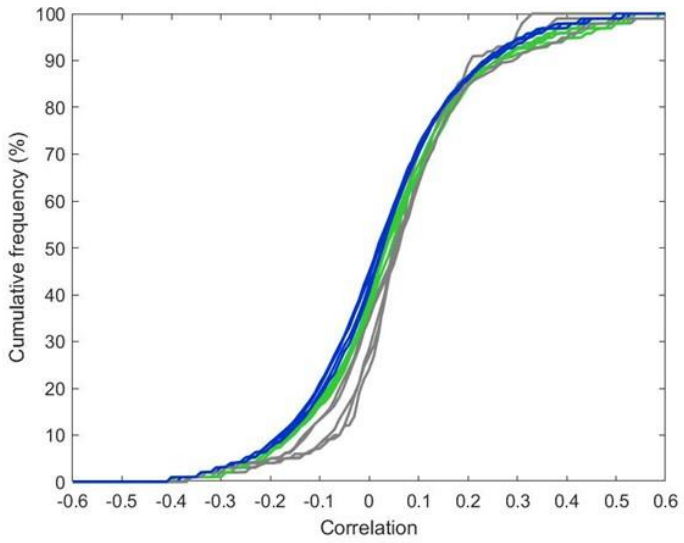

Figure 5: CFD of the correlation between modelled and observed flow speeds at BeSete during the reference period for different durations. Blue: 12-24hr, green: 24-72hr and grey: 72hr<.

Despite the fact that the CFDs of the accuracy indicators calculated during the reference period varied with the event duration, the corresponding cumulative frequencies of the correlation indicator calculated during wind, wave or stratification events were not tied to the duration of the events, regardless of the station (Figure 6 for wind events).

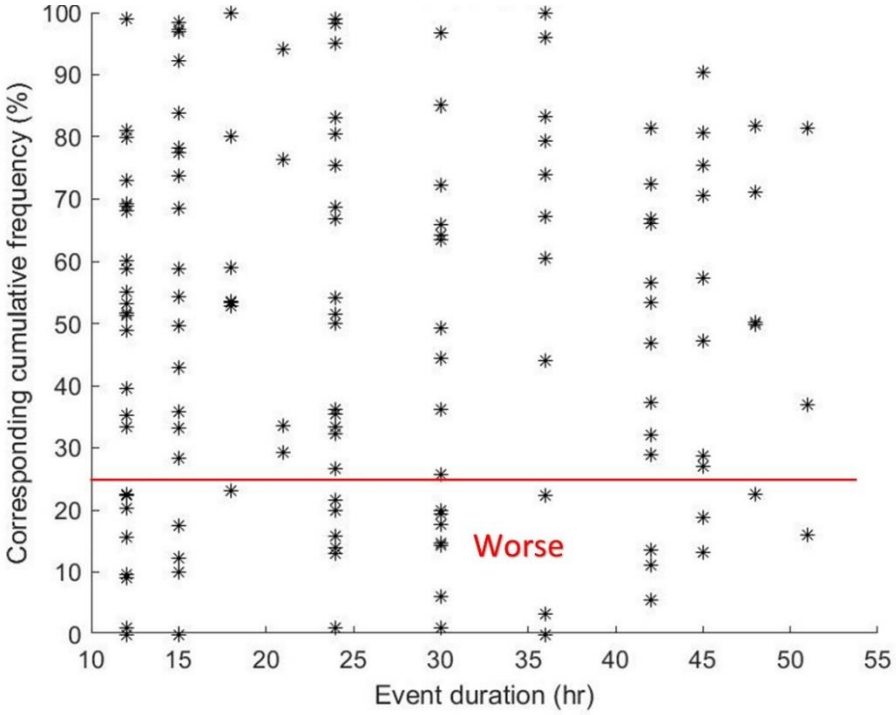

Figure 6: Corresponding cumulative frequency of the wind's correlation. Scatter plot of the wind event duration in relation to the corresponding cumulative frequency of the correlation between modelled and observed current speed. Events with a corresponding cumulative frequency below 25% are considered worse during the event than during the reference period.

Overall, the proportion of events where the model performed worse during the events than during the reference period was low no matter the event type. The average ratio worse ranged

from 25% for the wind events to 35% for the wave events (table 2). For the stratification events, which were only studied at BeSete and POEM, the model performed worse during the events than during the reference period for 25% and 33% of the events on average, respectively. However, the assessment of the model's performance varied greatly depending on the indicator, with the HH indicating a 13% ratio worse and the RMSE showing a 45% ratio worse in the wind events for instance (table 2).

Table 2: The ratio of events worse during the event than during the reference period per indicator, per station and per event type.

Event type	Wind								Waves								Stratification								
Indicator \ Station	RMSE	Bias	HH	SI	Relative bias	Correlation	Mean/Stat./ Type	Nr. of events	RMSE	Bias	HH	SI	Relative bias	Correlation	Mean/Stat./ Type	Nr. of events	RMSE	Bias	HH	SI	Relative bias	Correlation	Mean/Stat./ Type	Nr. of events	Mean/ station
Creus	50	50	28	33	28	33	37	18	67	67	0	0	0	0	22	3									30
LD	56	41	30	33	22	22	34	27	40	40	20	20	20	40	30	5									32
Lion	58	28	19	25	17	27	29	36	40	40	20	0	20	60	30	5									29
Planier	25	42	17	21	24	25	26	24	20	60	20	40	20	40	33	5									30
Mesurho	59	32	9	27	21	36	31	22	67	33	0	0	33	33	28	3									29
POEM	50	0	0	50	0	0	17	2	100	100	100	0	100	0	67	1	33	33	33	67	0	33	33	3	39
SOLA	33	0	0	33	0	0	11	3	0	0	0	100	100	0	33	1									22
BeSete	25	42	0	0	23	17	18	12	100	0	0	0	0	100	33	1	25	50	25	25	0	25	25	4	25
Mean/Ind./type	45	29	13	28	17	20	25		54	43	20	20	37	34	35		29	42	29	46	0	29	29		
Unit	%	%	%	%	%	%	%		%	%	%	%	%	%	%		%	%	%	%	%	%	%		%

When comparing the model's performance across event types and stations, it was worse during wave events than during wind events at shallow stations (except at the Mesurho station in front of the Rhone River mouth), while no trend could be observed at deep stations (figure 7A). During the wave events, the model performed similarly across all stations, with all stations indicating the model was worse than during the reference period less than 33% of the time on average, except at the POEM station, where the ratio worse reached 67% (Table 2). During the wind events, the model performed slightly better at the shallow stations (ratio worse ranging from 11% to 31%) than at the deep stations (ratio worse ranging from 26% to 37%, Table 2). For both event types, absolute indicators (RMSE and bias) displayed worse model performance than relative indicators (Figure 7B). All indicators except SI displayed worse model performance during wave events than during wind events (Figure 7B).

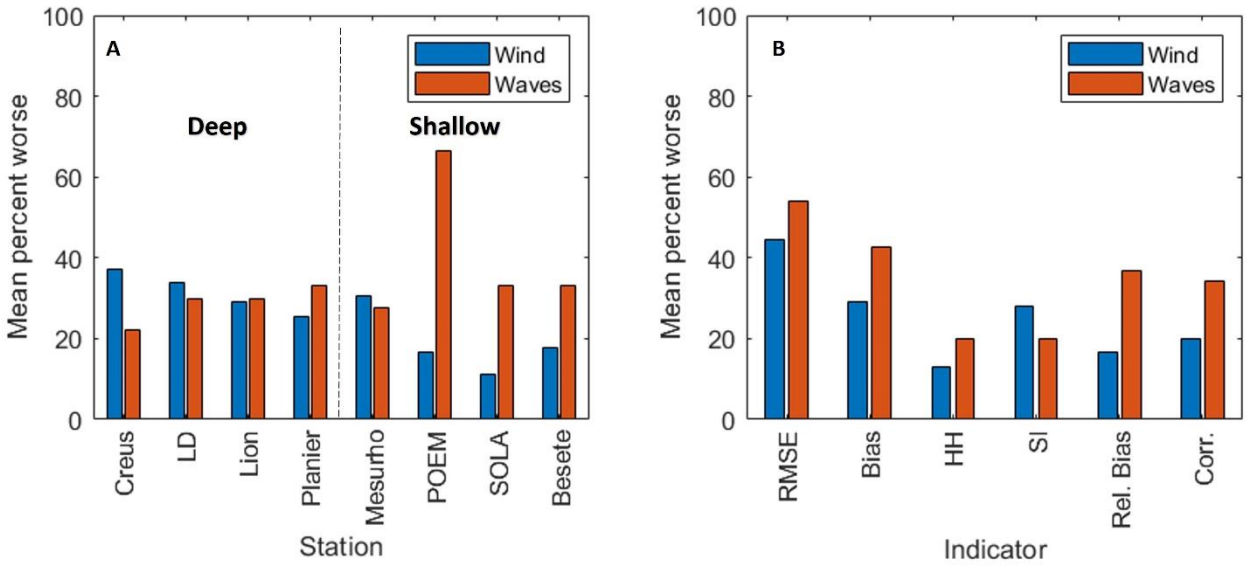

Figure 7: Mean percent worse per station and indicator for wind and wave events. Histograms of the mean percent of wind/wave events worse during the events than during the reference period. A) Per station, B) Per indicator.

1.5 Discussion

The present study quantified various indicators to describe the deviation between observed and simulated flow speed across shallow and deep stations within a highly dynamic region, during and outside short term events of three types (wind, waves, stratification).

The assessment of ocean model accuracy has largely been implemented by comparing simulated and observed hydrological variables (temperature and salinity; e.g. Gustafsson et al., 1998; Reffray et al., 2004; André et al., 2005; Kara et al., 2006; Chelton et al., 2007; Pairaud et al., 2011; Renault et al., 2012; Marzocchi et al., 2015; Seyfried et al., 2017; Akhtar et al., 2018) as their dynamics integrates transport (velocity) and mixing (turbulent kinetic energy) in ocean circulation models. However, hydrological variables are little informative about transport and mixing when well-mixed conditions prevail, which is often the case in coastal areas (Gill, 1982; Holt et al., 2009). The ability of coastal circulation models to simulate flow speed and not only hydrological parameters has been shown in short-term and/or local studies (Petrenko et al., 2005; Halliwell et al., 2011; Ross et al., 2016). The present study compliments these model assessments, whilst exceeding them in space and time. Using data from multiple stations, particularly shallow versus deep ones, enabled us to test the model's performance under a variety of coastal processes, such as fresh water mixing in the Rhône River prodelta (Estournel et al., 2001) where the Mesurho stations is located, wind driven Eckman flow at SOLA/BeSete/POEM (Davies et al., 1998; Lapouyade & Durrieu de Madron, 2001; Schaeffer et al., 2011; Estournel et al., 2016) and dense water cascading at Creus/LD/Planier (Ulses et al., 2008; Estournel et al., 2016). Using data spanning multiple years, particularly during summer (stratified) and winter (well-mixed), enabled us to test the model's performance under a variety of climatological forcings, such as swell flows

at SOLA/BeSete/POEM (Mikolajczak et al., 2020), stratified flows at Creus/LD/Planier/Mesurho (Petrenko et al., 2005) and wind dynamics at all stations (Molcard et al., 2002).

Contrary to expectations, the indicators did not display a worse model performance during wind, wave or stratification events, when model assumptions were expected to be violated, than outside those events. The absolute indicators (RMSE and bias) showed that the model was worse during the events more often than the relative indicators, probably because during those events, the currents are generally stronger than during the reference period. During wind events, coastal circulation simulations in the Gulf of Lion have been shown to dramatically change with the wind's spatial gradient (Estournel et al., 2003). Hence, an adequate spatial resolution of the wind field is essential to improve ocean circulation model performance. The present study ocean circulation simulations were forced by atmospheric field outputs from downscaled coupled air-sea simulations at the finest resolution available for the area at the time of the simulations (1/12°, NMfree12, Hamon et al., 2016). This is not generally the case, as some ocean models reported discrepancies between observed and modelled near-surface meteorological parameters during strong wind events (Rainaud et al., 2016). One way to improve the simulations' accuracy during strong wind events is to use the bidirectional atmospheric coupling technique (Gustafsson et al., 1998; Chelton et al., 2007; Schaeffer et al., 2011; Akhtar et al., 2018). Two-ways air-sea coupling performed better than one-way atmospheric forcing during autumn storms, when the sea surface cools rapidly (Seyfried et al., 2017). However, Renault et al. (2012) found little differences between the coupled and uncoupled atmosphere-ocean simulations in the Gulf of Lion area when comparing observed and modelled wind speed intensity and sea surface temperature.

Similarly, the model's performance was not systematically worse during wave events, although it was slightly worse during wave than during wind events. Therefore, incorporating the effects of waves on the coastal circulation simulations should be considered. When comparing a hydrostatic, quasi-hydrostatic and nonhydrostatic model, Marshall et al. (1997) suggested the quasi-hydrostatic and nonhydrostatic models are preferred for small scale phenomena, but found no difference between the three models at large scales with coarse resolution (1° horizontal resolution). In the Gulf of Lion, Michaud et al. (2012) showed that a fully coupled current-wave model would improve flow speed simulations in the surf zone (0-15 m water depth). However, outside the surf zone, deviations between observed and simulated flow speeds at POEM and Mesurho (same as in the present study) were similar regardless of wave forcing.

Another model assumption which could affect the model's performance is the Boussinesq approximation, which is violated during highly stratified conditions. During summer, incorrect representation of the stratification in the Gulf of Lion led to a misplacement of the NC in the simulations compared to the field observations (Petrenko et al., 2005). In the modelled salinity and temperature, a summer stratification period is clearly visible. However, the stratification index was set at a limit where both thermal and fresh water stratification was present. Thus, the stratification events at POEM and Besete were mainly due to freshwater input and none corresponded to a worse model performance. These are better results than in the study of Yang & Khangaonkar (2009), who found a large bias (4-15cm/s) and RMSE (6-18cm/s) during salinity stratification over a two week period when comparing measured and simulated flow speed in an estuary in the USA using the hydrodynamic FVCOM model with an unstructured grid (horizontal resolution 15-400 m).

In the Gulf of Lion, Estournel et al. (2001) qualitatively compared simulations of the Rhône plume to radar observations and showed that the SYMPHONIE model can reproduce the spatial variation of the current in front of the river mouth outside of strong wind events. In the present study however, the indicators showed that the deviations between simulation and observation were larger at the continuously stratified Mesurho station, than at the other shallow stations during the reference period. Of course, the Mesurho station is the only station that still has stratification during the reference period. Moreover, it is possible there is a higher horizontal heterogeneity at this station, since it is located right at the Rhône river mouth. Therefore, if the model doesn't reproduce the currents at exactly the right place, the error could be higher.

Despite the model not performing worse in case of wave and wind events than during the reference period, this is no guarantee that the model performs well overall. After all, it is possible the model also performs poorly during the reference period. However, our SYMPHONIE model configuration still performs equally well or even better than other models when performing similar studies. In the present study, the model's uncertainty during the reference period was bigger than the measuring device's accuracy. This is generally the case among the few studies that assess model performance quantitatively, since ADCPs are usually configured to provide velocity measurements with an error less than 1 cm/s (RDI, 2007).

For example, while comparing Glazur60 simulations (horizontal resolution of 1/64° hence 1.3 to 1.7 km) to the data of a fixed ADCP mooring, Barrier et al. (2016) found a bias between simulations and observations of 3.5 cm/s at 90 m and 7 cm/s at 20 m depth over an 11 month integration period. Similarly, while evaluating the effect of boundary conditions on simulations using the SoFLA-HYCOM model configuration (1/25° hence 3.5 to 4 km horizontal resolution) at shallow

stations around the Strait of Florida, the mean bias and the RMSE calculated between simulations and observations over a one year period ranged from -3.5 cm/s to 8.2 cm/s for the bias and from 5 to 13 cm/s for the RMSE, depending on the model's configuration and the station (Kourafalou et al., 2009). Also, Mikolajczak (2019) compared simulations obtained with another SYMPHONIE configuration than the one in this study (horizontal resolution ranging from 300 m to 7 km) to the same dataset as in the present study over a two month period (which included several wave events). The bias was 4 cm/s at the Mesurho station and -4 cm/s at the POEM station whilst the RMSEs were 10 cm/s and 8 cm/s, respectively. Despite flow speed simulations not being as precise as ADCP measurements, it is remarkable that the present study's bias and RMSE values were smaller than the values reported in all the aforementioned studies.

A common feature of the aforementioned studies is that they evaluated model performance over longer periods than the present study (weeks versus days), and thus included specific events such as strong wind (Kourafalou et al., 2009) or wave events (Mikolajczak, 2019) when the model's performance was expected to be at its worst. However, the present study showed this is not necessarily the case. Moreover, over long integration durations such as in the aforementioned studies, the relative importance of these short term events is likely to be negligible, which explains their high correlation values between modelled and observed current speeds. After all, the integration duration over which the indicator is calculated can alter model performance assessment as the systematic bias and the RMSE are more robust with increasing integration duration (Lopuhaä et al., 2005). Despite the present study's choice to restrict the integration duration to match the events' durations, the RMSE and bias estimates were similar to values calculated over two months (Mikolajczak, 2019). The correlation indicator was the only indicator

which improved with integration duration. The low correlation between simulated and observed flow speed calculated over short integration periods (less than a few days) at all stations indicated that the simulation failed to reproduce the short term flow dynamics. However, overall transport was fairly well simulated, as indicated by the bias. This limitation raises the question of how short term (days) velocity dynamics' inaccuracies (days) alter particle tracking simulations (used in e.g. larval dispersal studies like Briton et al., 2018).

One possible cause for model inaccuracy is resolution. The model performed better at shallow stations than at deep ones outside and during wind events, while the nearshore area is expected to experience a wider range of temporal frequencies in the current energy spectrum. Particularly short frequency ones, due to flow energy dissipation in the coastal boundary layer. In this study, the better model performance at the shallow stations could be due to the refinement of the horizontal spatial resolution, thanks to the adaptive resolution of the curvilinear grid. This could explain the improved bias and RMSE in the present study compared to the one of Mikolajczak (2019) at the POEM station, since the horizontal resolution in the two simulations was different (80 m vs. 300 m horizontal resolutions, resp.). Unfortunately, due to the low number of papers comparing simulations with flow speed observations, the added value of a finer horizontal resolution for flow speed simulations is difficult to assess. However, many do compare different model configurations to other types of observations (Thoppil et al., 2011; Kirtman et al., 2012; Putman & He, 2013; Ringler et al., 2013; Akhtar et al., 2018; Kvile et al., 2018; Ridenour et al., 2019). Ringler et al. (2013) compared their global ocean simulations with varying spatial resolution (7.5km-15km) to sea surface height observations and concluded the configuration with the finest resolution was the best one.

In conclusion, a validation of simulated current speeds was performed to quantify the uncertainty of the model during wind, wave and stratification events. The simulated current speed was compared to in situ flow speed observations from fixed moorings. Multiple indicators were calculated to evaluate the performance of the model. In absence of wind, wave or stratification events, the model performed better at shallow stations than at deep stations. Absolute indicators such as bias and RMSE displayed higher model uncertainty than relative indicators. Overall, the model did not perform notably worse during events than outside of events. However, the model's performance was lower during wave events than during wind events at shallow stations.

1.6 Acknowledgments

Some current observations were obtained within the framework of the French national observation services MOOSE (https://www.moose-network.fr/) and COAST-HF (https://coast-hf.fr/). Wave data were provided by the Centre d'études et d'expertise sur les risques, l'environnement, la mobilité et l'aménagement, the Direction Régionale de l'environnement de l'aménagement et du logement of the Occitanie region and the Observatoire Océanologique de Banyuls (https://candhis.cerema.fr/).

1.7 References

Akhtar, N., Brauch, J., & Ahrens, B. (2018). Climate modeling over the Mediterranean Sea: impact of resolution and ocean coupling. Climate Dynamics, 51(3), 933–948. https://doi.org/10.1007/s00382-017-3570-8

Aloisi, J. C., Got, H., & Monaco, A. (1973). Carte géologique du précontinent languedocien au 1/250000ième. International Institute for Aerial Survey and Earth Sciences, Netherlands.

André, G., Garreau, P., Garnier, V., & Fraunié, P. (2005). Modelled variability of the sea surface circulation in the North-western Mediterranean Sea and in the Gulf of Lions. Ocean Dynamics, 55(3–4), 294–308. https://doi.org/10.1007/s10236-005-0013-6

Banque hydro (n.d.). http://www.hydro.eaufrance.fr/, accessed 17/05/2021

Barrier, N., Petrenko, A. A., & Ourmières, Y. (2016). Strong intrusions of the Northern Mediterranean Current on the eastern Gulf of Lion: insights from in-situ observations and high resolution numerical modelling. Ocean Dynamics, 66(3), 313–327. https://doi.org/10.1007/s10236-016-0921-7

Bentsen, M., Evensen, G., Drange, H., & Jenkins, A. D. (1999). Coordinate transformation on a sphere using conformal mapping. Monthly Weather Review, 127(12), 2733–2740. https://doi.org/10.1175/1520-0493(1999)127<2733:CTOASU>2.0.CO;2

Bourrin, F., Many, G., Durrieu de Madron, X., Martín, J., Puig, P., Houpert, L., Testor, P., Kunesch, S., Mahiouz, K., & Béguery, L. (2015). Glider monitoring of shelf suspended particle dynamics and transport during storm and flooding conditions. Continental Shelf Research 109, 135–149. https://doi.org/10.1016/j.csr.2015.08.031

Boussinesq, J. (1903). Théorie analytique de la chaleur mise en harmonie avec la thermodynamique et avec la théorie mécanique de la lumière: Refroidissement et échauffement par rayonnement, conductibilité des tiges, lames et masses cristallines, courants de convection, théorie. In Cours de physique mathématique de la Faculté des sciences (2nd ed.). Gauthiers-Vars.

Briton, F., Cortese, D., Duhaut, T., & Guizien, K. (2018). High-resolution modelling of ocean circulation can reveal retention spots important for biodiversity conservation. Aquatic Conservation: Marine and Freshwater Ecosystems, 28(4), 882–893. https://doi.org/10.1002/aqc.2901

Cai, X., Zhang, Y. J., Shen, J., Wang, H., Wang, Z., Qin, Q., & Ye, F. (2020). A Numerical Study of Hypoxia in Chesapeake Bay Using an Unstructured Grid Model: Validation and Sensitivity to Bathymetry Representation. Journal of the American Water Resources Association, 1–24. https://doi.org/10.1111/1752-1688.12887

CANDHIS (n.d.), Centre d'Archivage National des Données de Houle In situ, http://candhis.cetmef.developpement-durable.gouv.fr, accessed 01/06/2021.

Chassignet, E. P., Hurlburt, H. E., Smedstad, O. M., Halliwell, G. R., Hogan, P. J., Wallcraft, A. J., Baraille, R., & Bleck, R. (2007). The HYCOM (HYbrid Coordinate Ocean Model) data assimilative system. Journal of Marine Systems, 65(1-4 SPEC. ISS.), 60–83. https://doi.org/10.1016/j.jmarsys.2005.09.016

Chelton, D. B., Schlax, M. G., & Samelson, R. M. (2007). Summertime coupling between sea surface temperature and wind stress in the California current system. Journal of Physical Oceanography, 37(3), 495–517. https://doi.org/10.1175/JPO3025.1

Clark, P. U., Pisias, N. G., Stocker, T. F., & Weaver, A. J. (2019). The role of the thermohaline circulation in abrupt climate change. Encyclopedia of Ocean Sciences, 415(February), 405–411. https://doi.org/10.1016/B978-0-12-409548-9.11625-2

Cowen, R. K., Lwiza, K. M. M., Sponaugle, S., Paris, C. B., & Olson, D. B. (2000). Connectivity of marine populations: Open or closed? Science, 287(5454), 857–859. https://doi.org/10.1126/science.287.5454.857

Davies, A. M., Kwong, S. C. M., & Flather, R. A. (1998). A three-dimensional model of wind-driven circulation on the shelf: Application to the storm of January 1993. Continental Shelf Research, 18(2–4), 289–340. https://doi.org/10.1016/S0278-4343(97)00060-5

Dohan, K., Fabrice, B., Centurioni, L., Cronin, M., Lagerloef, G., Lee, D.-K., Lumpkin, R., Maximenko, N. A., Niiler, P. P., & Hiroshi, U. (2010). Measuring the Global Ocean Surface Circulation with Satellite and In Situ Observations. January, 237–248. https://doi.org/10.5270/oceanobs09.cwp.23

Drevillon, M., Bahurel, P., Bazin, D., Benkiran, M., Beuvier, J., Crosnier, L., Drillet, Y., Durand, E., Fabardines, M., Hermosa, I. G., Giordan, C., Hernandez, F., Chune, S. L., Le, P., Lellouche, J., Levier, B., Melet, A., Obaton, D., Paul, J., Peltier, M., Peyrot, D., Von Schuckmann, K. & Thomas-couroux, C. (2018). Learning about Copernicus Marine Environment Monitoring Service CMEMS : A Practical Introduction to the Use of the European Operational Oceanography Service. https://doi.org/10.17125/gov2018.ch25.695

Dufois, F., Garreau, P., Le Hir, P., & Forget, P. (2008). Wave- and current-induced bottom shear stress distribution in the Gulf of Lions. Continental Shelf Research, 28(15), 1920–1934. https://doi.org/10.1016/j.csr.2008.03.028

Dulière, V., Gypens, N., Lancelot, C., Luyten, P., & Lacroix, G. (2019). Origin of nitrogen in the English Channel and Southern Bight of the North Sea ecosystems. Hydrobiologia, 845(1), 13–33. https://doi.org/10.1007/s10750-017-3419-5

Dumas, F., & Langlois, G. (2009). MARS Model for Applications at Regional Scale Scientific model description.

Durrieu de Madron X., Heussner S., Delsaut N., Kunesch S., & Menniti C. (2019). BILLION observatory data. SEANOE. https://doi.org/10.17882/45980

Estournel, C., Broche, P., Marsaleix, P., Devenon, J. L., Auclair, F., & Vehil, R. (2001). The Rhone River plume in unsteady conditions: Numerical and experimental results. Estuarine, Coastal and Shelf Science, 53(1), 25–38. https://doi.org/10.1006/ecss.2000.0685

Estournel, C., Durrieu de Madron, X., Marsaleix, P., Auclair, F., Julliand, C., & Vehil, R. (2003). Observation and modeling of the winter coastal oceanic circulation in the Gulf of Lion under wind conditions influenced by the continental orography (FETCH experiment). Journal of Geophysical Research: Oceans, 108(3), 1–19. https://doi.org/10.1029/2001jc000825

Estournel, C., Testor, P., Damien, P., D'Ortenzio, F., Marsaleix, P., Conan, P., Kessouri, F., Durrieu de Madron, X., Coppola, L., Lellouche, J. M., Belamari, S., Mortier, L., Ulses, C., Bouin, M. N., & Prieur, L. (2016). High resolution modeling of dense water formation in the north-western Mediterranean during winter 2012–2013: Processes and budget. Journal of Geophysical Research: Oceans, 121(7), 5367–5392. https://doi.org/10.1002/2016JC011935

Falkowski, P. G., Barber, R. T., & Smetacek, V. (1998). Biogeochemical controls and feedbacks on ocean primary production. Science, 281(5374), 200–206. https://doi.org/10.1126/science.281.5374.200

Fisher, A. W., Sanford, L. P., & Scully, M. E. (2018). Wind-wave effects on Estuarine Turbulence: A comparison of observations and second-moment closure predictions. Journal of Physical Oceanography, 48(4), 905–923. https://doi.org/10.1175/JPO-D-17-0133.1

Fofonoff, N. P., & Millard, R. C. (1983). Algorithms for computation of fundamental properties of seawater. UNESCO Technical Papers in Marine Science, 44, 53. http://darchive.mblwhoilibrary.org:8080/handle/1912/2470

Gentil, M., Many, G., de Madron, X. D., Cauchy, P., Pairaud, I., Testor, P., Verney, R., & Bourrin, F. (2020). Glider-based active acoustic monitoring of currents and turbidity in the coastal zone. Remote Sensing, 12(18). https://doi.org/10.3390/RS12182875

Gill, A. E. (1982). Atmosphere–Ocean Dynamics. International Geophysics Series. https://books.google.fr/books?hl=nl&lr=&id=lypfDAAAQBAJ&oi=fnd&pg=PP1&dq=atmosphere+ocean+dynamics&ots=MsziwO6jrl&sig=2-VQjQky1C6LtDP6ZvbJ25xWRFI#v=onepage&q=Brunt&f=false

Guizien, K. (2009). Spatial variability of wave conditions in the Gulf of Lions (NW Mediterranean sea). Life and Environment, 59(3/4), 261–270. https://www.researchgate.net/publication/250306276

Guizien, K., Barthélemy, E., & Inall, M. E. (1999). Internal tide generation at a shelf break by an oblique barotropic tide: Observations and analytical modeling. Journal of Geophysical Research: Oceans, 104(C7), 15655–15668. https://doi.org/10.1029/1999jc900089

Guizien, K., Charles, F., Lantoine, F., & Naudin, J. J. (2007). Nearshore dynamics of nutrients and chlorophyll during Mediterranean-type flash-floods. Aquatic Living Resources, 20(1), 3–14. https://doi.org/10.1051/alr:2007011

Gustafsson, N., Nyberg, L., & Omstedt, A. (1998). Coupling of a high-resolution atmospheric model and an ocean model for the Baltic Sea. Monthly Weather Review, 126(11), 2822–2846. https://doi.org/10.1175/1520-0493(1998)126<2822:COAHRA>2.0.CO;2

Halliwell, J. R., Shay, L. K., Brewster, J. K., & Teague, W. J. (2011). Evaluation and sensitivity analysis of an ocean model response to Hurricane Ivan. Monthly Weather Review, 139(3), 921–945. https://doi.org/10.1175/2010MWR3104.1

Hamon, M., Beuvier, J., Somot, S., Lellouche, J. M., Greiner, E., Jordà, G., Bouin, M. N., Arsouze, T., Béranger, K., Sevault, F., Dubois, C., Drevillon, M., & Drillet, Y. (2016). Design and validation of MEDRYS, a Mediterranean Sea reanalysis over the period 1992-2013. Ocean Science, 12(2), 577–599. https://doi.org/10.5194/os-12-577-2016

Hanna, S., & Heinold D. (1985) Development and application of a simple method for evaluating air quality models. American Petroleum Institute, 4409

Holt, J., Harle, J., Proctor, R., Michel, S., Ashworth, M., Batstone, C., Allen, I., Holmes, R., Smyth, T., Haines, K., Bretherton, D., & Smith, G. (2009). Modelling the global coastal ocean. Philosophical Transactions of the Royal Society A: Mathematical, Physical and Engineering Sciences, 367(1890), 939–951. https://doi.org/10.1098/rsta.2008.0210

Houpert, L., Durrieu de Madron, X., Testor, P., Bosse, A., D'Ortenzio, F., Bouin, M. N., Dausse, D., Le Goff, H., Kunesch, S., Labaste, M., Coppola, L., Mortier, L., & Raimbault, P. (2016). Observations of open-ocean deep convection in the northwestern Mediterranean Sea:

Seasonal and interannual variability of mixing and deep water masses for the 2007-2013 Period. Journal of Geophysical Research: Oceans, 121(11), 8139–8171. https://doi.org/10.1002/2016JC011857

Hu, Z. Y., Doglioli, A. M., Petrenko, A. A., Marsaleix, P., & Dekeyser, I. (2009). Numerical simulations of eddies in the Gulf of Lion. Ocean Modelling, 28(4), 203–208. https://doi.org/10.1016/j.ocemod.2009.02.004

Hu, Z. Y., Petrenko, A. A., Doglioli, A. M., & Dekeyser, I. (2011). Study of a mesoscale anticyclonic eddy in the western part of the Gulf of Lion. Journal of Marine Systems, 88(1), 3–11. https://doi.org/10.1016/j.jmarsys.2011.02.008

James, I. D. (2002). Modelling pollution dispersion, the ecosystem and water quality in coastal waters: A review. Environmental Modelling and Software, 17(4), 363–385. https://doi.org/10.1016/S1364-8152(01)00080-9

Kara, A. B., Barron, C. N., Martin, P. J., Smedstad, L. F., & Rhodes, R. C. (2006). Validation of interannual simulations from the 1/8° global Navy Coastal Ocean Model (NCOM). Ocean Modelling, 11(3–4), 376–398. https://doi.org/10.1016/j.ocemod.2005.01.003

Kirtman, B. P., Bitz, C., Bryan, F., Collins, W., Dennis, J., Hearn, N., Kinter, J. L., Richard, I. I. I., Clement, L., Siqueira, L., Stan, C., Tomas, R., & Vertenstein, M. (2012). Impact of ocean model resolution on CCSM climate simulations. 1303–1328. https://doi.org/10.1007/s00382-012-1500-3

Kourafalou, V.H., Peng, G., Kang, H., Hogan, P.J., Smedstad, O.M., & Weisberg, R.H. (2009) Evaluation of Global Ocean Data Assimilation Experiment products on South Florida

nested simulations with the Hybrid Coordinate Ocean Model. Ocean Dynamics 59(1), 47–66 . https://doi.org/10.1007/s10236-008-0160-7

Kvile, K. Ø., Romagnoni, G., Dagestad, K. F., Langangen, Ø., & Kristiansen, T. (2018). Sensitivity of modelled North Sea cod larvae transport to vertical behaviour, ocean model resolution and interannual variation in ocean dynamics. ICES Journal of Marine Science, 75(7), 2013–2024. https://doi.org/10.1093/icesjms/fsy039

Lapouyade, A., & Durrieu de Madron, X. (2001). Seasonal variability of the advective transport of particulate matter and organic carbon in the Gulf of Lion (NW Mediterranean). Oceanologica Acta, 24(3), 295–312. https://doi.org/10.1016/S0399-1784(01)01148-3

Lazure, P., & Dumas, F. (2008). An external-internal mode coupling for a 3D hydrodynamical model for applications at regional scale (MARS). Advances in Water Resources, 31(2), 233–250. https://doi.org/10.1016/j.advwatres.2007.06.010

Le Provost, C., & Lyard, F. H. (2000). How can we improve a global ocean tide model at a regional scale? A test on the Yellow Sea and the East China Sea. Journal of geophysical research, 105(C4), 8707–8725.

Lopuhaä, H. P., Dekking, F. M., Kraaikamp, C., & Meester, L. E. (2005). A Modern Introduction to Probability and Statistics: Understanding Why and How. Springer. https://doi.org/10.1198/jasa.2006.s72

Ludwig, W., Dumont, E., Meybeck, M., & Heussner, S. (2009). River discharges of water and nutrients to the Mediterranean and Black Sea: Major drivers for ecosystem changes during past and future decades? Progress in Oceanography, 80(3–4), 199–217. https://doi.org/10.1016/j.pocean.2009.02.001

Mader, J., Rubio, A., Novellino, A., Alba, M., Corgnati, L., Mantovani, C., Griffa, A., Gorringe, P. & Fernandez, V. (2016). The European HF Radar inventory. EuroGOOS publications.

Mannarini, G., & Carelli, L. (2019). Waves and ocean currents for energy efficient navigation. Geoscientific Model Development Discussions, February, 1–47. https://doi.org/10.5194/gmd-2018-292

Mansui, J., Darmon, G., Ballerini, T., van Canneyt, O., Ourmieres, Y., & Miaud, C. (2020). Predicting marine litter accumulation patterns in the Mediterranean basin: Spatio-temporal variability and comparison with empirical data. Progress in Oceanography, 182, 102268. https://doi.org/10.1016/j.pocean.2020.102268

Many, G., Bourrin, F., Durrieu de Madron, X., Ody, A., Doxaran, D., & Cauchy, P. (2018). Glider and satellite monitoring of the variability of the suspended particle distribution and size in the Rhône ROFI. Progress in Oceanography, 163, 123–135. https://doi.org/10.1016/j.pocean.2017.05.006

Many, G., Bourrin, F., Durrieu de Madron, X., Pairaud, I., Gangloff, A., Doxaran, D., Ody, A., Verney, R., Menniti, C., Le Berre, D., & Jacquet, M. (2016). Particle assemblage characterization in the Rhone River ROFI. Journal of Marine Systems, 157, 39–51. https://doi.org/10.1016/j.jmarsys.2015.12.010

Marsaleix, P., Auclair, F., Duhaut, T., Estournel, C., Nguyen, C., & Ulses, C. (2012). Alternatives to the Robert-Asselin filter. Ocean Modelling, 41, 53–66. https://doi.org/10.1016/j.ocemod.2011.11.002

Marsaleix, P., Auclair, F., & Estournel, C. (2009a). Low-order pressure gradient schemes in sigma coordinate models: The seamount test revisited. Ocean Modelling, 30(2–3), 169–177. https://doi.org/10.1016/j.ocemod.2009.06.011

Marsaleix, P., Auclair, F., Floor, J. W., Herrmann, M. J., Estournel, C., Pairaud, I., & Ulses, C. (2008). Energy conservation issues in sigma-coordinate free-surface ocean models. Ocean Modelling, 20(1), 61–89. https://doi.org/10.1016/j.ocemod.2007.07.005

Marsaleix, P., Estournel, C., Kondrachoff, V., & Vehil, R. (1998). A numerical study of the formation of the Rhone River plume. Journal of Marine Systems, 14(1–2), 99–115. https://doi.org/10.1016/S0924-7963(97)00011-0

Marsaleix, P., Ulses, C., Pairaud, I., Herrmann, M. J., Floor, J. W., Estournel, C., & Auclair, F. (2009b). Open boundary conditions for internal gravity wave modelling using polarization relations. Ocean Modelling, 29(1), 27–42. https://doi.org/10.1016/j.ocemod.2009.02.010

Marshall, J., Hill, C., Perelman, L., & Adcroft, A. (1997). Hydrostatic, quasi-hydrostatic, and nonhydrostatic ocean modeling. Journal of Geophysical Research C: Oceans, 102(C3), 5733–5752. https://doi.org/10.1029/96JC02776

Marzocchi, A., Hirschi, J. J. M., Holliday, N. P., Cunningham, S. A., Blaker, A. T., & Coward, A. C. (2015). The North Atlantic subpolar circulation in an eddy-resolving global ocean model. Journal of Marine Systems, 142, 126–143. https://doi.org/10.1016/j.jmarsys.2014.10.007

McCarthy, G. D., Haigh, I. D., Hirschi, J. J. M., Grist, J. P., & Smeed, D. A. (2015). Ocean impact on decadal Atlantic climate variability revealed by sea-level observations. Nature, 521(7553), 508–510. https://doi.org/10.1038/nature14491

McDougall, T. J., Greatbatch, R. J., & Lu, Y. (2002). On conservation equations in oceanography: How accurate are Boussinesq ocean models? Journal of Physical Oceanography, 32(5), 1574–1584. https://doi.org/10.1175/1520-0485(2002)032<1574:OCEIOH>2.0.CO;2

Mentaschi, L., Besio, G., Cassola, F., & Mazzino, A. (2013). Problems in RMSE-based wave model validations. Ocean Modelling, 72, 53–58. https://doi.org/10.1016/j.ocemod.2013.08.003

Michaud, H., Marsaleix, P., Leredde, Y., Estournel, C., Bourrin, F., Lyard, F., Mayet, C., & Ardhuin, F. (2012). Three-dimensional modelling of wave-induced current from the surf zone to the inner shelf. Ocean Science, 8(4), 657–681. https://doi.org/10.5194/os-8-657-2012

Mikolajczak, G. (2019). Dynamique de l'eau et des apports particulaires originaires du Rhône sur la marge continentale du Golfe du Lion. [Doctoral dissertation, Toulouse university]

Mikolajczak, G., Estournel, C., Ulses, C., Marsaleix, P., Bourrin, F., Martín, J., Pairaud, I., Puig, P., Leredde, Y., Many, G., Seyfried, L., & Durrieu de Madron, X. (2020). Impact of storms on residence times and export of coastal waters during a mild autumn/winter period in the Gulf of Lion. Continental Shelf Research, 207, 104192.

Millot, C. (1990). The Gulf of Lions' hydrodynamics. Continental Shelf Research, 10(9–11), 885–894. https://doi.org/10.1016/0278-4343(90)90065-T

Molcard, A., Pinardi, N., Iskandarani, M., & Haidvogel, D. B. (2002). Wind driven general circulation of the Mediterranean Sea simulated with a spectral element ocean model. Dynamics of Atmospheres and Oceans, 35(2), 97–130. https://doi.org/10.1016/S0377-0265(01)00080-X

Moore, A. M., Arango, H. G., Broquet, G., Powell, B. S., Weaver, A. T., & Zavala-Garay, J. (2011). The Regional Ocean Modeling System (ROMS) 4-dimensional variational data assimilation

systems. Part I - System overview and formulation. Progress in Oceanography, 91(1), 34–49. https://doi.org/10.1016/j.pocean.2011.05.004

Pairaud, I., Gatti, J., Bensoussan, N., Verney, R., & Garreau, P. (2011). Hydrology and circulation in a coastal area off Marseille: Validation of a nested 3D model with observations. Journal of Marine Systems, 88(1), 20–33. https://doi.org/10.1016/j.jmarsys.2011.02.010

Pairaud I., Repecaud M., Ravel C., Fuchs R., Arnaud M., Champelovier A., Rabouille C., Bombled B., Toussaint F., Garcia F., Raimbault P., Verney R., Meule S., Gaufres P., Bonnat A. & Cadiou J.-F. (2016). MesuRho. Plateforme instrumentée de suivi des paramètres environnementaux à l'embouchure du Rhône . Mesures à haute résolution dans l'environnement marin côtier. Schmitt, F.G. et Lefebvre A. (Eds.). CNRS Alpha. ISBN : 978-2-271-08592-4. pp.73- 87 .

Petrenko, A., Leredde, Y., & Marsaleix, P. (2005). Circulation in a stratified and wind-forced Gulf of Lions, NW Mediterranean Sea: In situ and modeling data. Continental Shelf Research, 25(1), 7–27. https://doi.org/10.1016/j.csr.2004.09.004

Prandtl, L. (1925). 7. Bericht über Untersuchungen zur ausgebildeten Turbulenz. ZAMM-Journal of Applied Mathematics and Mechanics/Zeitschrift für Angewandte Mathematik und Mechanik, 5(2), 136-139.

Putman, N. F. (2018). Marine migrations. Current Biology, 28(17), R972–R976. https://doi.org/10.1016/j.cub.2018.07.036

Putman, N. F., & He, R. (2013). Tracking the long-distance dispersal of marine organisms: Sensitivity to ocean model resolution. Journal of the Royal Society Interface, 10(81). https://doi.org/10.1098/rsif.2012.0979

Rainaud, R., Lebeaupin Brossier, C., Ducrocq, V., Giordani, H., Nuret, M., Fourrié, N., Bouin, M. N., Taupier-Letage, I., & Legain, D. (2016). Characterization of air–sea exchanges over the Western Mediterranean Sea during HyMeX SOP1 using the AROME–WMED model. Quarterly Journal of the Royal Meteorological Society, 142(August), 173–187. https://doi.org/10.1002/qj.2480

RDI Instruments. (2007). Accoustic Doppler Current Profiler Technical Manual. P/N 957-6150-00

Reffray, G., Fraunié, P., & Marsaleix, P. (2004). Secondary flows induced by wind forcing in the Rhône region of freshwater influence. Ocean Dynamics, 54(2), 179–196. https://doi.org/10.1007/s10236-003-0079-y

Renault, L., Chiggiato, J., Warner, J. C., Gomez, M., Vizoso, G., & Tintoré, J. (2012). Coupled atmosphere-ocean-wave simulations of a storm event over the Gulf of Lion and Balearic Sea. Journal of Geophysical Research: Oceans, 117(C9), n/a-n/a. https://doi.org/10.1029/2012JC007924

Ridenour, N. A., Hu, X., Jafarikhasragh, S., Landy, J. C., Lukovich, J. V., Stadnyk, T. A., Sydor, K., Myers, P. G., & Barber, D. G. (2019). Sensitivity of freshwater dynamics to ocean model resolution and river discharge forcing in the Hudson Bay Complex. Journal of Marine Systems, 196(May), 48–64. https://doi.org/10.1016/j.jmarsys.2019.04.002

Ringler, T., Petersen, M., Higdon, R. L., Jacobsen, D., Jones, P. W., & Maltrud, M. (2013). A multi-resolution approach to global ocean modeling. Ocean Modelling, 69, 211–232. https://doi.org/10.1016/j.ocemod.2013.04.010

Ross, N. O., Fraysse, M., Pinazo, C., Pairaud, I. (2016). Impact of an intrusion by the Northern Current on the biogeochemistry in the eastern Gulf of Lion, NW Mediterranean . Estuarine Coastal And Shelf Science , 170, 1-9. https://doi.org/10.1016/j.ecss.2015.12.022

Schaeffer, A., Garreau, P., Molcard, A., Fraunié, P., & Seity, Y. (2011). Influence of high-resolution wind forcing on hydrodynamic modeling of the Gulf of Lions. Ocean Dynamics, 61(11), 1823–1844. https://doi.org/10.1007/s10236-011-0442-3

Schroeder, K., Millot, C., Bengara, L., Ben Ismail, S., Bensi, M., Borghini, M., Budillon, G., Cardin, V., Coppola, L., Curtil, C., Drago, A., El Moumni, B., Font, J., Fuda, J. L., García-Lafuente, J., Gasparini, G. P., Kontoyiannis, H., Lefevre, D., Puig, P., Raimbault, P., Rougier, G.,Salat, J., Sammari, C., Sánchez Garrido, J. C., Sanchez-Roman, A., Sparnocchia, S., Tamburini, C., Taupier-Letage, I., Theocharis, A., Vargas-Yáñez, M., Vetrano, A. (2013). Long-term monitoring programme of the hydrological variability in the Mediterranean Sea: A first overview of the HYDROCHANGES network. Ocean Science, 9(2), 301–324. https://doi.org/10.5194/os-9-301-2013

Sextant (1996). Système Acquisition Validation Exploitation de Données des Navires de l'INSU - Projet SAVED https://sextant.ifremer.fr/record/6f6e95e9-8e97-48d6-b536-b40f2ad87402/, accessed 04/06/2021.

Seyfried, L., Marsaleix, P., Richard, E., & Estournel, C. (2017). Modelling deep-water formation in the north-west Mediterranean Sea with a new air-sea coupled model: Sensitivity to turbulent flux parameterizations. Ocean Science, 13(6), 1093–1112. https://doi.org/10.5194/os-13-1093-2017

Siedler, G., Gould, J., & Church, J. A. (2001). Ocean circulation and climate: observing and modelling the global ocean. Elsevier Ltd.

SIROCCO (n.d.), https://sirocco.obs-mip.fr/ocean-models/s-model/, accessed 17/05/2021

Smith, S. D. (1988). Coefficients for sea surface wind stress, heat flux, and wind profiles as a function of wind speed and temperature. Journal of Geophysical Research: Oceans, 93(C12), 15467–15472. https://doi.org/10.1029/JC093iC12p15467

Somot, S., Sevault, F., Déqué, M., & Crépon, M. (2008). 21st century climate change scenario for the Mediterranean using a coupled atmosphere-ocean regional climate model. Global and Planetary Change, 63(2–3), 112–126. https://doi.org/10.1016/j.gloplacha.2007.10.003

Testor, P., DeYoung, B., Rudnick, D. L., Glenn, S., Hayes, D., Lee, C., Pattiaratchi, C. B., Hill, K. L., Heslop, E., Turpin, V., Alenius, P., Barrera, C., Barth, J., Beaird, N., Becu, G., Bosse, A., Bourrin, F., Brearley, A., Chao, Y., Chen, S., Chiggiato, J., Coppola, L., Crout, R., Cummings, J., Curry, B., Curry, R., Davis, R., Desai, K., DiMarco, S., Edwards, C., Fielding, S., Fer, I., Frajka-Williams, E., Gildor, H., Goni, G., Gutierrez, D., Hanson, S., Haugan, P., Hebert, D., Heiderich, J., Heywood, K. J., Hogan, P., Houpert, L., Huh, S., Inall, M.E., Ishii, M., Ito, S., Itoh, S., Jan, S., Kaiser, J., Karstensen, J., Kirkpatrick, B., Klymak, J., Kohut, J., Krahmann, G., Krug, M., McClatchie, S., Marin, F., Mauri, E., Mehra, A., Meredith, M.P., Miles, T., Morell, J., Mortier, L., Nicholson, S., O'Callaghan, J., O'Conchubhair, D., Oke, P.R., Sanz, .P., Palmer, M., Park, J., Perivoliotis, L., Poulain, P.M., Perry, R., Queste, B., Rainville, L., Rehm, E., Roughan, M., Rome, N., Ross, T., Ruiz, S., Saba, G., Schaeffer, A., Schonau, M., Schroeder, K., Shimizu, Y., Sloyan, B.M., Smeed, D., Snowden, D.P., Song, Y., Swart, S., Tenreiro, M., Thompson, A.F., Tintore, J., Todd, R.E., Toro, C., Venables, H., Waterman, S., Watlington,

R., Wilson, D. (2019). OceanGliders: A component of the integrated GOOS. Frontiers in Marine Science, 6(July), 422. Frontiers Media S.A. https://doi.org/10.3389/fmars.2019.00422

Thoppil, P. G., Richman, J. G., & Hogan, P. J. (2011). Energetics of a global ocean circulation model compared to observations. Geophysical Research Letters, 38(15), 12–17. https://doi.org/10.1029/2011GL048347

Ulses, C., Estournel, C., Puig, P., Durrieu de Madron, X., & Marsaleix, P. (2008). Dense shelf water cascading in the northwestern Mediterranean during the cold winter 2005: Quantification of the export through the Gulf of Lion and the Catalan margin. Geophysical Research Letters, 35(7), . https://doi.org/10.1029/2008GL033257

Warner, J. C., Sherwood, C. R., Signell, R. P., Harris, C. K., & Arango, H. G. (2008). Development of a three-dimensional, regional, coupled wave, current, and sediment-transport model. Computers and Geosciences, 34(10), 1284–1306. https://doi.org/10.1016/j.cageo.2008.02.012

Yang, Z., & Khangaonkar, T. (2009). Modeling tidal circulation and stratification in Skagit River estuary using an unstructured grid ocean model. Ocean Modelling, 28(1–3), 34–49. https://doi.org/10.1016/j.ocemod.2008.07.004

Zhang, J. X., Sukhodolov Alexander, N., & Liu, H. (2014). Non-hydrostatic versus hydrostatic modelings of free surface flows. Journal of Hydrodynamics, 26(4), 512–522. https://doi.org/10.1016/S1001-6058(14)60058-5

1.8 Appendix A

Table A.1: Overview of all ocean current observation stations with the number of bins, the bin size, the measurement depth, the time step, the type of equipment, the latitude, the longitude and the source. For the ADCPs, only the maximum measurement depth is indicated (*).

	Nr. of bins	Bin size (m)	Meas. depth (m)	Time step (min)	Equipment (Frequency)	Latitude	Longitude	Source
Creus	1	x	295	30	SP-ADCM (2MHz)	42.39	3.321667	Schroeder et al., (2013)
LD	2	x	505 975	60	SP-ADCM (2MHz)	42.428050	3.544783	Durrieu de Madron et al., (2019)
Lion	5	x	152 246 501 1002 2330	30	SP-ADCM (2MHz)	42.037267	4.686133	Testor et al., (2018) ; Houpert et al., (2016); Durrieu de Madron et al., (2019)
Planier	2	x	505 975	60	SP-ADCM (2MHz)	43.015083	5.192133	Durrieu de Madron et al., (2019)
Mesurho	40	0.75	18.7*	10	ADCP (600 kHz)	43.32	4.87	Pairaud et al., (2016)
POEM	65	0.50	28.1*	60	ADCP (600kHz)	42.704167	3.06667	Bourrin et al., (2015)
SOLA	26	1.00	24.9*	20	ADCP (614.4 kHz)	42.488333	3.145	Unpublished Guizien
BeSete (2010-2011)	99	0.25	24.6*	20	ADCP (614.4 kHz)	43.333917	3.639617	Unpublished Leredde
BeSete (2012-2013)	54	0.50	24.4*	20	ADCP (614.4 kHz)	43.333917	3.639617	Unpublished Leredde

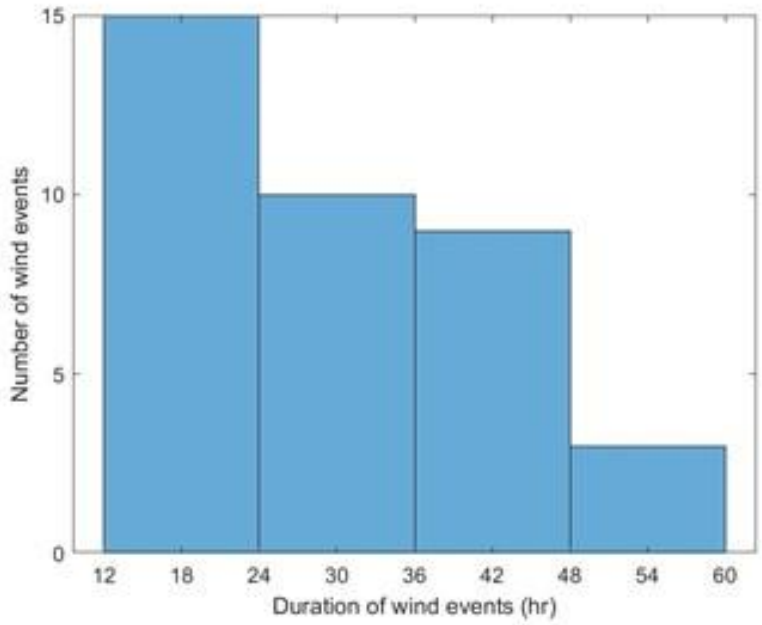

Figure A.1: Frequency histogram of the durations of the wind events.

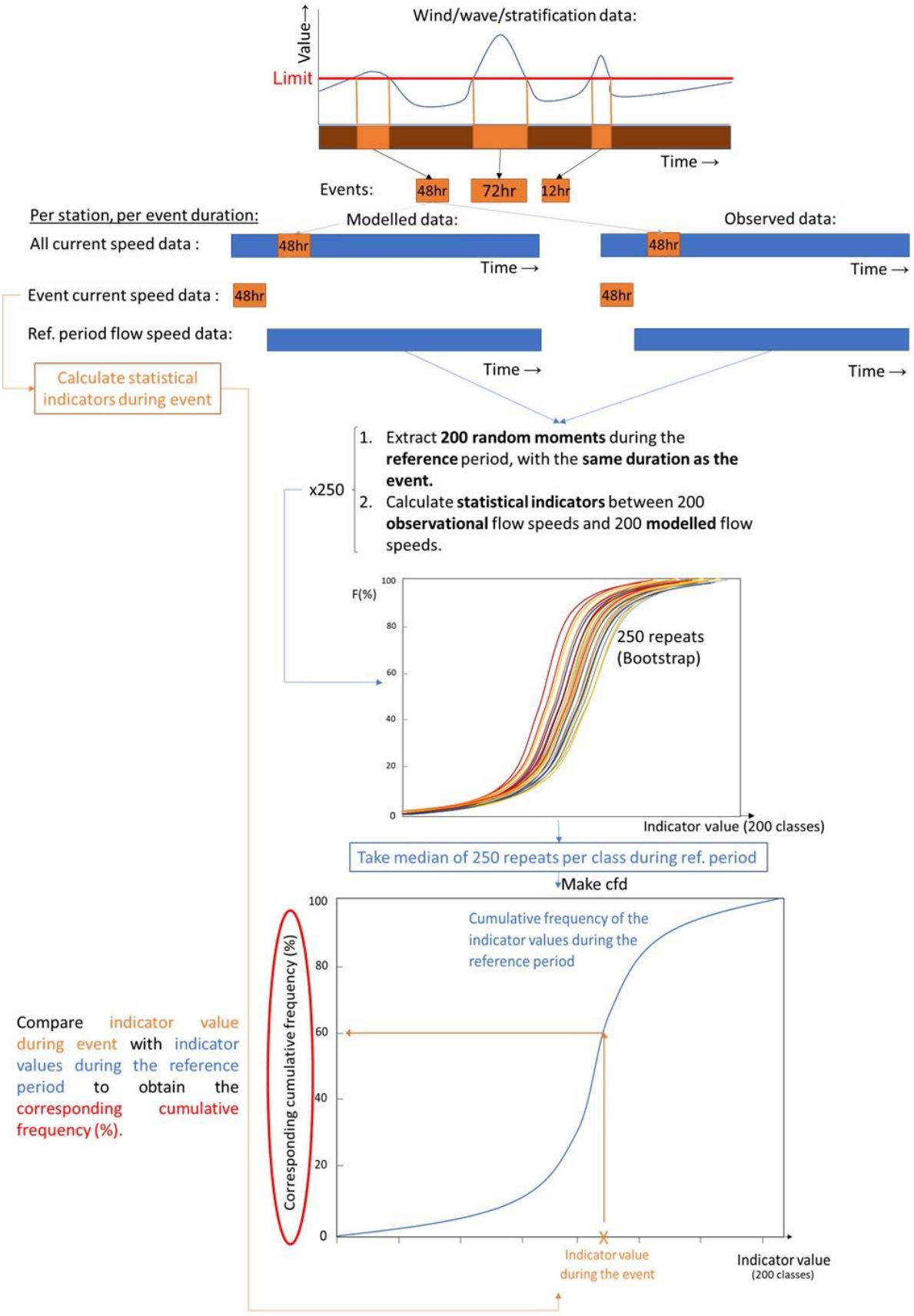

Figure A.2: Scheme on how to compare the uncertainty of the model during the event to the uncertainty of the model outside of the events.

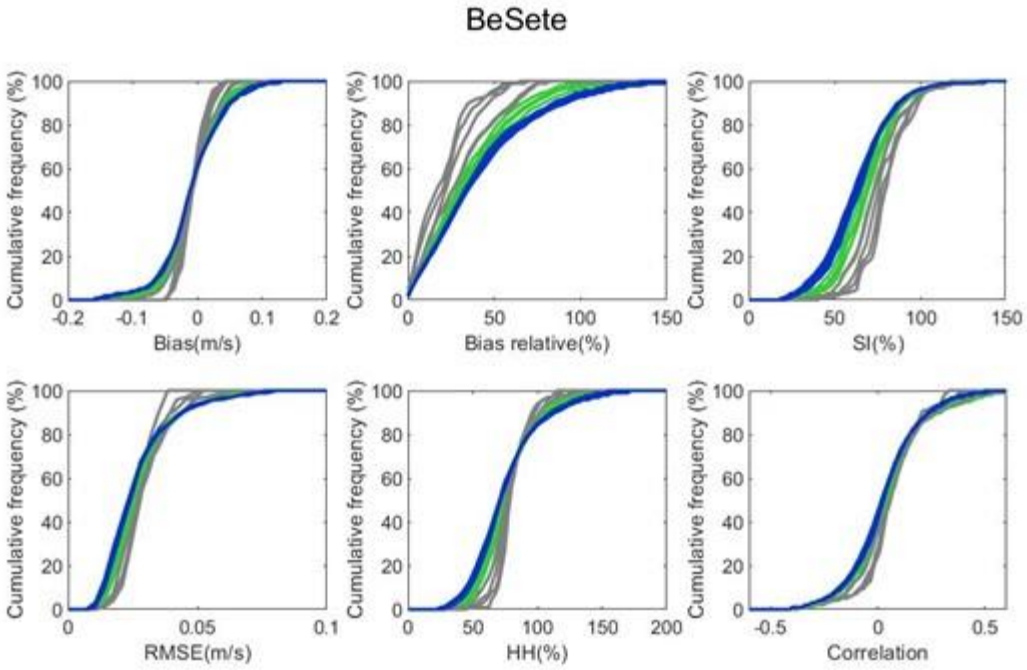

Figure A.3 Cumulative frequency distribution of the indicators calculated between modelled and observed flow speeds at BeSete during the reference period for different durations. Blue: 12-24hr, green: 24-72hr and grey: 72hr<.

1.9 Appendix B

$$T = C_D . \rho . U^2$$

Equation B.1: Wind stress at the sea surface..

$$N^2 = -\frac{g}{\rho_0}\frac{d\rho_0}{dz}$$

Equation B.2: The Brunt-Väisälä frequency

$$\text{Bias} = \frac{\sum_{i=1}^{Nd}\sum_{j=1}^{Nt}(M_{ij} - O_{ij})}{Nd . Nt}$$

Equation B.3: Bias

$$\text{Relative bias} = \frac{\sum_{i=1}^{Nd}\sum_{j=1}^{Nt}(M_{ij} - O_{ij})}{\sqrt{Nd . Nt \sum_{i=1}^{Nd}\sum_{j=1}^{Nt} M_{ij} O_{ij}}}$$

Equation B.4: Relative bias

$$SI = \sqrt{\frac{\sum_{i=1}^{Nd}\sum_{j=1}^{Nt}[(M_{ij} - \bar{M}) - (O_{ij} - \bar{O})]^2}{\sum_{i=1}^{Nd}\sum_{j=1}^{Nt} M_{ij} . O_{ij}}}$$

Equation B.5: Scatter index

$$RMSE = \sqrt{\frac{\sum_{i=1}^{Nd}\sum_{j=1}^{Nt}(M_{ij} - O_{ij})^2}{Nd . Nt}}$$

Equation B.6: Root mean square error

$$HH = \sqrt{\frac{\sum_{i=1}^{Nd}\sum_{j=1}^{Nt}(M_{ij} - O_{ij})^2}{\sum_{i=1}^{Nd}\sum_{j=1}^{Nt}(M_{ij} . O_{ij})}}$$

Equation B.7: Hanna & Heinold index

$$\text{Corr.} = \frac{\sum_{i=1}^{Nd}\sum_{j=1}^{Nt}[(M_{ij} - \bar{M}) * (O_{ij} - \bar{O})]^2}{\sqrt{\sum_{i=1}^{Nd}\sum_{j=1}^{Nt}(M_{ij} - \bar{M})^2 . \sum_{i=1}^{Nd}\sum_{j=1}^{Nt}(O_{ij} - \bar{O})^2}}$$

Equation B.8: Correlation

With :

- T the wind stress at the sea surface (Pa)
- C_D the drag coefficient
- ρ the density of the air (kg/m³)
- U the wind speed (m/s)
- N^2 the Brunt-Väisälä freq. (1/s²)
- g the gravitational acceleration (m/s²)
- ρ_0 the density of the seawater (kg/m³)
- z the depth of the seawater (m)
- M_{ij} the modelled current speed at depth i and time j (m/s)
- O_{ij} the observed current speed at depth i and time j (m/s)
- Nd the number of depth levels
- Nt the number of timesteps
- $\bar{M}$ the average modelled current speed over depth and time (m/s)
- $\bar{O}$ the average observed current speed and time (m/s)

Chapter 2: The spatiotemporal distribution of Eulerian model uncertainty in the Gulf of Lion

2.1 Introduction

The Gulf of Lion is located at the French Mediterranean coast. The Mediterranean has summers which are warm and dry and the winters are mild and wet (Lionello et al., 2006). During spring, there is usually a thermocline development. This stratification generally disappears in winter (Millot, 1990). A clear pycnocline can also be caused by the outflow of rivers during spring and autumn. The biggest river that flows into the Gulf of Lion is the Rhône River, which causes a large plume of fresh water and sediment (Estournel et al., 2001). The Rhône's plume is affected by the general circulation in the Gulf of Lion (e.g. Northern Current) and spread by the wind (Estournel et al., 2001). The Gulf of Lion has a particular wind regime, with the Mistral starting from the Rhône channel and blowing from the north and the Tramontane blowing from the northwest starting between the Massif Central and the Alps (Millot, 1990; Petrenko et al., 2008). When these winds blow, their mean wind velocity exceeds 31 km/h for 20% of the time. The winds coming from the sea can generate waves of up to 7 m during storms, which is a strong contrast with the otherwise small waves (mean significant wave height 0.7m) measured in the Gulf of Lion (Guizien, 2009; Gervais et al., 2011; Mikolajczak, 2019). The continental winds can be observed all year, but are more frequent in winter (Sète weather station, from 2005 to 2009; Gervais et al., 2011). In winter, these winds are cold and dry and can cause dense water cascading over the canyons (Ulses et al., 2008b; Mikolajczak, 2019) and large water and sediment exports to deeper parts of the ocean

(Palanques et al., 2008; Mikolajczak et al., 2020). For example, around 750 km³ shelf water in the Gulf of Lion was transported to deeper water layers through cascading during the cold winter of 2005 (Canals et al., 2006; Ulses et al., 2008a; Mikolajczak et al., 2020). The multiple canyons present in the Gulf of Lion facilitate the descent of dense water, as a steeper bottom slope can cause a stronger flow of dense water (Ulses et al., 2008a).

It is clear that the Gulf of Lion's circulation is very heterogenous, both seasonally and spatially. This is where modelling comes in handy, as it can recreate the currents' dynamics in three dimensions over large areas and longer periods of time. Moreover, ocean models can be used on a variety of applications and scales, as mentioned in the introduction of chapter 1. The resolution of the model predisposes which processes can be observed/simulated. Recent technological advancements have made it possible to increase the ocean models' resolution. For climate studies, high resolution basin and global ocean models yield a resolution of 6-8 km (Hamon et al., 2016). When testing the performance of the global ocean model MPAS-Ocean, Ringler et al. (2013) found that the version of the model with a resolution of 7.5 km performed better than the one with a resolution of 15 km. Correctly quantifying the hydrodynamic model's uncertainties is an important step towards understanding its effect on modelled dispersal trajectories. Guizien et al. (2006) showed that larval dispersal simulations showed different retention rates with varying spatial resolutions. Moreover, Putman & He (2013) found that close to the coast, a high spatial and temporal resolution is necessary to correctly simulate the dispersal of marine organisms, whereas coarser spatial resolutions are allowed in the open sea. Briton et al. (2018), who used the SYMPHONIE2015 model to find retention spots for biodiversity conservation applications, used a minimum resolution of 80 m near the coast and maximum resolution of 2.7 km in the open sea. This is one of the highest resolutions

of the SYMPHONIE2015 model in the Gulf of Lion to date and this is why this configuration is used in this PhD.

However, resolution is not the only factor which can influence the model's performance.

In the previous chapter, the effect of model assumption violation during certain events (wind, waves, stratification) was tested. This chapter is going to further research the link between the model's error and several setting characteristics.

To test the effect of the waves on the model, the water depth is used as a proxy, as the influence of the waves reduces with increasing water depth (Faizal et al., 2011). The stratification events at the Mesurho station, which is closest to the Rhône River, were not included in the previous chapter because the periods without stratification were not abundant enough. This chapter considers the entire Gulf of Lion by adding the SAVED trajectory data and thus allows us to research the model's error distribution near the Rhône more deeply. Moreover, the differences between the model's bathymetry and the actual bathymetry can be an important source of error, particularly where steep bottom slopes occur, such as the canyons or at rocky coasts. Furthermore, the first chapter showed that there might be a link between the averaged observed current speed and the magnitude error, which is further investigated in this chapter.

In the previous chapter, the error on Eulerian velocities was integrated over the duration of the event. However, in dispersal studies, particle tracking relies on a Lagrangian approach, meaning the instant velocity along a track. Thus, the model's uncertainty will affect the particles' drift trajectory every step of the way. This is why chapter 2 examines the instant error distribution during the same study period (2010 - June 2013) and over the entire Gulf of Lion.

In this chapter, the instant difference between observation and simulation is calculated for every timestep and depth level for eight moorings and for trajectory data. The distributions of the magnitude error were assessed to find differences in model inaccuracy in either time or space. In time, intra- and interseasonal differences in error distribution were tested. In space, the error distributions at shallow and deep stations and of trajectory data over multiple bathymetry zones were analysed. When spatial differences were detected, the relationship with some environmental (depth, stratification, current speed, bottom steepness) and a modelling characteristic (resolution) was tested.

2.2 Materials & Methods

Most of the materials and methods used in chapter two are similar to the ones used in chapter one. However, since the comparison techniques to calculate the model's uncertainty are different and additional data was included, a thorough explanation of all materials and methods is given, even though some of it was already discussed in chapter one.

2.2.1 Observations

Current velocity data was gathered over the Gulf of Lion between 2010 and June 2013. Table 2.1 shows the periods for which the data was acquired. On figure 2.1, the positions of the fixed moorings are depicted and so is the steepness of the ocean floor. The steepness at every station is mentioned in table 2.2. There are four shallow water stations:

- **BeSete**
- **POEM,** Observational Platform of the Mediterranean Environment/ Plateforme d'Observation de l'Environnement Méditerranéen
- **Mesurho**, Measuring buoy at the mouth of the Rhône River
- **SOLA,** SOMLIT Observatory of the Arago Laboratory/ SOMLIT Observatoire de Laboratoire Arago

For these stations, an upward facing, moored ADCP (Acoustic Doppler Current Profiler) was used (figure 2.2a). There were also four deep stations, for which moored lines with one or more Single Point, Acoustic Doppler Current Meters (SP-ADCMs) on it were used (figure 2.2c):

- **Creus,** Cap de Creus canyon
- **LD**, Lacaze-Duthiers canyon
- **Lion**
- **Planier**

The **SAVED** data, Acquisition, Validation and Exploitation System of the Téthys II Data / Système Acquisition Validation Exploitation des Données du Téthys II, consisted of flow velocity data taken along vessel tracks, which can be seen in figure 2.3. This data was acquired with a downward facing, hull mounted ADCP on the Téthys II vessel (figure 2.2b). In this PhD, only the horizontal current velocity was used. This data was not considered in chapter 1 because it dealt with wave events, during which the boat is unlikely to set out.

Table 2.1: Timetable of acquired velocity data. SAVED is trajectory data, the rest are moorings. The seasons are organised per colour. Blue: winter (DJF), green: spring (MAM), purple: summer (JJA), orange: autumn (SON).

Year	2010												2011												2012												2013					
Month	1	2	3	4	5	6	7	8	9	10	11	12	1	2	3	4	5	6	7	8	9	10	11	12	1	2	3	4	5	6	7	8	9	10	11	12	1	2	3	4	5	6
Creus	X	X	X	X	X	X					X	X	X	X	X	X	X	X					X	X	X	X	X	X	X													
LD	X	X	X	X	X	X	X	X	X	X	X	X	X	X	X	X	X	X	X	X	X	X	X	X	X	X	X	X	X	X	X	X	X	X	X							
Lion	X	X	X	X	X	X	X	X	X	X	X	X	X	X	X	X	X	X	X	X	X	X	X	X	X	X	X	X	X	X	X	X	X	X	X	X	X	X	X	X	X	X
Planier	X	X	X	X	X	X	X	X	X	X	X	X	X	X	X	X	X	X	X	X	X	X	X	X	X	X	X	X	X	X	X	X	X	X	X							
Mesurho											X	X	X	X	X								X	X	X	X	X		X	X					X	X	X	X	X	X		
POEM														X	X	X																											
SOLA	X	X	X																																							
BeSete			X	X	X	X	X	X	X	X	X	X	X																		X	X	X	X	X	X	X	X	X	X		
SAVED		X	X	X	X	X	X		X	X	X	X	X	X	X	X	X	X	X		X		X	X		X	X	X	X	X	X	X	X	X	X	X	X	X	X	X	X	X

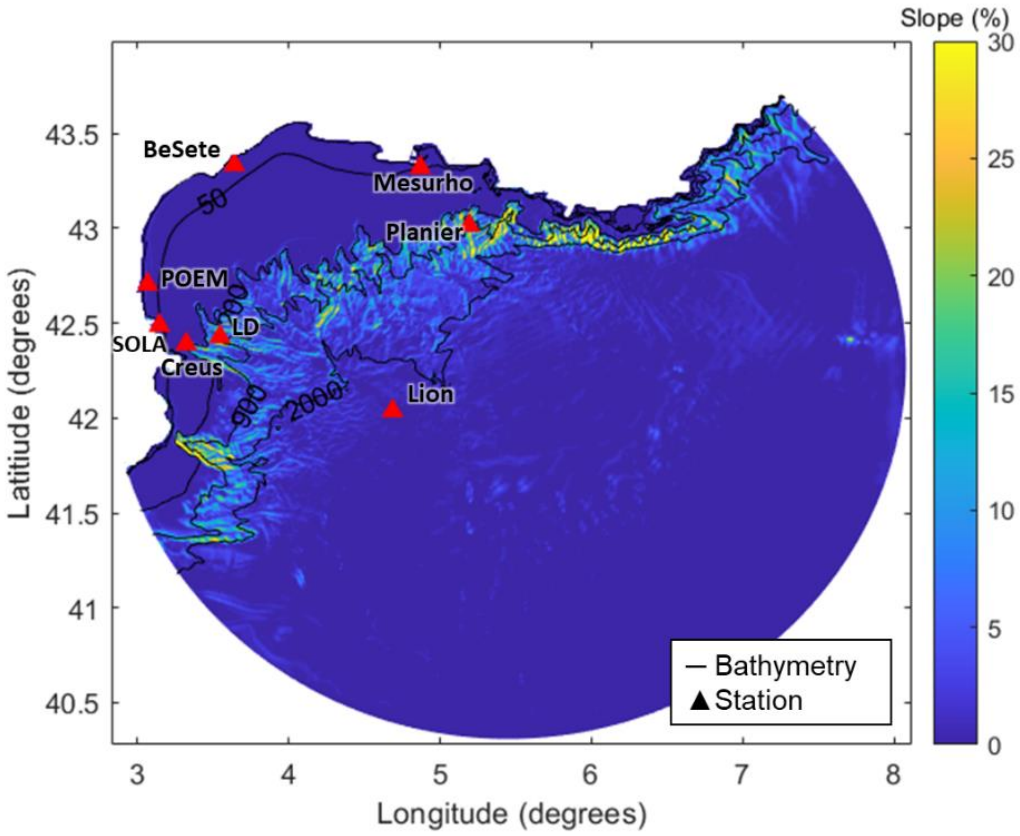

Figure 2.1: The Gulf of Lion's steepness of the ocean floor, including the bathymetry lines, and the positions of the fixed moorings.

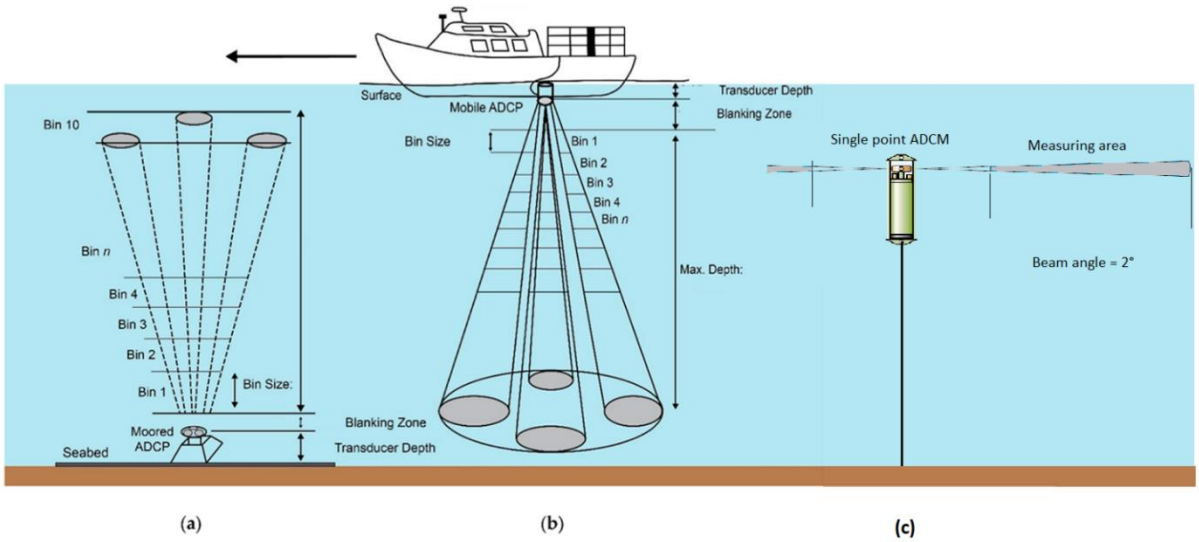

Figure 2.2: Fixed (a), mobile (b) ADCPs (Dwinovantyo et al., 2019) and a SP-ADCM (c) (AANDERAA 2001).

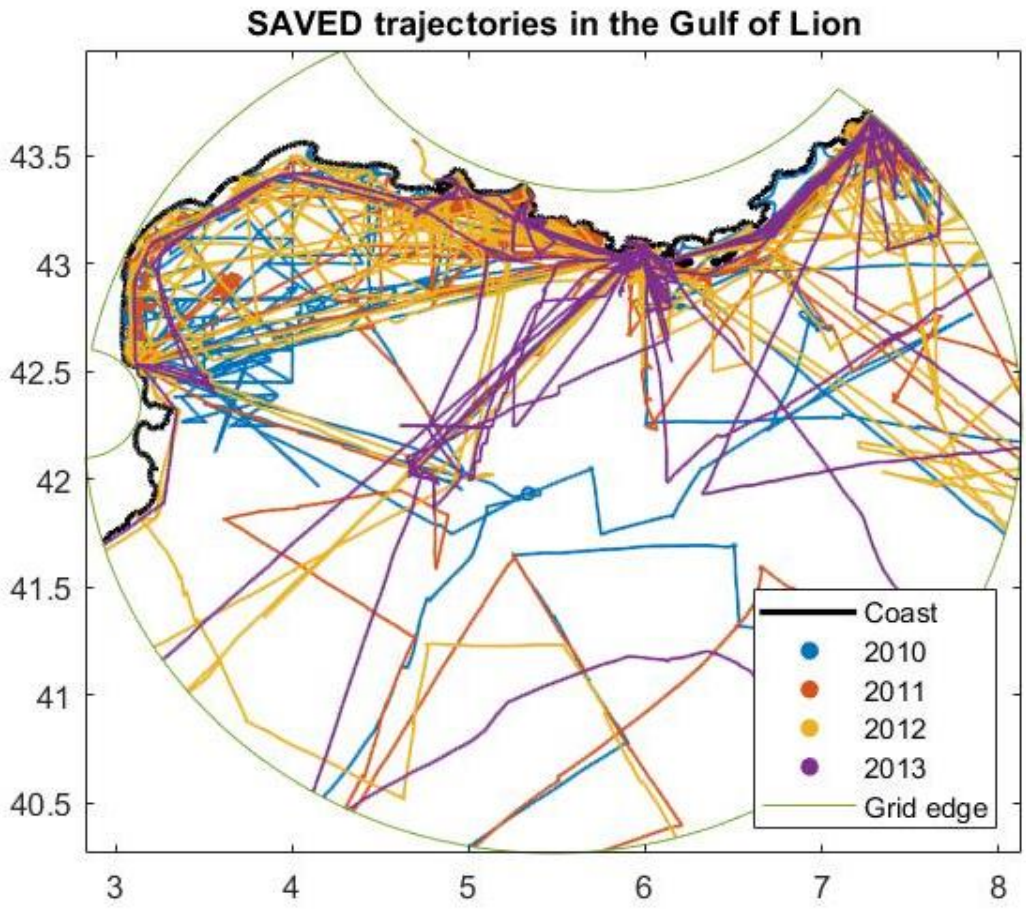

Figure 2.3: SAVED trajectories within the model grid for the years 2010-June2013.

Both ADCP and SP-ADCM devices use the Doppler effect to assess the current speed in the water. The Doppler effect expresses the change in sound wave frequency as a result of motion, which is clearly explained by RDI Instruments (1996): The change in frequency is directly proportional to the speed of the object producing the sound and is called the Doppler shift.

The bin sizes of the ADCPs used in this study vary from 25 centimeters to 4 meters with a bin count of 26 to 99 bins. The depth in table 2.2 is the depth at which the currents were measured for the SP-ADCMs. For the ADCPs, only the maximum depth at which measurements were taken is mentioned. This is not the maximum range of the machine. For example, the SOLA ADCP has 26 bins with a range of 1 m and thus has a range of 26 m. The ADCP was put at a depth of 27 m and takes the first measurement is taken at 2.1 m from the bottom. Therefore, he maximum depth is 24.9 m. The current meters take measurements at least every hour. Some take measurements every 30, 20 or 15 minutes and SAVED even takes a measurement every minute. Most ADCPs in this study use a frequency of around 600kHz, appart from SAVED, which uses a frequency of 150kHz. The SP-ADCMs all emit a frequency of around 2MHz.

$$M_{Obs} = \sqrt{{U_{Obs}}^2 + {V_{Obs}}^2}$$

Equation 2.1: The Pythagoras theorem is used to calculate the magnitude of the current calculated by the model.

$$\sigma_{Obs} = \operatorname{atan}\frac{V}{U}$$

Equation 2.2: Calculation of the angle from the North/East components (V and U resp.)

$$U_{Obs} = M_{Obs}.\cos(\sigma_{Obs})$$

$$V_{Obs} = M_{Obs}.\sin(\sigma_{Obs})$$

Equation 2.3 and 2.4: Calculation of North (V) and East (U) components based on the magnitude (M) and angle (σ).

Depending on the data, either the North/East components (V and U resp.) were provided, or a combination of the magnitude and angle. In case of the former, the magnitude was calculated using the Pythagoras theorem (equation 2.1) and angle was calculated using equation 2.2. In case of the latter, the North/East components were calculated using equation 2.3 and 2.4.

The observations were filtered for erronous data, as explained in chapter 1.

Table 2.2: Properties of the observations, including the number of bins, the bin size, the observational depth (*only max. depth for ADCPs), the time step, the type of equipment (emitted frequency), the position coordinates, the resolution of the model at these coordinates, the mean slope at these coordinates and the surrounding coordinates and the source. X: not applicable

	Nr. of bins	Bin size (m)	Obs. Depth (m)	Time step (min)	Equipment (Frequency)	Latitude (degrees)	Longitude (degrees)	Resolution (m)	mean Slope (%)	Source
Creus	1	x	295	30	SP-ADCM (2MHz)	42.39	3.3217	170	2.1	Schroeder et al., (2013)
LD	2	x	505 975	60	SP-ADCM (2MHz)	42.4281	3.5448	230	8.0	Durrieu de Madron et al., (2019)
Lion	5	x	152 246 501 1002 2330	30	SP-ADCM (2MHz)	42.0373	4.6861	620	0.6	Testor et al., (2018); Houpert et al., (2016); Durrieu de Madron et al., (2019)
Planier	2	x	505 975	60	SP-ADCM (2MHz)	43.0151	5.1921	440	8.1	Durrieu de Madron et al., (2019)
Mesurho	40	0.75	18.7*	10	ADCP (600 kHz)	43.32	4.87	330	1.8	Pairaud et al., (2016)
POEM	65	0.50	28.1*	60	ADCP (600kHz)	42.7042	3.0667	170	0.5	Bourrin et al., (2015)
SOLA	26	1.00	24.9*	20	ADCP (614.4 kHz)	42.4883	3.145	120	0.7	Unpublished Guizien
BeSete (2010-2011)	99	0.25	24.6*	20	ADCP (614.4 kHz)	43.3339	3.6396	330	0.4	Unpublished Leredde
BeSete (2012-2013)	54	0.50	24.4*	20	ADCP (614.4 kHz)	43.3339	3.6396	330	0.4	Unpublished Leredde
SAVED	60	4.00	244.3*	1	ADCP (150kHz)	Trajectory				SAVED (1996)

2.2.2 Model

The SYMPHONIE2015 model solves hydrostatic primitive equations to calculate the current velocities in the Gulf of Lion. In this thesis, the grid and setup as described in Briton et al. (2018) was used with an Arakawa C curvilinear grid under Boussinesq approximation (figure 2.5). Horizontal meshing is 680x710 which was adapted to the shape of the Gulf of Lion using a transformation of the Earth's spherical coordinates that preserves local angles. This bipolar grid allowed for higher resolution at the coastal moorings (110 m) than in the open ocean (3.13 km) (figure 2.5, 2.6). The water column was divided in 29 vertical sigma levels. At depths lower than 100 m, the vertical spacing is regular. At depths deeper than 100 m, the spacing is irregular, with spacing of 3.5 m at the surface that increases towards the bottom. The sea-surface and the open-sea boundary conditions were updated every 3 h from regional downscaled climatic simulations NM12-FREE (6–7 km horizontal resolution; Hamon et al., 2016). The atmospheric model ALADIN, which was forced by ERA-interim atmospheric reanalysis (every 3 h, 12 km horizontal resolution), was coupled with the oceanic model NEMO-MED 12 (Hamon et al., 2016). The discharge of twelve rivers was added to the open-boundary forcing: Agly, Argens, Aude, Baillaury, Ebro, Grand Rhône, Hérault, Orb, Petit Rhône, Tech, Têt and the Var. The model's output is saved four times per hour on minute 0, 20, 30 and 40 (figure 2.4).

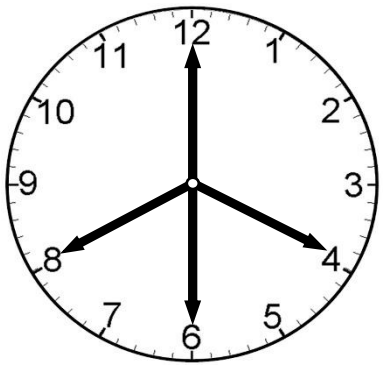

Figure 2.4: Extraction times. The model has output for every point on the grid every hour 20, 30 and 40 minutes past the hour and on the hour.

An example of the modelled current can be seen in figure 2.7 with strong currents near the coast and around the Northern Current.

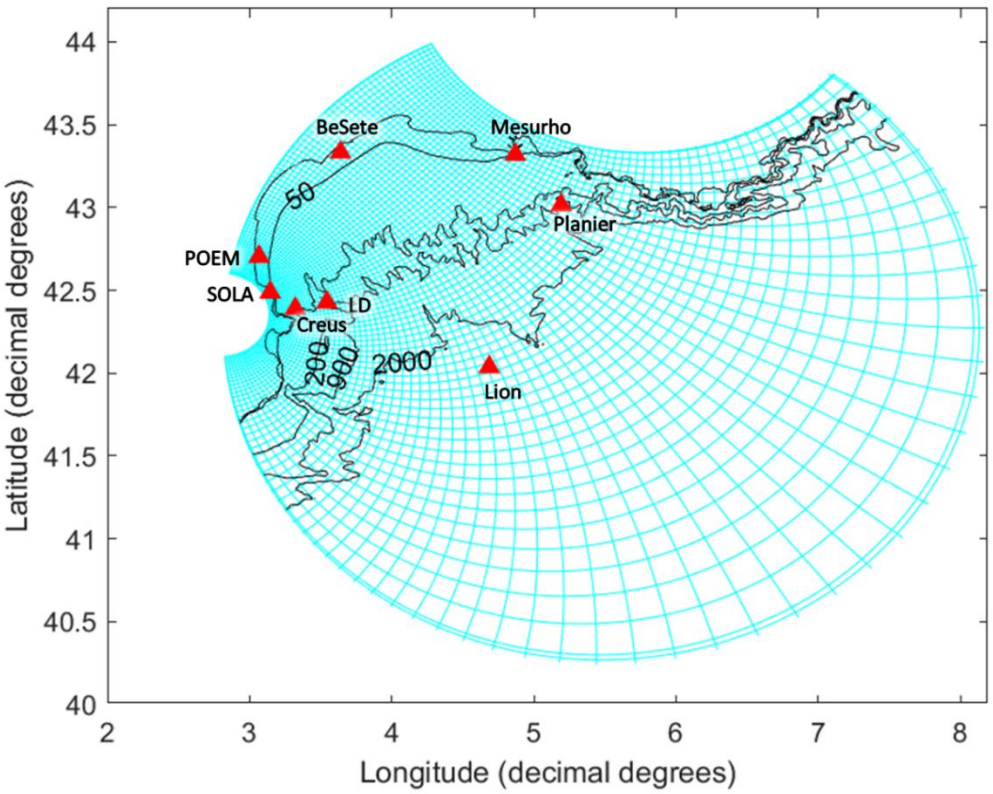

Figure 2.5: Model grid. Spatial extent of the simulated domain with the bipolar grid (680x710; with one blue line every 10 cells) and the 1-, 50-, 200-, 900-, and 2000 m bathymetric contours. Parameters for the projection were as follows: North pole (44.2°N, 5.3°E); South pole (42.37°N, 2.82°E); grid point (170; 710) corresponding to 47°N, S°E); and the reference latitude for Mercator projection was 52 °N (Briton et al.*, 2018).*

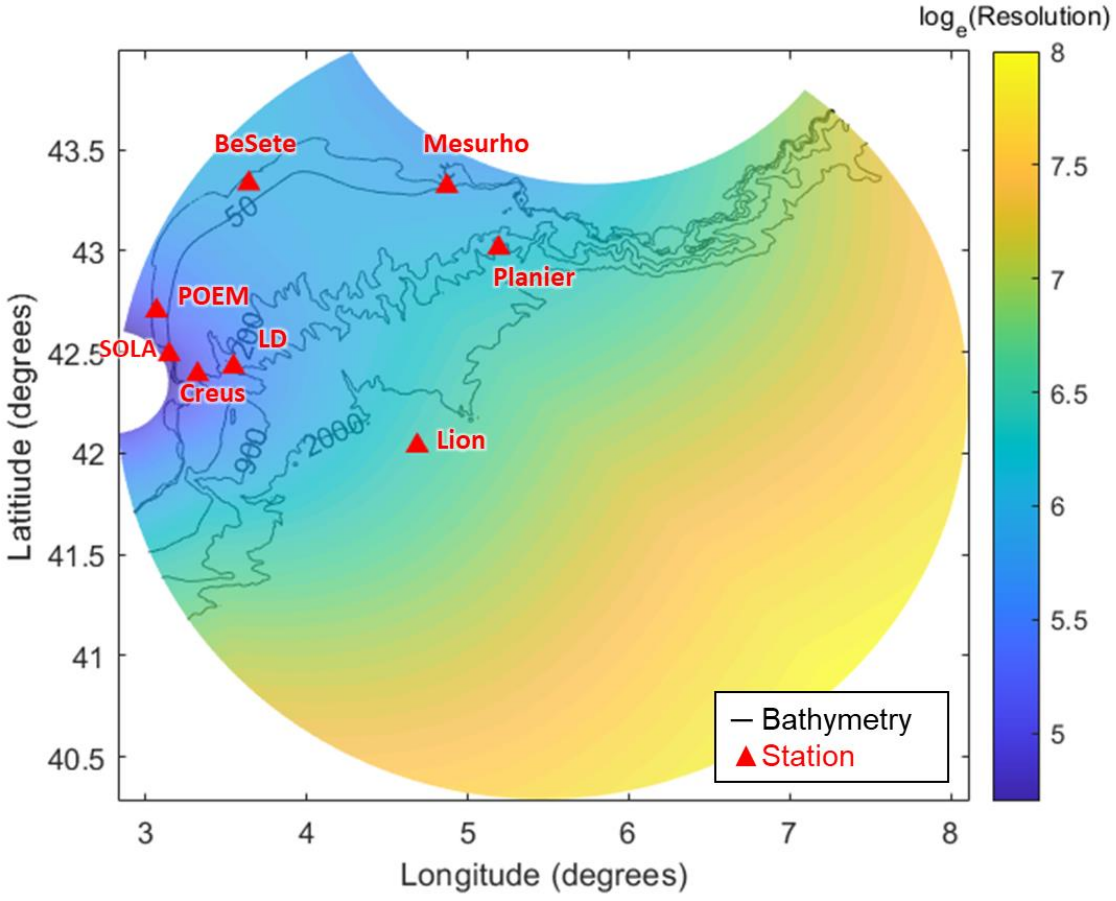

Figure 2.6: The natural logarithm of the resolution of the model in meters.

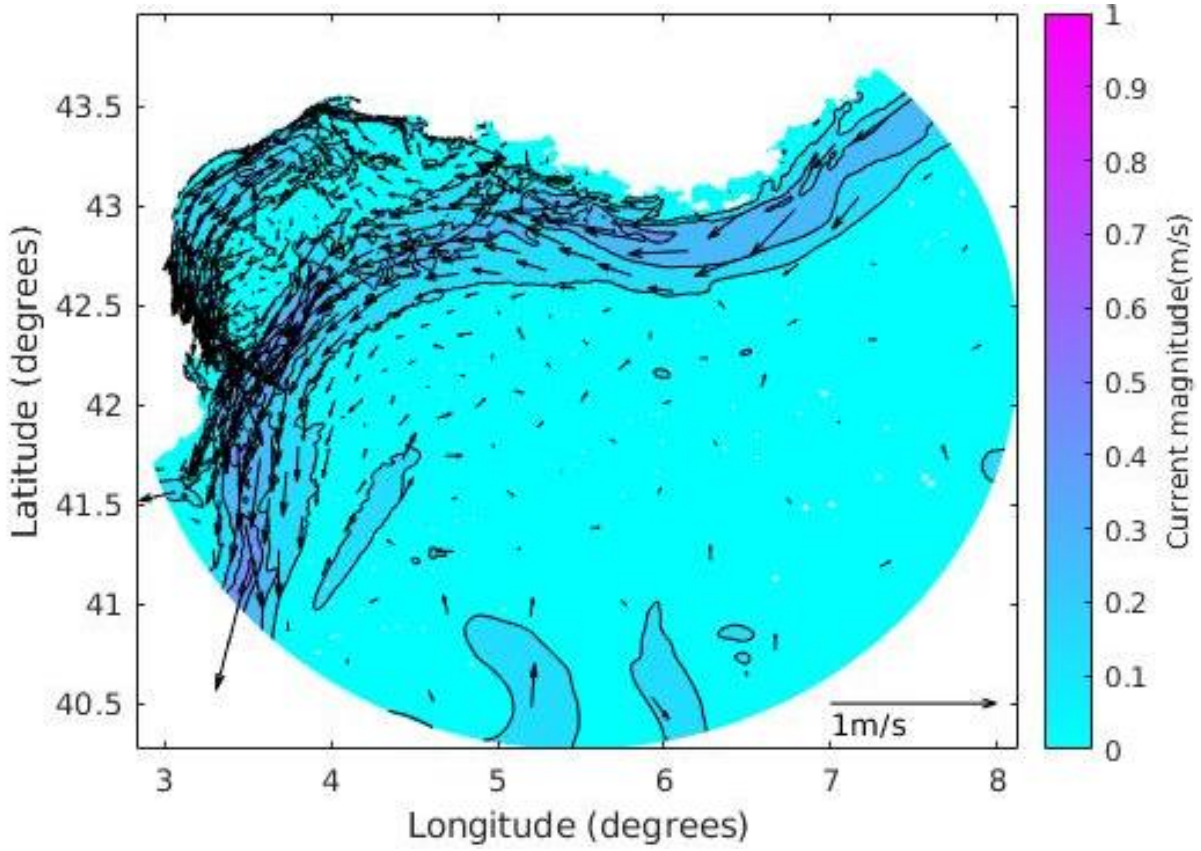

Figure 2.7: The modelled current according to the SYMPHONIE2015 model on 01/11/2010 00:30:20 for the 20th sigma level for every 30th grid point. The background colours and sizes of the arrows depict the magnitude.

2.2.3 Extraction

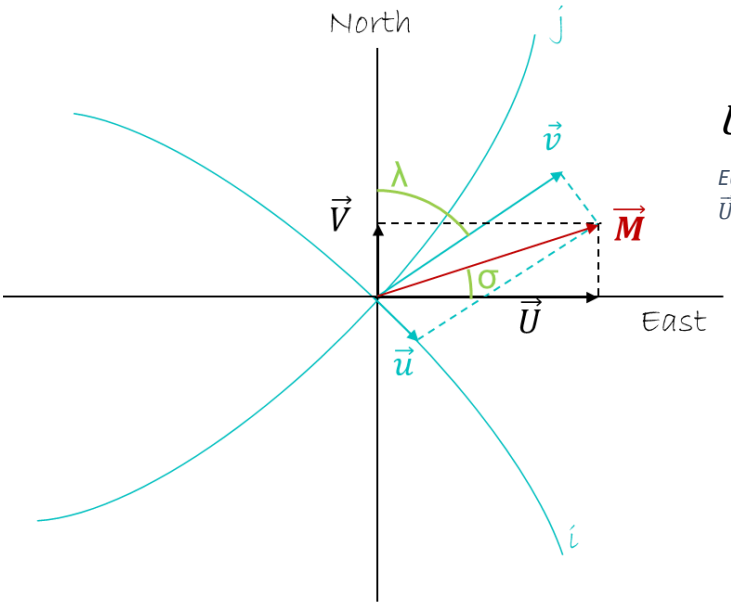

$$V_{Mod} = v.cos(\lambda) - u.sin(\lambda)$$

$$U_{Mod} = u.cos(\lambda) + v.sin(\lambda)$$

Equation 2.5 and 2.6 Equations on how to calculate $\vec{U}$ and $\vec{V}$ along the North/East axes.

Figure 2.8: Scheme on how to transform $\vec{u}$ and $\vec{v}$ along the axes of the model grid into $\vec{U}$ and $\vec{V}$ along the North/East axes.

The model output gives the $\vec{u}$ and $\vec{v}$ value of the current along the axes of the curvilinear grid described in figure 2.5, but not along the North/East axes. Therefore, a transformation must be done in order to know the currents along the North/East axes ($\vec{V}$ and $\vec{U}$ resp.) and figure 2.8 shows how the transformation from $\vec{u}$ and $\vec{v}$ along the grid's i and j axes into $\vec{U}$ and $\vec{V}$ along the North/East axes is calculated using the equations 2.5 and 2.6. To calculate the magnitude of the model, Pythagoras was applied (equation 2.1). Later, the angle of the current was calculated using equation 2.2.

The model's grid is staggered, meaning that when we take a closer look at a single grid cell, the vectors of all the current speeds grab on in different places (figure 2.9). It is the sum of the vectors u, v and w which form the velocity. Since the locations of the observation moorings don't overlap exactly with the points of the model grid, the data from the four grid points surrounding the observation point are extracted.

In figure 2.10, four grid cells like the ones in figure 2.9 are depicted next to each other in 2D from top view. If we take the blue dot, which represents the observation point, that means

that T1,2,3,4; u1,2,4,5 and v3,4,5,6 need to be extracted. Only the horizontal currents were analysed in this study and only the point closest to the observational point was used to assess the error.

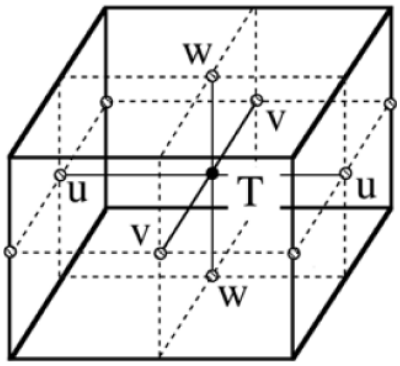

Figure 2.9: Representation of the Arakawa C grid (Mikolajczak 2019). u is the speed of the current entering or leaving the grid cell by the sides. v is the speed of the current entering or leaving the grid cell by the front and back. w describes the vertical movements of the water entering or leaving through the top and bottom of the grid cell. T, or temperature, is calculated in the middle of the grid cell.

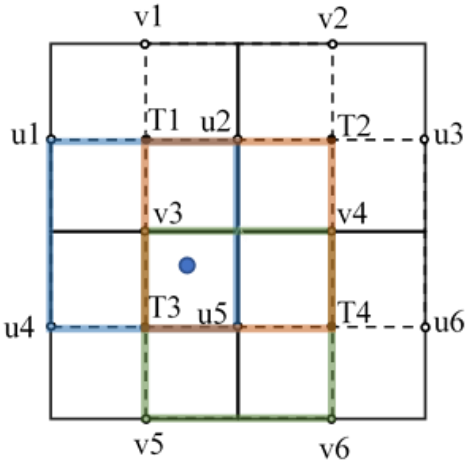

Figure 2.10: Four grid cells in 2D using the conformal projection (Bentsen et al.*, 1999). The blue dot is an observation point.*

However, the modelled currents $\vec{V}$ and $\vec{U}$ were calculated at different depths than the observations. On this vertical plane, the model values must be interpolated to velocity per observed depth instead of per sigma layer to compare between model and observation. Figure 2.11 shows a simplified scheme of the sigma levels and in combination with equation 2.7 and 2.8, it explains how to interpolate between the

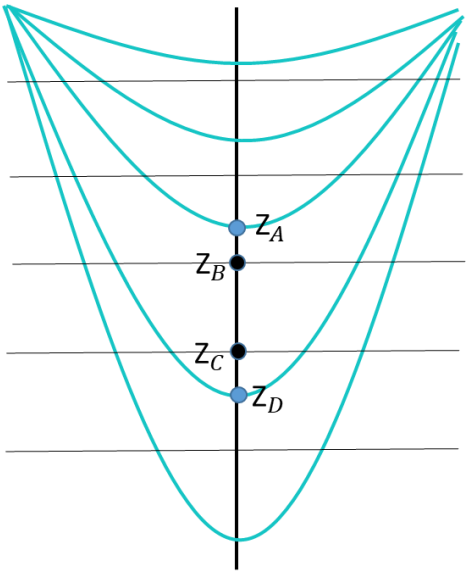

Figure 2.11: Scheme on how to rescale the modelled current speed from speed per sigma layer to speed per observed depth. In blue the sigma grid is depicted and the black lines are the observation depths. Z is the depth at points A, B, C and D.

$$M_B = M_A.\left(1 - \frac{|Z_B - Z_A|}{|Z_D - Z_A|}\right) + M_D.\left(\frac{|Z_B - Z_A|}{|Z_D - Z_A|}\right)$$

$$M_C = M_D.\left(1 - \frac{|Z_B - Z_A|}{|Z_D - Z_A|}\right) + M_A.\left(\frac{|Z_B - Z_A|}{|Z_D - Z_A|}\right)$$

Equation 2.7 and 2.8: Calculation of current speed per observational depth (Z), using the modelled current speed (M) per sigma layer.

sigma levels to recalculate the modelled current speed to have a speed per observed depth level. For deep moorings like e.g. Lion, observations were only taken at a few depths (Table 2.2) and thus model extractions were only made at the corresponding depths.

It must be mentioned that some of the observations were measured deeper than the model bathymetry. This could be due to the smoothing of the bathymetry or displacement of the buoy during storm events. In this case, the modelled current was not rescaled between the two sigma layers, as the observation point was beyond the scope of these layers. Therefore, at times when the observation was measured at a deeper level than the model bathymetry, the current was rescaled at a depth which was the same distance from the model bottom as the observation was from the real bottom (figure 2.12). This was only done for the deepest observation of the mooring, as other observations did not have this problem. This corresponds to all the extractions at 295 m depth of the Creus mooring, all the extractions at 975 m of the LD mooring, all but the last month of the Lion mooring at 2330 m depth and twelve months of the Planier mooring at 975 m depth.

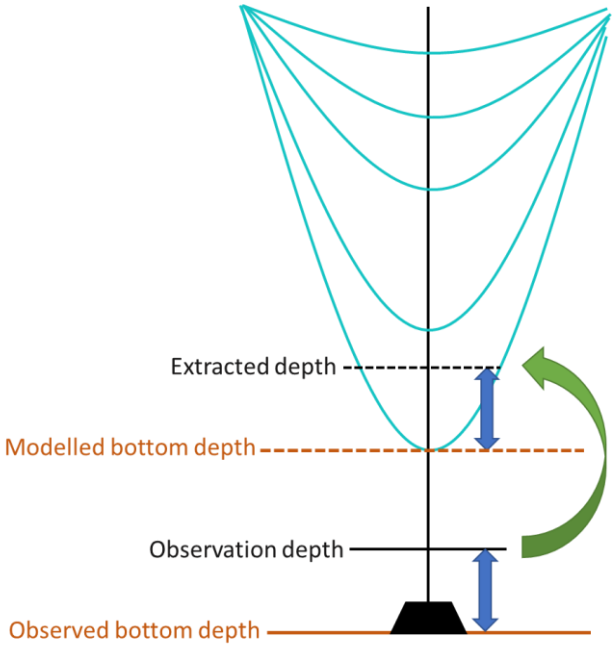

Figure 2.12: Scheme explaining where the extractions were taken in case the observation depth was deeper than the model bathymetry. The curved blue lines are the model sigma layers. The lowest sigma layer touches the modelled bottom depth. The extracted depth is the same distance from the modelled bottom as the observation depth is from the observed bottom depth.

2.2.4 Error vector calculation

$$\varepsilon_{\mathrm{East}} = \mathrm{U}_{\mathrm{Mod}} - \mathrm{U}_{\mathrm{Obs}}$$

$$\varepsilon_{\mathrm{North}} = \mathrm{V}_{\mathrm{Mod}} - \mathrm{V}_{\mathrm{Obs}}$$

Equation 2.9 and 2.10: Magnitude error calculation on the East and North axes. U is the current magnitude in the eastern direction. V is the current magnitude in the northern direction.

$$\varepsilon_{\mathrm{Magnitude}} = \sqrt{{\varepsilon_{\mathrm{East}}}^2 + {\varepsilon_{\mathrm{North}}}^2}$$

Equation 2.11: Total magnitude error calculation using the magnitude error on the East (ε_{East}) and North (ε_{North}) axes.

$$\varepsilon_{\mathrm{Angle}} = \mathrm{atan}\left(\frac{\varepsilon_{\mathrm{North}}}{\varepsilon_{\mathrm{East}}}\right)$$

Equation 2.12: Total angle error calculation using the magnitude error on the East (ε_{East}) and North (ε_{North}) axes.

Contrary to the previous chapter, the instant error vector is calculated for every depth level and every time step. The instant error vector calculation between observed and modelled current magnitude and angle is performed using equations 2.9-12. First, the difference between the observed and modelled East and North components is calculated (equations 2.9-10). These values are then used to calculate the magnitude of the error vector (equation 2.11) and the angle of the error vector (equation 2.12). The error vector was calculated for corresponding times and depths. After that, cumulative distribution frequency plots (cfd-plots) were made to assess the distribution of the error. In chapter 2, only difference in error distribution of the magnitude was assessed. The error of the angle shall be used in chapter 3.

2.2.5 Statistical methods

In order to test whether the error distribution is the same through time and space, the deviation between the cfd-plots was quantified and statistical tests were performed. The deviation quantification was performed on cfd-plots as a calculation of the difference in surface between the cfd-plots. The cfd-plot area was calculated by creating a relative cumulative frequency histogram with 200 classes and summing the surfaces of the bins. The

statistical tests which were used were the Wilcoxon rank sum test (WRS-test; α=0.5) and the Kolmogorov-Smirnov test (KS-test; α=0.5). The WRS-test gives information on whether the medians are significantly different and the KS-test tests whether the two complete distributions are significantly different. The WRS- and KS-tests perform a non-parametric test which allows the comparison of groups with different sample sizes. These tests were chosen because the data was non-normal (Shapiro Wilk test; α = 0.05) with unequal variance (F-test; α = 0.05) and had different sample sizes. The problem was that these tests were designed for small sample sizes, whilst my sample sizes are sometimes bigger than two million. This meant that they had enough power to detect the differences which were of no practical significance and declare them significantly different. In other words, almost all distributions were always significantly different, even if the deviation quantification was small. As a confirmation, a pre-analyses was done to see how the p-value evolved depending on the number of extracted points. Namely, the original error magnitude distribution over all stations and time was statistically (WRS-test) compared to itself, using a different amount of extracted points. The graph (appendix figure 2.A1) showed that the more points were extracted for the WRS-test, the smaller the p-value became (p = 0.9999 for 50 extraction points to p = 0.9961 for 100 000 extraction points). This is remarkable, as one would expect that the more points are extracted, the p-value would be closer to one as it is closer to the original dataset and thus more alike. This shows that the more data is used, the more the WRS-test becomes unnecessarily powerful, since there is a lower p-value for when more points are extracted.

To resolve this problem, a subsampling was performed of the original data. An X amount of points with equal intervals were selected on the y-axes of the cfd-plot (with X the number of extracted points) and the corresponding error values on the x-axes were selected.

The amount of datapoints to extract (X) was decided in another pre-analyses, which compared the difference in cfd-plot area between the two distributions to the p-value of the corresponding WRS-test. This was done for both the seasons (appendix figure 2.A2 A) and all stations from December to May (appendix figure 2.A2 B). The same pre-analysis was done on the KS-test, which was less sensitive, but still had a varying p-value depending on the sample size. The number of extracted points was calibrated in order to detect the difference between two CFDs when the difference in surface area was larger than 1.5 cm/s. Based on these pre-analyses, it was decided to extract 100 points from every distribution, as it still has plenty of power, as is shown in figure 2.A1. In short, to perform the KS-test and the WRS-test, 100 points were extracted at equal intervals from the original cfd-plots of the error magnitude.

2.2.6 Temporal and spatial difference in error distribution

The general outline of the temporal and spatial analyses of the differences in error distribution can be summarized as follows (table 2.3):

Table 2.3: Overview of temporal and spatial analyses

Temporal analyses	Intraseasonal		
	Interseasonal		
Spatial analyses	Top layer	Bathymetry zones	Shallow Moorings
	Bottom layer		Deep Moorings

To compare the error distributions in **time**, the error distributions of all seasons over the three and a half years (2010 - June 2013) were compared to each other. We searched for intra- and interseasonal differences.

Since the unstratified period starts in December (Houpert et al., 2015) and every season was chosen to have the same duration, the seasons were defined the same as in Somot (2005) and Somot et al. (2008):

- Winter: December-February
- Spring: March-May
- Summer: June-August
- Autumn: September-November

To compare the error distributions in **space**, only the data available during winter and spring months (December-May) was used, as the shallow stations had little data available for the summer and autumn months.

A step-by-step procedure was developed to compare the error distribution in space (figure 2.13). The first step was to see if trajectory data was available. In this study, the trajectory data of SAVED was available for most of the study period. This is why the water column was divided into two parts: The surface layer, which spans from the surface to the maximum range (R_{max}) of the trajectory data of the SAVED ADCP (≈200 m), and the bottom layer, which spans from the R_{max} to the bottom. A more visual representation of the water column and the data measurement equipment can be found in figure 2.14.

For **the surface layer**, the trajectory data is the only data which has trajectory data over a variety of latitudes and longitudes, which is why the SAVED data is treated first (figure 2.13A). Based on the results from chapter 1, it was clear that the model's error varied based on depth and position of the station. This why the difference in magnitude error distribution was originally divided per bathymetry. The hypothesized bathymetry zones, later called "alleged bathymetry zones", can be seen in figure 2.14 A.

The alleged bathymetry zones are:

- 0-50 m: The shallow zone
- 50-200 m: The continental shelf
- 200-900 m: The canyon head
- 900-2000 m: The canyon lower reach
- 2000 m <: The abyssal plain

If there is no significant difference in error distribution between the alleged bathymetry zones, they are grouped into the actual bathymetry zones. If not, they remain separate.

The next step is to test the error distributions of the mooring data and the trajectory data within the same bathymetry zone (figure 2.13A). In this case, all the shallow stations belonged to the same bathymetry zone and their error magnitude distributions were compared to each other. The data with similar error distributions is grouped.

Next, **the bottom layer** (200 m - bottom; figure 2.13B and 2.14B) is researched. Here, the error distribution of the mooring stations present in this layer are tested against each other. The Lion station is the only station which has four SP-ADCMs in the bottom layer and one in the surface layer (152 m; figure 2.14B). Therefore, the one in the surface layer is not taken into account for the analysis in the surface layer nor for the one in the deep layer. Only the error distributions acquired with the SP-ADCMs in the bottom layer are compared to the other moorings present in the deep layer. Mooring stations with similar magnitude error distributions are grouped.

How to create distribution zones:

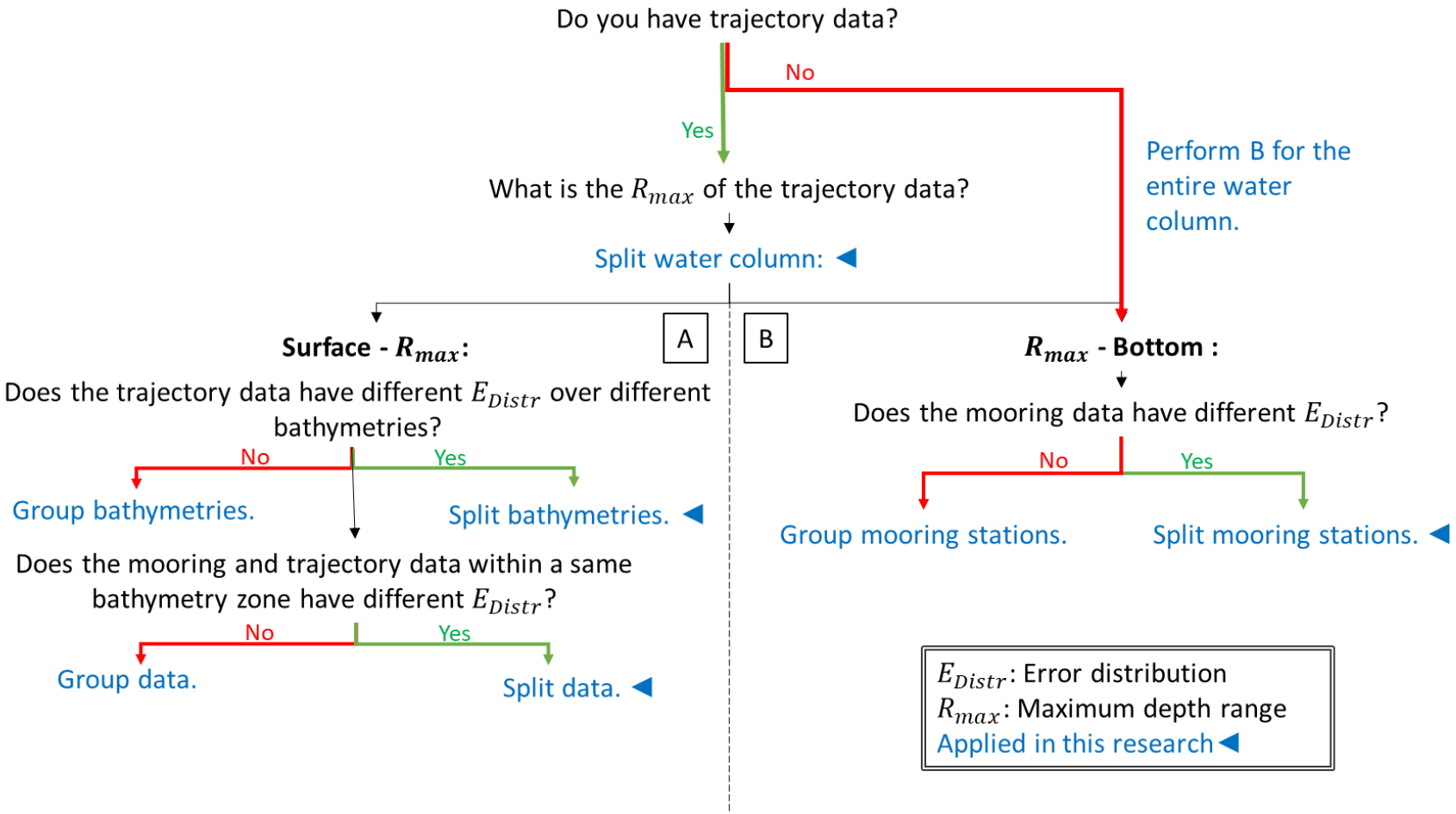

Figure 2.13: Scheme on how to build distribution zones.

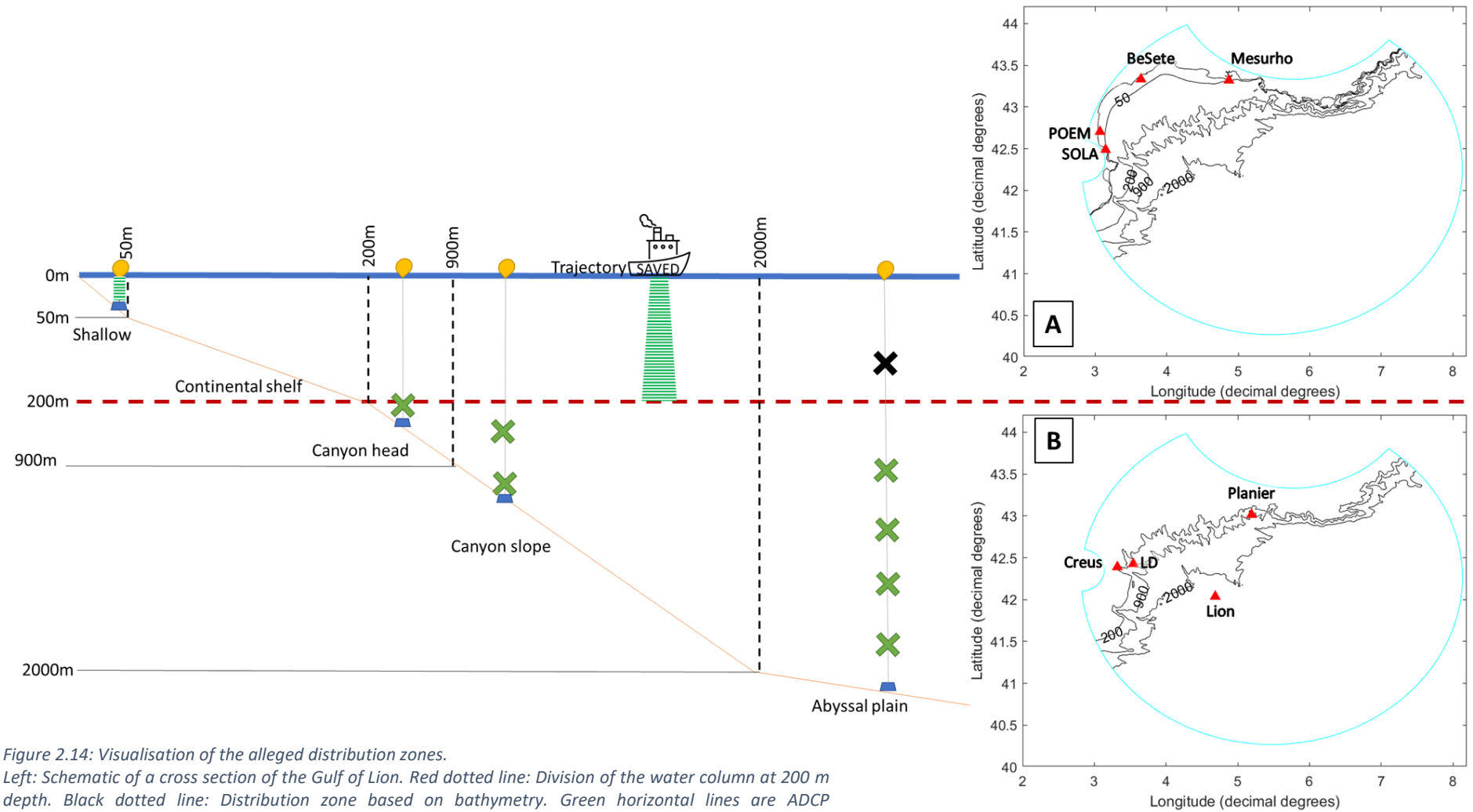

Figure 2.14: Visualisation of the alleged distribution zones.
Left: Schematic of a cross section of the Gulf of Lion. Red dotted line: Division of the water column at 200 m depth. Black dotted line: Distribution zone based on bathymetry. Green horizontal lines are ADCP measurements over the entire water column (max. 200 m). Green crosses are SP-ADCM measurements at several depths. Black crosses are SP-ADCM measurements that are not taken into account.
A: Distribution zones in the top water layer (0-200 m).
B: Distribution zones in the bottom water layer (200 m <).

2.2.7 Environmental and modelling characteristics

When spatial differences were detected, the relationship with some environmental and modelling characteristics was tested. Namely the stratification, the depth of the observations, the correlation between the observed current speed and the error magnitude, the steepness of the slope and the resolution of the model.

The **stratification** was calculated using the Brunt–Väisälä frequency (chapter 1 annex B equation B2). Only the shallow stations were considered, since those were the only ones with modelled profile data for salinity and temperature. In other words, these were the only stations with enough vertical levels to make a thorough assessment of the vertical stratification. The link between the stratification index and the mean of the error magnitude over depth was assessed.

Moreover, the correlation between the magnitude error and the **speed of the observed current** was calculated.

Furthermore, boxplots were made of the error magnitude per station and compared to the deepest observation **depth**, the **steepness of the slope** and the **resolution** of the model at these stations. These values can be found in table 2.2.

The **slope** was calculated using equation 2.13 in one direction and 2.14 in the other, which calculates the percentage of the slope over the grid resolution. It is the slope in percentage over the resolution of the grid, not per meter. Then, the maximum of the absolutes of the two directions was taken (equation 2.15). This was done at the grid point closest to the observational point and the eight surrounding grid points. The mean of these nine values is the eventual slope which can be found in table 2.2. The mean was taken because some

stations are located in the valley of a canyon. At the bottom of the valley, the slope is flat, whilst they are surrounded by steep slopes.

$$P_{i\to j} = \frac{Z_{(j+1,i)} + Z_{(j-1,i)}}{\frac{2\pi R}{360}\sqrt{\left[lat_{(j+1,i)} - lat_{(j-1,i)}\right]^2 + \left[\left(lon_{(j+1,i)} - lon_{(j-1,i)}\right) * \cos\left(lat_{(j,i)}\right)\right]^2}}$$

$$P_{j\to i} = \frac{Z_{(j,i+1)} + Z_{(j,i-1)}}{\frac{2\pi R}{360}\sqrt{\left[lat_{(j,i+1)} - lat_{(j,i-1)}\right]^2 + \left[\left(lon_{(j,i+1)} - lon_{(j,i-1)}\right) * \cos\left(lat_{(j,i)}\right)\right]^2}}$$

Equation 2.13 and 2.14: The slope P (%) of the ocean bottom in both directions at grid coordinates i,j . Z is the depth, lat is latitude, lon is longitude, R is the radius of the earth.

$$P = \max\left(|P_{i\to j}|, |P_{j\to i}|\right)$$

Equation 2.15: The maximum of the slopes in both directions P (%).

2.3 Results

2.3.1 Temporal variability of the error magnitude distribution

The intra- and interseasonal difference in error distribution was assessed for all seasons from 2010 to June 2013. Figure 2.15 shows the cfd-plots of all seasons. The **intraseasonal difference** in error distribution, which is the variation within one season (colour) for different years, is slightly smaller than the **interseasonal variation**, which is the variation between different seasons for the same year (line style). The exception to this is summer 2013, during which the model has a bigger error than during the summers of other years. The winter and spring seasons are quite alike and autumn is either similar to spring or summer (figure 2.15).

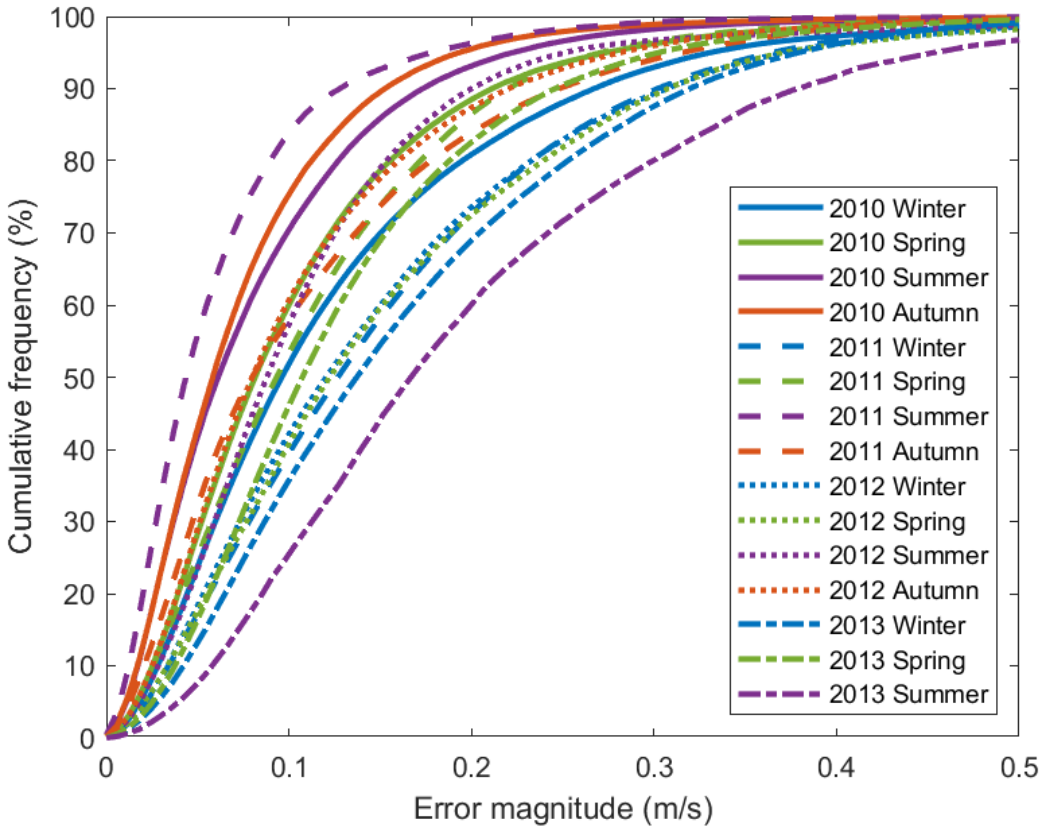

Figure 2.15: The cfd-plots of the error on the magnitude for all seasons. The years are ordered per line style. 2010 has a full line (-), 2011 has stripes (- -), 2012 has dots(⋯) and 2013 has dots and stripes (· -). The seasons are ordered per colour. Winter is blue, spring is green, summer is purple and autumn is dark orange.

On figure 2.16, the heatmap of the area between the error magnitude cfd-plots is shown and figure 2.17 shows this data in two scatter plots. These figures show largely the same information as explained before.

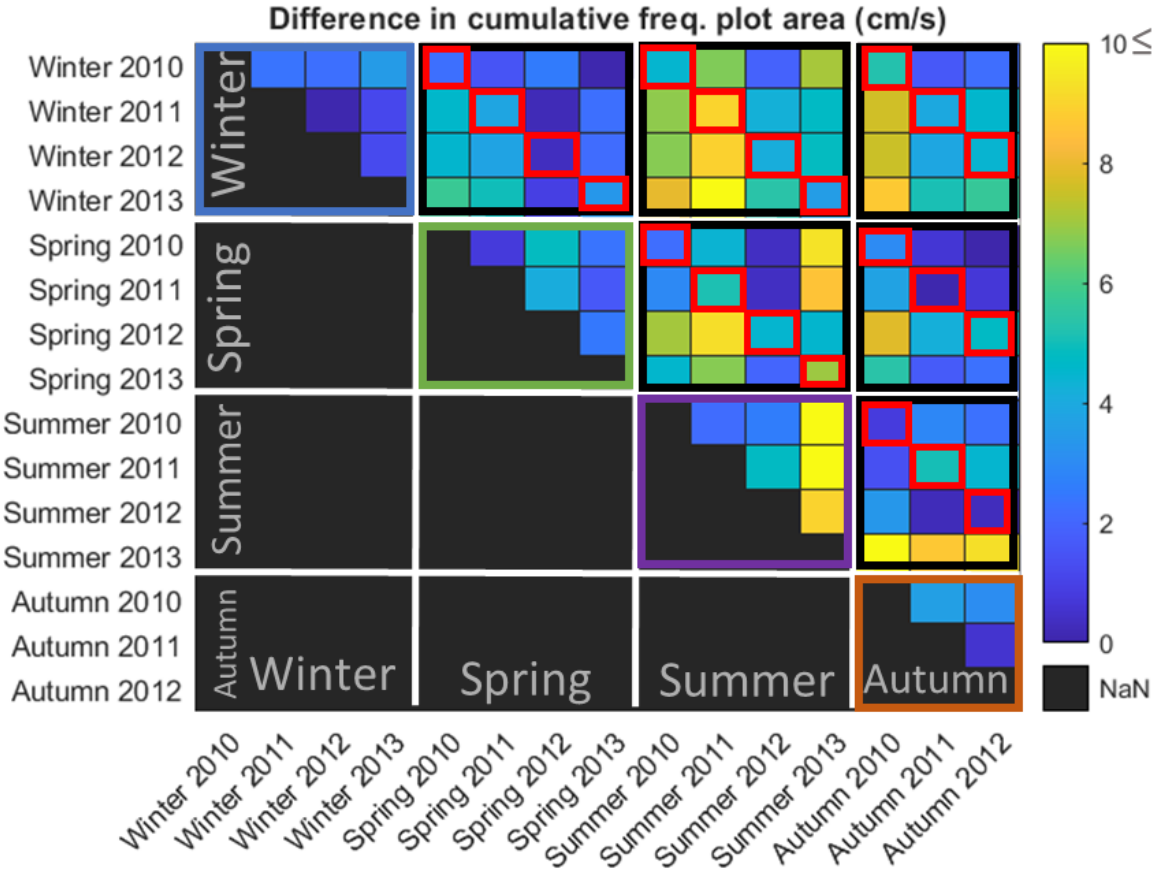

Figure 2.16: Heatplot of the surfaces between the cfd-plots of the seasons, showing intraseasonal (winter=blue, spring=green, summer=purple, autumn=orange) and interseasonal (same years=red).

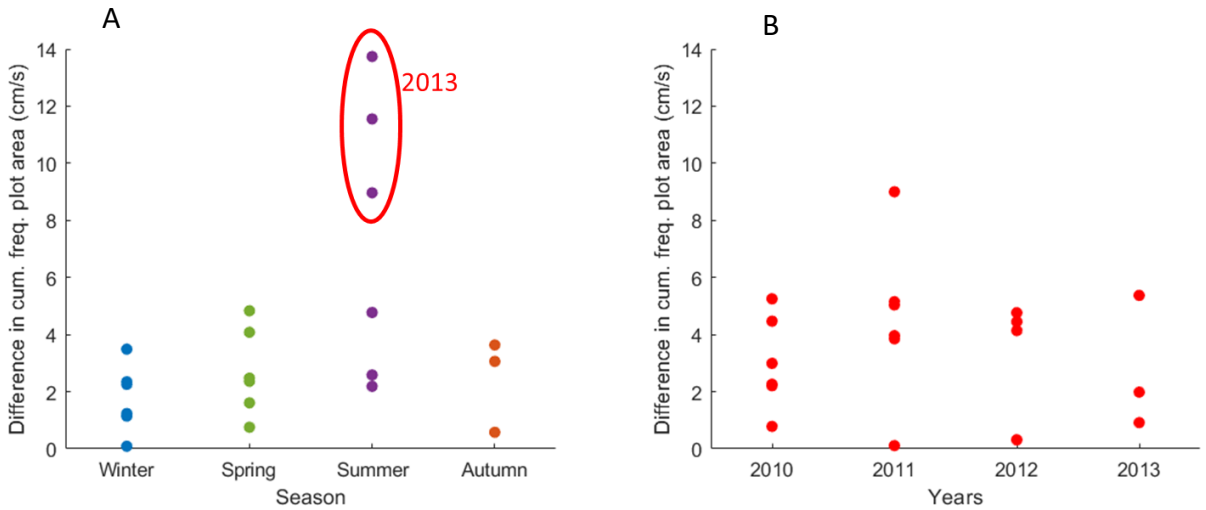

Figure 2.17: Scatter plot of the difference in cumulative frequency plot area compared to seasons as depicted in figure 2.14. A) Intraseasonal variation (winter=blue, spring= green, summer=purple) B) Interseasonal variation

Namely, the intraseasonal difference in error distribution is slightly smaller than or equal to the interseasonal difference (figure 2.16, 2.17). The exception to this is summer 2013, which is shown in figure 2.16 to have a very different error distribution than the other seasons.

Table 2.4 shows the p-values of the WRS-test between the medians of the seasons. They show that although the area between some of the error magnitude cfd-plots is quite small, the zero hypothesis that the medians of the distributions are identical, is often rejected. This can be seen within the seasons of the same year (background colours), which in figure 2.16 seem quite similar, but often have a p-value < 0.05 in table 2.4. The amount of times there is a significant difference in intraseasonal median error distribution (frame colours) is slightly smaller than the interseasonal difference (background colours) according to the WRS-test (12 out of 21 intraseasonal p-values < 0.05 VS 15 out of 21 interseasonal p-values < 0.05, resp.). The intraseasonal difference in error distribution for summer is quite large, with all p-values rejecting the H0 that the median error distributions for the summers of different years are similar.

The KS-test rejects the H0 of equal distributions less than the WRS-test rejects the one of equal medians. Table 2.5 does show that the intraseasonal difference (frame colours) in error distribution is slightly smaller than the interseasonal difference (background colours), according to the KS-test (6 out of 21 intraseasonal p-values < 0.05 VS 11 out of 21 interseasonal p-values < 0.05, resp.). It also shows that the error distributions of winter are often quite similar to those of spring and the error distributions of autumn were similar to those of either spring or summer.

Although the intraseasonal variation is smaller than the interseasonal one when eliminating summer 2013, the difference in variation is still quite small when comparing figure 2.17A to B.

Table 2.4: P-values of the WRS-test between the seasons, organised per season (frame colours): winter (blue), spring (green), summer (purple), autumn (orange) for all years (background colours): 2010 (yellow), 2011 (light orange), 2012 (brown), 2013 (red). The p-values which are significantly different (<0.05) are in bold.

P-values WRS-test 100 points		Winter				Spring				Summer				Autumn		
		2010	2011	2012	2013	2010	2011	2012	2013	2010	2011	2012	2013	2010	2011	2012
Winter	2010		0.0645	0.1182	**0.0084**	0.1753	0.5570	0.0801	0.4242	**0.0007**	**0**	0.3491	**0**	**0.0001**	0.2072	0.1700
	2011			0.7764	0.4570	**0.0011**	**0.0117**	0.9309	0.2063	**0**	**0**	**0.0032**	**0.0089**	**0**	**0.0030**	**0.0012**
	2012				0.2906	**0.0032**	**0.0281**	0.8567	0.3553	**0**	**0**	**0.0091**	**0.0042**	**0**	**0.0070**	**0.0036**
	2013					**0**	**0.0009**	0.3875	**0.0356**	**0**	**0**	**0.0002**	0.0598	**0**	**0.0002**	**0.0001**
Spring	2010						0.3955	**0.0018**	**0.0197**	0.0285	0	0.6031	0	**0.0054**	0.9885	0.9866
	2011							**0.0165**	0.1555	0.0033	**0**	0.6736	0	**0.0004**	0.4776	0.3862
	2012								0.2539	0	0	0.0049	0.0074	**0**	**0.0042**	**0.0019**
	2013									0	0	0.0557	0.0001	**0**	**0.0367**	**0.0197**
Summer	2010										**0.0158**	**0.0064**	**0**	0.6183	**0.0432**	**0.0333**
	2011											**0**	**0**	**0.0429**	**0**	**0**
	2012												**0**	**0.0007**	0.6630	0.5848
	2013													**0**	**0**	**0**
Autumn	2010														**0.0109**	**0.0066**
	2011															0.9942
	2012															

Table 2.5: P-values of the KS-test between the seasons, organised per season(frame colours): winter (blue), spring (green), summer (purple), autumn (orange) for all years (background colours): 2010 (yellow), 2011 (light orange), 2012 (brown), 2013 (red). The p-values which are significantly different (<0.05) are in bold.

P-values KS-test 100 points		Winter				Spring				Summer				Autumn		
		2010	2011	2012	2013	2010	2011	2012	2013	2010	2011	2012	2013	2010	2011	2012
Winter	2010		0.3499	0.5626	0.1024	0.7992	0.9926	0.4496	0.7992	**0.0327**	**0**	0.6828	**0.0006**	**0.0054**	0.6828	0.7992
	2011			1	0.9995	**0.0138**	0.1438	1	0.5626	**0.0001**	**0**	**0.0215**	0.1438	**0**	**0.0327**	**0.0138**
	2012				0.9627	**0.0327**	0.2659	1	0.6828	**0.0004**	**0**	**0.0327**	0.0715	**0**	0.0715	**0.0489**
	2013					**0.0019**	**0.0327**	0.9926	0.1976	**0**	**0**	**0.0032**	0.4496	**0**	**0.0054**	**0.0019**
Spring	2010						0.9627	**0.0327**	0.1976	0.2659	**0.0004**	0.9926	**0**	0.1024	0.9995	1
	2011							0.1976	0.6828	**0.0489**	**0**	0.9926	**0.0001**	**0.0087**	0.7992	0.8972
	2012								0.5626	**0.0001**	**0**	**0.0327**	0.1024	**0**	**0.0489**	**0.0327**
	2013									**0.0006**	**0**	0.4496	**0.0019**	**0.0001**	0.0715	0.1438
Summer	2010										0.1438	**0.0489**	**0**	0.9926	0.3499	0.3499
	2011											**0**	**0**	0.2659	**0.0019**	**0.0006**
	2012												**0**	**0.0138**	0.6828	0.9627
	2013													**0**	**0**	**0**
Autumn	2010														0.0715	0.1438
	2011															0.9995
	2012															

2.3.2 Spatial variability of the error magnitude distribution

The error distributions of all stations can be seen in figure 2.18. The deep stations LD and Planier have the lowest magnitude error, then the shallow stations SOLA, POEM and BeSete follow together with the Lion station and the SAVED data of 50-200 m. The Creus data is similar to the shallow stations and Lion until the cumulative frequency of 50 %, after which the error becomes much larger. At the Mesurho station, together with the other SAVED bathymetries, the model's error is larger than at the other stations.

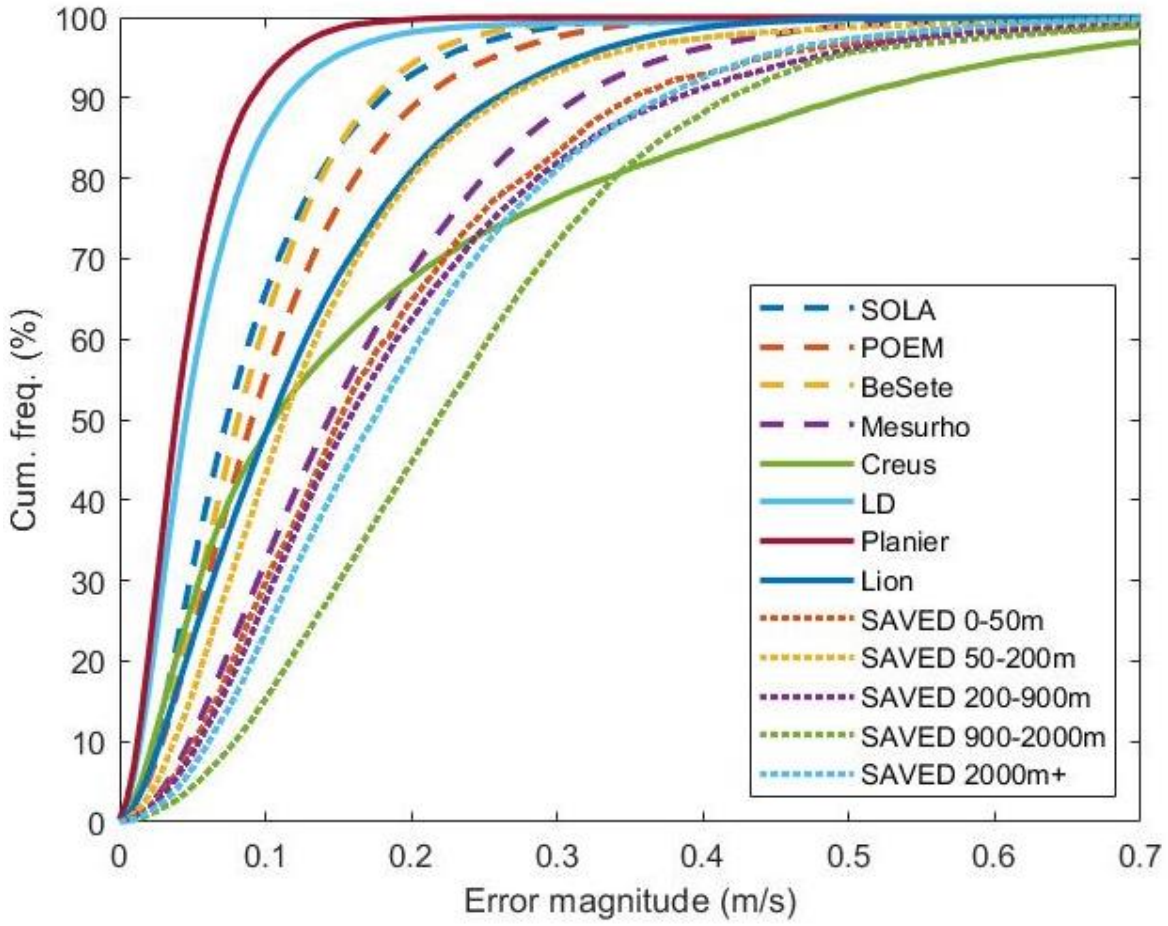

Figure 2.18: Cumulative frequency distributions of all moorings and trajectory data. The shallow stations are indicated in stripes (- -), the deep stations are indicated in full lines (-) and the SAVED trajectory bathymetry zones are indicated in dots (···).

Hereafter, the differences in error distribution of the **surface layer** (0-200 m) will be discussed, starting with the alleged bathymetry zones of the SAVED trajectory data. Figure 2.19 shows the cfd-plots of the error distributions in these alleged bathymetry zones. Adjacent zones are not very similar to each other, while the zones 0-50 m, 200-900 m and 2000 m < are quite similar to each other. The error distribution of the bathymetry zones 50-200 m and 900-2000m are quite different from all other distributions. This is confirmed by figure 2.20, which shows the surface between the cfd-plots. On the diagonal starting on column/row 2, the adjacent bathymetry zones are shown, which have a larger surface between them (3.985-5.531 cm^2/s) than the ones that are not adjacent. The same is shown by the WRS-test, where all adjacent bathymetry zones have a p-value smaller than 0.05, rejecting the zero hypothesis that the medians are the same (table 2.6). The KS-test on the other hand, does not reject the null hypothesis that the bathymetry zones 0-50 m and 50-200 m come from the same error distribution and the same for 900-2000 m and 2000 m < (table 2.7). Since all the medians of adjacent bathymetry zones are significantly different, it was decided to accept the alleged bathymetry zones as the actual bathymetry zones for the remainder of the study: 0-50 m, 50-200 m, 200-900 m, 900-2000 m and 2000 m <.

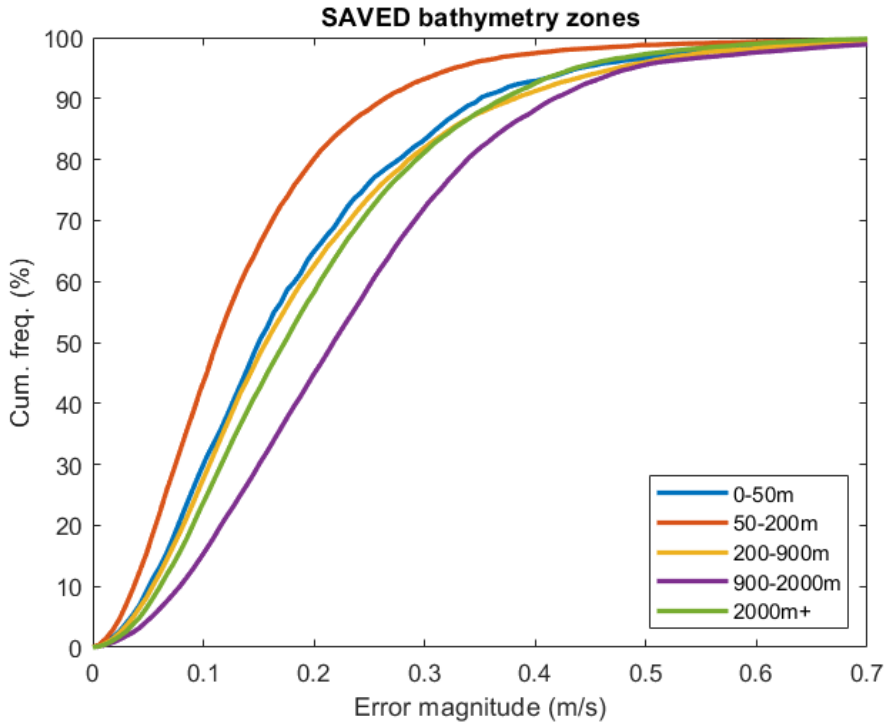

Figure 2.19: The cfd-plots of the error magnitude of the SAVED trajectory data, grouped per alleged bathymetry zone.

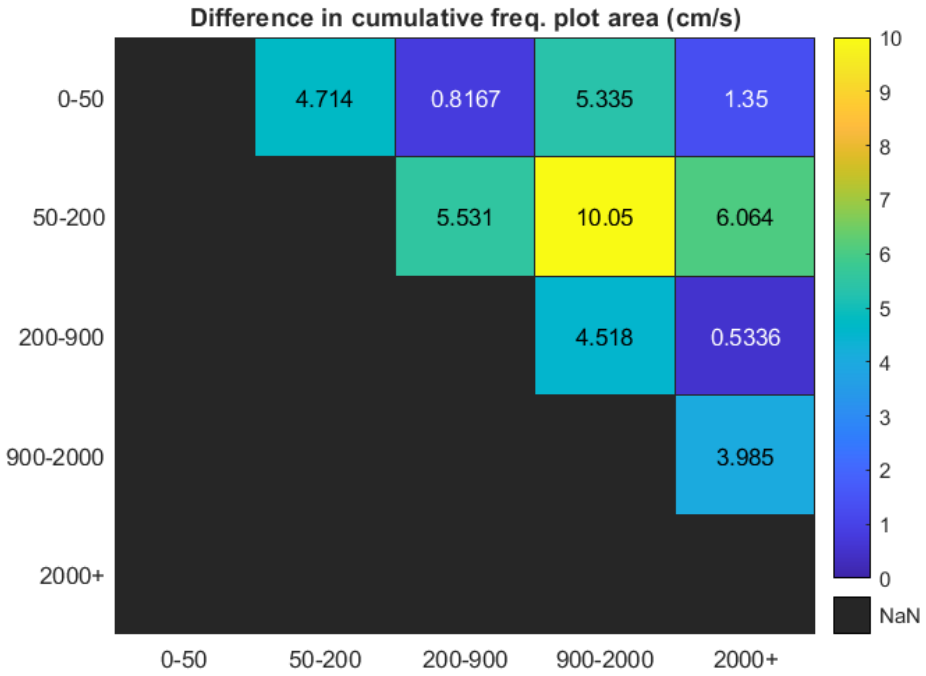

Figure 2.20: The heatmap of the surface between the cfd-plots of the error magnitude of the SAVED trajectory data, grouped per alleged bathymetry zone (m).

Table 2.6: The p-values of the WRS-test between the distributions of the SAVED bathymetry data, grouped per alleged bathymetry zone.

p-values WRS-test 100 points	0-50 m	50-200 m	200-900 m	900-2000 m	2000 m <
0-50 m		**0.0068**	0.6718	**0.0019**	0.2681
50-200 m			**0.0018**	**0**	**0.0001**
200-900 m				**0.0074**	0.5034
900-2000 m					**0.0329**
2000 m <					

Table 2.7: The p-values of the KS-test between the distributions of the SAVED bathymetry data, grouped per alleged bathymetry zone.

p-values KS-test 100 points	0-50 m	50-200 m	200-900 m	900-2000 m	2000 m <
0-50 m		0.1024	1	**0.0138**	0.7992
50-200 m			**0.0489**	**0**	**0.0054**
200-900 m				**0.0489**	0.9926
900-2000 m					0.2659
2000 m <					

Within the coastal bathymetry zone of 0-50 m, one can find the shallow stations SOLA, BeSete, Mesurho and POEM and SAVED trajectory data. Figure 2.21 shows the cfd-plots of the error magnitude. Two groups are distinguishable: SOLA, BeSete and POEM on one hand and SAVED 0-50 m and Mesurho on the other hand. This is confirmed by the heatmap of the surface areas in figure 2.22, where the shallow stations SOLA, BeSete and POEM have much smaller surface areas between them and Mesurho and SAVED 0-50 m are very different from all other stations apart from to each other. Both the WRS-test (table 2.8) and the KS-test (table 2.9) confirm this.

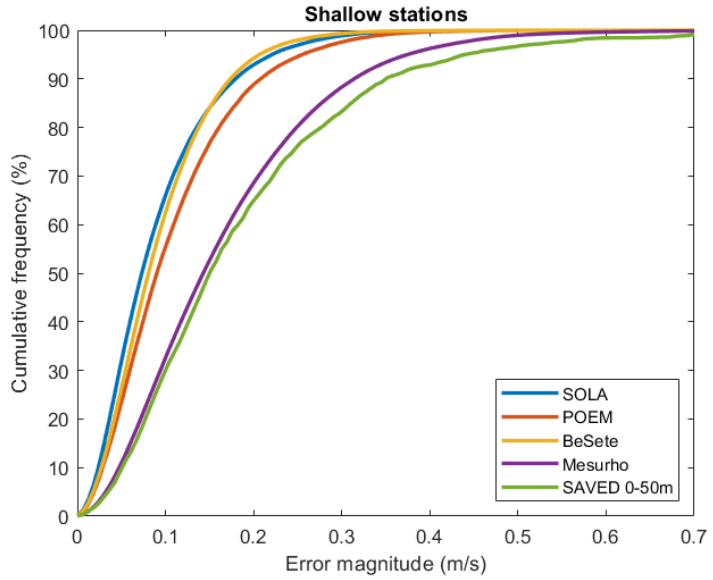

Figure 2.21: The cfd-plots of the error magnitude of the shallow stations (SOLA, POEM, BeSete, Mesurho) and the SAVED trajectory data between the bathymetries of 0-50 m.

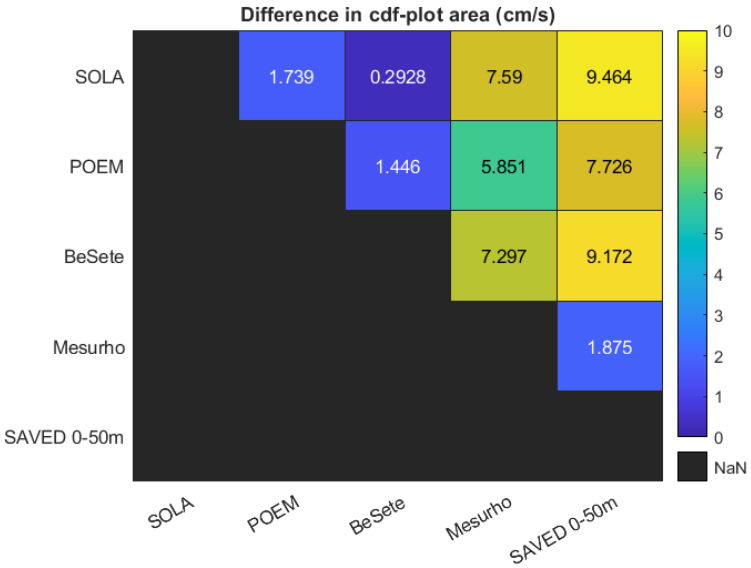

Figure 2.22: The heatmap of the surface between the cfd-plots of the error magnitude of the SAVED trajectory data, grouped per alleged bathymetry zone.

Table 2.8: P-values of the KW-test between the shallow stations (SOLA, POEM, BeSete, Mesurho) and the SAVED trajectory data between the bathymetries of 0-50 m.

P-values WRS-test 100 points	**SOLA**	**POEM**	**BeSete**	**Mesurho**	**SAVED 0-50 m**
SOLA		0.0818	0.4836	**0**	**0**
POEM			0.2599	**0.0001**	**0**
BeSete				**0**	**0**
Mesurho					0.4836
SAVED 0-50 m					

Table 2.9: P-values of the KS-test between the shallow stations (SOLA, POEM, BeSete, Mesurho) and the SAVED trajectory data between the bathymetries of 0-50 m

P-values KS-test 100 points	**SOLA**	**POEM**	**BeSete**	**Mesurho**	**SAVED 0-50 m**
SOLA		0.4496	0.9926	**0**	**0**
POEM			0.8972	**0.0032**	**0.0006**
BeSete				**0**	**0**
Mesurho					0.9995
SAVED 0-50 m					

Since there was a clear grouping between the stations on the west side of the Gulf of Lion and the SAVED 0-50 m and Mesurho data on the east side of the Gulf of Lion, it raised the question whether an additional separation between the east and west of the Gulf of Lion was necessary. This hypothesis is supported by the fact that there is a lot of SAVED data acquired close to the Mesurho station. The SAVED 0-50 m and 50-200 m trajectory data was separated into two by the longitude of E4.8°, which is just west of the Mesurho station. The difference in error distribution between the east and west was tested of the 0-50 m bathymetry zone and the 50-200 m bathymetry zone. Figure 2.23 shows the cfd-plots of the magnitude error distribution. The error distributions at longitudes smaller than or equal to E 4.8° are depicted

with a full line and those at bigger longitudes are depicted with a dashed line. The bathymetry zone from 0-50 m (blue) seems to show a bigger difference between the east and west side of the Gulf of Lion than the 50-200 m zone (red). This is confirmed by table 2.10, which shows the area between the cfd-plots and the p-values of the WRS-test and the KS-test between the error distributions of the east and west side of the Gulf of Lion. Since the null hypothesis that the median (KW-test, table 2.10) and the distribution (WRS-test, table 2.10) are the same between the left and right side of the Gulf of Lion is rejected for the bathymetry zone of 0-50m, the data in this bathymetry zone is divided in two.

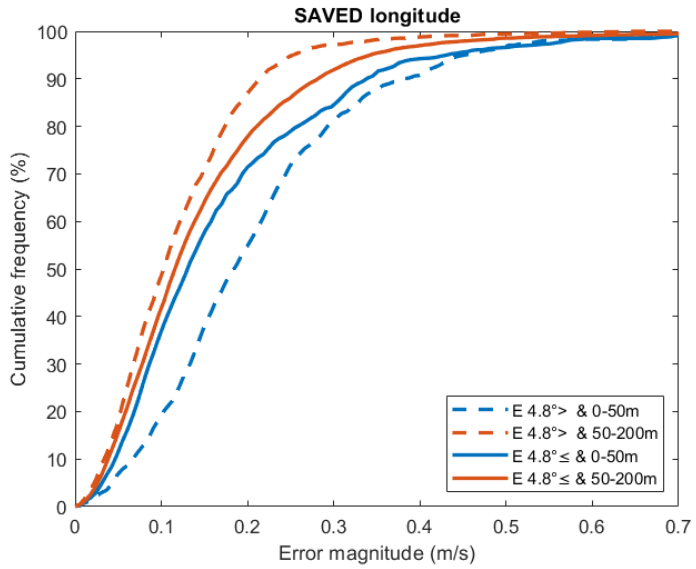

Figure 2.23: The cfd-plots of the error magnitude of the SAVED trajectory data between the bathymetries of 0-50 m and 50-200m left and right of E 4.8°.

Table 2.10: The p-values of the KW – and KS-test and the cfd-plot area between the error magnitude of the SAVED trajectory data between the bathymetries of 0-50 m and 50-200 m left and right of E 4.8°.

	0-50 m	**50-200 m**
The cfd-plot area (cm/s)	3.8964	2.5641
P-value WRS-test 100 extracted points	**0.0054**	0.1619
P-value KS-test 100 extracted points	**0.0138**	0.6828

In the **bottom layer** (200 m <), the error distributions of the deep stations were compared to each other. Figure 2.24 shows the cfd-plots of the error magnitude of the deep stations Creus, LD, Planier and Lion. From this figure, it is clear that the error distributions of LD and Planier are quite similar. The first halves of Lion and Creus overlap as well, but then they differentiate quite largely. This is confirmed by the heatmap of the surface between the cfd-plots in figure 2.25. Only the surface between LD and Planier is small, while the others are quite large. The WRS-test shows that the zero hypothesis of equal medians cannot be rejected for LD and Planier, but the same is true for Lion and Creus (table 2.11). When looking back at the cfd-plots in figure 2.24, it can be seen that their medians lie very closely together. What is interesting is that the KS-test also states that the zero hypothesis of equal distributions between the Lion and Creus stations cannot be rejected, even though the distributions have very different shapes after the 50% cumulative frequency (table 2.12).

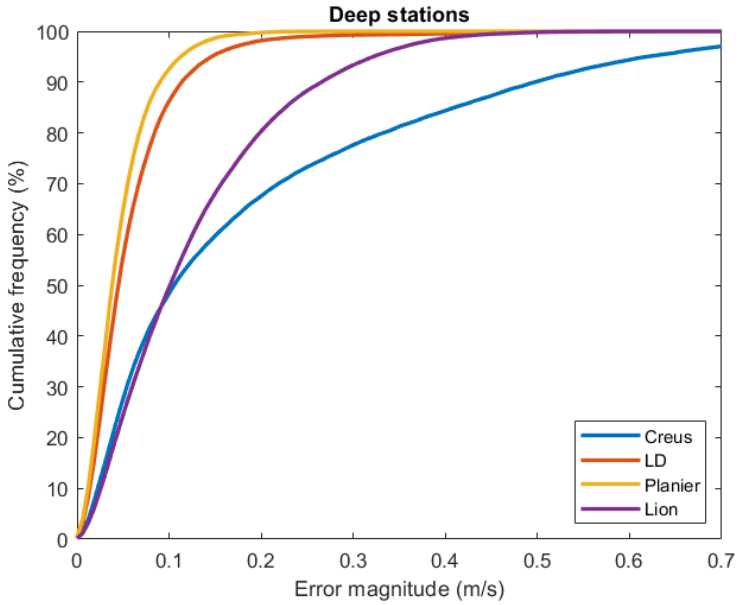

Figure 2.24: The cfd-plots of the error magnitude of the deep stations Creus, LD, Planier and Lion.

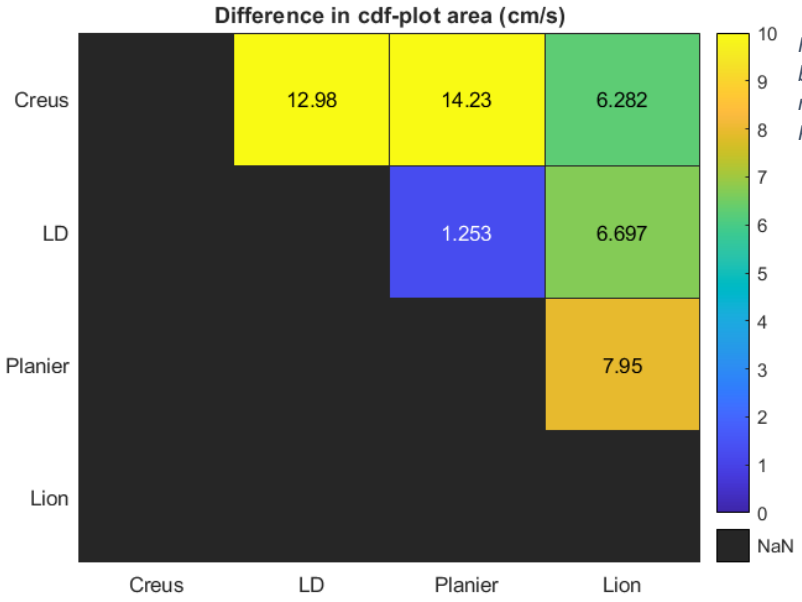

Figure 2.25: The heatmap of the surface between the cfd-plots of the error magnitude of the deep stations Creus, LD, Planier and Lion.

Table 2.11: The p-values of the WRS-test between the deep stations Creus, LD, Planier and Lion.

P-value WRS-test 100 points	Creus	LD	Planier	Lion
Creus		**0**	**0**	0.3380
LD			0.1211	**0**
Planier				**0**
Lion				

Table 2.12: The p-values of the KS-test between the deep stations Creus, LD, Planier and Lion.

P-value KS-test 100 points	Creus	LD	Planier	Lion
Creus		**0**	**0**	0.1438
LD			0.6828	**0**
Planier				**0**
Lion				

In conclusion, several error distributions could be grouped, as shown in table 2.13. In the shallow water layer, the SAVED data was split into five bathymetry zones. Then, within the 0-50 m bathymetry zone, two groups could be found: SOLA & BeSete & POEM and Mesurho & SAVED 0-50 m. In the deep water layer, two more groups could be defined: LD & Planier and Lion & Creus. In total, eight groups were created.

Table 2.13: Overview of the magnitude error distribution groups.

Shallow water layer (0-200m depth)	0-50m bathymetry zone	**SOLA & BeSete & POEM**	**1**
		Mesurho & SAVED 0-50m	**2**
	50-200m bathymetry zone		**3**
	200-900m bathymetry zone		**4**
	900-2000m bathymetry zone		**5**
	2000m< bathymetry zone		**6**
Deep water layer (200m-bottom)		**LD & Planier**	**7**
		Lion & Creus	**8**

2.3.3 Spatiotemporal variability of the error distribution

Figure 2.26 shows the error magnitude of the groups of the stations per season. Only the groups of Lion & Creus and LD & Planier show a difference between the seasons, with the model having a higher error during spring.

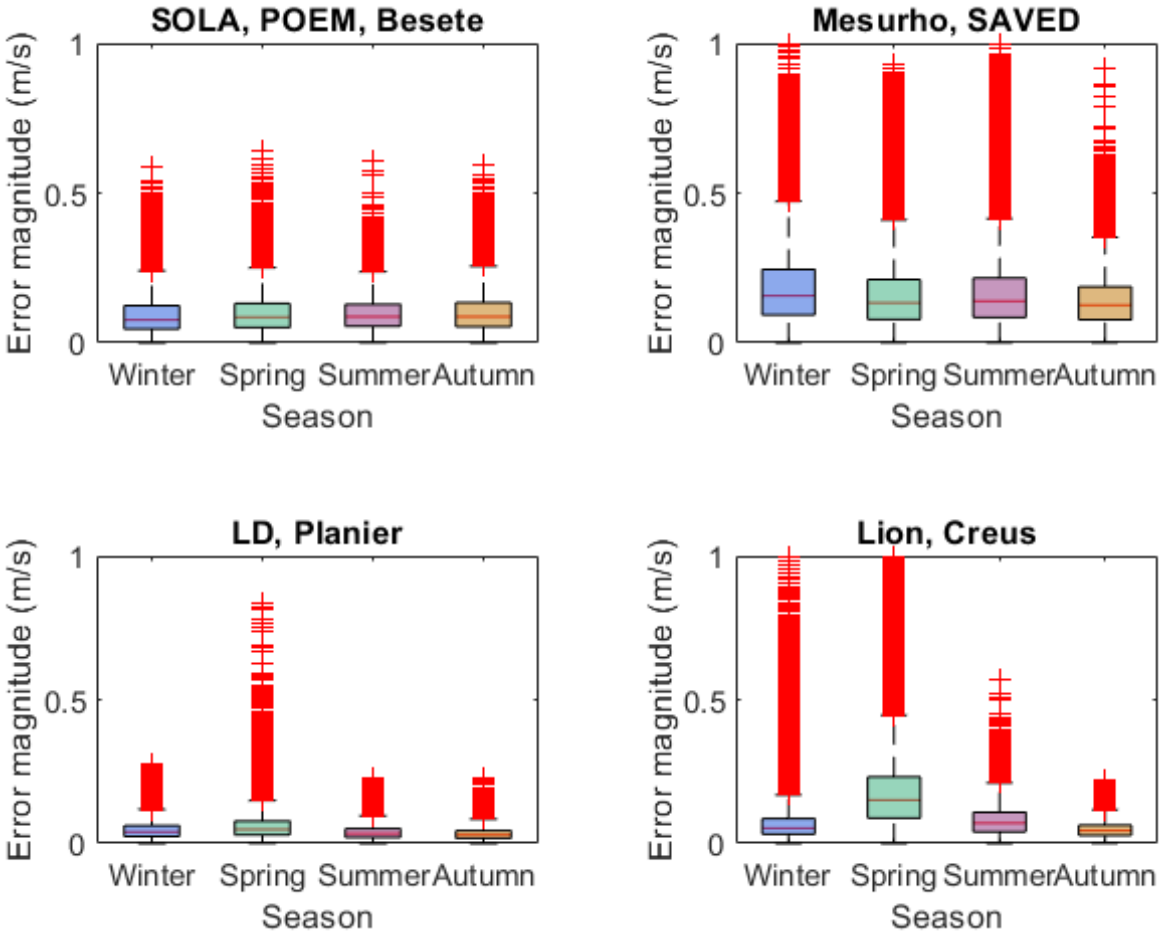

Figure 2.26: Boxplots of the error magnitude per group of stations, per season.

2.3.4 Environmental and modelling characteristics

The five characteristics discussed in this section are: Resolution, observed speed, steepness of the slope, depth and stratification. Since there is so little difference between the seasons for the different spatial groups (section 2.3.3), these setting variables are only discussed for the different moorings and the trajectory data (space) and not for the different seasons (time).

2.3.4.1 Current magnitude

Figure 2.27 shows the cfd-plots of the observed current magnitude. Their shape is very similar to the ones in figure 2.18, where the cfd-plots of the error magnitude were shown. The shallow stations all have quite similar current speeds. Their error distributions are also similar, except for the Mesurho station, where the model has a bigger error. This is also the station with one of the lowest correlations between observed current magnitude and error magnitude, together with BeSete (table 2.14). The Lion station has similar observed current speeds to the

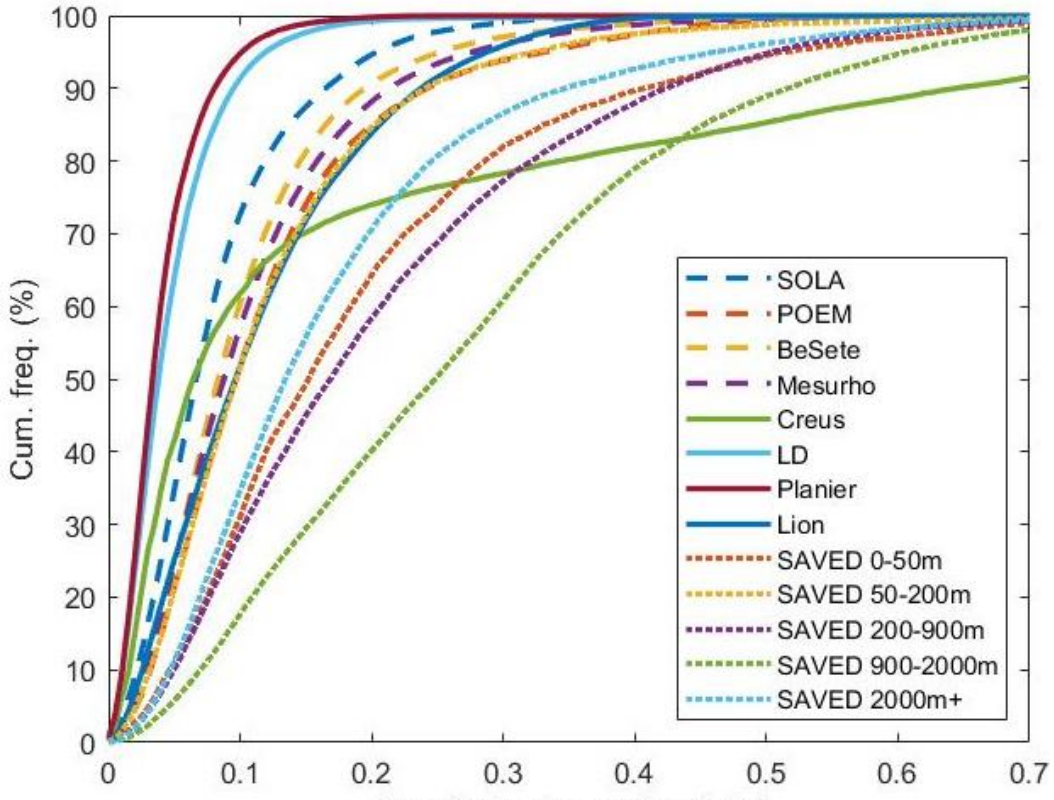

Figure 2.27: The cfd-plots of the observed current magnitude per station and SAVED bathymetry zone.

shallow stations and one of the highest correlations between observed current speed and magnitude error. At the Creus station, 30% of the observed current magnitudes are above 15cm/s, which could explain the higher error at this station given the 0.60 correlation. The SAVED bathymetries have even stronger currents and also a bigger error, since there are strong correlation values. The stations LD and Planier have the smallest observed currents, and the smallest error.

Hence, the correlation between observed current magnitude and error magnitude is quite large, which can be seen in table 2.14 and figure 2.29. This is especially the case for the deep stations and most of the SAVED bathymetry zones.

Table 2.14: Correlation between the error magnitude and the observed current magnitude per station or SAVED bathymetry zone.

Station	Correlation
SOLA	0.42
POEM	0.43
BeSete	0.25
Mesurho	0.34
Creus	0.60
LD	0.67
Planier	0.82
Lion	0.84
SAVED 0-50 m	0.69
SAVED 50-200 m	0.81
SAVED 200-900 m	0.84
SAVED 900-2000 m	0.78
SAVED 2000 m <	0.49

In figure 2.28, the scatter plot is shown of the error magnitude VS the observed magnitude per corresponding quantile, hence the cfd-plot of error magnitude (figure 2.18) VS the cfd-plot of the observation magnitude (figure 2.27). Most stations are located closely to or underneath the first bisector, which indicates when the error magnitude is the same size as the observed current magnitude. The stations located underneath the first bisector have an error magnitude smaller than the observed current magnitude, such as Mesurho, SOLA, Creus and several SAVED bathymetries.

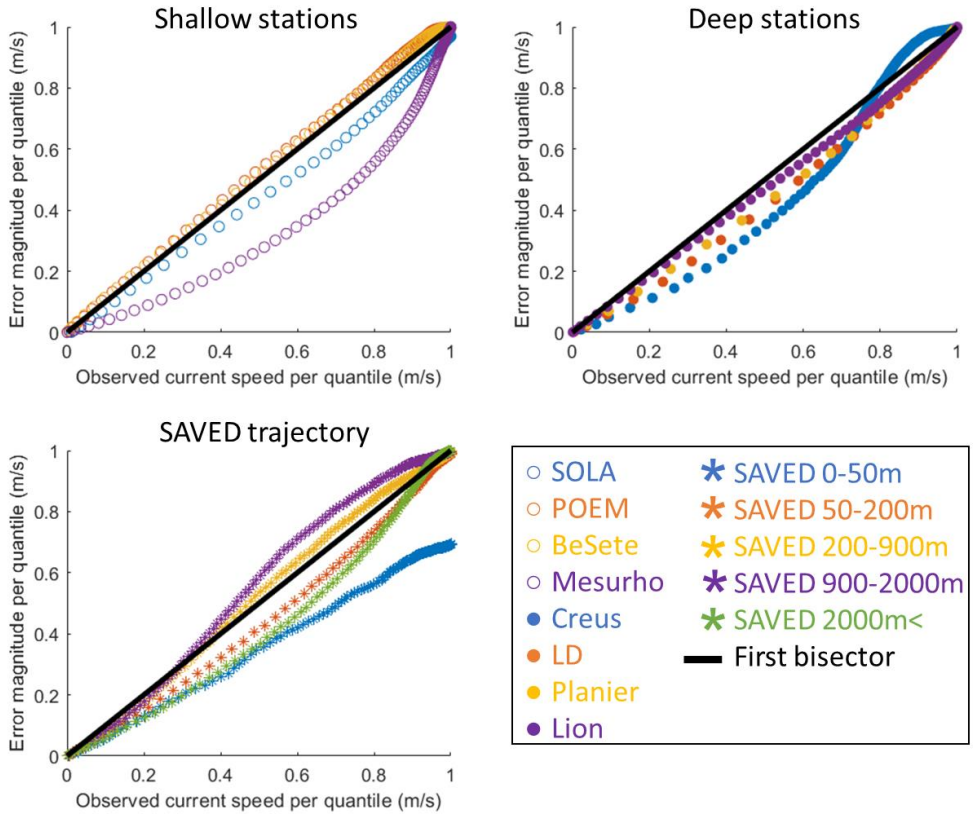

Figure 2.28: Scatter plot of the quantiles of the error magnitude vs the quantiles of the observed current speed for all observations.

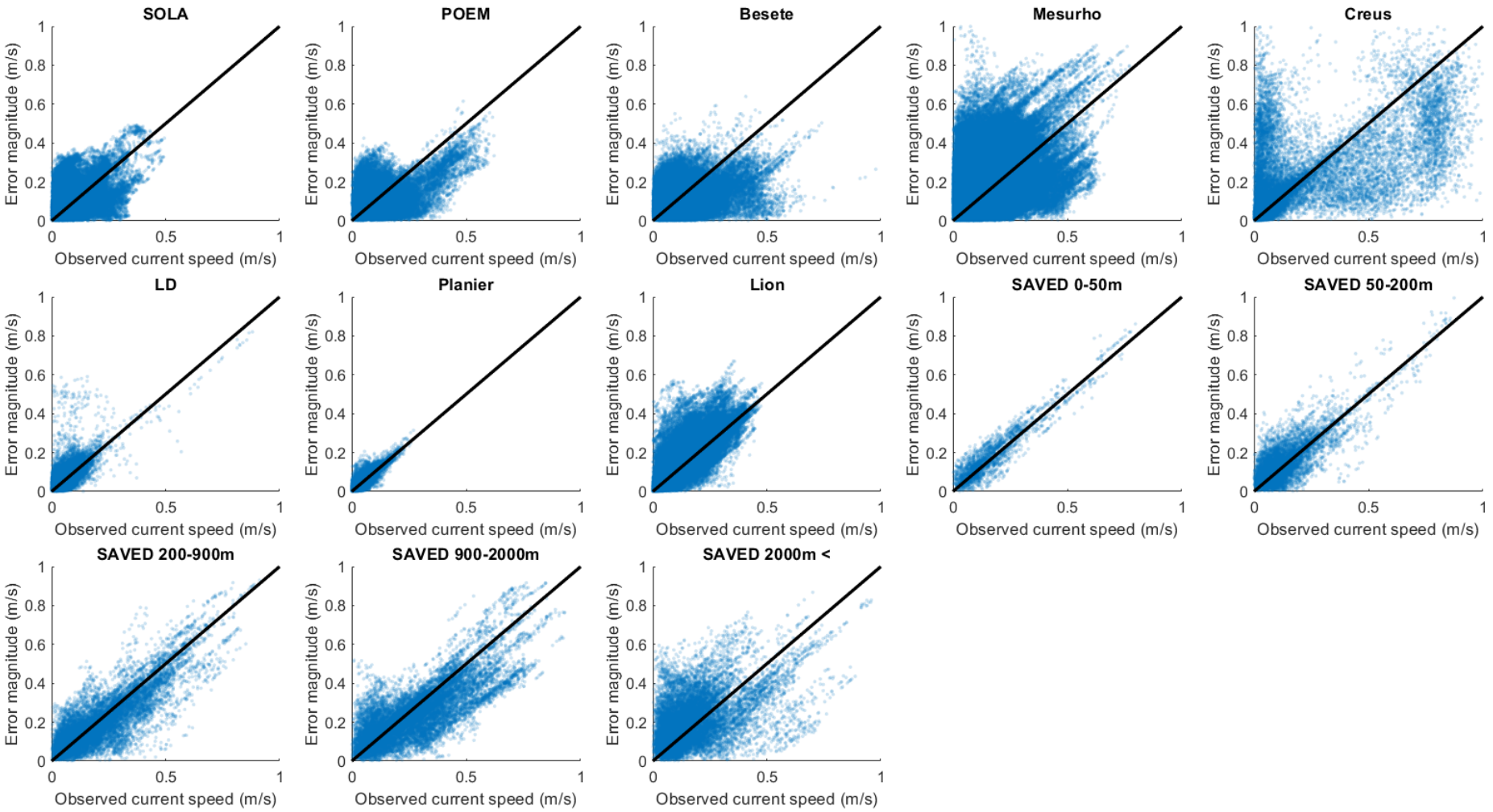

Figure 2.29: Scatter plot of the error magnitude VS the observed current magnitude for all observations. The black line is the first bisector.

2.3.4.2 Stratification

When looking at the stratification per station in figure 2.30, it is clear that the stratification levels at Mesurho are much higher than those of the other stations. No pattern can be found between the stratification and the error magnitude.

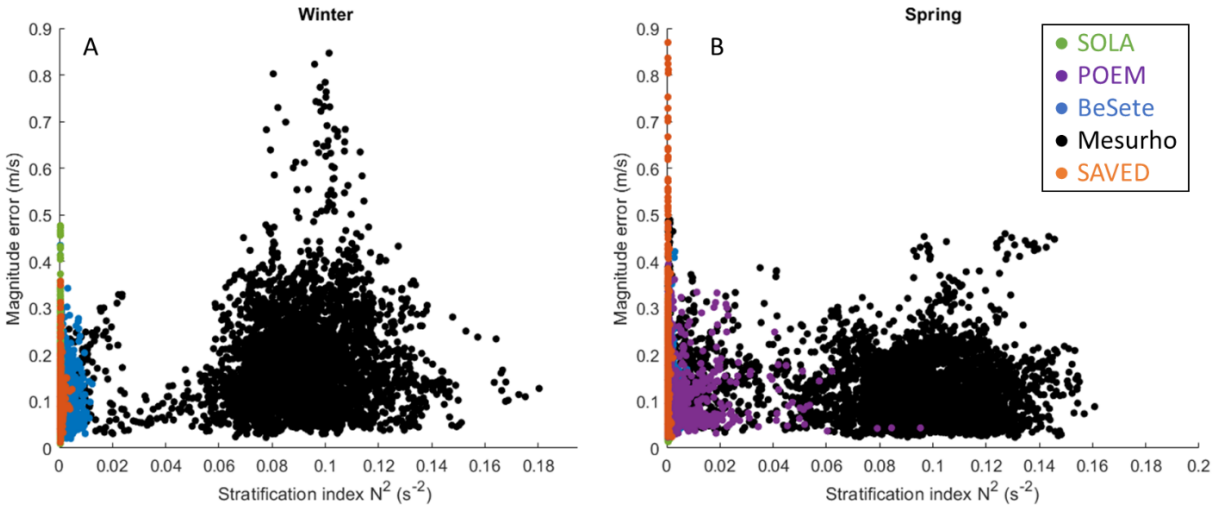

Figure 2.30: Scatter plot of the mean error magnitude over the entire water column compared to the maximum stratification over the entire water column per station for winter (A) and spring (B).

2.3.4.3 Resolution, slope and depth

The error magnitude is not correlated to the resolution of the model's grid (figure 2.31A), nor the slope of the model's bathymetry (figure 2.31B), nor the depth of the station for the fixed moorings (figure 2.31C). The correlations between the SAVED data and the resolution, the slope and the depth are 0.02, 0.01 and 0.02 respectively, so there is no correlation.

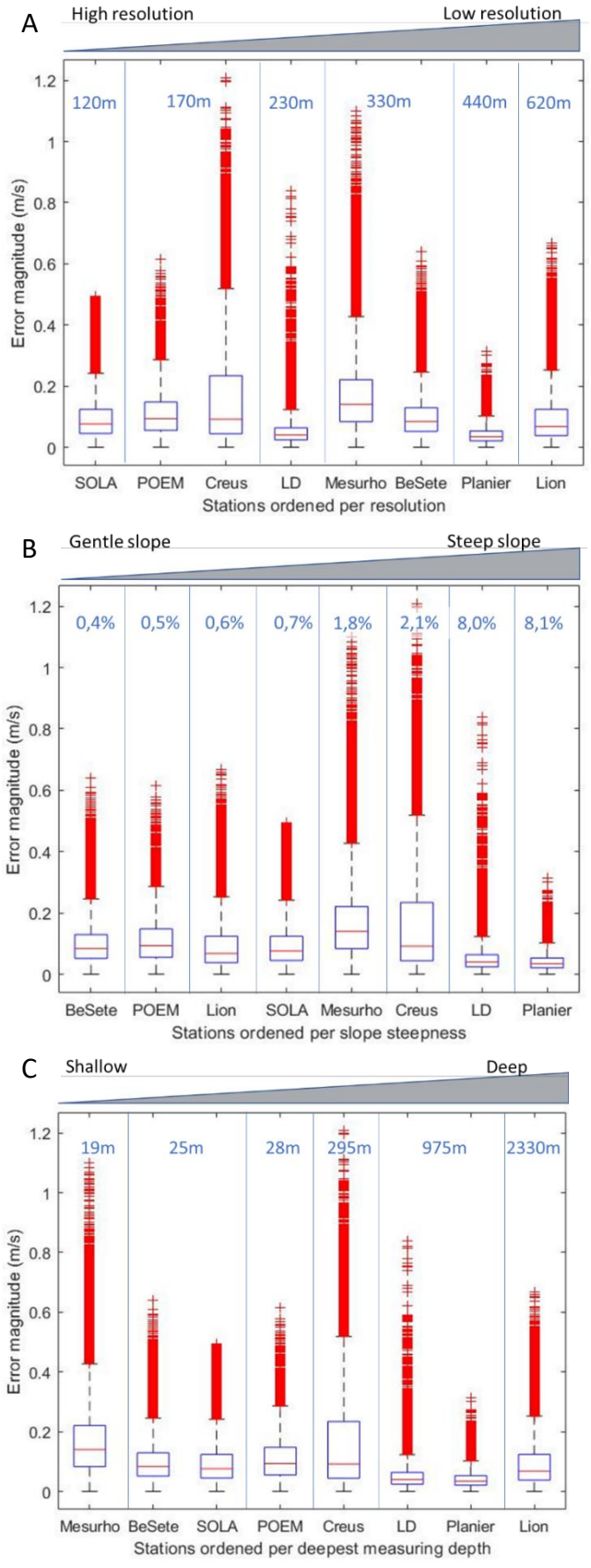

Figure 2.31: Boxplots of the error magnitudes of the stations ordered per A) resolution B) slope and C) deepest measuring depth.

2.3.4.4 Comparing characteristics

Table 2.15 shows when the environmental and modelling characteristics are similar within groups. What is remarkable is that within every group the stations' resolution is different. This indicates that the model's error distribution is not correlated to the model's resolution for as far as we can tell. Moreover, Mesurho and SAVED 0-50 m, which belong to the same group, have different values for every single setting variable. This indicates that although their error distributions are similar, the reason for the error of the model at these stations is likely different. The group of Creus and Lion show the same thing.

Table 2.15: Similarities within the group depending on the setting variable. An X indicates that within the group, the setting variable was different for the different stations. "V" indicates they were similar, "X" indicates they were different.

GROUP	RES.	SLOPE	SPEED	DEPTH	STRAT.
SOLA, POEM, BESETE	X	V	V	V	V
MESURHO, SAVED 0-50 M	X	X	X	V	X
LD, PLANIER	X	V	V	V	V
LION, CREUS	X	X	X	X	V

2.4 Discussion

The present study calculated the instant difference between observed and simulated flow speed at every depth level across the Gulf of Lion from 2010 to June 2013 using fixed moorings and trajectory data to assess the spatiotemporal differences in error distribution.

In space, eight groups were made based on the water layer and bathymetry zones. In the surface layer (0-200 m), the error distribution of the adjacent bathymetry zones of the SAVED data were all considered significantly different. For the shallowest bathymetry zone of 0-50m, two groups of error distributions could be distinguished. The error distributions at the stations SOLA, BeSete and POEM were similar, as well as those of the Mesurho station and the SAVED 0-50 m data. In the bottom layer (200 m - bottom), the error distribution of the four deep moorings could be organised in two groups: The LD and Planier station had similar error distributions as well as the Lion and Creus station.

In time, the intraseasonal differences in error distributions were slightly smaller than the interseasonal ones. The error distributions during the winter season were similar to the ones of the spring seasons and the error distributions of autumn were either similar to those of summer or spring.

The main circulation features in the Gulf of Lion are caused by ocean-atmosphere interaction (Schaeffer et al., 2011). These processes happening in the top layer also have an effect on deeper layers, such as for example inertial oscillations (Petrenko, 2003), up- and down welling (Millot, 1979), dense water formation (Ulses et al., 2008a) and eddy currents (Hu et al., 2009; Escudier, 2015). Another factor which influences the Gulf of Lion's circulation is freshwater input, which is why the Mesurho station at the mouth of the Rhône River is an interesting addition to this study (Marsaleix et al., 1998; Estournel et al., 2001; Reffray et al., 2004).

The offshore bathymetry zones had lower resolutions. Hence, one hypothesis to explain the spatial variability in the error magnitude distribution over the SAVED bathymetry zones, could be a difference in resolution. However, we found no link between the error magnitude distribution of the SAVED trajectory data and the resolution. The same is true for the shallow and deep moorings. Very few papers use flow speed observations to assess the effect of ocean model resolution on the performance of the model. However, most studies testing resolution do find better results with higher resolution models (Kirtman et al., 2012; Putman & He, 2013; Ringler et al., 2013) or state that a change in resolution has a big effect on the study's results (Guizien et al., 2006; Kvile et al., 2018), but more research needs to be done comparing hydrodynamic observations to assess if at the present study's resolutions, an even higher resolution would still improve the model. Based on this data, there is no link between the model's performance and its resolution. However, we didn't test different resolutions in the same place, we only tested different resolutions at different places. Therefore, there could be other factors affecting the error magnitude distributions in these places.

Another possible explanation which could explain the differences in error magnitude distribution is the steepness of the bottom slope. The bathymetry was smoothed before vertical meshing to prevent false vertical velocities due to hydrostatic inconsistency (Beckmann & Haidvogel, 1993; Haidvogel et al., 1993). This was done by limiting the relative water depth variation to 15% between grid points by applying iterative Laplacian diffusion to the initial bathymetry (Briton et al., 2018). This smoothing could potentially affect the performance of the model, as it creates an intrinsic error in the horizontal pressure gradient term (Sikirić et al., 2009). However, in this study, there was no effect of bottom steepness on the performance of the model. Contrary to my results, Blumberg & Georgas (2008) found that the New York Harbor Observing and Prediction System (NYHOPS) was highly sensitive to

bathymetry in the New York/New Jersey estuary. They hypothesized that this was due to the strong tidal changes, which could explain why my results are different, since the Gulf of Lion is microtidal.

The observed current speed on the other hand, does affect the model's error distribution. The higher the observed current speed, the higher the error. This is especially the case for the deep stations and the SAVED bathymetry zones. This is similar to the results in chapter 1, where it was already suggested that stronger currents lead to a bigger absolute error. The biggest difference with this study is that, in chapter 1, the indicators were averaged over the entire water column and over the event durations. Here, the instant error is calculated at every instant and at every depth level. Nonetheless, the results of both chapters correspond, with bigger errors at locations with bigger current magnitudes. Overall, one would expect faster currents near the coast, but this not the case for the Lion and Creus station, which have even faster currents than the shallow stations. When looking at the cumulative error distributions, the stations Lion and Creus are similar until the median, but after the Creus station has much higher error magnitude and observed current magnitude values. At the Lion station, the fast currents are due to deep convection during winter and spring (Houpert et al., 2016; Testor et al., 2018). The high observed current speed and error at the Creus station is possibly due to cascading events (Mikolajczak et al., 2020). The cascading events at the Creus station are caused by cold, strong, continental winds. The Cap de Creus canyon, which is where the Creus station was moored, has a large export of water of 1230 km^3 and 1750 km^3 for autumn and winter respectively (Mikolajczak et al., 2020). Ulses et al. (2008a) simulated and observed the dense water cascading in the Cap de Creus canyon and the Lacaze-Duthiers canyon (where the LD mooring is located), for 40 days from mid-February to March 2005. They estimated the water export to be 170 km^3 at the Lacaze-Duthiers canyon and 1010 km^3 at the

Cap de Creus canyon. This large difference in volume could explain why the Creus station shows a higher median error than the LD station.

When looking at the shallow stations, the correlation between observed current speed and error magnitude is smaller than at the deep stations. That being said, there is still a strong correlation. But, this means the error at these stations could be explained by a combination of the current speed and another variable. One explanation could be wave interaction, as shallower depths have bigger wave-current interactions (Mellor, 2008). However, in chapter 1, it was already shown that wave events do not have a notable effect on the performance of the model. Moreover, the results in this chapter show no link between the error magnitude distribution and the deepest measuring depth for both the fixed moorings and the SAVED data. Of course, the SAVED data was obtained by a hull-mounted ADCP, which was probably rarely deployed when there were waves. Furthermore, large wave events are rare in the Gulf of Lion (Guizien, 2009). Moreover, it is difficult to tell whether error magnitude is affected by deepest measuring depth in this study, as most shallow stations are moored at similar depths and there is a big difference in measuring depth between the shallow and deep stations. That being said, Mikolajczak (2019) compared the performance of a different configuration of the SYMPHONIE model with and without wave coupling and found no difference between the two. Since the model does not perform worse during wave events than during the reference period (chapter 1), this chapter shows no link between deepest measuring depth and the model's error and other literature shows no improvement when coupling a wave model to the SYMPHONIE2015 model, the effect of waves on the performance of the model seems negligible, but more research is necessary.

When looking at the shallowest bathymetry zone (0-50 m), the Mesurho station has a much higher error than the other shallow stations, despite the observed current speeds being similar

to the other shallow stations. The difference in error distribution of the Mesurho station with the other shallow stations is likely because of the Rhône River outflow. This is surprising, as chapter 1 showed that stratification had no notable effect on the performance of the model. However, the Mesurho station was not included in this study, as the water column at this station was always stratified, thus it could not be compared to reference periods. Since the stratification index (N^2) at Mesurho is a lot higher (up to 10 times) than at SOLA, POEM and BeSete, it is possible the model is only affected by stratification if the stratification is strong enough. Moreover, in a simulation using the MARS3D-RHOMA configuration with river discharge observations around the Rhône area, they found low correlations (0.1-0.5) between the observed and modelled salinity at Frioul (~35 km from Mesurho). Furthermore, there was an underestimation of 6-57% of the current speed measured by a hull-mounted ADCP (Pairaud et al., 2011). Overall, the model seems to reproduce the current rather well in stratified conditions, but it is possible that extreme salinity stratification can still impede with the model's calculations. Therefore, more research is required to fully understand the effect of strong, continuous stratification on the model's accuracy.

The error distribution of the Mesurho station can be grouped with the one of the SAVED 0-50m data. This is possibly due to the fact there is three times more SAVED 0-50 m data to the east of E4.8° than to the west. Hence, a lot of the SAVED data points were measured close to the Mesurho station. This raised the question if the SAVED data itself had longitudinal differences. Indeed, east and west of E 4.8° there was a difference in error distribution and median, but only for the data from the coast to the bathymetry line of 50 m. One possible hypothesis is that the effect the Rhône River's extreme stratification on the error distribution is limited to the shallowest bathymetry zone. Another possibility for the higher errors for the SAVED data could be that the observations themselves had a lower precision, since the SAVED

measured current velocities are corrected for the boat's own movement using a satellite. It is possible this correction is not precise enough, reducing the accuracy of the measurements. Moreover, the magnitude error of the SAVED data has a very high correlation with observed current speed, which explains the higher error for this data, since the SAVED data often measured high current magnitudes (Petrenko et al., 2005; Petrenko et al., 2017).

The stratification might not only affect the error magnitude in space, but also in time, as the seasonal variability in the surface layer circulation is largely due to meteorological forcing (Roussenov et al., 1995; Zavatarelli & Mellor, 1995; Pinardi & Masetti, 2000), e.g. thermal stratification and strong wind events. The seasonal differences between the error distribution of the magnitude were assessed to study the uncertainty of the model during different seasons. An interseasonal effect on the error distribution could be observed, indicating that the model's performance is different depending on the season.

The fact that the error distribution is more similar within the same season of different years than between different seasons is unsurprising, since every season has its own processes, some of which may not be easy to reproduce by the model.

The Gulf of Lion is especially susceptible to strong wind events (Millot, 1990). The Mistral and Tramontane winds can induce up- and down welling events all year long (Millot, 1979; Johns et al., 1992; Ulses et al., 2008b). In winter, these are cold and dry winds that cool the surface and create dense water formation (Hua & Thomasset, 1983; Millot, 1990; Madec et al., 1996; Estournel et al., 2003; Ulses et al., 2008a,b; Estournel et al., 2016). This could explain why the winter seasons have some of the highest median errors, as there is a high correlation between current speed (due to for example cascading) and the model's error. Therefore, it is possible that the model has difficulty recreating dense water formation. A study which used the SYMPHONIE model to study dense shelf water cascading in the Cap de Creus found high

correlations (0.69-0.93) between the modelled and observed current speed in the canyon when averaged over an almost five-month period. However, when looking at the periods with dense water cascading, large instant differences in observed and modelled current can be found where the model underestimates the current (Ulses et al., 2008a).

The error distributions of spring are similar to those of winter, because it is a transitioning season before the summer thermal stratification sets in (Millot, 1990). The error distributions of autumn either behave like those of spring, since it is the other transitioning season, or they are similar to those of summer, depending on when the water column becomes stratified that year. Moderate stratification has already been shown to have little effect on the performance of the model in chapter 1, which is probably why the summer seasons have the lowest median error. The good model performance during summer indicates that the model can incorporate the effects of thermal stratification on the currents quite well. The exception to this is the summer season of 2013. For this period, most data came from SAVED observations, which, as explained in the previous paragraph, is likely due to the high currents measured along the trajectories.

When performing a spatiotemporal cross-reference, it was clear the error magnitude within a group didn't change according to the season, apart from for the group of Lion & Creus and LD & Planier. This is likely because these stations have higher current speeds during the spring season due to deep convection and dense water cascading as previously mentioned (Ulses et al., 2008a; Mikolajczak et al., 2020).

A possible explanation for the model's performance not being linked to characteristics like slope steepness and resolution, but being strongly correlated to current speed, is that the model's atmospheric forcing is not great. If there are uncertainties in the atmospheric model, this will have an effect on the circulation model as shown by Chaudhuri et al. (2016), who

found that uncertainties in atmospheric forcing can cause substantial errors in modelled sea surface temperature at tropical and mid-latitude regions. These errors mainly occurred in the surface layer up to 1000 m.

In conclusion, there are spatial and seasonal differences in the performance of the model. Since ocean models are important tools to simulate transport in the ocean, it is necessary to take into account these differences in performance. In space, the differences in performance are mostly due to current speeds, since high current speeds are less well reproduced. Another possible factor affecting the model's performance could be extreme salinity stratification, which is observed at the Mesurho station. The summer is best reproduced, while the winter is the least well reproduced. This could be because the winter season has higher current speeds at some stations due to cascading and/or deep water convection. Overall, more research is needed comparing in situ hydrodynamic observations to model simulations in order to test its performance under different spatiotemporal variables. In the future, this research could be used to take into account the spatial and seasonal differences in model performance when interpreting dispersal simulations in the Gulf of Lion.

2.5 References

AANDERAA Instruments, N. N. (2001). Data Collecting Instruments for Land Sea and Air Aanderaa Instruments Recording Current Meter. AANDERAA RCM documentation.

Beckmann, A., & Haidvogel, D. B. (1993). Numerical simulation of flow around a tall isolated seamount. Part I: problem formulation and model accuracy. Journal of Physical Oceanography, 23(8), 1736–1753. https://doi.org/10.1175/1520-0485(1993)023<1736:NSOFAA>2.0.CO;2

Blumberg, A., & Georgas, N. (2008). Quantifying Uncertainty in Estuarine and Coastal Ocean Circulation Modeling. Journal of Hydraulic Engineering, 134(4), 403–415. https://doi.org/10.1061/(ASCE)0733-9429(2008)134

Bourrin, F., Many, G., Durrieu de Madron, X., Martín, J., Puig, P., Houpert, L., Testor, P., Kunesch, S., Mahiouz, K., Béguery, L. (2015). Glider monitoring of shelf suspended particle dynamics and transport during storm and flooding conditions. Continental Shelf Research 109, 135–149. https://doi.org/10.1016/j.csr.2015.08.031

Briton, F., Cortese, D., Duhaut, T., & Guizien, K. (2018). High-resolution modelling of ocean circulation can reveal retention spots important for biodiversity conservation. Aquatic Conservation: Marine and Freshwater Ecosystems, 28(4), 882–893. https://doi.org/10.1002/aqc.2901

Canals, M., Puig, P., Durrieu de Madron, X., Heussner, S., Palanques, A., & Fabres, J. (2006). Flushing submarine canyons. Nature, 444, 354–357. https://doi.org/10.1038/nature05271

Chaudhuri, A. H., Ponte, R. M., & Forget, G. (2016). Impact of uncertainties in atmospheric boundary conditions on ocean model solutions. Ocean Modelling, 100, 96–108. https://doi.org/10.1016/j.ocemod.2016.02.003

Durrieu de Madron X., Heussner S., Delsaut N., Kunesch S., & Menniti C. (2019). BILLION observatory data. SEANOE. https://doi.org/10.17882/45980

Dwinovantyo, A., Manik, H. M., Prartono, T., Susilohadi, S., & Mukai, T. (2019). Variation of Zooplankton mean volume backscattering strength from Moored and Mobile ADCP instruments for diel vertical migration observation. Applied Sciences (Switzerland), 9(9). https://doi.org/10.3390/app9091851

Escudier, R. (2015). Mesoscale eddies in the western Mediterranean Sea : characterization and understanding from satellite observations and model simulations.

Estournel, C., Broche, P., Marsaleix, P., Devenon, J. L., Auclair, F., & Vehil, R. (2001). The Rhône River plume in unsteady conditions: Numerical and experimental results. Estuarine, Coastal and Shelf Science, 53(1), 25–38. https://doi.org/10.1006/ecss.2000.0685

Estournel, C., De Madron, X. D., Marsaleix, P., Auclair, F., Julliand, C., & Vehil, R. (2003). Observation and modeling of the winter coastal oceanic circulation in the Gulf of Lion under wind conditions influenced by the continental orography (FETCH experiment). Journal of Geophysical Research: Oceans, 108(3), 8059. https://doi.org/10.1029/2001jc000825

Estournel, C., Testor, P., Damien, P., D'Ortenzio, F., Marsaleix, P., Conan, P., Kessouri, F., Durrieu de Madron, X., Coppola, L., Lellouche, J. M., Belamari, S., Mortier, L., Ulses, C., Bouin, M. N., & Prieur, L. (2016). High resolution modeling of dense water formation in the north-western Mediterranean during winter 2012–2013: Processes and budget.

Journal of Geophysical Research: Oceans, 121(7), 5367–5392. https://doi.org/10.1002/2016JC011935

Faizal, M., Ahmed, M. R., Kim, C. G., & Lee, Y. H. (2011). Experimental investigation of waterwave characteristics in awave channel. International Journal of Fluid Mechanics Research, 38(2), 167–178. https://doi.org/10.1615/InterJFluidMechRes.v38.i2.60

Gervais, M., Balouin, Y., & Belon, R. (2011). Morphological response and coastal dynamics associated with major storm events along the Gulf of Lions Coastline, France. https://doi.org/10.1016/j.geomorph.2011.07.035

Guizien, K. (2009). Spatial variability of wave conditions in the Gulf of Lions (NW Mediterranean Sea). Life and Environment, 59(3/4), 261–270. https://www.researchgate.net/publication/250306276

Guizien, K., Brochier, T., Duchêne, J. C., Koh, B. S., & Marsaleix, P. (2006). Dispersal of Owenia fusiformis larvae by wind-driven currents: Turbulence, swimming behaviour and mortality in a three-dimensional stochastic model. Marine Ecology Progress Series, 311(1986), 47–66. https://doi.org/10.3354/meps311047

Haidvogel, D. B., Beckmann, A., Chapman, D. C., & Ray-Qing Lin. (1993). Numerical simulation of flow around a tall isolated seamount. Part II: resonant generation of trapped waves. Journal of Physical Oceanography, 23(11), 2373–2391. https://doi.org/10.1175/1520-0485(1993)023<2373:NSOFAA>2.0.CO;2

Hamon, M., Beuvier, J., Somot, S., Lellouche, J. M., Greiner, E., Jordà, G., Bouin, M. N., Arsouze, T., Béranger, K., Sevault, F., Dubois, C., Drevillon, M., & Drillet, Y. (2016). Design and validation of MEDRYS, a Mediterranean Sea reanalysis over the period 1992-2013. Ocean Science, 12(2), 577–599. https://doi.org/10.5194/os-12-577-2016

Houpert, L., Durrieu de Madron, X., Testor, P., Bosse, A., D'Ortenzio, F., Bouin, M. N., Dausse, D., Le Goff, H., Kunesch, S., Labaste, M., Coppola, L., Mortier, L., & Raimbault, P. (2016). Observations of open-ocean deep convection in the northwestern Mediterranean Sea: Seasonal and interannual variability of mixing and deep water masses for the 2007-2013 Period. Journal of Geophysical Research: Oceans, 121(11), 8139–8171. https://doi.org/10.1002/2016JC011857

Houpert, L., Testor, P., de Madron, X. D., Somot, S., D'Ortenzio, F., Estournel, C., & Lavigne, H. (2015). Seasonal cycle of the mixed layer, the seasonal thermocline and the upper-ocean heat storage rate in the Mediterranean Sea derived from observations. Progress in Oceanography, 132, 333–352. https://doi.org/10.1016/j.pocean.2014.11.004

Hu, Z. Y., Doglioli, A. M., Petrenko, A. A., Marsaleix, P., & Dekeyser, I. (2009). Numerical simulations of eddies in the Gulf of Lion. Ocean Modelling, 28(4), 203–208. https://doi.org/10.1016/j.ocemod.2009.02.004

Hua, B.-L., & Thomasset, F. (1983). A numerical study of the effects of coastline geometry on wind-induced upwelling in the Gulf of Lions. Journal of Physical Oceanography, 13, 678–694.

Johns, B., Marsaleix, P., Estournel, C., & Véhil, R. (1992). On the wind-driven coastal upwelling in the Gulf of Lions. Journal of Marine Systems, 3(4–5), 309–320. https://doi.org/10.1016/0924-7963(92)90008-V

Kirtman, B. P., Bitz, C., Bryan, F., Collins, W., Dennis, J., Hearn, N., Kinter, J. L., Richard, I. I. I., Clement, L., Siqueira, L., Stan, C., Tomas, R., & Vertenstein, M. (2012). Impact of ocean model resolution on CCSM climate simulations. 1303–1328. https://doi.org/10.1007/s00382-012-1500-3

Kvile, K. Ø., Romagnoni, G., Dagestad, K. F., Langangen, Ø., & Kristiansen, T. (2018). Sensitivity of modelled North Sea cod larvae transport to vertical behaviour, ocean model resolution and interannual variation in ocean dynamics. ICES Journal of Marine Science, 75(7), 2013–2024. https://doi.org/10.1093/icesjms/fsy039

Lionello, P., Malanotte-Rizzoli, P., Boscolo, R., Alpert, P., Artale, V., Li, L., Luterbacher, J., May, W., Trigo, R., Tsimplis, M., Ulbrich, U., & Xoplaki, E. (2006). The Mediterranean Climate: An Overview of the Main Characteristics and Issues. Developments in Earth and Environmental Sciences, 4, 1–26.

Madec, G., Lott, F., Delecluse, P., & Crépon, M. (1996). Large-scale preconditioning of deep-water formation in the northwestern Mediterranean Sea. Journal of Physical Oceanography, 26(8), 1393–1408. https://doi.org/10.1175/1520-0485(1996)026<1393:LSPODW>2.0.CO;2

Marsaleix, P., Estournel, C., Kondrachoff, V., & Vehil, R. (1998). A numerical study of the formation of the Rhone River plume. Journal of Marine Systems, 14(1–2), 99–115. https://doi.org/10.1016/S0924-7963(97)00011-0

Mellor, G. L. (2008). The depth-dependent current and wave interaction equations: A revision. Journal of Physical Oceanography, 38(11), 2587–2596. https://doi.org/10.1175/2008JPO3971.1

Mikolajczak, G. (2019). Dynamique de l'eau et des apports particulaires originaires du Rhône sur la marge continentale du Golfe du Lion. [Doctoral dissertation, Toulouse university]

Mikolajczak, G., Estournel, C., Ulses, C., Marsaleix, P., Bourrin, F., Martín, J., Pairaud, I., Puig, P., Leredde, Y., Many, G., Seyfried, L., & Durrieu de Madron, X. (2020). Impact of storms on residence times and export of coastal waters during a mild autumn/winter period

in the Gulf of Lion. Continental Shelf Research, 207, 104192. https://doi.org/10.1016/j.csr.2020.104192

Millot, C. (1979). Wind induced upwellings in the Gulf of Lions. Oceanologica Acta, 2(3), 261–274.

Millot, C. (1990). The Gulf of Lions' hydrodynamics. Continental Shelf Research, 10(9–11), 885–894. https://doi.org/10.1016/0278-4343(90)90065-T 4

Pairaud, I. L., Gatti, J., Bensoussan, N., Verney, R., & Garreau, P. (2011). Hydrology and circulation in a coastal area off Marseille: Validation of a nested 3D model with observations. Journal of Marine Systems, 88(1), 20–33. https://doi.org/10.1016/j.jmarsys.2011.02.010

Pairaud, I., Répécaud, C., Ravel, M., Fuchs, R., Arnaud, M., Champelovier, A., Rabouille, C., Bombled, B., Toussaint, F., Garcia, F. (2016) MesuRho: Plateforme instrumentée de suivi des paramètres environnementaux à l'embouchure du Rhône. In Mesures Haute Résolution dans L'environnement Marin Côtier; Schmitt, F.G., Lefebvre, A., Eds.; Presses du CNRS: Paris, France

Palanques, A., Guillén, J., Puig, P., & Durrieu de Madron, X. (2008). Storm-driven shelf-to-canyon suspended sediment transport at the southwestern Gulf of Lions. Continental Shelf Research, 28(15), 1947–1956. https://doi.org/10.1016/j.csr.2008.03.020

Petrenko, A. (2003). Variability of circulation features in the Gulf of Lion NW Mediterranean Sea. Importance of inertial currents. Oceanologica Acta, 26(4), 323–338. https://doi.org/10.1016/S0399-1784(03)00038-0

Petrenko, A. A., Doglioli, A. M., Nencioli, F., Kersalé, M., Hu, Z., & d'Ovidio, F. (2017). A review of the LATEX project: mesoscale to submesoscale processes in a coastal environment. In Ocean Dynamics (Vol. 67, Issues 3–4). https://doi.org/10.1007/s10236-017-1040-9

Petrenko, A., Dufau, C., & Estournel, C. (2008). Barotropic eastward currents in the western Gulf of Lion, north-western Mediterranean Sea, during stratified conditions. Journal of Marine Systems, 74(1–2), 406–428. https://doi.org/10.1016/j.jmarsys.2008.03.004

Petrenko, A., Leredde, Y., & Marsaleix, P. (2005). Circulation in a stratified and wind-forced Gulf of Lions, NW Mediterranean Sea: In situ and modeling data. Continental Shelf Research, 25(1), 7–27. https://doi.org/10.1016/j.csr.2004.09.004

Pinardi, N., & Masetti, E. (2000). Variability of the large scale general circulation of the Mediterranean Sea from observations and modelling: A review. Palaeogeography, Palaeoclimatology, Palaeoecology, 158(3–4), 153–173. https://doi.org/10.1016/S0031-0182(00)00048-1

Putman, N. F., & He, R. (2013). Tracking the long-distance dispersal of marine organisms: Sensitivity to ocean model resolution. Journal of the Royal Society Interface, 10(81). https://doi.org/10.1098/rsif.2012.0979

RDI Instruments. (1996). Acoustic Doppler current profiler: Principles of operation, a practical primer. (Vol. 00, Issue January). RD Instruments.

Reffray, G., Fraunié, P., & Marsaleix, P. (2004). Secondary flows induced by wind forcing in the Rhône region of freshwater influence. Ocean Dynamics, 54(2), 179–196. https://doi.org/10.1007/s10236-003-0079-y

Ridenour, N. A., Hu, X., Jafarikhasragh, S., Landy, J. C., Lukovich, J. V., Stadnyk, T. A., Sydor, K., Myers, P. G., & Barber, D. G. (2019). Sensitivity of freshwater dynamics to ocean model resolution and river discharge forcing in the Hudson Bay Complex. Journal of Marine Systems, 196(May), 48–64. https://doi.org/10.1016/j.jmarsys.2019.04.002

Ringler, T., Petersen, M., Higdon, R. L., Jacobsen, D., Jones, P. W., & Maltrud, M. (2013). A multi-resolution approach to global ocean modeling. Ocean Modelling, 69, 211–232. https://doi.org/10.1016/j.ocemod.2013.04.010

Roussenov, V., Stanev, E., Artale, V., & Pinardi, N. (1995). A seasonal model of the Mediterranean Sea general circulation. Journal of Geophysical Research, 100(C7), 515–538.

SAVED (1996) Système Acquisition Validation Exploitation de Données des Navires de l'INSU - Projet SAVED -. https://sextant.ifremer.fr/record/6f6e95e9-8e97-48d6-b536-b40f2ad87402/

Schaeffer, A., Garreau, P., Molcard, A., Fraunié, P., & Seity, Y. (2011). Influence of high-resolution wind forcing on hydrodynamic modeling of the Gulf of Lions. Ocean Dynamics, 61(11), 1823–1844. https://doi.org/10.1007/s10236-011-0442-3

Schroeder, K., Millot, C., Bengara, L., Ben Ismail, S., Bensi, M., Borghini, M., Budillon, G., Cardin, V., Coppola, L., Curtil, C., Drago, A., El Moumni, B., Font, J., Fuda, J. L., García-Lafuente, J., Gasparini, G. P., Kontoyiannis, H., Lefevre, D., Puig, P., Raimbault, P., Rougier, G.,Salat, J., Sammari, C., Sánchez Garrido, J. C., Sanchez-Roman, A., Sparnocchia, S., Tamburini, C., Taupier-Letage, I., Theocharis, A., Vargas-Yáñez, M., Vetrano, A. (2013). Long-term monitoring programme of the hydrological variability in the Mediterranean Sea: A first overview of the HYDROCHANGES network. Ocean Science, 9(2), 301–324. https://doi.org/10.5194/os-9-301-2013

Sikirić, M. D., Janeković, I., & Kuzmić, M. (2009). A new approach to bathymetry smoothing in sigma-coordinate ocean models. Ocean Modelling, 29(2), 128–136. https://doi.org/10.1016/j.ocemod.2009.03.009

Somot, S. (2005). Modélisation climatique du bassin méditerranéen: variabilité et scénarios de changement climatique. 347.

Somot, S., Sevault, F., Déqué, M., & Crépon, M. (2008). 21st century climate change scenario for the Mediterranean using a coupled atmosphere-ocean regional climate model. Global and Planetary Change, 63(2–3), 112–126. https://doi.org/10.1016/j.gloplacha.2007.10.003

Testor, P., Bosse, A., Houpert, L., Margirier, F., Mortier, L., Legoff, H., Dausse, D., Labaste, M., Karstensen, J., Hayes, D., Olita, A., Ribotti, A., Schroeder, K., Chiggiato, J., Onken, R., Heslop, E., Mourre, B., D'ortenzio, F., Mayot, N., Lavigne, H., de Fommervault, O., Coppola, L., Prieur, L., Taillandier, V., Durrieu de Madron, X., Bourrin, F., Many, G., Damien, P., Estournel, C., Marsaleix, P., Taupier-Letage, I., Raimbault, P., Waldman, R., Bouin, M. N., Giordani, H., Caniaux, G., Somot, S., Ducrocq, V., Conan, P. (2018). Multiscale Observations of Deep Convection in the Northwestern Mediterranean Sea During Winter 2012–2013 Using Multiple Platforms. Journal of Geophysical Research: Oceans, 123(3), 1745–1776. https://doi.org/10.1002/2016JC012671

Ulses, C., Estournel, C., Bonnin, J., Durrieu de Madron, X., & Marsaleix, P. (2008b). Impact of storms and dense water cascading on shelf-slope exchanges in the Gulf of Lion (NW Mediterranean). Journal of Geophysical Research, 113(C2), C02010. https://doi.org/10.1029/2006JC003795

Ulses, C., Estournel, C., Puig, P., Durrieu de Madron, X., & Marsaleix, P. (2008a). Dense shelf water cascading in the northwestern Mediterranean during the cold winter 2005: Quantification of the export through the Gulf of Lion and the Catalan margin. Geophysical Research Letters, 35(7), n/a-n/a. https://doi.org/10.1029/2008GL033257

Zavatarelli, M., & Mellor, G. L. (1995). A numerical study of the Mediterranean Sea circulation. Journal of Physical Oceanography, 25(6), 1384–1414.

2.6 Appendix

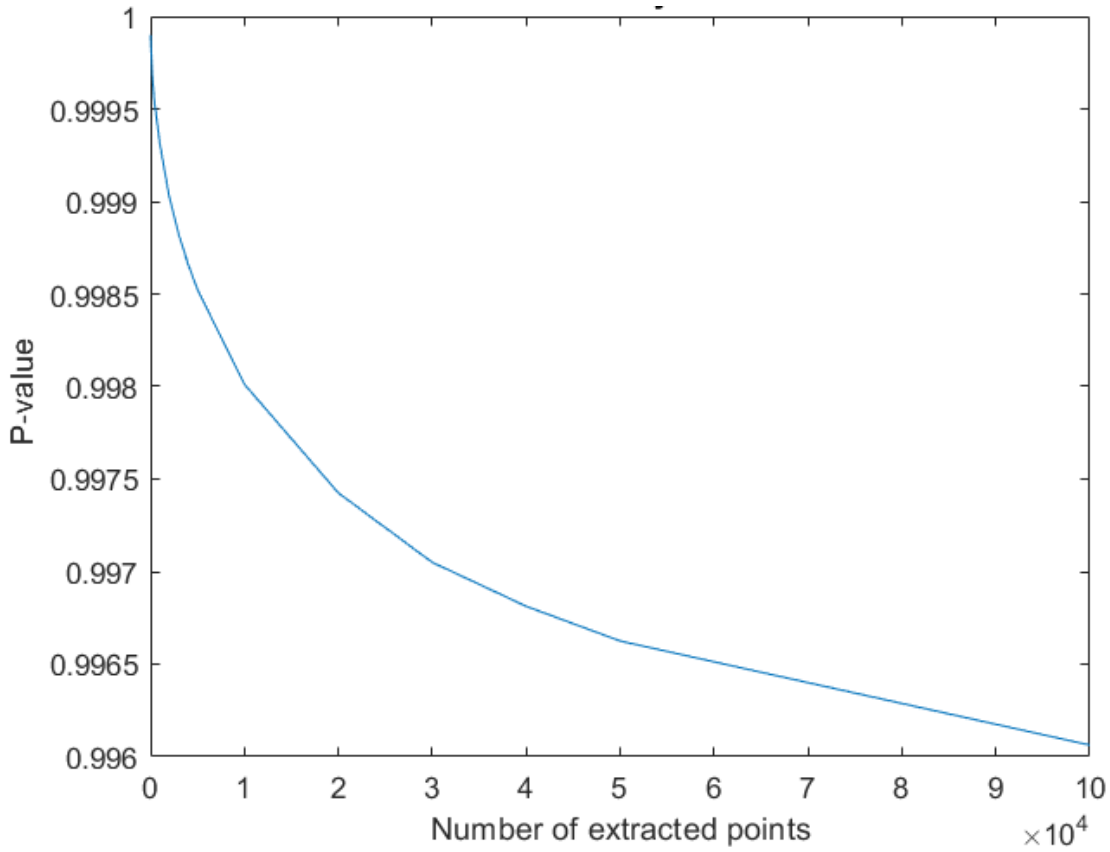

Figure 2.A1: Plot comparing the p-value of the WRS-test between the total distribution of the current error magnitude and the same distribution with a limited number of points extracted.

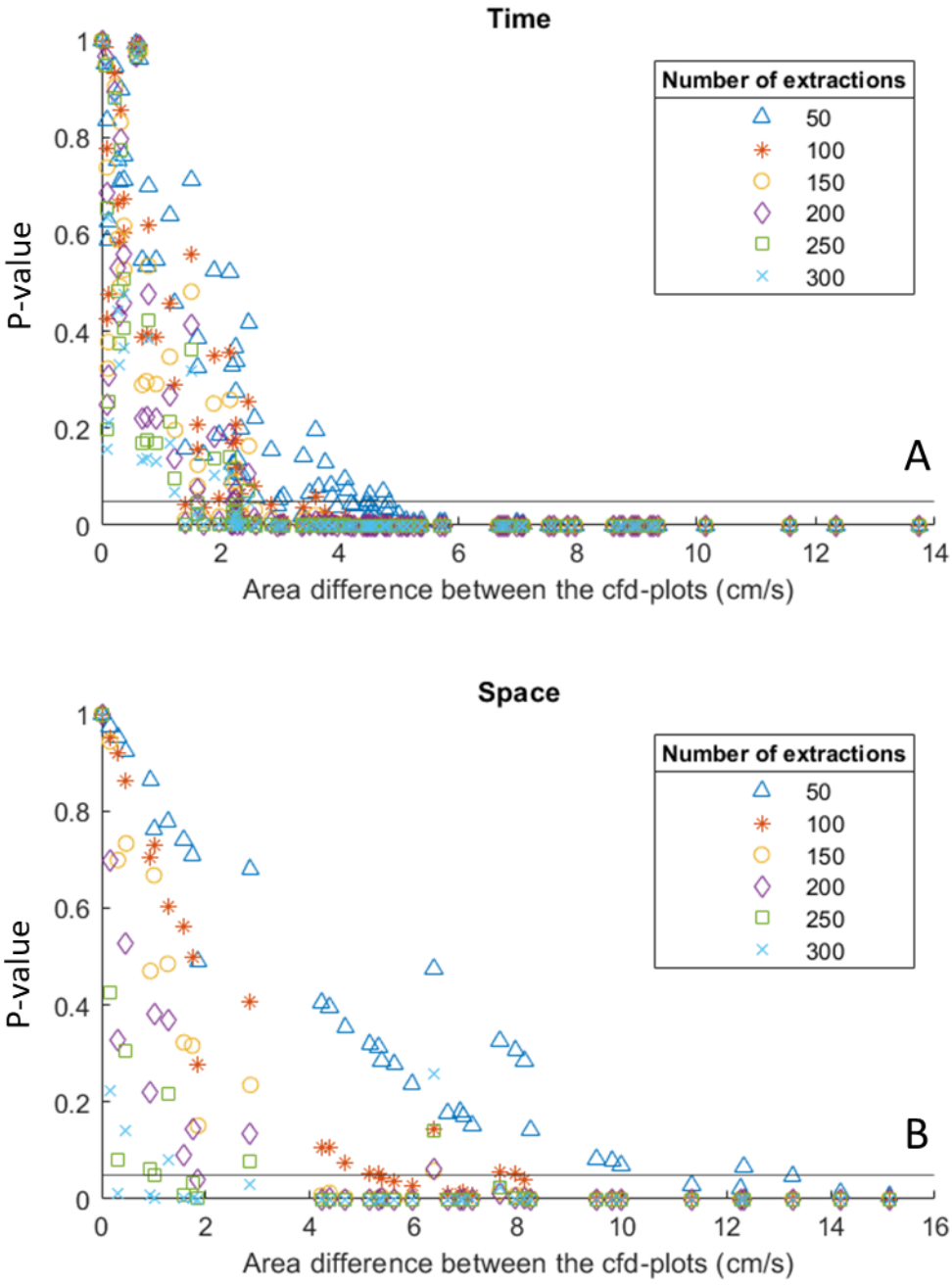

Figure 2.A2: Scatter plot comparing the p-value of the WRS-test to the area difference between de cfd-plots for all seasons (A) and all stations (B).

Chapter 3: The integration of ocean model uncertainty into Lagrangian dispersal simulations to assess its effect on larval connectivity in the Gulf of Lion.

3.1 Introduction

Recent years have seen a rise of anthropogenic influences on the ocean and this increased stress reduces the effectiveness of the ecosystem services (Douvere, 2008; Collie et al., 2013). These anthropogenic influences can cause habitat fragmentation, which can lead to a reduction in biodiversity and population abundance (Saunders et al., 1991; Fahrig, 2003; Boström et al., 2006; Cushman, 2006; Ha & Williams, 2018; Yeager et al., 2020).

An example of habitat fragmentation is the creation of a port on an otherwise sandy ocean bottom. Of course, the new port is a loss of habitat for species surviving in sandy habitats, but when looking at it from another angle, it is also creating additional hard substrate, which could be beneficial for hard substrate species. The question is whether this new hard substrate can be colonised by organisms or the opposite, where do we install artificial hard substrate to help protect marine biodiversity?

The Gulf of Lion possesses several patches of hard substrate (natural reefs), which are hotspots for biodiversity. This is why some of them were incorporated into MPAs. In the Gulf of Lion there are several MPAs, among which: The “Parc Marin de la Côte Bleue” (https://parcmarincotebleue.fr/), the “Réserve Naturelle Marine de Cérbere-Banyuls”

(https://www.reserves-naturelles.org/cerbere-banyuls) and the “Parc Naturel Marin de Golfe du Lion” (https://parc-marin-golfe-lion.fr/) (Padrón, 2015). Furthermore, artificial reefs have been installed to help degraded natural habitats and fisheries recover (Wilson, 2002; Claudet & Pelletier, 2004; Seaman, 2007). Recently, there has been an increased interest in MPAs and artificial reefs (Jones et al., 1993; Cocklin et al., 1998; Pomeroy, 1999; Halpern, 2003; Claudet & Pelletier, 2004; Costello, 2014). Rocky habitats, both natural and artificial, house sessile benthic invertebrates, which play an important part in fish trophic networks (Ardizzone et al., 1996; Martens et al., 2006; Blouet et al., submitted). However, how are sessile species able to colonise new habitat?

Most benthic marine species have a biphasic life cycle where the larval development is pelagic and the adults are sedentary (Young, 1990; Shanks, 2009; Nolasco et al., 2018; Swearer et al., 2019). Understanding pelagic larval dispersal, and thus population spread (Levins, 1969; Gaines & Lafferty, 1995; Gaylord & Gaines, 2000), is key to species protection and management (Gaines et al., 2003; Palumbi, 2004; Treml et al., 2008). For example, it can help us understand how the species would react to global change (Trakhtenbrot et al., 2005; Treml et al., 2008).

Most pelagic larvae are so minuscule that observing them in situ is extremely difficult. This is why biophysical ocean models are often used to study connectivity (Nolasco et al., 2018). Two types of models can be used to study connectivity: Eulerian and Lagrangian models. In an Eulerian model, the concentration of particles and their overall diffusion and advection is calculated, whereas in a Lagrangian model, the trajectory of each individual particle is calculated, which is why Lagrangian models take more time to compute when a large amount of particles is being tracked (Saidi et al., 2014).

Many studies assessed the sensitivity of dispersal models to life history traits such as behaviour, mortality, pelagic larval duration (PLD), spawn location and spawn period (e.g. Queiroga & Blanton, 2005; Fox et al., 2006; Guizien et al., 2006; Fiksen et al., 2007; Vikebø et al., 2007; Bolle et al., 2009; White et al., 2014; Briton et al., 2018). Kvile et al. (2018) compared transfer rates with and without vertical behaviour added to their model and found a mean difference in transfer rate of around 3% and a median of 1%.

Since models are often used to aid decision making (e.g. Beger et al., 2010; Kough et al., 2013; Andrello et al., 2015; Gallego et al., 2017; Bode et al., 2019), they need to be reliable. This is why it is important to quantify the model's uncertainties. Dispersal models (=connectivity simulations) are assessed using different techniques: Comparison of simulated larval settlement with in situ observations (e.g. Sponaugle et al., 2012), comparison of simulated surface drifters with observed ones (e.g. Carlson et al., 2016), using genetic parentage techniques (e.g. Bode et al., 2019), inter-model comparisons (e.g. Hufnagl et al., 2017) or intra-model comparisons (e.g. Huret et al., 2007; Putman & He 2013; Kvile et al., 2018). The deviation between observed and simulated connectivity can be due to uncertainties in biotic traits, but also due to the flow simulations as well. This is where the present study completes comes in, as it includes the error on the flow and assesses its direct influence on the dispersal model.

The mistake made by the hydrodynamical current simulation, which was quantified in the previous chapters, affects the larval trajectory every step of the way. This is why the instant error at every timestep (chapter 2) needs to be known to assess the effect of hydrodynamic models on simulated connectivity.

The aim of this study is to assess how the modelled flow uncertainty affects connectivity simulations. In the second chapter, the Eulerian uncertainty was assessed, which is integrated

into the Lagrangian dispersal model in this chapter. The effect of the flow velocity error on the modelled connectivity is assessed by adding the previously found velocity error to the modelled velocity and assessing the difference in connectivity matrices between the run with and without added error. Moreover, it was compared to connectivity variability arising from spawning period and PLD variation.

3.2 Materials & Methods

3.2.1 Adding flow uncertainty to a Lagrangian dispersal model

The model was the same SYMPHONIE model used in chapters one and two, but now we applied the Lagrangian routine. To study whether the uncertainty of the model has an effect on connectivity, the same Lagrangian trajectory model is run several times with an added noise and compared to a reference run without noise (figure 3.1, equation 3.1). The noise which is added is the statistical error distribution on the magnitude and angle as calculated in chapter two. It is the statistical error distribution over all data, which was used to simulate a noise velocity ($\vec{\varepsilon}_U$) to be added to the advection velocity $\vec{U}$ (equation 3.1) at each time step. This cumulative frequency distribution (figure 3.2) has 200 classes, made from the instant error calculated in chapter 2 at all stations combined and all months combined between 2010 and June 2013. At each time step, a random number between 0 and 100 % is chosen (y-axis) and the corresponding error magnitude (ε_U; figure 3.2A) and error angle (α; figure 3.2B) is determined.

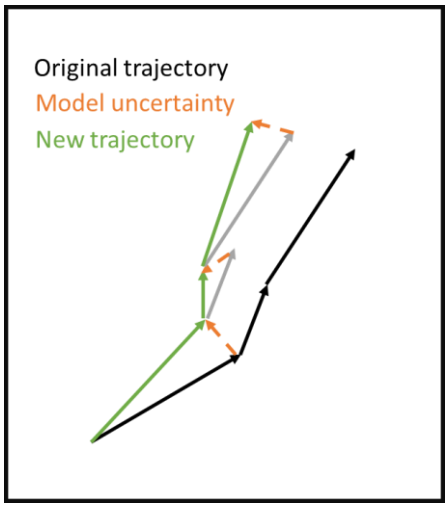

Figure 3.1: Visualisation of adding an uncertainty ($\vec{\varepsilon}_U$) to every step of the Lagrangian dispersal trajectory.

$$\frac{dX}{dt} = \vec{U} + \vec{\varepsilon}_U \text{ with } \vec{\varepsilon}_U \begin{cases} |\varepsilon_U|.cos\alpha \\ |\varepsilon_U|.sin\alpha \end{cases}$$

Equation 3.1: Lagrangian dispersal with added error. U is advection, ε is error, α is angle.

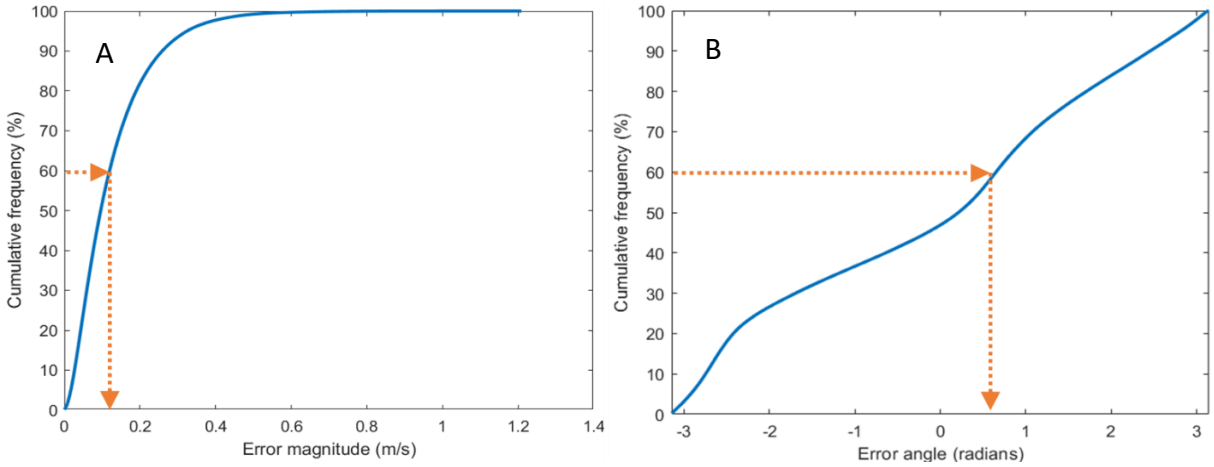

Figure 3.2: The cumulative frequency distribution of the original error (Ɛ) on the magnitude (A) and angle (B) for all data and all stations from 2010 to June 2013. The orange arrows are examples of a random number chosen between 0 and 100% (in this case 60%) on the y-axis and the noise added to the model trajectory is the complementary error value on the x-axis. This is done for both the error magnitude and angle.

3.2.2 Test cases

The different runs are all different multiples of the original error distribution (figure 3.2; table 3.1). The added magnitude error is varied (from half the original error magnitude to double the original error magnitude), the added angle error is always the same (figure 3.2B, Angle error*1). A caveat of the study is that only one particle was released per release location at a time, so no replication of the random selection was done.

Table 3.1: Specifications of the connectivity matrices $C^{e}_{i,j}$ calculated for every Lagrangian run performed in this research. With e = ε_U the added original error, with i the release period and j the PLD.

	Reference run: ε_U*0	**Half error:** ε_U/2	**Original error:** ε_U*1	**Double error:** ε_U*2
Release period 1: 1-12/06/2010	$C^{0}_{1,j}$	$C^{e/2}_{1,j}$	$C^{e}_{1,j}$	$C^{e*2}_{1,j}$
Release period 2: 13-24/06/2010	$C^{0}_{2,j}$	$C^{e/2}_{2,j}$	$C^{e}_{2,j}$	$C^{e*2}_{2,j}$
Release period 3: 19-30/07/2010	$C^{0}_{3,j}$	$C^{e/2}_{3,j}$	$C^{e}_{3,j}$	$C^{e*2}_{3,j}$

Neutrally buoyant particles were released 2 m above the bottom, every 100 m from eight artificial reef zones (figure 3.3, purple) every hour during three release periods: 1-12/06/2010, 13-24/06/2010 and 19-30/07/2010. These release periods are considered summer spawning periods since hard bottom benthic species in temperate seas spawn in summer (Weinberg & Weinberg, 1979; Coma et al., 1995; Santangelo et al., 2003; Tsounis et al., 2006). Ultimately, 1 267 776 particles were released in total. The artificial reef zones were also the arrival zones, together with ten natural reef zones (figure 3.3, green). The reef zones were described by Hentati (2017), Briton et al. (2018), Tournadre (2019) and Blouet et al. (2021).

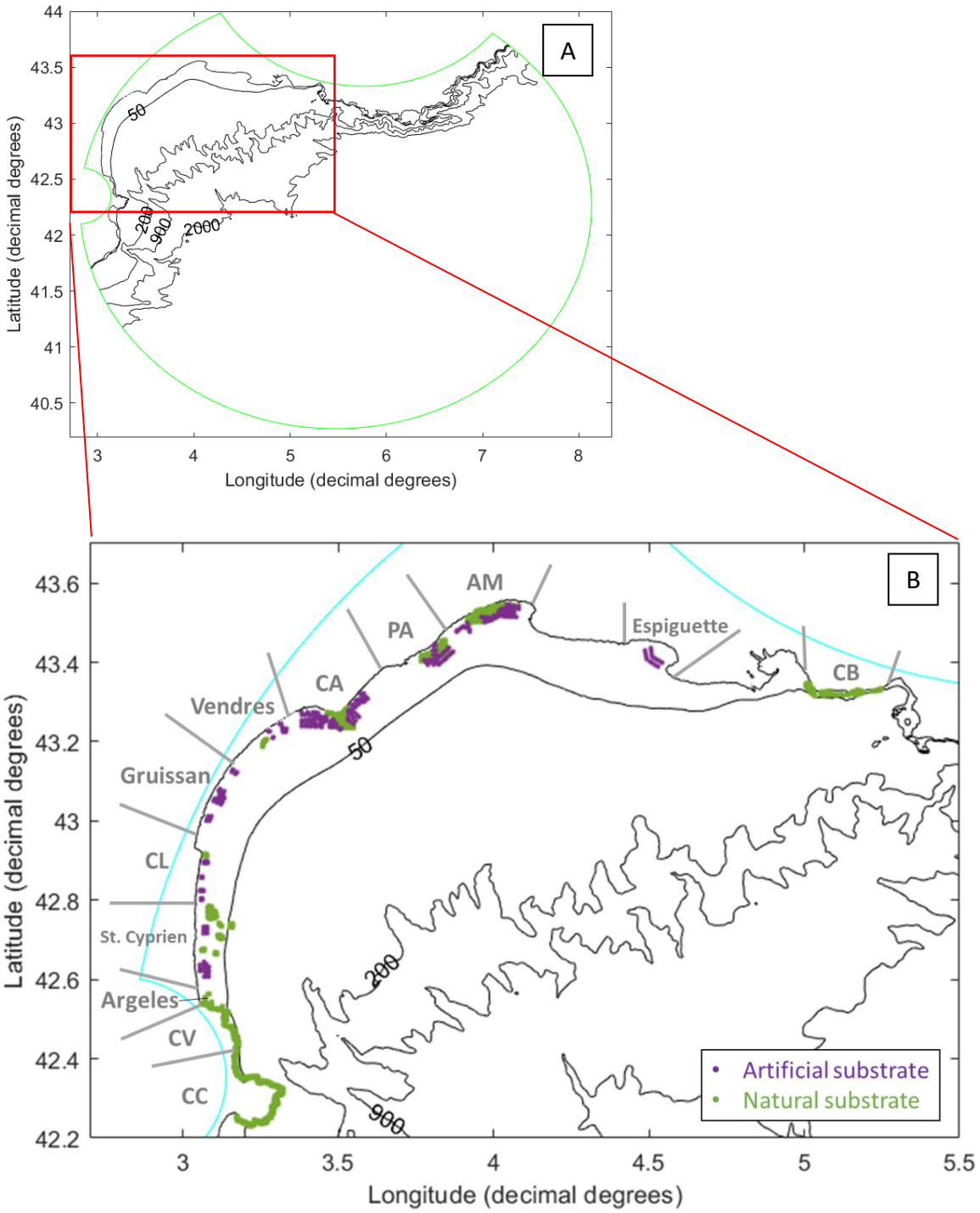

Figure 3.3: Bathymetry map of the Gulf of Lion showing the 1, 50, 200, 900 and 2000 m bathymetry lines.
A) Bathymetry map of the Gulf of Lion. The green oval depicts the edges of the model's grid.
B) Zoom on the release and arrival areas of the particles. The purple points are artificial reefs from which the particles are released. The green points are natural hard substrate. Both the artificial and the natural reefs are arrival zones.
CC: Cap de Creus; CV: Cap Vermeille; CL: Cap Leucate; CA: Cap d'Agde; PA: Plateau des Aresquiers; AM : Aigues Mortes; CB: Côte bleue.
Hentati (2017), Briton et al. (2018), Tournadre (2019), Blouet et al. (2021).

3.2.3 Connectivity calculation

The transfer rates were obtained by calculating the proportion of particles released from one zone and arriving in another. This was done after drift durations of 3.5, 7, 10.5, 14, 21, 28, 35 and 42 days, which are the PLDs of the simulated larvae. This range of PLDs was chosen so the study could be applicable to a multitude of hard substrate species.

These transfer rates form connectivity matrices between the artificial (arrival and release) reefs and the natural (arrival) reefs and were calculated for all four runs, for all eight PLDs and all three release periods. The arrival zones are the columns and the release zones are the rows. Every connectivity matrix had a size of 8x18x8 (Release zones x Arrival zones x PLDs).

The difference in transfer rates between the connectivity matrices with and without added noise for a same release period and PLD is the effect of the error on the modelled connectivity, namely the **model's connectivity sensitivity** (equation 3.2).

$$Cs_{i,j}^{e} = C_{i,j}^{e} - C_{i,j}^{0}$$

Equation 3.2: Connectivity sensitivity (Cs) calculation. C is the connectivity matrix, e the added noise, i the release period and j the PLD.

The relative difference in transfer rate is the difference between the connectivity matrices divided by the sum of the connectivity matrices, also called the **model's relative connectivity sensitivity** (equation 3.3).

$$Relative\ Cs_{i,j}^{e} = \frac{C_{i,j}^{e} - C_{i,j}^{0}}{C_{i,j}^{e} + C_{i,j}^{0}}$$

Equation 3.3: Relative connectivity sensitivity calculation. C is the connectivity matrix, e the added noise, i the release period and j the PLD.

To compare the sensitivity to the added noises, the PLD and the release periods, the number of **non-zero connections** was counted. These are the number of transfer rate percentages in the connectivity matrix different from zero.

Moreover, variability of the transfer rates between the different release periods and the added error (original error) were compared to each other.

First, the percentile range (90th percentile - 10th percentile) was calculated for all connectivity sensitivity matrices (equation 3.4 and table 3.2) for the original error (release periods (3) x PLDs (8) = 24 error variability results). This was called the **error variability** ($Var\ Cs^{e}_{i,j}$).

$$Var\ Cs^{e}_{i,j} = Q_{0.9}(Cs^{e}_{i,j}) - Q_{0.1}(Cs^{e}_{i,j})$$

Equation 3.4: Variability (Var) between connectivity sensitivity (Cs) for different release periods (i), PLDs(j) and original error added (e=ε_U). $Q_{0.9}$ is the 90th percentile, $Q_{0.1}$ is the 10th percentile.

Table 3.2: Connectivity sensitivity calculation of the original error (Cs^e) and error variability calculation for all PLDs (j) and original error added (e=ε_U). $Q_{0.9}$ is the 90th percentile, $Q_{0.1}$ is the 10th percentile

	Original error: ε_U*1		Reference run: ε_U*0		Connectivity sensitivity $Cs^{e}_{i,j}$	Error variability $Var\ Cs^{e}_{i,j}$
Release period 1: 1-12/06/2010	$C^{e}_{1,j}$	−	$C^{0}_{1,j}$	=	$Cs^{e}_{1,j}$	$Q_{0.9}(Cs^{e}_{1,j}) - Q_{0.1}(Cs^{e}_{1,j})$
Release period 2: 13-24/06/2010	$C^{e}_{2,j}$	−	$C^{0}_{2,j}$	=	$Cs^{e}_{2,j}$	$Q_{0.9}(Cs^{e}_{2,j}) - Q_{0.1}(Cs^{e}_{2,j})$
Release period 3: 19-30/07/2010	$C^{e}_{3,j}$	−	$C^{0}_{3,j}$	=	$Cs^{e}_{3,j}$	$Q_{0.9}(Cs^{e}_{3,j}) - Q_{0.1}(Cs^{e}_{3,j})$

The variability in transfer rates due to the release period was calculated by calculating the difference between reference run connectivity matrices in different release periods for the same PLD (equation 3.5) and calculating the percentile range of the resulting matrices (equation 3.6 and table 3.3). This was called the **release period variability**. Eventually, three percentile ranges corresponding to the three release period pairs were obtained per PLD (release period pairs (3) x PLDs (8) = 24 release period variability results).

$$C_{P_{i1\_i2,j}} = C^0_{i1,j} - C^0_{i2,j}$$

Equation 3.5: Difference in connectivity (C) between the release periods pairs ($C_{P_{i1\_i2,j}}$) for two different periods release (i1 and i2), for the reference run (C^0), for different PLDs(j).

$$Var\ Cp_{i1\_i2,j} = Q_{0.9}(Cp_{i1\_i2,j}) - Q_{0.1}(Cp_{i1\_i2,j})$$

Equation 3.6: Variability in connectivity sensitivity between the three release periods (Cp) for the reference run (C^0), for two release periods (i1 and i2), for different PLDs(j).

Table 3.3: Calculation of the difference in connectivity (Cp) between the different release periods (i1 and i2) and release period variability calculation for all PLDs (j). $Q_{0.9}$ is the 90th percentile, $Q_{0.1}$ is the 10th percentile

Release period i1 – Release period i2	$C_{P_{i1\_i2,j}}$	Release period variability $Var\ Cp_{i1\_i2,j}$
Release period 1 – Release period 2	$C_{P_{1\_2,j}} = C^0_{1,j} - C^0_{2,j}$	$Q_{0.9}(Cp_{1\_2,j}) - Q_{0.1}(Cp_{1\_2,j})$
Release period 2 – Release period 3	$C_{P_{2\_3,j}} = C^0_{2,j} - C^0_{3,j}$	$Q_{0.9}(Cp_{2\_3,j}) - Q_{0.1}(Cp_{2\_3,j})$
Release period 1 – Release period 3	$C_{P_{1\_3,j}} = C^0_{1,j} - C^0_{3,j}$	$Q_{0.9}(Cp_{1\_3,j}) - Q_{0.1}(Cp_{1\_3,j})$

3.3 Results

When running the model without added noise (reference run) the connectivity between the release zones St. Cyprien, CL, Gruissan, Vendres and the arrival zones northwest of CA is rather small, while the arrival zones south of CA are quite well connected to them (figure 3.4). Some zones, such as Espiguette and CB, receive almost no particles. Overall transfer rates are quite small (0-0.6% for a PLD of 7 days). The transfer rates drop drastically with increasing PLD. There are big differences in connectivity depending on the release period, but periods one and three are quite alike.

When the original error is added to the modelled velocity (figure 3.5), some zones seem to receive more larvae, like CA and AM, whilst others receive no larvae at all. The release zones St. Cyprien, CL, Gruissan, Vendres are still not or barely connected to the arrival zones northwest of CA, apart from during the second release period.

Figure 3.6 shows the model's connectivity sensitivity for the original error. Overall, most zones show no difference in transfer rate (green) when an error is added to the model. Some zones to the north, like AM and CA, seem to have an increase in transfer rate (yellow) when an error is added, but for the zones to south, the difference in transfer rate systematically decreases. For most zones, the difference in transfer rates seems to change randomly. When the model's connectivity sensitivity is not equal to zero, most zones show an increase (yellow). The difference in transfer rates decreased with increasing PLD (notice the difference in colour scale between the different PLDs) and there was a big difference in the model's connectivity sensitivity between the different release periods.

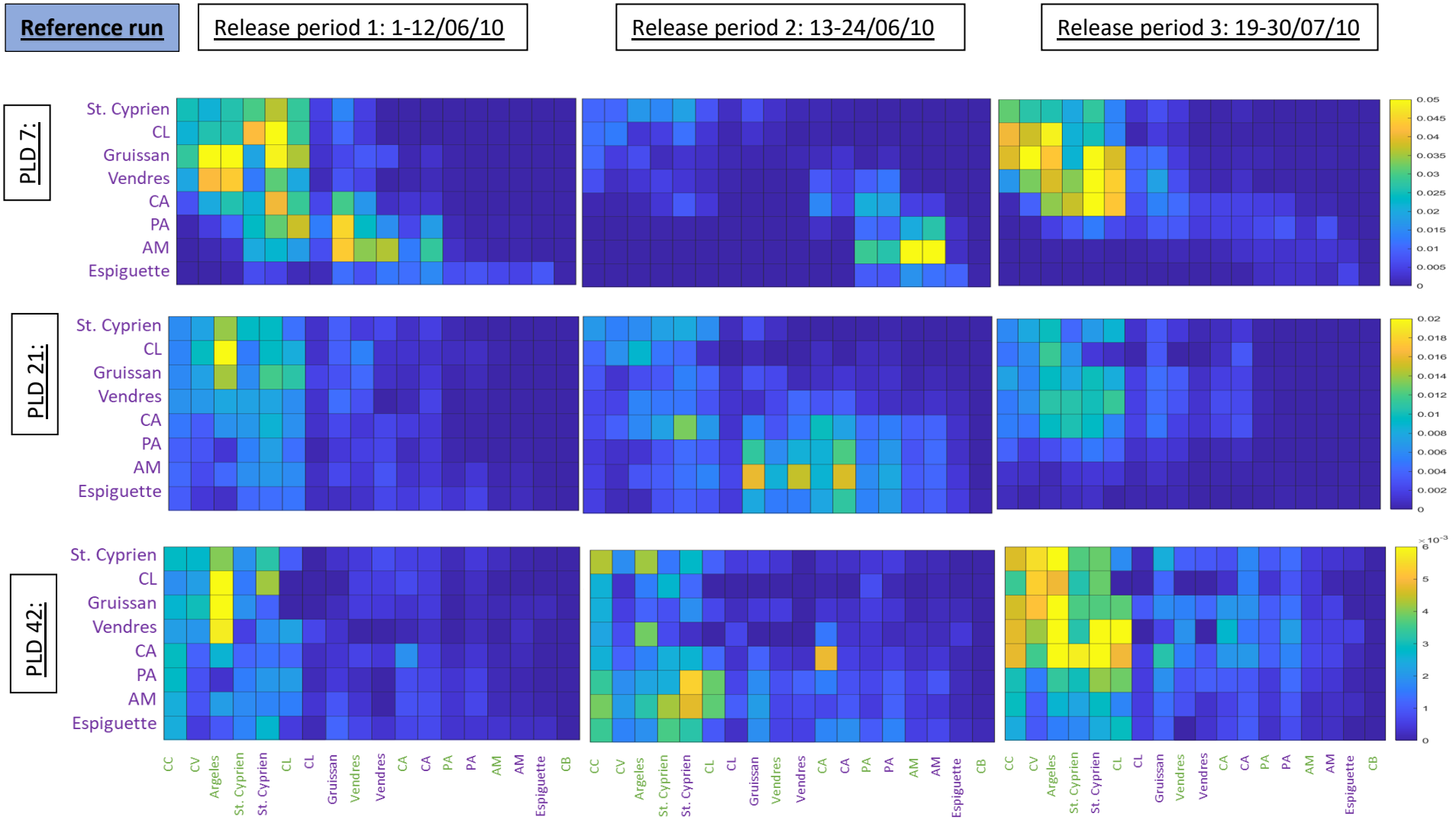

Figure 3.4: Transfer rates (%) for the reference run for different release periods and different PLDs (days). The natural substrate zones are depicted in green and the artificial substrate zones are depicted in purple. On the y-axes are the release zones, on the x-axis are the arrival zones. Every square is the average transfer rate between the two zones. Notice the difference in colour scales.

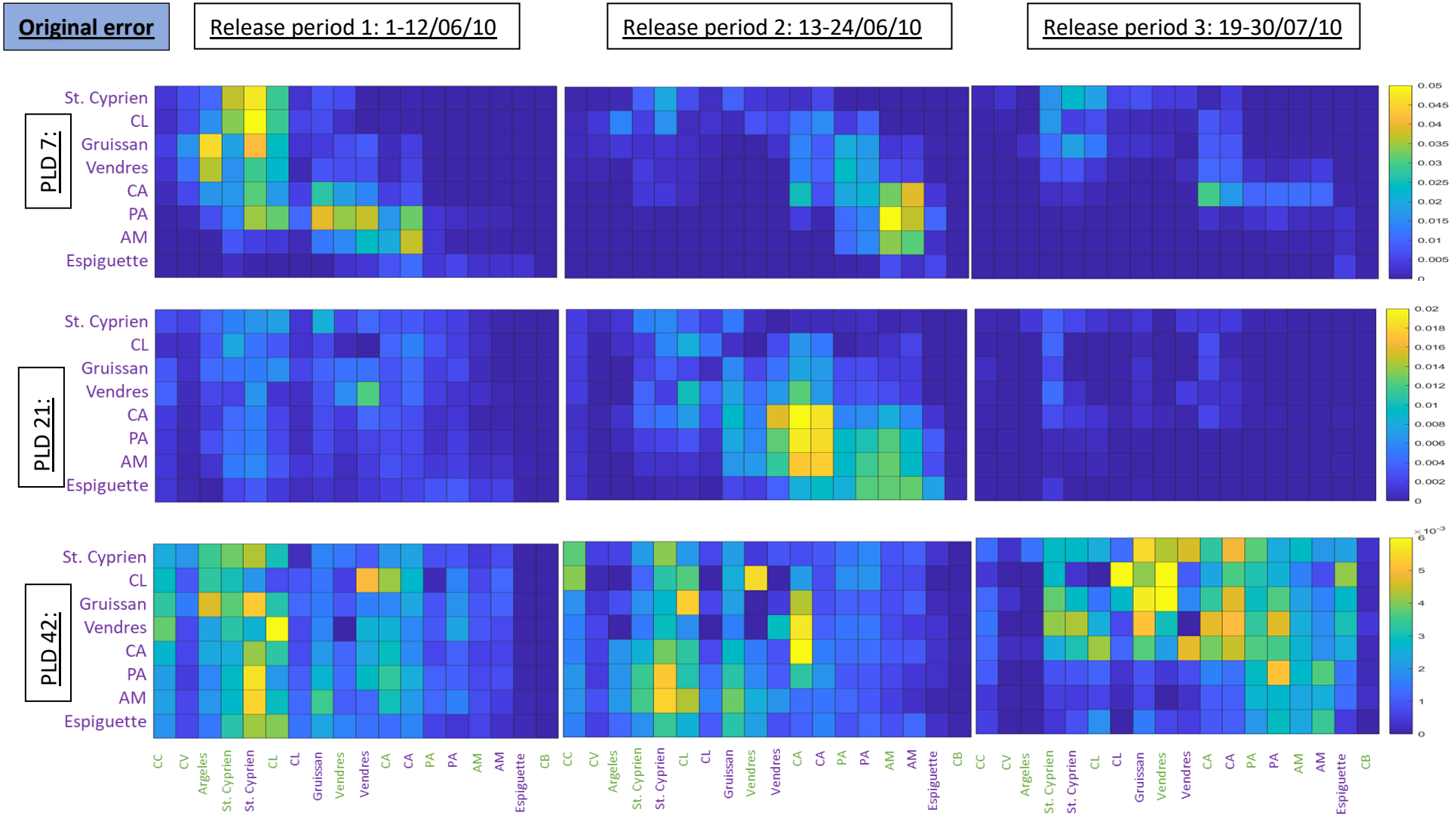

Figure 3.5: Transfer rates (%) for the original error run for different release periods and different PLDs (days). The natural substrate zones are depicted in green and the artificial substrate zones are depicted in purple. On the y-axes are the release zones, on the x-axis are the arrival zones. Every square is the average transfer rate between the two zones. Notice the difference in colour scales.

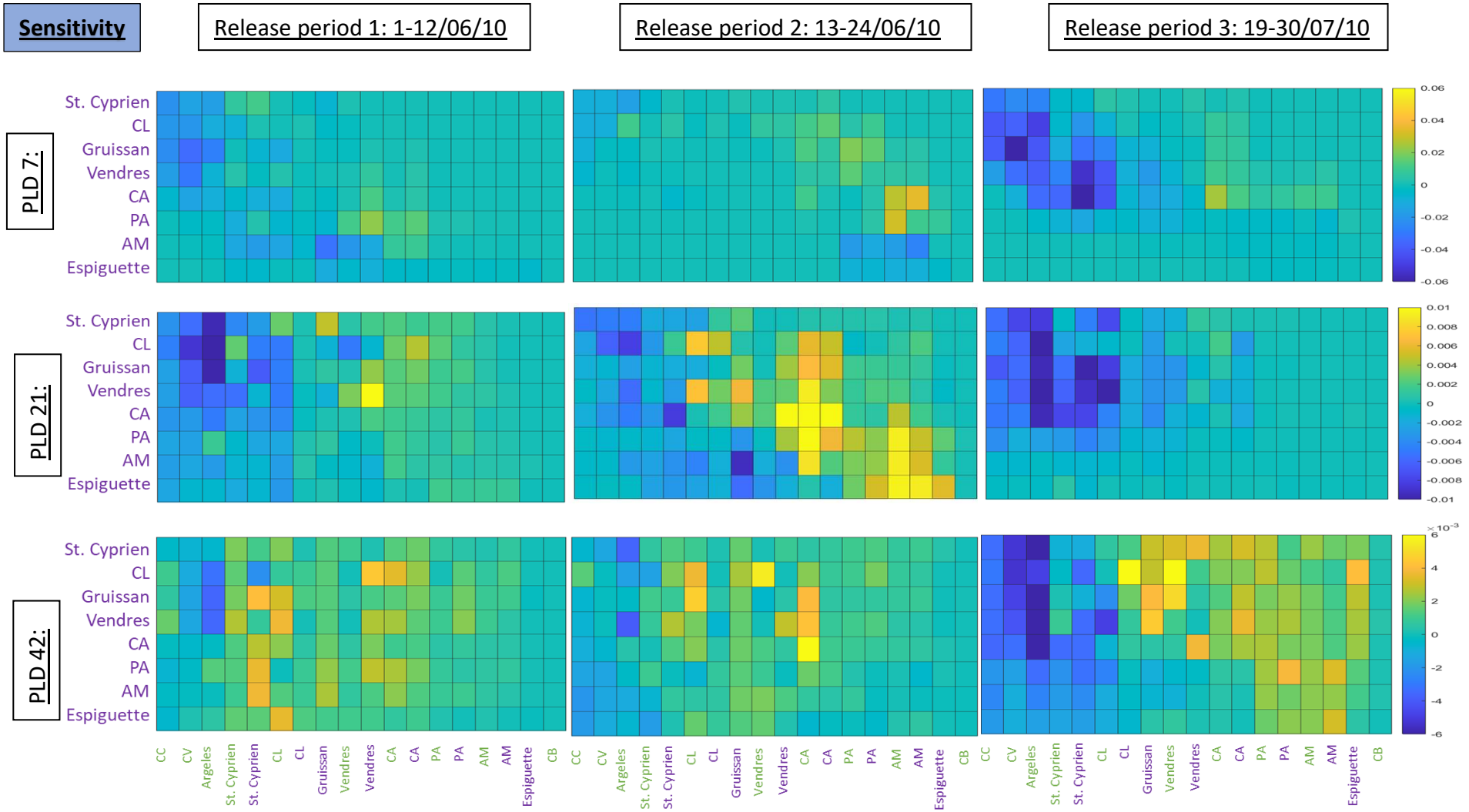

Figure 3.6: Difference in transfer rates (%) between the connectivity matrices with and without added error for different release periods and different PLDs (days). The natural substrate zones are depicted in green and the artificial substrate zones are depicted in purple. On the y-axes are the release zones, on the x-axis are the arrival zones. Every square is the average transfer rate between the two zones. Notice the difference in colour scales.

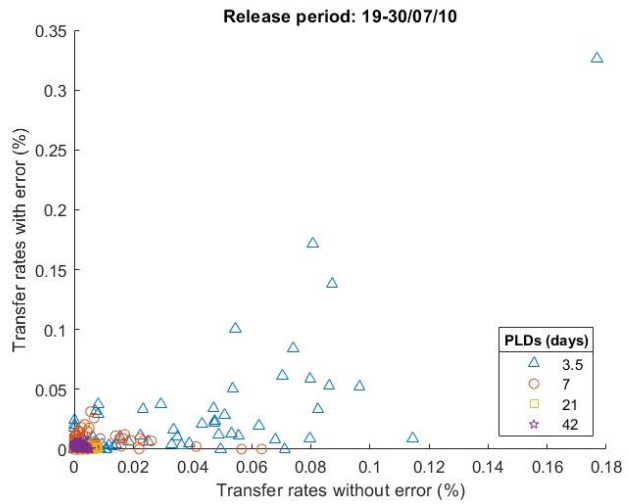

Figure 3.7: Transfer rates (%) per zone without (x-axis) versus with (y-axis) error (original error) for different PLDs.

Figure 3.7 shows that there is no clear correlation between the transfer rates with and without error.

Figure 3.8 shows that overall, the median of the model's connectivity sensitivity is around zero, meaning adding an error does not affect the connectivity in most cases. However, when it is not zero, the model often has a lower connectivity when an error is added to the model (negative) for small PLDs. For large PLDs, the model has a higher connectivity (positive) with an added error. Furthermore, the smallest added error (E/2) shows a smaller connectivity sensitivity than the other error laws (colours). It seems that the connectivity sensitivity decreases with increasing PLD in figure 3.8, but when looking at figure 3.9, which shows the relative connectivity sensitivity, it becomes clear that an increasing PLD decreases the connectivity overall and not the sensitivity.

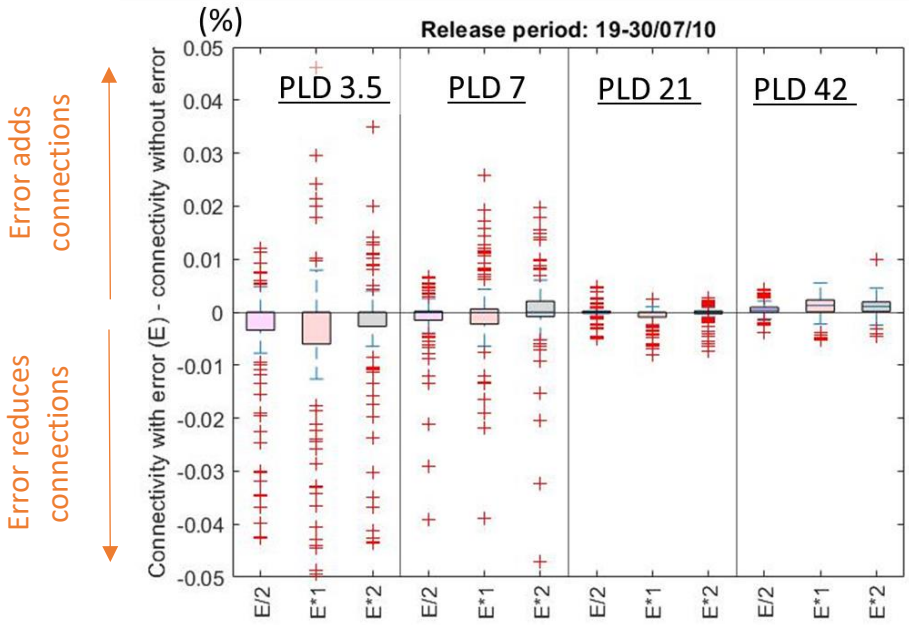

*Figure 3.8: Boxplots of connectivity sensitivity for three (E/2, E*1, E*2) different error magnitudes and the PLDs of 3.5, 7, 21 and 42 days.*

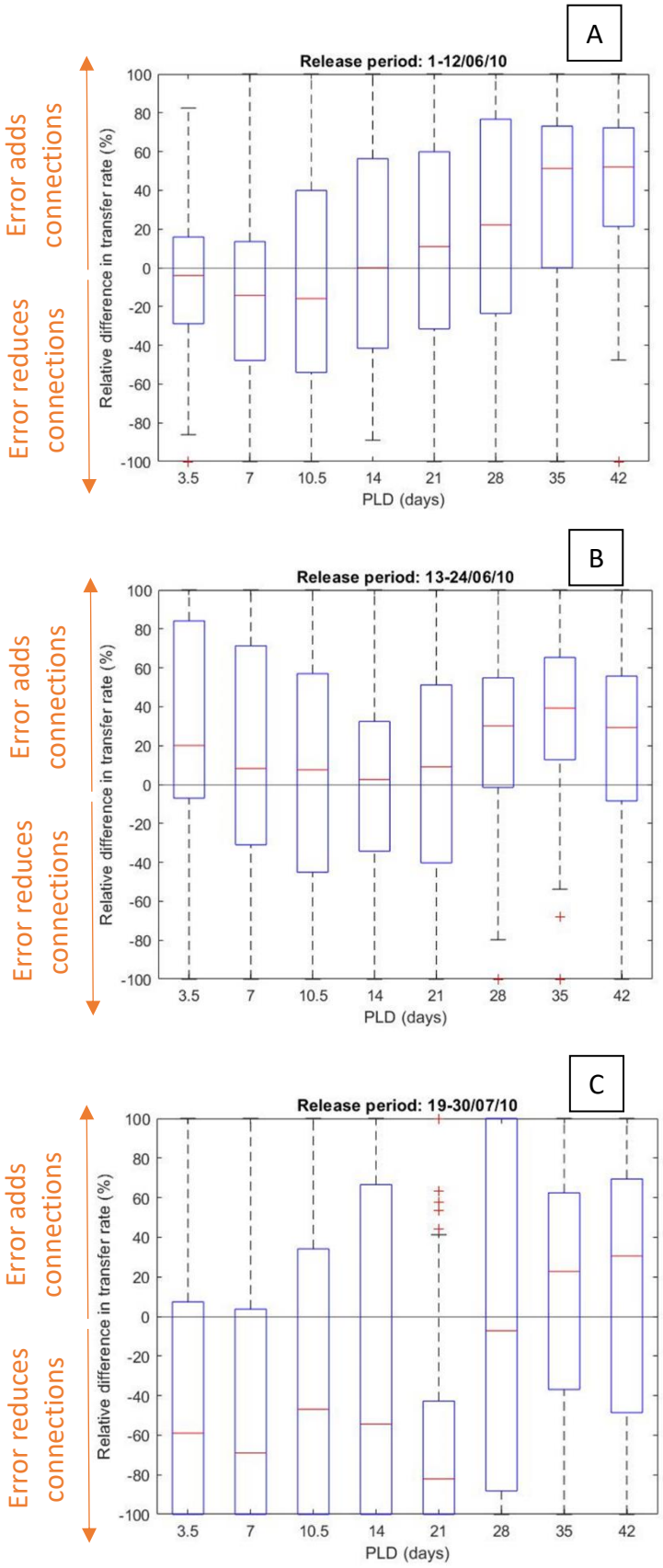

Figure 3.9: Boxplots of the model's relative connectivity sensitivity over all error magnitudes, per PLD and for all release periods (A,B,C) and PLDs

The relative differences are quite large, with medians higher than 40% and fluctuations between -100% and 100%. Moreover, there is a lot of variability in transfer rate between the release periods. Overall, it seems that for small PLDs, the relative difference is either close to zero or is negative (added error reduces connections), whilst for large errors, the relative difference becomes positive.

Figure 3.10 gives information on how the PLD affects the structure of the connectivity. The number of non-zero connections increased with the PLD for PLD up to 45 days, and was similar in the reference run (black line) and in the runs with error (coloured lines), no matter the intensity of the error. Therefore, deviation in the number of non-zero connections between the reference run and runs with error was comparable to the deviation among release periods in the reference run.

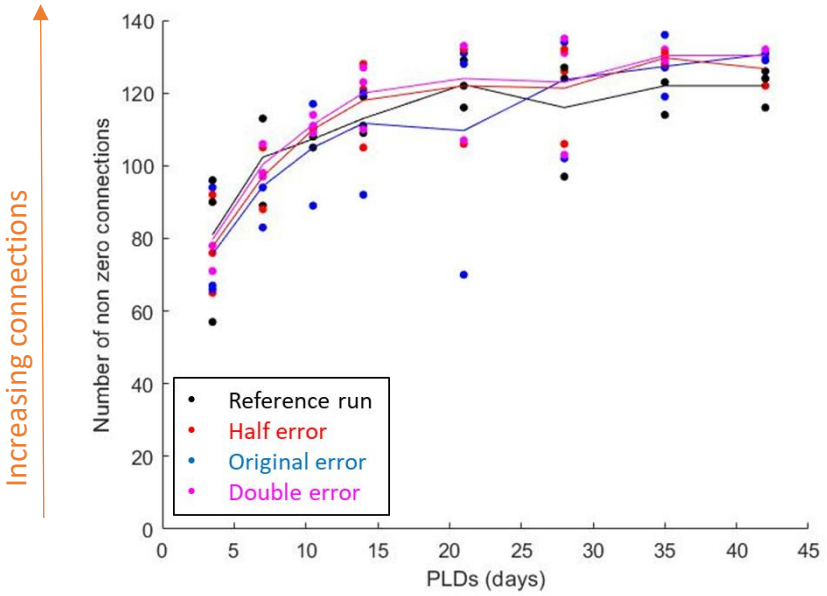

Figure 3.10: The number of non-zero connections per PLDs (x-axes), for all added noises (colours) and for all periods. The lines are the means of all three periods.

Figure 3.11 shows how the error and the release period affect the intensity of the transfer rate by showing the percentage range in transfer rate. Here, the release period variability is just as big as the error variability after a PLD of ten days. Thus, adding a velocity uncertainty in dispersal simulations affected connectivity patterns in the same order of magnitude as the uncertainty on release periods.

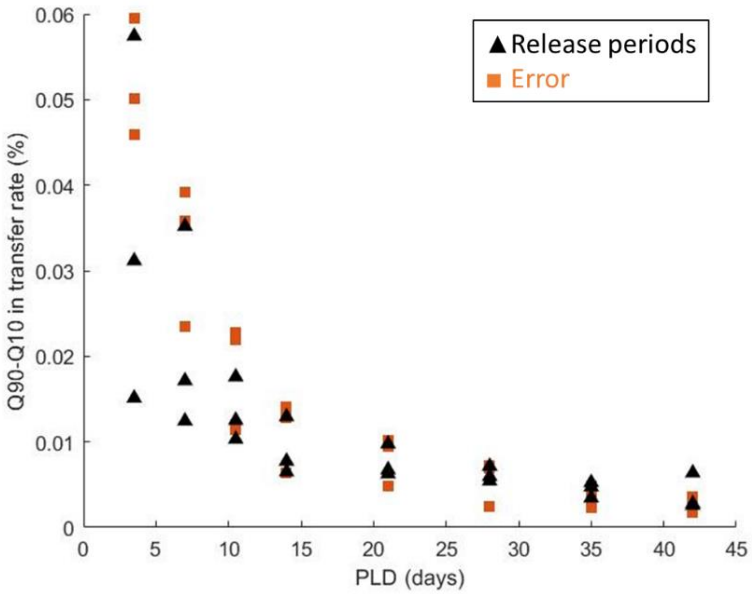

Figure 3.11: Variability in transfer rates according to the release periods ($Var\ Cp_j$) and the original error ($Var\ Cs^e_{i,j}$). Q10 stands for 10th percentile and Q90 for the 90th percentile.

3.4 Discussion

In the present study, we compared the modelled connectivity with and without added magnitude and angle error. For most zones, the connectivity doesn't change when an error is added. However, when the connectivity does change, there is usually less connectivity when an error is added for short PLDs and more connectivity for large PLDs. Moreover, the smallest error added (E/2) causes the smallest connectivity sensitivity. Lastly, after a PLD of 10 days, adding an error to the model affects the intensity of the transfer rate just as much as a different release period does and the structure of the connectivity (number of non-zero elements) is the same with or without an added error.

Previously, larval dispersal models have been validated with in situ observations (gene flow, tagging) or their sensitivity to biotic (PLD, behaviour, release location, release timing) and abiotic (grid resolution in time and space) parameters were assessed (e.g. Thorrold et al., 2002; Edwards et al., 2008; Kough & Paris, 2015; Monroy et al., 2017; Kvile et al., 2018; Bode et al., 2019). However, the novelty of this study is that it uses the instant flow uncertainties quantified through comparisons with in situ observations (chapter 2) to assess the larval dispersal model's sensitivity to flow error. To my knowledge, this is the only study to do so. The purpose of this study was to assess the effect of the model's flow error on transport and connectivity simulations.

Therefore, some biological features, like mortality and behaviour, were not included in this study. This was primarily done because these properties are often species specific, which would narrow down the relevance of the study. However, behaviour and mortality have both been proven to have a large effect on larval dispersal patterns (Cowen et al., 2000; Queiroga & Blanton, 2005; Cowen et al., 2006; Fox et al., 2006; Fiksen et al., 2007; Vikebø et al., 2007;

Bolle et al., 2009; Huebert et al., 2011; Treml et al., 2015). For mortality however, less than 10% of 524 dispersal studies included a species-specific mortality rate (Swearer et al., 2019). This is likely due to the lack of in situ mortality observations (Swearer et al., 2019). Moreover, several studies have found that the mortality is often overestimated (White et al., 2014; Johnson et al., 2015). For behaviour, Cowen et al. (2006) found that their total recruitment was 3% lower for passively dispersing larvae than when behaviour was incorporated into the model. Fox et al. (2006) found that at least 4.4% more larvae drifted offshore when no behaviour was added. The microscopic sizes of the larvae make in situ observations of the larval behaviour very difficult. Out of 524 dispersal studies, over 50% assumed passively dispersing larvae (Swearer et al., 2019), just like the present study. Furthermore, Kvile et al. (2018) tested their model's sensitivity to resolution and vertical swimming behaviour and found resolution was more influential. In other words, the relative importance of these properties is still in question. Moreover, Bode et al. (2019) found that adding behaviour to their fish larvae dispersal model gave better results than with passive larvae, but including incorrect behaviour assumptions gave the worst results. This stresses the negative effect of biological model uncertainties on dispersal model results. Therefore, although making models as realistic as possible is every modellers dream, making them overly detailed in one regard while ignoring other, equally important factors, defeats the point (May, 2014). Given the sampling difficulties and the fact that most of these traits are still ongoingly being researched, the individually based models themselves likely have uncertainties (Swearer et al., 2019). This validates the decision to not include mortality or behaviour in the present study.

The only life cycle traits which were added were spawning location, spawning period and PLD. For the release location, Blouet et al. (submitted) found that the location of artificial reefs influenced the colonisation more than the immersion time or depth. The release location of

the particles can thus not be neglected when assessing connectivity. Moreover, the retention rates can vary significantly with varying distance between release locations (Guizien et al., 2006; Briton et al., 2018).

Moreover, the results in the present study showed big differences in the model's connectivity sensitivity with varying release period. After all, several studies showed that the connectivity is heavily impacted by the release period (e.g. Hugget et al., 2003; Donahue et al., 2015; Treml et al., 2015; Romero-Torres et al., 2017; Guizien et al., 2012; Hufnagl et al., 2017; Meerhoff et al., 2020). Kough & Paris (2015) found that the release period strongly affects the connectivity and that vertical larval behaviour increased connections. Bolle et al. (2009) found up to 11% difference in transport rate between release periods which were one month apart.

In fact, in the present study, the differences in transfer rate intensity between the release periods are similar to the differences in transfer rate caused by adding an error after ten PLDs. This means that the uncertainty on the release period can affect the transfer rate just as much as the uncertainty on flow velocity. Moreover, when looking at the structure, the number of non-zero connections is not affected by adding an error.

One way this could be further analysed in future studies, is by calculating the correlation between the connectivity matrixes like the technique applied in Padrón et al. (2018) for different release periods and for the matrices with and without error. For the release periods, the correlation is expected to be low, since there are big differences in connectivity according to release periods. But will the connectivity correlation between the different release periods be higher or lower than between the matrices with and without error?

After all, in the present study, the relative difference in connectivity is quite high when an error is added. Of course, part of the high relative difference can be explained by the very low

transfer rates, making the slightest difference of high relative importance. These low transfer rates correspond with the findings of Briton et al. (2018).

For the PLD, Padrón et al. (2018) found that the genetic and simulated connectivity corresponded quite well for a PLD of 7 days. However, given the high relative differences in connectivity found in this PhD, it is likely their results would remain unchanged when taking the model's uncertainty into account. In correspondence with Padrón et al. (2018) their findings, my results from the reference run show that the Côte Bleue (CB) barely received any larvae, whilst Port Aresquieres (PA), Cap d'Agde (CA) and Cape Vermeille (CV) do.

One caveat of the study in chapter 3 is that only a single particle was released per release point per release moment. Since the added error is chosen randomly from an error distribution, the study should be repeated multiple times or several particles should be released at exactly the same place and time, to compensate for the random selection.

It must be stressed that for most zones, PLDs and release periods, the absolute difference in connectivity between the model's runs with and without error are very close to or equal to zero. This means that more often than not, the simulated connectivity is not gravely affected by the model's uncertainty. In the present study, when the connectivity is affected by the error, it is often an underestimation for short PLDs and an overestimation for long PLDs.

Since this is a novel study, it cannot be compared to similar studies. What is interesting however, is that when Sponaugle et al. (2012) compared modelled connectivity with in situ observations, they also found an under- or overestimation, depending on the arrival zone. The difference with our study is that they included life-cycle traits like mortality and behaviour. Moreover, in the present study, only a few zones had systematic under- or overestimation and most had random changes in transfer rates depending on the release period and PLD. However, Carlson et al. (2016) also found similar results when validating the ROMS model in

the Adriatic Sea with surface drifters. In some zones their model overestimated the connection percentages, whilst in others, they were underestimated, but overall they state the virtual particles results showed “remarkable agreement” with the drifter results.

Shanks (2009) states that passively dispersing particles, like the ones in the present study, accurately portray the dispersal distance for PLDs smaller than one day, but that they are overestimated for longer PLDs, since they found including behaviour into the model reduces dispersal distance. Therefore, a perspective could be to include larval behaviour. After all, many studies found that larval behaviour increases retention and/or connectivity since less particles were lost off-shore (Robins et al., 2013; Shanks, 2009; Kough & Paris, 2015).

3.5 Acknowledgments

I would like to thank the master students Thibaud Tournadre (2019) for creating the input files with the release zones for the SYMPHONIE2015 model and Skandar Hentati (2017) for the Matlab scripts that calculated the connectivity matrices.

3.6 References

Andrello, M., Jacobi, M. N., Manel, S., Thuiller, W., & Mouillot, D. (2015). Extending networks of protected areas to optimize connectivity and population growth rate. Ecography, 38(3), 273–282. https://doi.org/10.1111/ecog.00975

Ardizzone, G.D., Belluscio, A., Gravina, M.F., Somaschini, A. (1996). Colonization and Disappearance of Mytilus galloprovincialis Lam. on an Artificial Habitat in the Mediterranean Sea. Estuarine, Coastal and Shelf Science, 43, 665–676. https://doi.org/10.1006/ecss.1996.0095

Beger, M., Linke, S., Watts, M., Game, E., Treml, E., Ball, I., & Possingham, H. P. (2010). Incorporating asymmetric connectivity into spatial decision making for conservation. Conservation Letters, 3(5), 359–368. https://doi.org/10.1111/j.1755-263X.2010.00123.x

Blouet, S., Bramanti, L., & Katell, G. (submitted). Artificial reefs geographical location matters more than its age and depth for sessile invertebrate colonization in the Gulf of Lion (NorthWestern Mediterranean Sea) Sylvain. BioRxiv, 6. https://doi.org/10.1101/2021.10.08.463669

Blouet, S., Quittet, L., Agin, G., Thorin, S., Dalias, N., Marobin, D., Lenfant, P., Guizien, K., (2021). Database of the location and typology of artificial reefs in the Gulf of Lion (NW Mediterranean Sea).

Bode, M., Leis, J. M., Mason, L. B., Williamson, D. H., Harrison, H. B., Choukroun, S., & Jones, G. P. (2019). Successful validation of a larval dispersal model using genetic parentage data. PLoS Biology, 17(7), 1–13. https://doi.org/10.1371/journal.pbio.3000380

Bolle, L. J., Dickey-Collas, M., Van Beek, J. K. L., Erftemeijer, P. L. A., Witte, J. I., Van Der Veer, H. W., & Rijnsdorp, A. D. (2009). Variability in transport of fish eggs and larvae. III. Effects of hydrodynamics and larval behaviour on recruitment in plaice. Marine Ecology Progress Series, 390(September), 195–211. https://doi.org/10.3354/meps08177

Boström, C., Jackson, E. L., & Simenstad, C. A. (2006). Seagrass landscapes and their effects on associated fauna: A review. Estuarine, Coastal and Shelf Science, 68(3–4), 383–403. https://doi.org/10.1016/j.ecss.2006.01.026

Briton, F., Cortese, D., Duhaut, T., & Guizien, K. (2018). High-resolution modelling of ocean circulation can reveal retention spots important for biodiversity conservation. Aquatic Conservation: Marine and Freshwater Ecosystems, 28(4), 882–893. https://doi.org/10.1002/aqc.2901

Carlson, D. F., Griffa, A., Zambianchi, E., Suaria, G., Corgnati, L., Magaldi, M. G., Poulain, P. M., Russo, A., Bellomo, L., Mantovani, C., Celentano, P., Molcard, A., & Borghini, M. (2016). Observed and modeled surface Lagrangian transport between coastal regions in the Adriatic Sea with implications for marine protected areas. Continental Shelf Research, 118(May 2019), 23–48. https://doi.org/10.1016/j.csr.2016.02.012

Claudet, J. & Pelletier, D. (2004). Marine protected areas and artificial reefs: A review of the interactions between management and scientific studies. Aquatic Living Resources, 17(2), 129–138. https://doi.org/10.1051/alr:2004017

Cocklin C., Craw M., McAuley I. (1998). Marine reserves in New Zealand: Use rights, public attitudes, and social impacts. Coastal Management, 26, 213-231

Collie, J. S., Vic Adamowicz, W. L., Beck, M. W., Craig, B., Essington, T. E., Fluharty, D., Rice, J., & Sanchirico, J. N. (2013). Marine spatial planning in practice. Estuarine, Coastal and Shelf Science, 117, 1–11. https://doi.org/10.1016/j.ecss.2012.11.010

Coma, R., Ribes, R. M., Zabala, M., & Gilil, J. M. (1995). Reproduction and cycle of gonadal development in the Mediterranean gorgonian Paramuricea clavata. Marine Ecolology Progress Series, 117, 173-183.

Costello, M. J. (2014). Long live Marine Reserves: A review of experiences and benefits. Biological Conservation, 176, 289–296. https://doi.org/10.1016/j.biocon.2014.04.023

Cowen, R. K., Kamazima, L. M. M., Sponaugle, S., Paris, C. B., & Olsen, D. B. (2000). Connectivity of Marine Populations: Open or Closed? Science, 287(5760), 522–527. https://doi.org/10.1126/science.1122039

Cowen, R. K., Paris, C. B., & Srinivasan, A. (2006). Scaling of connectivity in marine populations. Science, 311(5760), 522–527. https://doi.org/10.1126/science.1122039

Cushman, S. A. (2006). Effects of habitat loss and fragmentation on amphibians: A review and prospectus. Biological Conservation, 128(2), 231–240. https://doi.org/10.1016/j.biocon.2005.09.031

Donahue, M. J., Karnauskas, M., Toews, C., & Paris, C. B. (2015). Location is not everything: Timing of spawning aggregations optimizes larval replenishment. PLoS ONE, 10(6), 1–14. https://doi.org/10.1371/journal.pone.0130694

Douvere, F. (2008). The importance of marine spatial planning in advancing ecosystem-based sea use management. Marine Policy, 32(5), 762–771. https://doi.org/10.1016/j.marpol.2008.03.021

Edwards, K. P., Hare, J. A., & Werner, F. E. (2008). Dispersal of black sea bass (Centropristis striata) larvae on the southeast U.S. continental shelf: Results of a coupled vertical

larval behavior - 3D circulation model. Fisheries Oceanography, 17(4), 299–315. https://doi.org/10.1111/j.1365-2419.2008.00480.x

Fahrig, L. (2003). Effects of Habitat Fragmentation on Biodiversity. Annual Review of Ecology, Evolution, and Systematics, 34, 487–515. https://doi.org/10.1146/annurev.ecolsys.34.011802.132419

Fiksen, Ø., Jørgensen, C., Kristiansen, T., Vikebø, F., & Huse, G. (2007). Linking behavioural ecology and oceanography: Larval behaviour determines growth, mortality and dispersal. Marine Ecology Progress Series, 347, 195–205. https://doi.org/10.3354/meps06978

Fox, C. J., McCloghrie, P., Young, E. F., & Nash, R. D. M. (2006). The importance of individual behaviour for successful settlement of juvenile plaice (Pleuronectes platessa L.): A modelling and field study in the eastern Irish Sea. Fisheries Oceanography, 15(4), 301–313. https://doi.org/10.1111/j.1365-2419.2005.00396.x

Gaines, S. D., Gaylord, B., & Largier, J. L. (2003). Avoiding current oversights in marine reserve design. Ecological Applications, 13(1 SUPPL.), 32–46. https://doi.org/10.1890/1051-0761(2003)013[0032:acoimr]2.0.co;2

Gaines, S. D., & Lafferty, K. D. (1995) Modeling the dynamics of marine species: the importance of incorporating larval dispersal. Ecology of marine invertebrate larvae. CRC Press, Boca Raton, 389–412

Gallego, A., Gibb, F. M., Tullet, D., & Wright, P. J. (2017). Bio-physical connectivity patterns of benthic marine species used in the designation of Scottish nature conservation marine protected areas. ICES Journal of Marine Science, 74(6), 1797–1811. https://doi.org/10.1093/icesjms/fsw174

Gaylord, B., & Gaines, S. D. (2000). Temperature or transport? Range limits in marine species mediated solely by flow. American Naturalist, 155(6), 769–789. https://doi.org/10.1086/303357

Guizien, K., Belharet, M., Marsaleix, P., & Guarini, J. M. (2012). Using larval dispersal simulations for marine protected area design: Application to the Gulf of Lions (northwest Mediterranean). Limnology and Oceanography, 57(4), 1099–1112. https://doi.org/10.4319/lo.2012.57.4.1099

Guizien, K., Brochier, T., Duchêne, J. C., Koh, B. S., & Marsaleix, P. (2006). Dispersal of Owenia fusiformis larvae by wind-driven currents: Turbulence, swimming behaviour and mortality in a three-dimensional stochastic model. Marine Ecology Progress Series, 311(1986), 47–66. https://doi.org/10.3354/meps311047

Ha, G., & Williams, S. L. (2018). Eelgrass community dominated by native omnivores in Bodega Bay, California, USA. Bulletin of Marine Science, 94(4), 1333–1353. https://doi.org/10.5343/bms.2017.1091

Halpern, B. (2003). The impact of marine reserves: Do reserves work and does reserve size matter? Ecological Applications, 13, 117-137.

Hentati, S. (2017). Analyse du rôle des Récifs Artificiels dans la dynamique de métapopulation des gorgones : Approche numérique [Master thesis, Institut national agronomique de Tunesie]

Huebert, K. B., Cowen, R. K., & Sponaugle, S. (2011). Vertical migrations of reef fish larvae in the straits of florida and effects on larval transport. Limnology and Oceanography, 56(5), 1653–1666. https://doi.org/10.4319/lo.2011.56.5.1653

Hufnagl, M., Payne, M., Lacroix, G., Bolle, L. J., Daewel, U., Dickey-Collas, M., Gerkema, T., Huret, M., Janssen, F., Kreus, M., Pätsch, J., Pohlmann, T., Ruardij, P., Schrum, C.,

Skogen, M. D., Tiessen, M. C. H., Petitgas, P., van Beek, J. K. L., van der Veer, H. W., & Callies, U. (2017). Variation that can be expected when using particle tracking models in connectivity studies. Journal of Sea Research, 127(May 2016), 133–149. https://doi.org/10.1016/j.seares.2017.04.009

Huggett, J., Fréon, P., Mullon, C., & Penven, P. (2003). Modelling the transport success of anchovy Engraulis encrasicolus eggs and larvae in the southern Benguela: The effect of spatio-temporal spawning patterns. Marine Ecology Progress Series, 250(March 2003), 247–262. https://doi.org/10.3354/meps250247

Huret, M., Runge, J. A., Chen, C., Cowles, G., Xu, Q., & Pringle, J. M. (2007). Dispersal modeling of fish early life stages : sensitivity with application to Atlantic cod in the western Gulf of Maine. 347, 261–274. https://doi.org/10.3354/meps06983

Johnson, D. W., Christie, M. R., Stallings, C. D., Pusack, T. J., & Hixon, M. A. (2015). Using post-settlement demography to estimate larval survivorship: a coral reef fish example. Oecologia, 179(3), 729–739. https://doi.org/10.1007/s00442-015-3368-5

Jones G.P., Cole R.C. & Battershill C.N. (1993) Marine Reserves: Do they work? In: NIWA (Ed.), The Ecology of Temperate Reefs: Proceedings of the Second International Temperate Reef Symposium, Auckland, New Zealand, pp. 29-45.

Kough, A. S., & Paris, C. B. (2015). The influence of spawning periodicity on population connectivity. Coral Reefs, 34(3), 753-757.

Kough, A. S., Paris, C. B., & Butler IV, M. J. (2013). Larval Connectivity and the International Management of Fisheries. PLoS ONE, 8(6). https://doi.org/10.1371/journal.pone.0064970

Kvile, K. Ø., Romagnoni, G., Dagestad, K. F., Langangen, Ø., & Kristiansen, T. (2018). Sensitivity of modelled North Sea cod larvae transport to vertical behaviour, ocean model

resolution and interannual variation in ocean dynamics. ICES Journal of Marine Science, 75(7), 2013–2024. https://doi.org/10.1093/icesjms/fsy039

Levins, R. (1969). Some Demographic and Genetic Consequences of Environmental Heterogeneity for Biological Control. American Entomologist, 15(3), 237–240.

Martens, K., Queiroga, H., Cunha, M.R., Cunha, A., Moreira, M.H., Quintino, V., Rodrigues, A.M., Seroôdio, J., Warwick, R.M. (Eds.) (2006). Marine Biodiversity: Patterns and Processes, Assessment, Threats, Management and Conservation. Springer Netherlands, Dordrecht. https://doi.org/10.1007/1-4020-4697-9

May, R. M. (2004). Uses and Abuses of Mathematics in Biology. Science, 303(5659), 790–793. https://doi.org/10.1126/science.1094442

Meerhoff, E., Defeo, O., Combes, V., Franco, B. C., Matano, R. P., Piola, A. R., Vaca, F. H., & Celentano, E. (2020). Assessment of larval connectivity in a sandy beach mole crab through a coupled bio-oceanographic model. Estuarine, Coastal and Shelf Science, 246(September). https://doi.org/10.1016/j.ecss.2020.107035

Monroy, P., Rossi, V., Ser-Giacomi, E., López, C., & Hernández-García, E. (2017). Sensitivity and robustness of larval connectivity diagnostics obtained from Lagrangian Flow Networks. ICES Journal of Marine Science, 74(6), 1763–1779. https://doi.org/10.1093/icesjms/fsw235

Nolasco, R., Gomes, I., Peteiro, L., Albuquerque, R., Luna, T., Dubert, J., Swearer, S. E., & Queiroga, H. (2018). Independent estimates of marine population connectivity are more concordant when accounting for uncertainties in larval origins. Scientific Reports, 8(1), 1–16. https://doi.org/10.1038/s41598-018-19833-w

Padrón, M. (2015). Evaluation of conservation efficiency for gorgonian species at a regional scale based on an existing Marine Protected Area network and modeling scenarios

accounting for hydrodynamics. [Doctoral dissertation, Université Pierre et Marie Curie, Università di Bologna]

Padrón, M., Costantini, F., Baksay, S., Bramanti, L., & Guizien, K. (2018). Passive larval transport explains recent gene flow in a Mediterranean gorgonian. Coral Reefs, 37(2), 495–506. https://doi.org/10.1007/s00338-018-1674-1

Palumbi, S. R. (2004). Marine reserves and Ocean neighborhoods: The spatial scale of marine populations and their management. Annual Review of Environment and Resources, 29, 31–68. https://doi.org/10.1146/annurev.energy.29.062403.102254

Pomeroy, C. (1999) Social considerations for marine resource management: Evidence from Big Creek Ecological Reserve. Reports of California Cooperative Oceanic Fisheries Investigations Rep. 40, 118-125.

Putman, N. F., & He, R. (2013). Tracking the long-distance dispersal of marine organisms: Sensitivity to ocean model resolution. Journal of the Royal Society Interface, 10(81). https://doi.org/10.1098/rsif.2012.0979

Queiroga, H., & Blanton, J. (2005). Interactions between behaviour and physical forcing in the control of horizontal transport of decapod crustacean larvae. Advances in marine biology, 47, 107-214.

Robins, P. E., Neill, S. P., Giménez, L., Stuart, R., Jenkins, S. R., & Malham, S. K. (2013). Physical and biological controls on larval dispersal and connectivity in a highly energetic shelf sea. Limnology and Oceanography, 58(2), 505–524. https://doi.org/10.4319/lo.2013.58.2.0505

Romero-Torres, M., Acosta, A., & Treml, E. A. (2017). The regional structure of spawning phenology and the potential consequences for connectivity of coral assemblages

across the Eastern Tropical Pacific. ICES Journal of Marine Science, 74(3), 613–624. https://doi.org/10.1093/icesjms/fsw218

Saidi, M. S., Rismanian, M., Monjezi, M., Zendehbad, M., & Fatehiboroujeni, S. (2014). Comparison between Lagrangian and Eulerian approaches in predicting motion of micron-sized particles in laminar flows. Atmospheric Environment, 89, 199–206. https://doi.org/10.1016/j.atmosenv.2014.01.069

Santangelo, G., Carletti, E., Maggi, E., Bramanti, L. (2003) Reproduction and population sexual structure of the overexploited Mediterranean red coral Corallium rubrum. Marine Ecology Progress Series, 248, 99–108

Saunders, D., Hobbs, R., & Margules, C. (1991). Biological Consequences of Ecosystem Fragmentation: A Review. Conservation Biology, 5(1), 18–32. https://doi.org/10.1111/j.1523-1739.1991.tb00384.x

Seaman, W. (2007). Artificial habitats and the restoration of degraded marine ecosystems and fisheries. Hydrobiologia, 580(1), 143–155. https://doi.org/10.1007/s10750-006-0457-9

Shanks, A. L. (2009). Pelagic larval duration and dispersal distance revisited. Biological Bulletin, 216(3), 373–385. https://doi.org/10.2307/25548167

Sponaugle, S., Paris, C., Walter, K. D., Kourafalou, V., & D'Alessandro, E. (2012). Observed and modeled larval settlement of a reef fish to the Florida Keys. Marine Ecology Progress Series, 453, 201–212. https://doi.org/10.3354/meps09641

Swearer, S. E., Treml, E. A., & Shima, J. S. S. (2019). A Review of Biophysical Models of Marine Larval Dispersal. In Oceanography and Marine Biology (Vol. 57, pp. 325–356). CRC Press.

Thorrold, S. R., Jones, G. P., Hellberg, M. E., Burton, R. S., Swearer, S. E., Neigel, J. E., Morgan, S. G., & Warner, R. R. (2002). Quantifying larval retention and connectivity in marine populations with artificial and natural markers. Bulletin of Marine Science, 70(1 SUPPL.), 291–308.

Tournadre, T. (2019). Analyse de la connectivité océanologique au sein des réseaux de substrats durs naturels et artificiels du Golfe du Lion. [Master thesis, Université de Rennes]

Trakhtenbrot, A., Nathan, R., Perry, G., & Richardson, D. M. (2005). The importance of long-distance dispersal in biodiversity conservation. Diversity and Distributions, 11(2), 173–181. https://doi.org/10.1111/j.1366-9516.2005.00156.x

Treml, E. A., Ford, J. R., Black, K. P., & Swearer, S. E. (2015). Identifying the key biophysical drivers, connectivity outcomes, and metapopulation consequences of larval dispersal in the sea. Movement Ecology, 3(1), 1–16. https://doi.org/10.1186/s40462-015-0045-6

Treml, E. A., Halpin, P. N., Urban, D. L., & Pratson, L. F. (2008). Modeling Population Connectivity by Ocean Currents, a Graph-theoretic Approach for Marine Conservation. Landscape Ecology, 23(1), 19–36.

Tsounis, G., Rossi, S., Aranguren, M., Gili, J. M., & Arntz, W. (2006). Effects of spatial variability and colony size on the reproductive output and gonadal development cycle of the Mediterranean red coral (Corallium rubrum L.). Marine Biology, 148(3), 513–527. https://doi.org/10.1007/s00227-005-0100-8

Vikebø, F., Jørgensen, C., Kristiansen, T., & Fiksen, Ø. (2007). Drift, growth, and survival of larval Northeast Arctic cod with simple rules of behaviour. Marine Ecology Progress Series, 347, 207–219. https://doi.org/10.3354/meps06979

Weinberg, S., & Weinberg, F. (1979). The life cycle of a gorgonian: Eunicella singularis (Esper, 1794). Bijdragen tot de Dierkunde, 48(2), 127-140.

White, J. W., Morgan, S. G., & Fisher, J. L. (2014). Planktonic larval mortality rates are lower than widely expected. Ecology, 95(12), 3344–3353. https://doi.org/10.1890/13-2248.1

Wilson, K. (2002). Restoration of Hong Kong fisheries through deployment of artificial reefs in marine protected areas. ICES Journal of Marine Science 59, 157–163. https://doi.org/10.1006/jmsc.2002.1186

Yeager, L. A., Estrada, J., Holt, K., Keyser, S. R., & Oke, T. A. (2020). Are Habitat Fragmentation Effects Stronger in Marine Systems? A Review and Meta-analysis. Current Landscape Ecology Reports, 5(3), 58–67. https://doi.org/10.1007/s40823-020-00053-w

Young, C.M. (1990). Larval ecology of marine invertebrates: a sesquicentennial history. Ophelia 32(1–2), 1–48.

General conclusions and perspectives

With increasing anthropogenic pressures on the ocean, the need to protect biodiversity in the ocean is bigger than ever. In order to give sound advice on where and why to implement MPAs, the connectivity in coastal areas must be thoroughly understood. Connectivity analyses have been performed using a variety of techniques, such as genetic analyses (Hedgecock et al., 2007) and artificial or natural tags (Thorrold et al., 2002). However, the small sizes of the dispersing larvae compared to the vastness of the ocean makes determining larval dispersal patterns in situ rather laborious. This is why hydrodynamical ocean models are often used to study larval dispersal. The red thread throughout this PhD is analysing the uncertainty of the SYMPHONIE2015 model and its effect on larval dispersal simulations.

In the first chapter, the robustness of the model to assumption violation was tested. This was done by calculating six relative and absolute statistical indicators during and outside of wind, wave and stratification events. During these events, either the model's turbulent closure, the hydrostatic assumption or the Boussinesq approximation wasn't respected. The results showed that the model's performance is not affected by these events. Moreover, the absolute indicators showed the model performed worse during the events more often than the relative indicators. This is probably because during wave and wind events, higher current speeds can occur and absolute indicators increase with current speed.

Since the uncertainty of the model affects the larval trajectory at every step, in the second chapter, the instant error was calculated (contrary to the first chapter, where the error was integrated over the event duration). Then, the cumulative error distributions were compared to each other in space and time. In time, the intraseasonal differences in error distributions were smaller than the interseasonal ones. In space, eight groups of error distributions could

be formed. Lastly, the spatial groups were compared to modelling (resolution) and environmental (stratification, depth, bathymetry and current speed) characteristics. No link was found between the model's performance and the resolution. Similar to chapter one, no link was found between the model's performance and stratification and wave interaction (water depth as proxy). What was also suggested in chapter one, was a link between the model's performance and the current speed. This was confirmed in chapter two, as a strong correlation between the current speed and the error distributions was found.

In chapter three, the overall instant error which was found in chapter two was added as noise to the Lagrangian dispersal simulations and compared to the original run to assess the effect of the models' error on connectivity. The noise added was the overall instant error over all stations and the entire study period. This was done three times with different multiples of this error magnitude distribution: Half error, original error and double error. The larvae were released during summer 2010 from eight artificial hard substrate zones. These artificial substrate zones were also the arrival zones, together with ten natural hard substrate zones. The results show that the median difference in transfer rate between the runs with and without noise is zero for most zones. Some zones had systematic under- or overestimation, whilst in other zones, the difference in transfer rate when adding noise was random. However, when there is a difference in transfer rate, the runs with noise often underestimate the connectivity for small PLDs and overestimate for large PLDs. Moreover, the relative difference in transfer rate can vary from -100% to 100%, even though the median is around zero. Moreover, after 10 PLDs a different release zone affects the connectivity just as much as adding an error to the model.

During this PhD, an extensive amount of current velocity observations was gathered. There was less data available during the autumn and summer months. Therefore, it would be nice if

in the future, more current observation data was available during these periods. Additional mooring data at shallow depths during the summer and autumn months could make it possible for the study to be repeated with more robustness for these seasons. Moreover, only the winter and spring months were used for the spatial analyses in chapter two and performing the same study for all four seasons could be interesting.

Since model validation with hydrodynamic data is quite rare, this study aids in quantifying the uncertainty of the SYMPHONIE2015. Moreover, the finding that the model is not sensitive to intrinsic assumption violation, is very interesting. However, the true novelty of this study is that it first quantifies the uncertainty of the model using current observations, to then perform an intramodel comparison to its own error (chapter three).

Padrón et al. (2018) found that the simulated connectivity corresponded with their genetic findings. They also found that that the Côte Bleue (CB) and Espiguette were barely connected to the rest of the Gulf of Lion. This is thought-provoking, as these zones are close to the Mesurho station, which had the biggest error of all shallow stations. Despite the large error in these zones, the model's connectivity simulation still corresponds to the observed genetic analyses by Padrón et al. (2018).

A perspective for chapter three could be to further extend the number of multiples in error magnitude added to the model (e.g. one tenth). The reason several multiples of the error magnitude were added as a noise, was to see the effect on connectivity of the different magnitudes. Since no difference in transfer rate was found between the different multiples of magnitude, perhaps it would be interesting to also add varying multiples of angle error as a noise and see how this affects the simulated connectivity. Furthermore, one could go deeper into the connectivity between the different zones and study the parentage (=origin) of the particles.

In chapter three, a single particle was released every 100 m per zone every hour during three release periods. One perspective for this chapter should be to release multiple particles from the same spot at the same time and use them as repeats to compensate for the randomly selected noise from the error distribution.

Another way to prevent a change in results due to the random selection, it to add a constant error magnitude over the entire Gulf of Lion and see how that would affect connectivity.

Of course, this wouldn't be very realistic, as chapter 2 clearly showed spatial differences in error. Therefore, the noise could be added to the model depending on the error distribution groups defined in chapter 2. In other words, the noise added to the trajectory of the particle would depend on where the particle was, as the noise would be selected from the error distribution that belonged to the group found at this place. Since these error distributions are defined using observational data from these places, the added noise would be closer to the actual error the particle would experience.

Moreover, given the strong correlation between observed current speed and the model's error magnitude which was found in chapter 2, it could also be interesting to add a noise to the modelled velocity in chapter 3 which is proportionate to the current speed.

Of course, given the complexity and particularity of the Gulf of Lion, the results of such studies could only be applied to this region, which reduces the scope and applicability of the results. This is the case for the entire PhD anyhow, as all observations were gathered in the Gulf of Lion, within three and a half years (2010 - June 2013) and only one model (SYMPHONIE2015) was used. Nevertheless, this PhD gave way to the development of several new techniques to study the uncertainty of ocean models used for larval dispersal, such as the analyses of the model's instant error distribution according to space and time (chapter 2) and the intramodel

comparison to its own error (chapter 3). It is the first study to quantify the uncertainty of the connectivity matrix caused by flow speed uncertainties.

The development of new research techniques and the quantification of the uncertainties of existing research methods is imperative to quality science, especially since connectivity and dispersal will be crucial for benthic species persistence in the face of climate change. This PhD seeks to put an error bar around dispersal simulations and is a first step to aiding future management decisions.

References

Hedgecock, D., Barber, P. H., & Edmands, S. (2007). Genetic approaches to measuring connectivity. Oceanography, 20(SPL.ISS. 3), 70–79. https://doi.org/10.5670/oceanog.2007.30

Padrón, M., Costantini, F., Baksay, S., Bramanti, L., & Guizien, K. (2018). Passive larval transport explains recent gene flow in a Mediterranean gorgonian. Coral Reefs, 37(2), 495–506. https://doi.org/10.1007/s00338-018-1674-1

Thorrold, S. R., Jones, G. P., Hellberg, M. E., Burton, R. S., Swearer, S. E., Neigel, J. E., Morgan, S. G., & Warner, R. R. (2002). Quantifying larval retention and connectivity in marine populations with artificial and natural markers. Bulletin of Marine Science, 70(1 SUPPL.), 291–308.

Table of figures

General introduction

Chapter 1

Chapter 2

Chapter 3

Table of tables

Chapter 1

Chapter 2

Chapter 3

French summary

L'océan a un impact important sur l'atmosphère, les terres et la biosphère. Il couvre 71% de la surface de la terre (Hoegh-Guldberg et al., 2014) et fournit de nombreux services écosystémiques tels que la nourriture, les transports et le tourisme (Barbier, 2017). La littérature indique que ces services augmentent avec l'augmentation de la biodiversité (Loreau et al., 2001 ; Tilman, 2001 ; Sala & Knowlton, 2006 ; Worm et al., 2006 ; Butler et al., 2007 ; Hector & Bagchi, 2007 ; Palumbi et al., 2009). Malgré son importance, il est continuellement menacé par des influences anthropiques telles que la surpêche (Christensen et al., 2007), la pollution (Sindermann, 1995), l'acidification (Hoegh-Guldberg et al., 2014) et le réchauffement climatique (Hoegh-Guldberg et al. , 2014). De plus, le nombre de personnes vivant le long de la côte ne cesse d'augmenter (Small & Nicholls, 2003 ; Neumann et al., 2015). Ce stress accru sur l'océan peut créer des conflits entre les différents services écosystémiques, réduisant leur efficacité (Douvere, 2008 ; Collie et al., 2013).

L'augmentation des influences anthropiques sur l'océan peut également provoquer une fragmentation de l'habitat. La fragmentation de l'habitat peut entraîner une réduction de la biodiversité et de l'abondance de la population (Saunders et al., 1991 ; Fahrig, 2003 ; Boström et al., 2006 ; Cushman, 2006 ; Ha & Williams, 2018 ; Yeager et al., 2020). Un exemple de fragmentation de l'habitat est la création d'un port sur un fond océanique autrement sablonneux. Bien sûr, le nouveau port est une perte d'habitat pour les espèces survivant dans les habitats sablonneux, mais vu sous un autre angle, il crée également un substrat dur supplémentaire, ce qui pourrait être bénéfique pour les espèces à substrat dur. La question

est de savoir si ce nouveau substrat dur peut être colonisé par des organismes ou au contraire, où installer un substrat dur artificiel pour aider à protéger la biodiversité marine ?

L'augmentation du stress sur l'environnement marin est la raison pour laquelle la planification spatiale marine (PSM) est de plus en plus appliquée (Foley et al., 2010 ; Lubchenco & Sutley, 2010). Malheureusement, de nombreux MSP sont principalement basés sur la croissance économique, alias la croissance bleue, plutôt que sur la conservation marine (Qiu & Jones, 2013 ; Frazão Santos et al., 2018).

Heureusement, il y a eu un intérêt accru pour la protection des océans du monde (Sala et al., 2018) avec de plus en plus d'aires marines protégées (AMP) mises en œuvre dans les MSP (Lubchenco & Grorud-Colvert, 2015 ; Sala et al., 2018). Lors de la Convention des Nations Unies sur la diversité biologique (CDB) en 2010, il a été décidé que d'ici 2020, 10 % de l'océan devrait être protégé (Sala et al., 2018). Cependant, Sala et al. (2018) ont constaté que seulement 3,6% de l'océan se trouve en fait dans une AMP, car bon nombre des AMP signalées ne sont pas encore installées ou ne sont pas suffisamment protégées des activités d'extraction. De plus, les scientifiques affirment qu'au moins 30 % devraient être protégés pour protéger correctement la biodiversité de l'océan (O'Leary et al., 2016 ; Sala et al., 2018). De plus, même dans les AMP sans prélèvement, la biomasse et la biodiversité n'augmentent pas nécessairement pour les invertébrés, puisque la plupart d'entre eux ont été mis en œuvre pour soutenir la pêche (Lester et al., 2009 ; Guizien et al., 2012). C'est pourquoi donner des conseils scientifiques judicieux sur l'emplacement d'installation des AMP est crucial pour la protection des espèces de tous les taxons.

Pour bien comprendre comment protéger les invertébrés sessiles, il faut regarder leur cycle de vie, car la plupart d'entre eux ont un stade larvaire pélagique (Thorson, 1946 ; Young, 1990), qui a des durées variables, même au sein d'une même espèce (Scheltema, 1986 ; Victor, 1986

; Guizien et al., 2020). Les quatre étapes de leur cycle de vie sont : l'initiation de l'émigration, le transport et le mouvement, l'établissement et le recrutement (Pineda et al., 2007). La persistance d'une espèce dépend aussi fortement des interactions au sein de la population. Bien entendu, différentes espèces vivant dans le même habitat peuvent également interagir entre elles via la prédation, la compétition, le parasitisme, le mutualisme ou le commensalisme (Lang & Benbow, 2013). C'est ce qu'on appelle une communauté et la dispersion entre différentes communautés forme des métacommunautés (Wilson, 1992).

Malheureusement, les AMP sont souvent installées dans des lieux à forte biodiversité (Briton et al., 2018), sans tenir compte du fonctionnement des métapopulations ou des métacommunautés (Halpern & Warner, 2003). Dans le Golfe du Lion, il existe trois AMP : Le « Parc Marin de la Côte Bleue » (https://parcmarincotebleue.fr/), la « Réserve Naturelle Marine de Cérbere - Banyuls » (https://www.reserves-naturelles.org/cerbere-banyuls) et le « Parc Naturel Marin de Golfe du Lion » (https://parc-marin-golfe-lion.fr/) (Padrón, 2015). Le plus souvent, la taille de la réserve est beaucoup plus petite que l'étendue spatiale de l'espèce (Allison et al., 1998 ; Palumbi, 2004 ; Gaines et al., 2010). Une solution serait d'agrandir les AMP, mais compte tenu de l'augmentation du nombre de personnes vivant sur le littoral évoquée précédemment, il s'agit d'un scénario improbable. Une autre option est de créer un réseau d'AMP connectées, car plusieurs études en ont montré les bénéfices (Crowder et al., 2000 ; Neubert, 2003 ; Costello & Polasky, 2008). La dispersion larvaire joue un rôle déterminant dans le succès des AMP.

Cette thèse cherche à comprendre la deuxième étape de la dispersion larvaire : le transport et le mouvement, qui est un processus fortement influencé par les courants océaniques. Les courants océaniques sont régulés par divers facteurs. Non seulement la bathymétrie et la salinité ont un effet, mais aussi les influences atmosphériques telles que le vent et la

température. Lorsqu'on regarde le climat méditerranéen en particulier, il a un climat assez particulier en raison de sa position latitudinale. Les hivers sont humides et doux, en raison de la position de la ceinture de vent d'ouest à cette période. En été, le temps est chaud et sec pendant plusieurs mois, car il est sous l'influence des systèmes anticycloniques subtropicaux (Harding et al., 2009). La Méditerranée est une mer semi-fermée qui est reliée à la mer Rouge par le canal de Suez, à la mer Noire par la mer de Marmara et à l'océan Atlantique par le détroit de Gibraltar. Les caractéristiques de la circulation générale de la Méditerranée ont également été décrites par de nombreux autres articles (par exemple Malanotte-Rizzoli & Bergamasco, 1991 ; Robinson & Golnaraghi, 1993 ; Millot, 1994 ; Roussenov et al., 1995 ; Pinardi & Masetti, 2000 ; Molcard et al. al., 2002). Dans les eaux peu profondes (0-500 m), il y a un afflux d'eau de l'Atlantique à travers le détroit de Gibraltar. En Méditerranée orientale, elle devient l'eau intermédiaire levantine (300-800 m). À travers le détroit de Sicile, cette eau plus chaude et plus salée peut à nouveau se déplacer vers l'ouest. Une fois là, l'eau peut se densifier et se transformer en eau profonde sous la force constante des vents froids et secs (MEDOC GROUP, 1969 ; Lascaratos, 1993 ; Theocharis et al., 1993 ; Marshall & Schott, 1999 ; Pinardi & Masetti, 2000 ; Mikolajczak, 2019). En Méditerranée nord-occidentale, on trouve le Courant Nord, qui est constitué des eaux intermédiaires mentionnées précédemment (Millot, 1999 ; Barrier et al., 2016 ; Mikolajczak, 2019). Il longe le plateau continental du Golfe du Lion, qui est la partie de la mer Méditerranée sur laquelle se concentre cette thèse.

Le Golfe du Lion est situé dans la partie nord-ouest de la mer Méditerranée microtidale et possède un large plateau continental d'une profondeur moyenne de 70 m (Aloisi et al., 1973). Il est délimité par une rupture de plateau abrupte, incisée par un réseau dense de canyons sous-marins. Sa circulation côtière résulte principalement de l'interaction entre le Courant Nord thermohaline, qui s'écoule le long de la rupture du plateau du nord-est au sud-ouest et

les fréquents vents continentaux soufflant du nord et du nord-ouest (Mistral et Tramontane resp.), qui induisent une convection hivernale (Millot, 1990). Ces vents sont froids et secs, ce qui rend l'eau plus froide et donc plus dense. Cela les fait couler au fond dans un processus appelé cascade d'eau de plateau dense. Les canyons jouent un rôle important dans le guidage de cette eau dense vers les parties plus profondes de l'océan (Herrmann et al., 2008 ; Puig et al., 2008 ; Ulses et al., 2008 ; Puig et al., 2013 ; Mikolajczak, 2019) . Les vents du sud-est et du sud, qui soufflent moins fréquemment, se produisent principalement de l'automne au printemps et peuvent provoquer de grosses houles. Cependant, les vagues dans le Golfe du Lion sont généralement assez petites (Guizien, 2009). La circulation côtière du Golfe du Lion est également influencée par le débit sortant de l'un des plus grands fleuves méditerranéens, le Rhône, et d'une série de fleuves plus petits avec des régimes de crues éclair typiquement méditerranéens (Guizien et al., 2007 ; Ludwig et al., 2009). La taille du panache d'eau douce du Rhône dépend des conditions atmosphériques, de la force du débit du fleuve et de la circulation de l'eau de mer (Millot, 1990 ; Many et al., 2016 ; Many et al., 2018). Les couches superficielles du Golfe du Lion peuvent se stratifier thermiquement entre le printemps et l'automne et sont déstabilisées de manière récurrente près du rivage par l'upwelling côtier (Millot, 1990 ; Petrenko et al., 2005). Les sédiments côtiers du Golfe du Lion sont constitués de sable, de limons, de boue et de quelques plaques de substrat rocheux dur (Aloïsi, 1973 ; Bourrin, 2007). Récemment, plusieurs récifs artificiels ont été installés (Blouet et al., 2021), augmentant la quantité de substrat dur. De plus, des récifs artificiels ont été installés pour aider les habitats naturels dégradés et les pêcheries à se rétablir (Wilson, 2002; Claudet et Pelletier, 2004; Seaman, 2007). Les habitats rocheux, tant naturels qu'artificiels, abritent des invertébrés benthiques, qui jouent un rôle important dans les réseaux trophiques des poissons (Ardizzone et al., 1996 ; Martens et al., 2006 ; Blouet et al., soumis).

Lorsqu'on anticipe la dispersion des êtres vivants, il est important de prendre en compte que les résultats obtenus ne sont que temporairement pertinents. À savoir, la dynamique de la population, la propagation et l'habitat changent constamment en raison de causes naturelles ou anthropiques. C'est pourquoi la quantification des incertitudes des simulations est importante, car de cette façon, l'incertitude autour des simulations de prévision peut être anticipée. Par exemple, le réchauffement climatique provoque un déplacement géographique de l'habitat convenable pour de nombreuses espèces (Chen et al. , 2011). Pour survivre à cela, ils peuvent soit se déplacer vers un habitat plus approprié, soit évoluer, ces deux processus nécessitent une dispersion (Berg et al., 2010; Bellard et al., 2012).

Bien que la dispersion ait été étudiée in situ par le biais, par exemple, de techniques génétiques (Hedgecock et al., 2007) et de marquage (par exemple, Bailey, 1997), elle est souvent modélisée à l'aide de modèles biophysiques constitués de deux facteurs : facteurs biologiques et physiques. Les facteurs biologiques comprennent la mortalité, la croissance, le comportement, la durée des larves pélagiques (DPL), la période de frai et la zone de frai. De nombreuses études ont évalué la sensibilité des modèles de dispersion aux traits d'histoire de vie tels que le comportement, la mortalité, la durée des larves pélagiques (DPL), l'emplacement et la période de frai (p. ex. Queiroga et Blanton, 2005; Fox et al., 2006; Guizien et al., 2006 ; Fiksen et al., 2007 ; Vikebø et al., 2007 ; Bolle et al., 2009 ; White et al., 2014 ; Briton et al., 2018). Cette thèse porte principalement sur les influences physiques sur la dispersion larvaire modélisée, à savoir l'écoulement des courants océaniques.

Malheureusement, les observations de vitesse océanique, qui sont nécessaires pour décrire ces processus de transport, sont souvent limitées dans le temps ou dans l'espace. Les radars satellites ou terrestres et les dériveurs lagrangiens peuvent mesurer les courants sur une vaste zone, mais uniquement près de la surface de l'océan (Dohan et al., 2010 ; Mader et al., 2016).

Certains courantomètres in situ fournissent des séries chronologiques de mesure de débit le long de profils verticaux (par exemple, Acoustic Doppler Current Profiler, ADCP), mais les mesures ponctuelles sont encore courantes (Schroeder et al., 2013 ; Durrieu de Madron et al., 2019). Les ADCP qui n'étaient auparavant déployés qu'à des mouillages fixes (Guizien et al., 1999) sont désormais montés sur des coques de navires (Sextant, 1996) ou sur des véhicules sous-marins autonomes (Dohan et al., 2010 ; Bourrin et al. 2015 ; Gentil et al 2020). Au final, les appareils de mesure des courants océaniques sont déployés soit sur le plan horizontal, soit sur le plan vertical, ce qui limite fortement leur applicabilité à l'étude des processus de transport. Pour cette raison, les processus de transport sont principalement étudiés à l'aide de simulations de courant sur l'ensemble de l'océan.

Les modèles de circulation océanique varient selon les différentes échelles et processus qu'ils visent à simuler. Les modèles de marée sont des modèles bidimensionnels, prédisant l'élévation de la surface de la mer et le transport d'écoulement horizontal intégré à la profondeur, dont la principale application est la navigation (Le Provost & Lyard, 2000). Les modèles de circulation océanique globale (OGCM) sont des modèles tridimensionnels résolvant la dynamique océanique à des échelles spatiales grossières partout sur terre (1/12°). Ils reposent soit sur le couplage atmosphérique pour les prévisions climatiques (Siedler et al., 2001 ; Chassignet et al., 2007 ; Somot et al., 2008). Les modèles de circulation côtière sont des modèles tridimensionnels forcés par des modèles atmosphériques, la plupart du temps sans interaction air-mer, simulant la dynamique des flux océaniques et l'hydrologie sur une zone limitée. Ces modèles visent à simuler des processus océaniques de méso-échelle à sous-méso-échelle, comme les tourbillons (Hu et al., 2009 ; Hu et al., 2011), les cascades d'eau dense (Ulses et al., 2008) et les panaches fluviaux (Marsaleix et al., 1998). Ils utilisent une résolution spatiale horizontale qui peut être plus précise que 100 m et une résolution verticale qui peut

être plus précise que 1 m (Estournel et al., 2003 ; Briton et al., 2018). De tels modèles sont considérés comme capables de décrire les processus contrôlant le transport des matières dissoutes et/ou particulaires dans une variété d'applications (marées noires, transfert terre-mer, modélisation des écosystèmes, connectivité des populations). Des modèles de circulation régionale ont également été couplés à des modèles de vagues pour le transport des sédiments et la prévision de l'érosion des plages (Ulses et al., 2008 ; Dufois et al., 2008 ; Warner et al., 2008). Des exemples de ces modèles sont le Modèle d'Applications à l'Echelle Régionale (MARS 3D ; Lazure & Dumas, 2008 ; Dumas & Langlois, 2009), le modèle Ecologique Hydrodynamique COuplé pour les mers du plateau régional (COHERENS ; Dulière et al., 2019), le Regional Ocean Modelling System (ROMS ; Moore et al., 2011) et SYMPHONIE (Marsaleix et al., 2008, 2009a).

Les modèles océaniques, comme tous les modèles, sont des approximations de la réalité, ce qui signifie qu'ils ne sont pas parfaits et comportent des incertitudes. Celles-ci sont soit liées à la mise en œuvre du modèle, soit aux hypothèses intrinsèques du modèle. La mise en œuvre du modèle inclut la résolution spatiale et temporelle des modes baroclines et la précision des données de forçage (forçage atmosphérique, ruissellement fluvial, bathymétrie et forçage en zone ouverte). La sensibilité à la résolution spatiale de la grille (Kirtman et al., 2012 ; Kvile et al., 2018 ; Cai et al., 2020) et au forçage atmosphérique et aux frontières ouvertes (Kourafalou et al., 2009) a été largement illustrée.

Étant donné que les modèles sont souvent utilisés pour aider à la prise de décision (par ex. Beger et al., 2010 ; Kough et al., 2013 ; Andrello et al., 2015 ; Gallego et al., 2017 ; Bode et al., 2019), ils ont besoin être fiable, c'est pourquoi de nombreuses techniques de validation différentes ont déjà été développées.

Par exemple, les simulations ont été comparées à des paramètres hydrologiques mesurés in situ comme la salinité et la température (par exemple Gustafsson et al., 1998; Reffray et al., 2004; André et al., 2005; Kara et al., 2006; Chelton et al. ., 2007 ; Pairaud et al., 2011 ; Renault et al., 2012 ; Marzocchi et al., 2015 ; Seyfried et al., 2017 ; Akhtar et al., 2018) ou les simulations ont été comparées à des paramètres hydrodynamiques mesurés in situ comme la vitesse et la direction du flux (chapitres 1 et 2, par exemple Petrenko et al., 2005 ; Halliwell et al., 2011 ; Ross et al., 2016).

L'évaluation de la précision des modèles océaniques a été largement mise en œuvre en comparant des variables hydrologiques simulées et observées (température et salinité ; ex. Gustafsson et al., 1998 ; Reffray et al., 2004 ; André et al., 2005 ; Kara et al., 2006 ; Chelton et al., 2007 ; Pairaud et al., 2011 ; Renault et al., 2012 ; Marzocchi et al., 2015 ; Seyfried et al., 2017 ; Akhtar et al., 2018) car leur dynamique intègre le transport (vitesse) et le mélange (énergie cinétique turbulente) dans les modèles de circulation océanique. Cependant, les variables hydrologiques sont peu informatives sur le transport et le mélange lorsque des conditions bien mélangées prévalent, ce qui est souvent le cas dans les zones côtières (Gill, 1982 ; Holt et al., 2009).

La capacité des modèles de circulation côtière à simuler la vitesse d'écoulement et pas seulement les paramètres hydrologiques a été démontrée dans des études à court terme et/ou locales (Petrenko et al., 2005 ; Halliwell et al., 2011 ; Ross et al., 2016).

D'autres techniques de validation sont les comparaisons inter-modèles (entre comparaisons de modèles ; ex. Delhez et al., 2004) ou les comparaisons intra-modèles (au sein de comparaisons de modèles ; ex. Ezer & Mellor, 2000 ; Seyfried et al., 2017 ; Ridenour et al., 2019).

Les incertitudes peuvent provenir des hypothèses intrinsèques du modèle, telles que l'hydrostaticité, l'approximation de Boussinesq, le schéma de fermeture turbulente et l'interaction air-mer. L'hypothèse hydrostatique selon laquelle la variation verticale de la pression est dominée par l'accélération de la gravité (entraînant des vitesses verticales négligeables par rapport aux vitesses horizontales) n'est pas satisfaite lors des événements de vagues (Marshall et al., 1997 ; Zhang et al., 2014). L'approximation de Boussinesq (les variations de densité peuvent être négligées sauf dans les termes associés au forçage de flottabilité) peut ne pas être respectée dans l'océan stratifié supérieur, puisque la densité de l'eau peut varier jusqu'à 5%, en particulier dans les zones côtières sous influence fluviale. Par conséquent, l'approximation de Boussinesq peut entraîner des inexactitudes dans la vitesse simulée eulérienne du même ordre de grandeur que la variation de la densité de l'eau (McDougall et al., 2002). La fermeture de la turbulence est également une partie vitale de tout modèle de dynamique d'écoulement car elle distribue l'énergie totale de l'écoulement entre l'énergie turbulente résultant de toutes les fluctuations de vitesse à l'échelle du sous-réseau et l'écoulement moyen (Boussinesq, 1903; Prandtl, 1925). Cette séparation de l'énergie d'écoulement est essentielle pour décrire les processus de transport et de mélange dans les simulations numériques. On s'attend à ce que la fermeture de la turbulence joue un rôle plus important lorsque le transfert énergétique se produit à des échelles plus petites que la grille spatio-temporelle, comme lors de vagues de vent (Fisher et al., 2018) ou d'inondations fluviales (Reffray et al., 2004) . Cela pose la question de savoir si les vitesses de courant modélisées sont valables pendant certaines périodes au cours de la simulation lorsque les hypothèses classiques des modèles océaniques ne sont pas remplies.

Dans cette thèse, l'incertitude du modèle océanique hydrostatique de Boussinesq SYMPHONIE (Marsaleix et al., 2008, 2009a, 2009b, 2012 ; SIROCCO, n.d.) est quantifiée. Il a

été mis en place pour effectuer des simulations de circulation océanique régionale à très haute résolution dans le Golfe du Lion (Briton et al., 2018). Une grille horizontale bipolaire curviligne de 680x710 a été utilisée pour mailler le Golfe du Lion avec une résolution de 80 m sur la côte et de 2,7 km en haute mer (Bentsen et al., 1999). Des coordonnées σ généralisées ont été utilisées pour le maillage vertical, avec 29 niveaux verticaux (Briton et al., 2018). Les simulations ont été réalisées sur la période 2010-juin 2013 et ont été forcées par les conditions aux limites de la surface de la mer et de la haute mer des simulations climatiques régionales à échelle réduite NM12-FREE (résolution horizontale de 6 à 7 km ; Hamon et al., 2016) et la débit de douze rivières (Agly, Argens, Aude, Baillaury, Ebre, Grand Rhône, Hérault, Orb, Petit Rhône, Tech, Têt, Var ; Banque Hydro, sd). Les pas de temps interne et externe du modèle étaient respectivement de 25,48 s et 1,59 s.

Les vitesses simulées ont été extraites quatre fois par heure aux minutes 0, 20, 30 et 40 pour correspondre aux heures de mesure des observations. Sur l'horizontale, les vitesses d'écoulement simulées ont été extraites au point de grille le plus proche de l'emplacement des observations (moins de 132 m de distance). Sur la verticale, les niveaux verticaux de la simulation ne correspondant pas aux profondeurs des observations, les vitesses simulées ont été interpolées à la même profondeur que les observations. Si la profondeur d'eau réelle était supérieure à la profondeur d'eau dans la simulation (écart bathymétrique), les vitesses simulées ont été interpolées à la profondeur à la même distance du fond que l'observation.

Dans le premier chapitre, afin de tester l'effet de la violation des hypothèses du modèle sur les performances du modèle, les incertitudes ont été évaluées séparément en présence de vent fort (fermeture de la turbulence ou fiabilité du forçage atmosphérique), des vagues (violation de l'hypothèse hydrostatique), dans des conditions stratifiées (Boussinesq violation

d'approximation) puis comparées aux incertitudes de la période de référence (conditions de vent faible, sans vagues et non stratifiées).

La vitesse du courant simulée a été comparée aux observations in situ de la vitesse d'écoulement à partir de quatre mouillages fixes peu profonds et quatre profonds. De multiples indicateurs ont été calculés pour évaluer la performance du modèle, à savoir : Le biais, le biais relatif, la corrélation, le RMSE, le SI et le HH.

Contrairement aux attentes, les indicateurs n'ont pas affiché de pires performances du modèle lors d'événements de vent, de vagues ou de stratification, lorsque les hypothèses du modèle devaient être violées, qu'en dehors de ces événements. Cependant, les performances du modèle étaient plus faibles lors d'événements de vagues que lors d'événements de vent dans les stations peu profondes. Les indicateurs absolus (RMSE et biais) ont montré que le modèle était plus souvent moins bon pendant les événements que les indicateurs relatifs, probablement parce que lors de ces événements, les courants sont généralement plus forts que pendant la période de référence. Lors d'événements éoliens, il a été démontré que les simulations de circulation côtière dans le Golfe du Lion changent considérablement avec le gradient spatial du vent (Estournel et al., 2003). Par conséquent, une résolution spatiale adéquate du champ de vent est essentielle pour améliorer les performances du modèle de circulation océanique. Les simulations de la circulation océanique de la présente étude ont été forcées par les sorties de champ atmosphérique de simulations couplées air-mer à échelle réduite à la résolution la plus fine disponible pour la région au moment des simulations (1/12°, NMfree12, Hamon et al., 2016). Ce n'est généralement pas le cas, car certains modèles océaniques ont signalé des écarts entre les paramètres météorologiques observés et modélisés près de la surface lors de vents forts (Rainaud et al., 2016). Une façon d'améliorer la précision des simulations lors de vents forts est d'utiliser la technique de couplage

atmosphérique bidirectionnel (Gustafsson et al., 1998 ; Chelton et al., 2007 ; Schaeffer et al., 2011 ; Akhtar et al., 2018). Le couplage air-mer bidirectionnel a donné de meilleurs résultats que le forçage atmosphérique unidirectionnel pendant les tempêtes d'automne, lorsque la surface de la mer se refroidit rapidement (Seyfried et al., 2017). Cependant, Renault et al. (2012) ont trouvé peu de différences entre les simulations atmosphère-océan couplées et non couplées dans la région du Golfe du Lion lors de la comparaison de l'intensité de la vitesse du vent observée et modélisée et de la température de surface de la mer.

De même, les performances du modèle n'étaient pas systématiquement pires lors d'événements de vagues, bien qu'elles soient légèrement pires lors d'événements de vagues que lors d'événements de vent. Par conséquent, l'intégration des effets des vagues sur les simulations de circulation côtière doit être envisagée. En comparant un modèle hydrostatique, quasi-hydrostatique et non hydrostatique, Marshall et al. (1997) ont suggéré que les modèles quasi-hydrostatiques et non hydrostatiques sont préférés pour les phénomènes à petite échelle, mais n'ont trouvé aucune différence entre les trois modèles à grande échelle avec une résolution grossière (résolution horizontale de 1°). Dans le Golfe du Lion, Michaud et al. (2012) ont montré qu'un modèle courant-onde couplé entièrement non hydrostatique améliorerait les simulations de vitesse d'écoulement dans la zone de surf (0-15 m de profondeur d'eau). Cependant, en dehors de la zone de surf, les écarts entre les vitesses d'écoulement observées et simulées à POEM et Mesurho (comme dans la présente étude) étaient similaires quel que soit le forçage des vagues.

Une autre hypothèse du modèle qui pourrait affecter les performances du modèle est l'approximation de Boussinesq, qui est violée dans des conditions hautement stratifiées. Durant l'été, une représentation incorrecte de la stratification dans le Golfe du Lion a conduit à un mauvais placement de la NC dans les simulations par rapport aux observations de terrain

(Petrenko et al., 2005). Dans la salinité et la température modélisées, une période de stratification estivale est clairement visible. Cependant, l'indice de stratification a été fixé à une limite où la stratification en eau douce et thermique était présente. Ainsi, les événements de stratification à POEM et à Besete étaient principalement dus à l'apport d'eau douce et aucun ne correspondait à une pire performance du modèle.

Dans le Golfe du Lion, Estournel et al. (2001) ont comparé qualitativement des simulations du panache du Rhône à des observations radar et ont montré que le modèle SYMPHONIE peut reproduire la variation spatiale du courant devant l'embouchure du fleuve en dehors des événements de vents forts. Cependant, au cours de la période de référence, les indicateurs ont montré que les écarts entre simulation et observation étaient plus importants à la station de Mesurho stratifiée en continu, qu'aux autres stations peu profondes.

Bien que le modèle ne fonctionne pas moins bien en cas d'événements de vagues et de vent que pendant la période de référence, ce ne garantit pas que le modèle fonctionne bien dans l'ensemble. Après tout, il est possible que le modèle fonctionne également mal pendant la période de référence. Cependant, notre configuration de modèle SYMPHONIE fonctionne toujours aussi bien, voire mieux, que d'autres modèles lors de la réalisation d'études similaires. Dans la présente étude, l'incertitude du modèle pendant la période de référence était plus grande que la précision de l'appareil de mesure. C'est généralement le cas parmi les rares études qui évaluent quantitativement les performances du modèle, car les ADCP sont généralement configurés pour fournir des mesures de vitesse avec une erreur inférieure à 1 cm/s (RDI, 2007).

Une cause possible de l'inexactitude du modèle est la résolution. Le modèle a mieux fonctionné dans les stations peu profondes que dans les stations profondes à l'extérieur et pendant les événements de vent, tandis que la zone littorale devrait connaître une plus large

gamme de fréquences temporelles dans le spectre énergétique actuel. Des fréquences particulièrement courtes, dues à la dissipation d'énergie du flux dans la couche limite côtière. Dans cette étude, les meilleures performances du modèle aux stations peu profondes pourraient être dues au raffinement de la résolution spatiale horizontale, grâce à la résolution adaptative de la grille curviligne. Cela pourrait expliquer l'amélioration du biais et de la RMSE dans la présente étude par rapport à celle de Mikolajczak (2019) à la station POEM, puisque la résolution horizontale dans les deux simulations était différente (résolutions horizontales de 100 m contre 300 m, resp.).

Le modèle SYMPHONIE2015 dispose également d'une routine lagrangienne pour étudier la dispersion larvaire. Dans un modèle lagrangien, la trajectoire de chaque particule individuelle est calculée (Saidi et al., 2014). Un autre objectif de cette thèse est d'évaluer la validité de la dispersion et de la connectivité simulées, ce que font les deuxième et troisième chapitres. Dans le deuxième chapitre, l'incertitude du modèle eulérien est calculée à chaque instant, alors que dans le premier chapitre, elle a été moyennée sur la durée de l'événement. Cependant, l'incertitude du modèle affectera la dérive des larves à chaque étape, c'est pourquoi l'erreur instantanée doit également être évaluée. Dans le deuxième chapitre, les variations spatio-temporelles de l'incertitude du modèle ont été recherchées et liées à la modélisation et aux caractéristiques environnementales. Les différences ont été évaluées en calculant la différence de surface entre les tracés cfd de l'erreur de magnitude. De plus, un sous-échantillonnage de 100 points a été effectué pour chaque distribution d'erreur, pour ensuite effectuer un test WRS et un test KS.

Dans l'espace, huit groupes ont été trouvés en fonction de la couche d'eau, des zones bathymétriques et de la station d'amarrage. Dans la couche de surface (0-200 m), la distribution d'erreur des zones bathymétriques des données SAVED a toutes été considérée

comme significativement différente. Pour la zone bathymétrique la moins profonde de 0 à 50 m, deux groupes de distributions d'erreurs ont pu être distingués. Les distributions d'erreurs aux stations SOLA, BeSete et POEM étaient similaires, ainsi que celles de la station Mesurho et les données SAVED 0-50 m. Dans la couche inférieure (200 m de fond), la distribution d'erreur des quatre mouillages pourrait être organisée en deux groupes : La station LD et Planier avaient des distributions d'erreur similaires ainsi que la station Lion et Creus. Aucun lien n'a été trouvé entre les performances du modèle et les caractéristiques de modélisation. Semblable au chapitre un, aucun lien n'a été trouvé entre les performances du modèle et la stratification et l'interaction des vagues (profondeur comme proxy). Ce qui a également été suggéré dans le premier chapitre, était un lien entre les performances du modèle et la vitesse actuelle. Cela a été confirmé dans le chapitre deux, car une forte corrélation entre la vitesse du courant et les distributions d'erreurs a été trouvée. La vitesse et l'erreur de courant élevées observées à la station de Creus sont peut-être dues à des événements en cascade (Mikolajczak et al., 2020).

La station Mesurho a une erreur beaucoup plus élevée que les autres stations peu profondes, bien que les vitesses de courant observées soient similaires aux autres stations peu profondes. La différence de distribution d'erreur de la station de Mesurho avec les autres stations peu profondes est probablement due à l'exutoire du Rhône. Ceci est surprenant, car le chapitre 1 a montré que la stratification n'avait pas d'effet notable sur les performances du modèle. Cependant, la station Mesurho n'a pas été incluse dans cette étude, car la colonne d'eau à cette station était toujours stratifiée, elle ne pouvait donc pas être comparée aux périodes de référence. Étant donné que l'indice de stratification (N^2) à Mesurho est beaucoup plus élevé (jusqu'à 10 fois) qu'à SOLA, POEM et BeSete, il est possible que le modèle ne soit affecté par la stratification que si la stratification est suffisamment forte.

Avec le temps, les différences intrasaisonnières dans les distributions d'erreurs étaient plus petites que les différences intersaisonnières. En hiver, les vents froids et secs qui refroidissent la surface et créent une formation d'eau dense (Hua & Thomasset, 1983 ; Millot, 1990 ; Madec et al., 1996 ; Estournel et al., 2003 ; Ulses et al., 2008; Estournel et al., 2016). Cela pourrait expliquer pourquoi les saisons d'hiver ont certaines des erreurs médianes les plus élevées, car il existe une forte corrélation entre la vitesse actuelle (en raison par exemple de cascading) et l'erreur du modèle. Par conséquent, il est possible que le modèle ait des difficultés à recréer une formation d'eau dense. Les distributions d'erreurs pendant la saison hivernale étaient similaires à celles des saisons printanières.

Dans le chapitre trois, l'erreur instantanée globale qui a été trouvée dans le chapitre deux a été ajoutée en tant que bruit aux simulations de dispersion lagrangienne. Les matrices de connectivité de ces exécutions ont été comparées à celles de l'exécution originale pour évaluer l'effet de l'erreur des modèles sur la connectivité. Le bruit ajouté était l'erreur instantanée globale sur toutes les stations et sur toute la période d'étude. Des particules à flottabilité neutre ont été libérées à 2 m au-dessus du fond, tous les 100 m à partir de huit zones de récifs artificiels toutes les heures pendant trois périodes de libération : 1-12/06/2010, 13-24/06/2010 et 19-30/07/2010. Ces périodes de lâcher sont considérées comme des périodes de frai estivale et ont été choisies parce que les espèces benthiques des mers tempérées fraient souvent en été (Weinberg & Weinberg, 1979; Coma et al., 1995; Santangelo et al., 2003; Tsounis et al., 2006). Les particules ont été libérées de huit zones de récifs artificiels dans tout le Golfe du Lion (décrite par Blouet et al., 2021). Ce sont aussi les zones d'arrivée, ainsi que dix zones de récifs naturels. Les zones récifales naturelles ont été décrites par Briton et al. (2018) et Blouet et al. (2021). Au total, 1 267 776 particules ont été libérées. Les taux de transfert ont été obtenus en calculant la proportion de particules libérées

d'une zone et arrivant dans une autre. Cela a été fait après des durées de dérive de 3,5, 7, 10,5, 14, 21, 28, 35 et 42 jours, qui sont les PLD des larves simulées.

Ces taux de transfert forment des matrices de connectivité entre les récifs naturels (arrivée) et les récifs artificiels (arrivée et relâchement), qui ont été calculés une fois pour les quatre passages (référence, demi-erreur, erreur d'origine, double erreur), pour les huit PLD et tous trois périodes de libération.

Les résultats montrent que la différence médiane de taux de transfert entre les passages avec et sans bruit est nulle pour la plupart des zones. Certaines zones avaient une sous-estimation ou une surestimation systématique, tandis que dans d'autres zones, la différence de taux de transfert lors de l'ajout de bruit était aléatoire. Cependant, lorsqu'il y a une différence de taux de transfert, les courses avec du bruit sous-estiment souvent la connectivité. La réduction de la connectivité avec une erreur supplémentaire pourrait signifier que l'incertitude du modèle fait dériver les particules vers la côte, les empêchant d'arriver aux zones d'arrivée. C'est un phénomène qui s'aggrave avec l'augmentation de la PLD. De plus, la différence relative de taux de transfert peut varier de -100 % à 100 %. En bref, l'incertitude du modèle n'affecte pas souvent la connectivité simulée, mais quand c'est le cas, elle peut être assez profonde, avec comme résultat une sous-estimation de la connectivité modélisée. Les taux de transfert variaient selon les périodes de libération, de la même manière que dans d'autres études (p. ex. Hugget et al., 2003 ; Donahue et al., 2015 ; Treml et al., 2015 ; Romero-Torres et al., 2017 ; Briton et al., 2018, Hufnagl et al., 2017, Meerhoff et al., 2020).

Au cours de cette thèse, une quantité importante d'observations de vitesse de courant a été recueillie. Étant donné que la validation du modèle avec des données hydrodynamiques est assez rare, cette étude aide à quantifier l'incertitude du SYMPHONIE2015. De plus, la constatation que le modèle n'est pas sensible à la violation des hypothèses intrinsèques est

très intéressante. Cependant, la vraie nouveauté de cette étude est qu'elle quantifie d'abord l'incertitude du modèle à partir des observations actuelles (chapitre deux), pour ensuite effectuer une comparaison intra-modèle à sa propre erreur (chapitre trois).

Une perspective pour le chapitre trois pourrait être d'exécuter plusieurs exécutions par bruit ajouté pour compenser le bruit sélectionné au hasard à partir de la distribution d'erreur. Une autre perspective pourrait être d'étendre davantage le nombre de multiples de magnitude d'erreur ajoutés au modèle (par exemple un dixième). La raison pour laquelle plusieurs multiples de l'amplitude d'erreur ont été ajoutés en tant que bruit était de voir la différence de connectivité entre les différentes amplitudes ajoutées en tant que bruit. Étant donné qu'aucune différence n'a été trouvée entre les différents multiples de magnitude, il serait peut-être intéressant d'ajouter également des multiples variables d'erreur d'angle sous forme de bruit et de voir comment cela affecte la connectivité simulée. De plus, on pourrait approfondir la connectivité entre les différentes zones et étudier la filiation (=origine) des particules.

Étant donné que toutes les observations ont été recueillies dans le Golfe du Lion, en trois ans et demi (2010 - juin 2013) et qu'un seul modèle (SYMPHONIE2015) a été utilisé, nos résultats ne sont applicables que dans le Golfe du Lion. Néanmoins, cette thèse a donné lieu au développement de plusieurs nouvelles techniques pour étudier l'incertitude des modèles océaniques utilisés pour la dispersion larvaire, comme la comparaison d'indicateurs statistiques pendant et en dehors de certains événements (chapitre 1), les analyses de la distribution des erreurs du modèle selon l'espace et le temps (chapitre 2) et la comparaison intramodèle à sa propre erreur (chapitre 3).

Le développement de n Les nouvelles techniques de recherche et la quantification des incertitudes des méthodes de recherche existantes sont impératives pour une science de

qualité. D'autant plus que la connectivité et la dispersion seront cruciales pour la persistance des espèces benthiques face au changement climatique. Cette thèse vise à mettre une barre d'erreur autour des simulations de dispersion et est une première étape pour aider les futures décisions de gestion.

References

Akhtar, N., Brauch, J., & Ahrens, B. (2018). Climate modeling over the Mediterranean Sea: impact of resolution and ocean coupling. Climate Dynamics, 51(3), 933–948. https://doi.org/10.1007/s00382-017-3570-8

Allison, G. W., Lubchenco, J., & Carr, M. H. (1998). Marine reserves are necessary but not sufficient for marine conservation. Ecological Applications, 8(1 SUPPL.), 79–92. https://doi.org/10.2307/2641365

Aloisi, J. C., Got, H., & Monaco, A. (1973). Carte géologique du précontinent languedocien au 1/250000ième. International Institute for Aerial Survey and Earth Sciences, Netherlands.

André, G., Garreau, P., Garnier, V., & Fraunié, P. (2005). Modelled variability of the sea surface circulation in the North-western Mediterranean Sea and in the Gulf of Lions. Ocean Dynamics, 55(3–4), 294–308. https://doi.org/10.1007/s10236-005-0013-6

Andrello, M., Jacobi, M. N., Manel, S., Thuiller, W., & Mouillot, D. (2015). Extending networks of protected areas to optimize connectivity and population growth rate. Ecography, 38(3), 273–282. https://doi.org/10.1111/ecog.00975

Ardizzone, G.D., Belluscio, A., Gravina, M.F., Somaschini, A. (1996). Colonization and Disappearance of Mytilus galloprovincialis Lam. on an Artificial Habitat in the Mediterranean Sea. Estuarine, Coastal and Shelf Science, 43, 665–676. https://doi.org/10.1006/ecss.1996.0095

Bailey, K. M. (1997). Structural dynamics and ecology of flatfish populations. Journal of Sea Research, 37(3–4), 269–280. https://doi.org/10.1016/S1385-1101(97)00018-X

Barbier, E. B. (2017). Marine ecosystem services. Current Biology, 27(11), R507–R510. https://doi.org/10.1016/j.cub.2017.03.020

Barrier, N., Petrenko, A. A., & Ourmières, Y. (2016). Strong intrusions of the Northern Mediterranean Current on the eastern Gulf of Lion: insights from in-situ observations and high resolution numerical modelling. Ocean Dynamics, 66(3), 313–327. https://doi.org/10.1007/s10236-016-0921-7

Beger, M., Linke, S., Watts, M., Game, E., Treml, E., Ball, I., & Possingham, H. P. (2010). Incorporating asymmetric connectivity into spatial decision making for conservation. Conservation Letters, 3(5), 359–368. https://doi.org/10.1111/j.1755-263X.2010.00123.x

Bellard, C., Bertelsmeier, C., Leadley, P., Thuiller, W., & Courchamp, F. (2012). Impacts of climate change on the future of biodiversity. Ecology Letters, 15(4), 365–377. https://doi.org/10.1111/j.1461-0248.2011.01736.x.Impacts

Berg, M. P., Toby Kiers, E., Driessen, G., van der Heijden, M., Kooi, B. W., Kuenen, F., Liefting, M., Verhoef, H. A., & Ellers, J. (2010). Adapt or disperse: Understanding species persistence in a changing world. Global Change Biology, 16(2), 587–598. https://doi.org/10.1111/j.1365-2486.2009.02014.x

Blouet, S., Bramanti, L., & Katell, G. (submitted). Artificial reefs geographical location matters more than its age and depth for sessile invertebrate colonization in the Gulf of Lion (NorthWestern Mediterranean Sea) Sylvain. BioRxiv, 6. https://doi.org/10.1101/2021.10.08.463669

Blouet, S., Quittet, L., Agin, G., Thorin, S., Dalias, N., Marobin, D., Lenfant, P., Guizien, K., (2021). Database of the location and typology of artificial reefs in the Gulf of Lion (NW Mediterranean Sea).

Bode, M., Leis, J. M., Mason, L. B., Williamson, D. H., Harrison, H. B., Choukroun, S., & Jones, G. P. (2019). Successful validation of a larval dispersal model using genetic parentage data. PLoS Biology, 17(7), 1–13. https://doi.org/10.1371/journal.pbio.3000380

Bolle, L. J., Dickey-Collas, M., Van Beek, J. K. L., Erftemeijer, P. L. A., Witte, J. I., Van Der Veer, H. W., & Rijnsdorp, A. D. (2009). Variability in transport of fish eggs and larvae. III. Effects of hydrodynamics and larval behaviour on recruitment in plaice. Marine Ecology Progress Series, 390(September), 195–211. https://doi.org/10.3354/meps08177

Boström, C., Jackson, E. L., & Simenstad, C. A. (2006). Seagrass landscapes and their effects on associated fauna: A review. Estuarine, Coastal and Shelf Science, 68(3–4), 383–403. https://doi.org/10.1016/j.ecss.2006.01.026

Bourrin, F., Many, G., Durrieu de Madron, X., Martín, J., Puig, P., Houpert, L., Testor, P., Kunesch, S., Mahiouz, K., Béguery, L. (2015). Glider monitoring of shelf suspended particle dynamics and transport during storm and flooding conditions. Continental Shelf Research 109, 135–149. https://doi.org/10.1016/j.csr.2015.08.031

Briton, F., Cortese, D., Duhaut, T., & Guizien, K. (2018). High-resolution modelling of ocean circulation can reveal retention spots important for biodiversity conservation. Aquatic Conservation: Marine and Freshwater Ecosystems, 28(4), 882–893. https://doi.org/10.1002/aqc.2901

Butler, S. J., Vickery, J. A., & Norris, K. (2007). Farmland biodiversity and the footprint of agriculture. Science, 315(5810), 381-384.

Cai, X., Zhang, Y. J., Shen, J., Wang, H., Wang, Z., Qin, Q., & Ye, F. (2020). A Numerical Study of Hypoxia in Chesapeake Bay Using an Unstructured Grid Model: Validation and

Sensitivity to Bathymetry Representation. Journal of the American Water Resources Association, 1–24. https://doi.org/10.1111/1752-1688.12887

Chassignet, E. P., Hurlburt, H. E., Smedstad, O. M., Halliwell, G. R., Hogan, P. J., Wallcraft, A. J., Baraille, R., & Bleck, R. (2007). The HYCOM (HYbrid Coordinate Ocean Model) data assimilative system. Journal of Marine Systems, 65(1-4 SPEC. ISS.), 60–83. https://doi.org/10.1016/j.jmarsys.2005.09.016

Chelton, D. B., Schlax, M. G., & Samelson, R. M. (2007). Summertime coupling between sea surface temperature and wind stress in the California current system. Journal of Physical Oceanography, 37(3), 495–517. https://doi.org/10.1175/JPO3025.1

Chen, I. C., Hill, J. K., Ohlemüller, R., Roy, D. B., & Thomas, C. D. (2011). Rapid range shifts of species associated with high levels of climate warming. Science, 333(6045), 1024–1026. https://doi.org/10.1126/science.1206432

Christensen, V., Aiken, K. A., & Villanueva, M. C. (2007). Threats to the ocean: On the role of ecosystem approaches to fisheries. Social Science Information, 46(1), 67–86. https://doi.org/10.1177/0539018407073656

Claudet, J. & Pelletier, D. (2004). Marine protected areas and artificial reefs: A review of the interactions between management and scientific studies. Aquatic Living Resources, 17(2), 129–138. https://doi.org/10.1051/alr:2004017

Collie, J. S., Vic Adamowicz, W. L., Beck, M. W., Craig, B., Essington, T. E., Fluharty, D., Rice, J., & Sanchirico, J. N. (2013). Marine spatial planning in practice. Estuarine, Coastal and Shelf Science, 117, 1–11. https://doi.org/10.1016/j.ecss.2012.11.010

Coma, R., Ribes, R. M., Zabala, M., & Gilil, J. M. (1995). Reproduction and cycle of gonadal development in the Mediterranean gorgonian Paramuricea clavata. Marine Ecolology Progress Series, 117, 173-183.

Costello, C., & Polasky, S. (2008). Optimal harvesting of stochastic spatial resources. Journal of Environmental Economics and Management, 56(1), 1–18. https://doi.org/10.1016/j.jeem.2008.03.001

Crowder, L. B., Lyman, S. J., Figueira, W. F., & Priddy, J. (2000). Source-sink population dynamics and the problem of siting marine reserves. Bulletin of Marine Science, 66(3), 799–820.

Cushman, S. A. (2006). Effects of habitat loss and fragmentation on amphibians: A review and prospectus. Biological Conservation, 128(2), 231–240. https://doi.org/10.1016/j.biocon.2005.09.031

Delhez, É. J. M., Damm, P., De Goede, E., De Kok, J. M., Dumas, F., Gerritsen, H., Jones, J. E., Ozer, J., Pohlmann, T., Rasch, P. S., Skogen, M., & Proctor, R. (2004). Variability of shelf-seas hydrodynamic models: Lessons from the NOMADS2 Project. Journal of Marine Systems, 45(1–2), 39–53. https://doi.org/10.1016/j.jmarsys.2003.09.003

Dohan, K., Fabrice, B., Centurioni, L., Cronin, M., Lagerloef, G., Lee, D.-K., Lumpkin, R., Maximenko, N. A., Niiler, P. P., & Hiroshi, U. (2010). Measuring the Global Ocean Surface Circulation with Satellite and In Situ Observations. January, 237–248. https://doi.org/10.5270/oceanobs09.cwp.23

Donahue, M. J., Karnauskas, M., Toews, C., & Paris, C. B. (2015). Location is not everything: Timing of spawning aggregations optimizes larval replenishment. PLoS ONE, 10(6), 1–14. https://doi.org/10.1371/journal.pone.0130694

Douvere, F. (2008). The importance of marine spatial planning in advancing ecosystem-based sea use management. Marine Policy, 32(5), 762–771. https://doi.org/10.1016/j.marpol.2008.03.021

Dufois, F., Garreau, P., Le Hir, P., & Forget, P. (2008). Wave- and current-induced bottom shear stress distribution in the Gulf of Lions. Continental Shelf Research, 28(15), 1920–1934. https://doi.org/10.1016/j.csr.2008.03.028

Dulière, V., Gypens, N., Lancelot, C., Luyten, P., & Lacroix, G. (2019). Origin of nitrogen in the English Channel and Southern Bight of the North Sea ecosystems. Hydrobiologia, 845(1), 13–33. https://doi.org/10.1007/s10750-017-3419-5

Dumas, F., & Langlois, G. (2009). MARS Model for Applications at Regional Scale Scientific model description.

Estournel, C., Broche, P., Marsaleix, P., Devenon, J. L., Auclair, F., & Vehil, R. (2001). The Rhone River plume in unsteady conditions: Numerical and experimental results. Estuarine, Coastal and Shelf Science, 53(1), 25–38. https://doi.org/10.1006/ecss.2000.0685

Estournel, C., De Madron, X. D., Marsaleix, P., Auclair, F., Julliand, C., & Vehil, R. (2003). Observation and modeling of the winter coastal oceanic circulation in the Gulf of Lion under wind conditions influenced by the continental orography (FETCH experiment). Journal of Geophysical Research: Oceans, 108(3), 8059. https://doi.org/10.1029/2001jc000825

Estournel, C., Testor, P., Damien, P., D'Ortenzio, F., Marsaleix, P., Conan, P., Kessouri, F., Durrieu de Madron, X., Coppola, L., Lellouche, J. M., Belamari, S., Mortier, L., Ulses, C., Bouin, M. N., & Prieur, L. (2016). High resolution modeling of dense water formation in the north-western Mediterranean during winter 2012–2013: Processes and budget. Journal of Geophysical Research: Oceans, 121(7), 5367–5392. https://doi.org/10.1002/2016JC011935

Ezer, T., & Mellor, G. L. (2000). Sensitivity studies with the North Atlantic sigma coordinate Princeton Ocean Model. Dynamics of Atmospheres and Oceans, 32(3–4), 185–208. https://doi.org/10.1016/S0377-0265(00)00047-6

Fahrig, L. (2003). Effects of Habitat Fragmentation on Biodiversity. Annual Review of Ecology, Evolution, and Systematics, 34, 487–515. https://doi.org/10.1146/annurev.ecolsys.34.011802.132419

Fiksen, Ø., Jørgensen, C., Kristiansen, T., Vikebø, F., & Huse, G. (2007). Linking behavioural ecology and oceanography: Larval behaviour determines growth, mortality and dispersal. Marine Ecology Progress Series, 347, 195–205. https://doi.org/10.3354/meps06978

Foley, M. M., Halpern, B. S., Micheli, F., Armsby, M. H., Caldwell, M. R., Crain, C. M., Prahler, E., Rohr, N., Sivas, D., Beck, M. W., Carr, M. H., Crowder, L. B., Emmett Duffy, J., Hacker, S. D., McLeod, K. L., Palumbi, S. R., Peterson, C. H., Regan, H. M., Ruckelshaus, M. H., Sandifer, P. A., Steneck, R. S. (2010). Guiding ecological principles for marine spatial planning. Marine Policy, 34(5), 955–966. https://doi.org/10.1016/j.marpol.2010.02.001

Fox, C. J., McCloghrie, P., Young, E. F., & Nash, R. D. M. (2006). The importance of individual behaviour for successful settlement of juvenile plaice (Pleuronectes platessa L.): A modelling and field study in the eastern Irish Sea. Fisheries Oceanography, 15(4), 301–313. https://doi.org/10.1111/j.1365-2419.2005.00396.x

Frazão Santos, C., Ehler, C. N., Agardy, T., Andrade, F., Orbach, M. K., & Crowder, L. B. (2018). Marine spatial planning. World Seas: An Environmental Evaluation Volume III: Ecological Issues and Environmental Impacts, September, 571–592. https://doi.org/10.1016/B978-0-12-805052-1.00033-4

Gallego, A., Gibb, F. M., Tullet, D., & Wright, P. J. (2017). Bio-physical connectivity patterns of benthic marine species used in the designation of Scottish nature conservation marine protected areas. ICES Journal of Marine Science, 74(6), 1797–1811. https://doi.org/10.1093/icesjms/fsw174

Gaines, S. D., White, C., Carr, M. H., & Palumbi, S. R. (2010). Designing marine reserve networks for both conservation and fisheries management. Proceedings of the National Academy of Sciences of the United States of America, 107(43), 18286–18293. https://doi.org/10.1073/pnas.0906473107

Gentil, M., Many, G., de Madron, X. D., Cauchy, P., Pairaud, I., Testor, P., Verney, R., & Bourrin, F. (2020). Glider-based active acoustic monitoring of currents and turbidity in the coastal zone. Remote Sensing, 12(18). https://doi.org/10.3390/RS12182875

Gill, A. E. (1982). Atmosphere–Ocean Dynamics. International Geophysics Series. https://books.google.fr/books?hl=nl&lr=&id=lypfDAAAQBAJ&oi=fnd&pg=PP1&dq=atmosphere+ocean+dynamics&ots=MsziwO6jrl&sig=2-VQjQky1C6LtDP6ZvbJ25xWRFI#v=onepage&q=Brunt&f=false

Guizien, K. (2009). Spatial variability of wave conditions in the Gulf of Lions (NW Mediterranean Sea). Life and Environment, 59(3/4), 261–270. https://www.researchgate.net/publication/250306276

Guizien, K., Barthélemy, E., & Inall, M. E. (1999). Internal tide generation at a shelf break by an oblique barotropic tide: Observations and analytical modeling. Journal of Geophysical Research: Oceans, 104(C7), 15655–15668. https://doi.org/10.1029/1999jc900089

Guizien, K., Belharet, M., Marsaleix, P., & Guarini, J. M. (2012). Using larval dispersal simulations for marine protected area design: Application to the Gulf of Lions

(northwest Mediterranean). Limnology and Oceanography, 57(4), 1099–1112. https://doi.org/10.4319/lo.2012.57.4.1099

Guizien, K., Brochier, T., Duchêne, J. C., Koh, B. S., & Marsaleix, P. (2006). Dispersal of Owenia fusiformis larvae by wind-driven currents: Turbulence, swimming behaviour and mortality in a three-dimensional stochastic model. Marine Ecology Progress Series, 311(1986), 47–66. https://doi.org/10.3354/meps311047

Guizien, K., Charles, F., Lantoine, F., & Naudin, J. J. (2007). Nearshore dynamics of nutrients and chlorophyll during Mediterranean-type flash-floods. Aquatic Living Resources, 20(1), 3–14. https://doi.org/10.1051/alr:2007011

Guizien, K., Viladrich, N., Martínez-Quintana, & Bramanti, L. (2020). Survive or swim: different relationships between migration potential and larval size in three sympatric Mediterranean octocorals. Scientific Reports, 10(1), 1–12. https://doi.org/10.1038/s41598-020-75099-1

Gustafsson, N., Nyberg, L., & Omstedt, A. (1998). Coupling of a high-resolution atmospheric model and an ocean model for the Baltic Sea. Monthly Weather Review, 126(11), 2822–2846. https://doi.org/10.1175/1520-0493(1998)126<2822:COAHRA>2.0.CO;2

Ha, G., & Williams, S. L. (2018). Eelgrass community dominated by native omnivores in Bodega Bay, California, USA. Bulletin of Marine Science, 94(4), 1333–1353. https://doi.org/10.5343/bms.2017.1091

Halpern, B. S., & Warner, R. R. (2003). Matching marine reserve design to reserve objectives. Proceedings of the Royal Society B: Biological Sciences, 270(1527), 1871–1878. https://doi.org/10.1098/rspb.2003.2405

Harding, A., Palutikof, J., & Holt, T. (2009). The climate system. The physical geography of the Mediterranean, 69-88.

Hector, A., & Bagchi, R. (2007). Biodiversity and ecosystem multifunctionality. Nature, 448(7150), 188-190.

Hedgecock, D., Barber, P. H., & Edmands, S. (2007). Genetic approaches to measuring connectivity. Oceanography, 20(SPL.ISS. 3), 70–79. https://doi.org/10.5670/oceanog.2007.30

Herrmann, M., Estournel, C., Déqué, M., Marsaleix, P., Sevault, F., & Somot, S. (2008). Dense water formation in the Gulf of Lions shelf: Impact of atmospheric interannual variability and climate change. Continental Shelf Research, 28(15), 2092–2112. https://doi.org/10.1016/j.csr.2008.03.003

Hoegh-Guldberg, O., Rongshuo, C., Poloczanska, E. S., Brewer, P. G., Sundby, S., Hilmi, K., Fabry J., V., & Sukgeun, J. (2014). The oceans. In Climate Change 2014: Impacts, Adaptation, and Vulnerability. Part B: Regional Aspects. Contribution of Working Group II to the Fifth Assessment Report of the Intergovernmental Panel on Climate Change [Barros, (Vol. 21, pp. 1655–1731). https://doi.org/10.1016/S1460-1567(02)80016-2

Holt, J., Harle, J., Proctor, R., Michel, S., Ashworth, M., Batstone, C., Allen, I., Holmes, R., Smyth, T., Haines, K., Bretherton, D., & Smith, G. (2009). Modelling the global coastal ocean. Philosophical Transactions of the Royal Society A: Mathematical, Physical and Engineering Sciences, 367(1890), 939–951. https://doi.org/10.1098/rsta.2008.0210

Hu, Z. Y., Doglioli, A. M., Petrenko, A. A., Marsaleix, P., & Dekeyser, I. (2009). Numerical simulations of eddies in the Gulf of Lion. Ocean Modelling, 28(4), 203–208. https://doi.org/10.1016/j.ocemod.2009.02.004

Hu, Z. Y., Petrenko, A. A., Doglioli, A. M., & Dekeyser, I. (2011). Study of a mesoscale anticyclonic eddy in the western part of the Gulf of Lion. Journal of Marine Systems, 88(1), 3–11. https://doi.org/10.1016/j.jmarsys.2011.02.008

Hua, B.-L., & Thomasset, F. (1983). A numerical study of the effects of coastline geometry on wind-induced upwelling in the Gulf of Lions. Journal of Physical Oceanography, 13, 678–694.

Hufnagl, M., Payne, M., Lacroix, G., Bolle, L. J., Daewel, U., Dickey-Collas, M., Gerkema, T., Huret, M., Janssen, F., Kreus, M., Pätsch, J., Pohlmann, T., Ruardij, P., Schrum, C., Skogen, M. D., Tiessen, M. C. H., Petitgas, P., van Beek, J. K. L., van der Veer, H. W., & Callies, U. (2017). Variation that can be expected when using particle tracking models in connectivity studies. Journal of Sea Research, 127(May 2016), 133–149. https://doi.org/10.1016/j.seares.2017.04.009

Huggett, J., Fréon, P., Mullon, C., & Penven, P. (2003). Modelling the transport success of anchovy Engraulis encrasicolus eggs and larvae in the southern Benguela: The effect of spatio-temporal spawning patterns. Marine Ecology Progress Series, 250(March 2003), 247–262. https://doi.org/10.3354/meps250247

Kara, A. B., Barron, C. N., Martin, P. J., Smedstad, L. F., & Rhodes, R. C. (2006). Validation of interannual simulations from the 1/8° global Navy Coastal Ocean Model (NCOM). Ocean Modelling, 11(3–4), 376–398. https://doi.org/10.1016/j.ocemod.2005.01.003

Kirtman, B. P., Bitz, C., Bryan, F., Collins, W., Dennis, J., Hearn, N., Kinter, J. L., Richard, I. I. I., Clement, L., Siqueira, L., Stan, C., Tomas, R., & Vertenstein, M. (2012). Impact of ocean model resolution on CCSM climate simulations. 1303–1328. https://doi.org/10.1007/s00382-012-1500-3

Kough, A. S., Paris, C. B., & Butler IV, M. J. (2013). Larval Connectivity and the International Management of Fisheries. PLoS ONE, 8(6). https://doi.org/10.1371/journal.pone.0064970

Kourafalou, V.H., Peng, G., Kang, H., Hogan, P.J., Smedstad, O.M., & Weisberg, R.H. (2009) Evaluation of Global Ocean Data Assimilation Experiment products on South Florida nested simulations with the Hybrid Coordinate Ocean Model. Ocean Dynamics 59(1), 47–66 . https://doi.org/10.1007/s10236-008-0160-7

Kvile, K. Ø., Romagnoni, G., Dagestad, K. F., Langangen, Ø., & Kristiansen, T. (2018). Sensitivity of modelled North Sea cod larvae transport to vertical behaviour, ocean model resolution and interannual variation in ocean dynamics. ICES Journal of Marine Science, 75(7), 2013–2024. https://doi.org/10.1093/icesjms/fsy039

Lang, J. M. & Benbow, M. E. (2013). Species Interactions and Competition. Nature Education Knowledge 4(4):8

Lascaratos, A. (1993). Estimation of deep and intermediate water mass formation rates in the Mediterranean Sea. Deep-Sea Research Part II, 40(6), 1327–1332. https://doi.org/10.1016/0967-0645(93)90072-U

Lazure, P., & Dumas, F. (2008). An external-internal mode coupling for a 3D hydrodynamical model for applications at regional scale (MARS). Advances in Water Resources, 31(2), 233–250. https://doi.org/10.1016/j.advwatres.2007.06.010

Le Provost, C., & Lyard, F. H. (2000). How can we improve a global ocean tide model at a regional scale? A test on the Yellow Sea and the East China Sea. Journal of geophysical research, 105(C4), 8707–8725.

Lester, S. E., Halpern, B. S., Grorud-Colvert, K., Lubchenco, J., Ruttenberg, B. I., Gaines, S. D., Airamé, S., & Warner, R. R. (2009). Biological effects within no-take marine reserves: A

global synthesis. Marine Ecology Progress Series, 384, 33–46. https://doi.org/10.3354/meps08029

Loreau, M., Naeem, S., Inchausti, P., Bengtsson, J., Grime, J.P., Hector, A., Hooper, D.U., Huston, M.A., Raffaelli, D., Schmid, B., Tilman, D. & Wardle, D.A. (2001). Biodiversity and ecosystem functioning: current knowledge and future challenges. Science, 294(5543), 804-808. https://doi.org/10.1126/science.1064088

Lubchenco, J., & Grorud-Colvert, K. (2015). Making waves: The science and politics of ocean protection. Science, 350(6259), 382–383. https://doi.org/10.1126/science.aad5443

Lubchenco, J. & Sutley, N. (2010). Proposed U.S. policy for ocean, coast, and Great Lakes stewardship. Policy forum. Science 328, 1485-1486. http://dx.doi.org/10.1126/

Madec, G., Lott, F., Delecluse, P., & Crépon, M. (1996). Large-scale preconditioning of deep-water formation in the northwestern Mediterranean Sea. Journal of Physical Oceanography, 26(8), 1393–1408. https://doi.org/10.1175/1520-0485(1996)026<1393:LSPODW>2.0.CO;2

Malanotte-Rizzoli, P., & Bergamasco, A. (1991). The wind and thermally driven circulation of the eastern Mediterranean Sea. Part II: The baroclinic case. Dynamics of Atmospheres and Oceans, 15(3-5), 355-419.

Many, G., Bourrin, F., Durrieu de Madron, X., Ody, A., Doxaran, D., & Cauchy, P. (2018). Glider and satellite monitoring of the variability of the suspended particle distribution and size in the Rhône ROFI. Progress in Oceanography, 163, 123–135. https://doi.org/10.1016/j.pocean.2017.05.006

Many, G., Bourrin, F., Durrieu de Madron, X., Pairaud, I., Gangloff, A., Doxaran, D., Ody, A., Verney, R., Menniti, C., Le Berre, D., & Jacquet, M. (2016). Particle assemblage

characterization in the Rhone River ROFI. Journal of Marine Systems, 157, 39–51. https://doi.org/10.1016/j.jmarsys.2015.12.010

Marshall, J., Hill, C., Perelman, L., & Adcroft, A. (1997). Hydrostatic, quasi-hydrostatic, and nonhydrostatic ocean modeling. Journal of Geophysical Research C: Oceans, 102(C3), 5733–5752. https://doi.org/10.1029/96JC02776

Marshall, J., & Schott, F. (1999). Open-Ocean Convection: Observations, Theory, and Models. Reviews of Geophysics, 37(98), 1–64.

Marsaleix, P., Auclair, F., Duhaut, T., Estournel, C., Nguyen, C., & Ulses, C. (2012). Alternatives to the Robert-Asselin filter. Ocean Modelling, 41, 53–66. https://doi.org/10.1016/j.ocemod.2011.11.002

Marsaleix, P., Auclair, F., & Estournel, C. (2009a). Low-order pressure gradient schemes in sigma coordinate models: The seamount test revisited. Ocean Modelling, 30(2–3), 169–177. https://doi.org/10.1016/j.ocemod.2009.06.011

Marsaleix, P., Auclair, F., Floor, J. W., Herrmann, M. J., Estournel, C., Pairaud, I., & Ulses, C. (2008). Energy conservation issues in sigma-coordinate free-surface ocean models. Ocean Modelling, 20(1), 61–89. https://doi.org/10.1016/j.ocemod.2007.07.005

Marsaleix, P., Estournel, C., Kondrachoff, V., & Vehil, R. (1998). A numerical study of the formation of the Rhone River plume. Journal of Marine Systems, 14(1–2), 99–115. https://doi.org/10.1016/S0924-7963(97)00011-0

Marsaleix, P., Ulses, C., Pairaud, I., Herrmann, M. J., Floor, J. W., Estournel, C., & Auclair, F. (2009b). Open boundary conditions for internal gravity wave modelling using polarization relations. Ocean Modelling, 29(1), 27–42. https://doi.org/10.1016/j.ocemod.2009.02.010

Martens, K., Queiroga, H., Cunha, M.R., Cunha, A., Moreira, M.H., Quintino, V., Rodrigues, A.M., Seroôdio, J., Warwick, R.M. (Eds.) (2006). Marine Biodiversity: Patterns and Processes, Assessment, Threats, Management and Conservation. Springer Netherlands, Dordrecht. https://doi.org/10.1007/1-4020-4697-9

Marzocchi, A., Hirschi, J. J. M., Holliday, N. P., Cunningham, S. A., Blaker, A. T., & Coward, A. C. (2015). The North Atlantic subpolar circulation in an eddy-resolving global ocean model. Journal of Marine Systems, 142, 126–143. https://doi.org/10.1016/j.jmarsys.2014.10.007

MEDOC GROUP (1969). Observation of Formation of Deep Water in the Mediterranean Sea, 1969. Nature, 227(5262), 1037–1040. https://doi.org/10.1038/2271037a0

Meerhoff, E., Defeo, O., Combes, V., Franco, B. C., Matano, R. P., Piola, A. R., Vaca, F. H., & Celentano, E. (2020). Assessment of larval connectivity in a sandy beach mole crab through a coupled bio-oceanographic model. Estuarine, Coastal and Shelf Science, 246(September). https://doi.org/10.1016/j.ecss.2020.107035

Michaud, H., Marsaleix, P., Leredde, Y., Estournel, C., Bourrin, F., Lyard, F., Mayet, C., & Ardhuin, F. (2012). Three-dimensional modelling of wave-induced current from the surf zone to the inner shelf. Ocean Science, 8(4), 657–681. https://doi.org/10.5194/os-8-657-2012

Mikolajczak, G. (2019). Dynamique de l'eau et des apports particulaires originaires du Rhône sur la marge continentale du Golfe du Lion. [Doctoral dissertation, Toulouse university]

Mikolajczak, G., Estournel, C., Ulses, C., Marsaleix, P., Bourrin, F., Martín, J., Pairaud, I., Puig, P., Leredde, Y., Many, G., Seyfried, L., & Durrieu de Madron, X. (2020). Impact of storms on residence times and export of coastal waters during a mild autumn/winter period

in the Gulf of Lion. Continental Shelf Research, 207, 104192. https://doi.org/10.1016/j.csr.2020.104192

Millot, C. (1990). The Gulf of Lions' hydrodynamics. Continental Shelf Research, 10(9–11), 885–894. https://doi.org/10.1016/0278-4343(90)90065-T

Millot, C. (1994). Models and data: a synergetic approach in the western Mediterranean Sea. In: Malanotte-Rizzoli, P., Robinson, A.R. (Eds.), Ocean Processes in Climate Dynamics: Global and Mediterranean Examples. Kluwer Academic Publishers, Dordrecht, The Netherlands, 1994, pp. 407–425

Millot, C. (1999). Circulation in the Western Mediterranean Sea. Journal of Marine Systems, 20(1–4), 423–442. https://doi.org/10.1016/S0924-7963(98)00078-5

Molcard, A., Pinardi, N., Iskandarani, M., & Haidvogel, D. B. (2002). Wind driven general circulation of the Mediterranean Sea simulated with a spectral element ocean model. Dynamics of Atmospheres and Oceans, 35(2), 97–130. https://doi.org/10.1016/S0377-0265(01)00080-X

Moore, A. M., Arango, H. G., Broquet, G., Powell, B. S., Weaver, A. T., & Zavala-Garay, J. (2011). The Regional Ocean Modeling System (ROMS) 4-dimensional variational data assimilation systems. Part I - System overview and formulation. Progress in Oceanography, 91(1), 34–49. https://doi.org/10.1016/j.pocean.2011.05.004

Neubert, M. G. (2003). Marine reserves and optimal harvesting. Ecology Letters, 6(9), 843-849.

Neumann, B., Vafeidis, A. T., Zimmermann, J., & Nicholls, R. J. (2015). Future coastal population growth and exposure to sea-level rise and coastal flooding - A global assessment. PLoS ONE, 10(3). https://doi.org/10.1371/journal.pone.0118571

O'Leary, B. C., Winther-Janson, M., Bainbridge, J. M., Aitken, J., Hawkins, J. P., & Roberts, C. M. (2016). Effective Coverage Targets for Ocean Protection. Conservation Letters, 9(6), 398–404. https://doi.org/10.1111/conl.12247

Padrón, M. (2015). Evaluation of conservation efficiency for gorgonian species at a regional scale based on an existing Marine Protected Area network and modeling scenarios accounting for hydrodynamics. [Doctoral dissertation, Université Pierre et Marie Curie, Università di Bologna]

Pairaud, I. L., Gatti, J., Bensoussan, N., Verney, R., & Garreau, P. (2011). Hydrology and circulation in a coastal area off Marseille: Validation of a nested 3D model with observations. Journal of Marine Systems, 88(1), 20–33. https://doi.org/10.1016/j.jmarsys.2011.02.010

Palumbi, S. R. (2004). Marine reserves and Ocean neighborhoods: The spatial scale of marine populations and their management. Annual Review of Environment and Resources, 29, 31–68. https://doi.org/10.1146/annurev.energy.29.062403.102254

Palumbi, S. R., Sandifer, P. A., Allan, J. D., Beck, M. W., Fautin, D. G., Fogarty, M. J., Halpera, B. S., Incze, L. S., Leong, J. A., Norse, E., Stachowicz, J. J., & Wall, D. H. (2009). Managing for ocean biodiversity to sustain marine ecosystem services. Frontiers in Ecology and the Environment, 7(4), 204–211. https://doi.org/10.1890/070135

Petrenko, A., Leredde, Y., & Marsaleix, P. (2005). Circulation in a stratified and wind-forced Gulf of Lions, NW Mediterranean Sea: In situ and modeling data. Continental Shelf Research, 25(1), 7–27. https://doi.org/10.1016/j.csr.2004.09.004

Pinardi, N., & Masetti, E. (2000). Variability of the large scale general circulation of the Mediterranean Sea from observations and modelling: A review. Palaeogeography,

Palaeoclimatology, Palaeoecology, 158(3–4), 153–173. https://doi.org/10.1016/S0031-0182(00)00048-1

Pineda, J., Hare, J. A., & Sponaugle, S. (2007). Larval transport and dispersal in the coastal ocean and consequences for population connectivity. Oceanography, 20(SPL.ISS. 3), 22–39. https://doi.org/10.5670/oceanog.2007.27

Puig, P., Madron, X. D. de, Salat, J., Schroeder, K., Martín, J., Karageorgis, A. P., Palanques, A., Roullier, F., Lopez-Jurado, J. L., Emelianov, M., Moutin, T., & Houpert, L. (2013). Thick bottom nepheloid layers in the western Mediterranean generated by deep dense shelf water cascading. Progress in Oceanography, 111, 1–23. https://doi.org/10.1016/j.pocean.2012.10.003

Puig, P., Palanques, A., Orange, D. L., Lastras, G., & Canals, M. (2008). Dense shelf water cascades and sedimentary furrow formation in the Cap de Creus Canyon, northwestern Mediterranean Sea. Continental Shelf Research, 28(15), 2017–2030. https://doi.org/10.1016/j.csr.2008.05.002

Qiu, W., & Jones, P. J. S. (2013). The emerging policy landscape for marine spatial planning in Europe. Marine Policy, 39(1), 182–190. https://doi.org/10.1016/j.marpol.2012.10.010

Queiroga, H., & Blanton, J. (2005). Interactions between behaviour and physical forcing in the control of horizontal transport of decapod crustacean larvae. Advances in marine biology, 47, 107-214.

RDI Instruments. (2007). Accoustic Doppler Current Profiler Technical Manual. P/N 957-6150-00

Reffray, G., Fraunié, P., & Marsaleix, P. (2004). Secondary flows induced by wind forcing in the Rhône region of freshwater influence. Ocean Dynamics, 54(2), 179–196. https://doi.org/10.1007/s10236-003-0079-y

Renault, L., Chiggiato, J., Warner, J. C., Gomez, M., Vizoso, G., & Tintoré, J. (2012). Coupled atmosphere-ocean-wave simulations of a storm event over the Gulf of Lion and Balearic Sea. Journal of Geophysical Research: Oceans, 117(C9), n/a-n/a. https://doi.org/10.1029/2012JC007924

Ridenour, N. A., Hu, X., Jafarikhasragh, S., Landy, J. C., Lukovich, J. V., Stadnyk, T. A., Sydor, K., Myers, P. G., & Barber, D. G. (2019). Sensitivity of freshwater dynamics to ocean model resolution and river discharge forcing in the Hudson Bay Complex. Journal of Marine Systems, 196(May), 48–64. https://doi.org/10.1016/j.jmarsys.2019.04.002

Robinson, A.R., Golnaraghi, M. (1993). Circulation and dynamics of the eastern Mediterranean Sea; quasi-synoptic data-driven simulations. Part II. Deep Sea Research. Topical Studies of Oceanography 40 (6), 1207–1246.

Romero-Torres, M., Acosta, A., & Treml, E. A. (2017). The regional structure of spawning phenology and the potential consequences for connectivity of coral assemblages across the Eastern Tropical Pacific. ICES Journal of Marine Science, 74(3), 613–624. https://doi.org/10.1093/icesjms/fsw218

Ross, N. O., Fraysse, M., Pinazo, C., Pairaud, I. (2016). Impact of an intrusion by the Northern Current on the biogeochemistry in the eastern Gulf of Lion, NW Mediterranean . Estuarine Coastal And Shelf Science , 170, 1-9. https://doi.org/10.1016/j.ecss.2015.12.022

Saidi, M. S., Rismanian, M., Monjezi, M., Zendehbad, M., & Fatehiboroujeni, S. (2014). Comparison between Lagrangian and Eulerian approaches in predicting motion of micron-sized particles in laminar flows. Atmospheric Environment, 89, 199–206. https://doi.org/10.1016/j.atmosenv.2014.01.069

Sala, E., & Knowlton, N. (2006). Global marine biodiversity trends. Annual Review of Environment and Resources, 31, 93–122. https://doi.org/10.1146/annurev.energy.31.020105.100235

Sala, E., Lubchenco, J., Grorud-Colvert, K., Novelli, C., Roberts, C., & Sumaila, U. R. (2018). Assessing real progress towards effective ocean protection. Marine Policy, 91(February 2018), 11–13. https://doi.org/10.1016/j.marpol.2018.02.004

Santangelo, G., Carletti, E., Maggi, E., Bramanti, L. (2003) Reproduction and population sexual structure of the overexploited Mediterranean red coral Corallium rubrum. Marine Ecology Progress Series, 248, 99–108

Saunders, D., Hobbs, R., & Margules, C. (1991). Biological Consequences of Ecosystem Fragmentation: A Review. Conservation Biology, 5(1), 18–32. https://doi.org/10.1111/j.1523-1739.1991.tb00384.x

Schaeffer, A., Garreau, P., Molcard, A., Fraunié, P., & Seity, Y. (2011). Influence of high-resolution wind forcing on hydrodynamic modeling of the Gulf of Lions. Ocean Dynamics, 61(11), 1823–1844. https://doi.org/10.1007/s10236-011-0442-3

Scheltema, R. S. (1986). On dispersal and planktonic larvae of benthic invertebrates: an eclectic overview and summary of problems. Bulletin of marine science, 39(2), 290-322.

Seaman, W. (2007). Artificial habitats and the restoration of degraded marine ecosystems and fisheries. Hydrobiologia, 580(1), 143–155. https://doi.org/10.1007/s10750-006-0457-9

Sextant (1996). Système Acquisition Validation Exploitation de Données des Navires de l'INSU - Projet SAVED https://sextant.ifremer.fr/record/6f6e95e9-8e97-48d6-b536-b40f2ad87402/, accessed 04/06/2021.

Seyfried, L., Marsaleix, P., Richard, E., & Estournel, C. (2017). Modelling deep-water formation in the north-west Mediterranean Sea with a new air-sea coupled model: Sensitivity to turbulent flux parameterizations. Ocean Science, 13(6), 1093–1112. https://doi.org/10.5194/os-13-1093-2017

Siedler, G., Gould, J., & Church, J. A. (2001). Ocean circulation and climate: observing and modelling the global ocean. Elsevier Ltd.

Sindermann, C. J. (1995). Ocean pollution: effects on living resources and humans. CRC press.

Small, C., & Nicholls, R. J. (2003). A global analysis of human settlement in coastal zones. Journal of Coastal Research, 19(3), 584–599.

Somot, S., Sevault, F., Déqué, M., & Crépon, M. (2008). 21st century climate change scenario for the Mediterranean using a coupled atmosphere-ocean regional climate model. Global and Planetary Change, 63(2–3), 112–126. https://doi.org/10.1016/j.gloplacha.2007.10.003

Theocharis, A., Georgopoulos, D., Lascaratos, A., & Nittis, K. (1993). Water masses and circulation in the central region of the Eastern Mediterranean. Deep-Sea Research II, 40(6), 1121–1142.

Thorson, G. (1946). Reproduction and larval development of Danish marine bottom invertebrates, with special reference to the planktonic larvae in the Sound (Oresund). Meddelelser fra Kommissionen For Danmarks Fiskeriog Havundersøkelser. Serie: Plankton IV: 1–523

Tilman, D. (2001). Functional Diversity. In Encyclopedia of Biodiversity volume 3, 109–120.

Treml, E. A., Ford, J. R., Black, K. P., & Swearer, S. E. (2015). Identifying the key biophysical drivers, connectivity outcomes, and metapopulation consequences of larval dispersal

in the sea. Movement Ecology, 3(1), 1–16. https://doi.org/10.1186/s40462-015-0045-6

Tsounis, G., Rossi, S., Aranguren, M., Gili, J. M., & Arntz, W. (2006). Effects of spatial variability and colony size on the reproductive output and gonadal development cycle of the Mediterranean red coral (Corallium rubrum L.). Marine Biology, 148(3), 513–527. https://doi.org/10.1007/s00227-005-0100-8

Ulses, C., Estournel, C., Bonnin, J., Durrieu de Madron, X., & Marsaleix, P. (2008). Impact of storms and dense water cascading on shelf-slope exchanges in the Gulf of Lion (NW Mediterranean). Journal of Geophysical Research, 113(C2), C02010. https://doi.org/10.1029/2006JC003795

Victor, B. C. (1986). Duration of the planktonic larval stage of one hundred species of Pacific and Atlantic wrasses (family Labridae). Marine Biology, 90(3), 317–326. https://doi.org/10.1007/BF00428555

Vikebø, F., Jørgensen, C., Kristiansen, T., & Fiksen, Ø. (2007). Drift, growth, and survival of larval Northeast Arctic cod with simple rules of behaviour. Marine Ecology Progress Series, 347, 207–219. https://doi.org/10.3354/meps06979

Warner, J. C., Sherwood, C. R., Signell, R. P., Harris, C. K., & Arango, H. G. (2008). Development of a three-dimensional, regional, coupled wave, current, and sediment-transport model. Computers and Geosciences, 34(10), 1284–1306. https://doi.org/10.1016/j.cageo.2008.02.012

Weinberg, S., & Weinberg, F. (1979). The life cycle of a gorgonian: Eunicella singularis (Esper, 1794). Bijdragen tot de Dierkunde, 48(2), 127-140.

White, J. W., Morgan, S. G., & Fisher, J. L. (2014). Planktonic larval mortality rates are lower than widely expected. Ecology, 95(12), 3344–3353. https://doi.org/10.1890/13-2248.1

Wilson, D. S. (1992). Complex Interactions in Metacommunities , with Implications for Biodiversity and Higher Levels of Selection. Ecology, 73(6), 1984–2000.

Wilson, K. (2002). Restoration of Hong Kong fisheries through deployment of artificial reefs in marine protected areas. ICES Journal of Marine Science 59, 157–163. https://doi.org/10.1006/jmsc.2002.1186

Worm, B., Barbier, E.B., Beaumont, N., Duffy, E.J., Folke, C., Halpern, B.S., Jackson, J.B.C., Lotze, H.K., Micheli, F., Palumbi, S.R., Sala, E., Selko, K.A., Stachowicz, J.J., & Watson, R. (2006). Impacts of biodiversity loss on ocean ecosystem services. Science, 314(5800), 787–790. https://doi.org/10.1126/science.1137946

Yeager, L. A., Estrada, J., Holt, K., Keyser, S. R., & Oke, T. A. (2020). Are Habitat Fragmentation Effects Stronger in Marine Systems? A Review and Meta-analysis. Current Landscape Ecology Reports, 5(3), 58–67. https://doi.org/10.1007/s40823-020-00053-w

Young, C.M. (1990). Larval ecology of marine invertebrates: a sesquicentennial history. Ophelia 32(1–2), 1–48.